North Carolina Agricultural and Technical State University

Aggie Digital Collections and Scholarship

2014

# Chemical Reactive Separations In Energy And Environmental Processes

Md Arif Khan
*North Carolina Agricultural and Technical State University*

Follow this and additional works at: https://digital.library.ncat.edu/theses

Chemical Reactive Separations in Energy and Environmental Processes

Md Arif Khan

North Carolina A&T State University

A thesis submitted to the graduate faculty

in partial fulfillment of the requirements for the degree of

MASTER OF SCIENCE

Department: Chemical, Biological and Bioengineering

Major: Chemical Engineering

Major Professor: Dr. Yusuf G. Adewuyi

Greensboro, North Carolina

2014

The Graduate School
North Carolina Agricultural and Technical State University
This is to certify that the Master's Thesis of


Md Arif Khan



has met the thesis requirements of
North Carolina Agricultural and Technical State University


Greensboro, North Carolina
2014


Approved by:


_____  _____
Dr. Yusuf G. Adewuyi                        Dr. Leonard Uitenham
Major Professor                            Committee Member


_____  _____
Dr. Stephen B. Knisley                      Dr. Lijun Wang
Department Chair                           Committee Member


_____
Dr. Sanjiv Sarin
Dean, The Graduate School

Biographical Sketch

Md Arif Khan was born on February 13, 1985, in Narsingdi, Bangladesh. He received his Bachelor's degree (BSc) in Chemical Engineering from Bangladesh University of Engineering and Technology (BUET), Dhaka, Bangladesh in 2008. He is currently a chemical engineering graduate student and candidate for Master's degree (MS) in chemical engineering at North Carolina Agricultural and Technical State University, Greensboro, North Carolina. He plans to pursue a Doctoral degree (PhD) upon graduation.

Dedication

I dedicate this thesis to my family members.

Acknowledgements

I wish to express my sincere gratitude to my academic advisor, Dr. Yusuf Adewuyi for his valuable guidelines and supervision throughout the entire research work. I am also thankful to my former colleagues, Dr. Vishwanath Deshmane and Nana Sakyi, who have helped me in conveying previous knowledge and in experimental and analytical works. I also wish to thank Mr. George Coleman, Lab Manager for the Chemical Engineering Program, for providing support in solving various machinery problems.

I thank Dr. Lijun Wang, for providing technical, intellectual and financial supports as a co-advisor. I also appreciate Dr. Leonard Uitenham for his time as a committee member. I also thank all the chemical engineering faculty members, all my class teachers and classmates for their warm and supportive behavior.

I acknowledge the NSF-CBET and USDA-NIFA for providing financial assistance for these projects which are subject of this thesis. I am very much grateful to Chemical, Biological and Bioengineering Department for providing financial aids and facilities, and to Dr. Shamsuddin Ilias, Chemical Engineering Program Director, for his valuable advice throughout my academic career.

Table of Contents

List of Figures

## List of Tables

Abstract

The main objective of this study was to investigate the application of chemical reactive

separation (reactive separation, advanced oxidation) in bio-oil upgradation and air pollution

control. Aspen simulation for reactive distillation of pyrolysis bio-oil for the reactive distillation

with n-butanol is carried out using RADFRAC module and UNIQUAC property method by

minimizing Gibbs free energy. The binary and ternary interaction and chemical and phase

equilibrium (CPE) between the components were studied to determine the azeotropes and

homogeneous region of mixture. The conversions for the esterification reactions were found to

be 70-90% for various simulated bio-oils, and water was separated from the ester products. All

the distillation column parameters such as condenser and reboiler heat duty, number of stages,

reflux ratio with different inlet conditions etc., were studied to develop a completely energy cost

minimized RD unit. The removal of nitric oxide (NO) from simulated flue gas in a bubble

column reactor at atmospheric pressure is investigated using combined aqueous persulfate

$(Na_2S_2O_8)$ and ferrous ethylenediamine tetraacetate ($Fe^{II}$-EDTA) systems. 0.1 M persulfate

solution with 0.01 M $Fe^{2+}$ was used as the optimum amount of absorption-oxidation reagents and

molar ratio of $Fe^{2+}$ and EDTA was found to be 1:1 for maximum NO conversion. NO absorption

experiments were carried out at 23-70 $^0$C, and comparative NO concentration profiles and

corresponding conversion (%) plotted. The results show significant improvement in NO removal

compared with thermally and $Fe^{2+}$ activated persulfate systems (at lower temperature 25-30%

and at higher temperature 5-10%) and almost 100% NO conversion can be achieved at 70 $^0$C.

The detailed chemistry and kinetics are discussed. Iron species' ($Fe^{2+}$, $Fe^{3+}$ and $Fe^{II}$-EDTA)

concentrations were measured spectrophotometrically to understand the simultaneous and

synergistic relationship between persulfate and $Fe^{II}$-EDTA in NO removal.

**CHAPTER 1**

**Introduction**

**1.1 General Introduction**

In the 21$^{st}$ century, sustainable energy sources and the environment are the biggest

concern due to the diminishing world energy reserves and the destruction of global

environmental sustainability by industrialization of human civilization. Energy drives the world

economy and is very important for supporting the successful functioning of all sectors of our

modern society, while its relentless use has directed the world to an environmental disaster. The

International Panel on Climate Control (IPCC) report predicted that global average temperature

can increase up to 1.8 °C to 4 °C by the year 2100, which could lead to the extinction of 20-30 %

of plant and animal species and increase of sea level by 18-59 cm catastrophically impacting

coastal based communities (IPCC, 2007). Consumption of fossil fuels is responsible for the

majority of $CO_2$ emissions. The concentration of $CO_2$ continues to grow and is predicted to

increase to over 390 ppm, or 39 % above pre-industrial point by the end of 2010. Green house

gas (GHG) emissions must be minimized to less than half the global emission levels of 1990, in

order to reduce global warming and related climate change impacts (IEA, 2007; IPCC, 2011).

Renewable energy sources offer the prospect to contribute to social and economic

progress, energy accessibility, safe and sound energy supply, climate change mitigation, and the

reduction of negative environmental and health impacts. In general, renewable energy is defined

as any form of energy obtained from sources that can be replenished by natural processes within

a reasonable period of time (IPCC, 2007). Biomass is a plentiful carbon-neutral renewable

energy source and can be obtained from any organic matter of vegetable or animal origin. It is

available in many forms and from different sources and heat, power, liquid and gaseous fuels can

be produced from biomass simultaneously (Bauen et al., 2009). It also serves as a feedstock for materials and, when produced and used on a sustainable basis, can significantly reduce GHG emissions compared to fossil fuels. Biomass resources are available in most of the countries, , rendering biomass a more uniformly spread energy supply option across the globe (Ragauskas et al., 2006).

Bioenergy is presently one of the largest renewable energy sources and is likely to remain for the first half of 21$^{st}$ century. On a global basis, for the year 2008, biomass offered about 10 % or 50.3 Exajoules (EJ) while other RE sources contributed to about 2.9 % of the total 492 (EJ) primary energy supply. However, the majority (roughly 60 %) of bioenergy came from the traditional biomass used in cooking and heating purposes in less developed countries. This traditional use of biomass creates negative health impacts by producing the high concentrations of particulate matter and carbon monoxide, among other pollutants (IPCC, 2011). Careful management of bioenergy can contribute incredibly to the global primary energy supply, can significantly reduce the green house gas emissions in additions to the other environmental benefits. It can deliver improvements in energy security, by replacing imported fossil fuels with domestic biomass; create opportunities for economic and social development in rural communities; and  offer possibility for using wastes and residues, reducing waste disposal problems, and making better use of resources (Bauen et al., 2009). In 2008, transport sector contributed about 33 % of total global final energy consumption (294 EJ), while the remaining 67 % was consumed in buildings, industry and agriculture sectors in the form of heat and electricity. However, only 2 % of the energy attributed to the transport sector was in the form of biofuels (IEA, 2010). In order to face the challenge of meeting the secure and sustainable energy

supply and reduction of green house gas emissions, exponential research and development in the field of biofuels is anticipated to play pivotal role in upcoming years.

Air pollution has become a serious threat to human health and ecology all over the world as well as in United States. Continuous increase in the use of fossil fuels in industries and automobiles is causing a steady increase in the level of pollutants in the atmosphere. The Environmental Protection Agency (EPA) has defined an air pollutant to be "any substance in the air that can cause harm to humans or the environment." Pollutants may be natural or man-made and may take the form of solid particles, liquid droplets or gases. The 1990 Clean Air Act Amendments (CAAA) lists 188 toxic air pollutants that EPA is required to control. These pollutants are divided into various groups, including particulate matter, volatile organic compounds (VOCs) and halogen compounds. Also included are more commonly-known pollutants such as lead, mercury and asbestos. The Act requires EPA to set air quality standards for "criteria pollutants". Currently, $NO_X$ (nitric oxide and its group of compounds) and five other major pollutants (ozone, lead, carbon monoxide, sulfur oxides and particulate matter) are listed as criteria pollutants. The law also requires EPA to periodically review the standards and revise them if appropriate to ensure that they provide the requisite amount of health and environmental protection and to update those standards as necessary.

Since the adoption of Clean Air Act in 1970, while the levels of $NO_2$ and $SO_2$ have decreased, the level of NO has actually increased by 20% (Environmental Defense Fund, 2010). The combustion of bio-fuel also emits higher $NO_X$ compared to petroleum fuels (Kiss, Dimian, & Rothenberg, 2007; A. A. Kiss, F. Omota, A. C. Dimian, & G. Rothenberg, 2006). The stricter control by state and regulatory agencies for $NO_X$ emission warrants the need for efficient and inexpensive NO removal technologies that can be easily retrofitted to existing power plants.

Currently, popular technologies for $NO_X$ abatement include SCR (selective catalytic reduction), SNCR (selective non-catalytic reduction), FGR (flue gas recirculation), thermal $deNO_X$ etc. All of these technologies suffer from some form of drawbacks including high operating and capital costs, high temperature and disposal problems. In this respect, $NO_X$ removal by aqueous scrubbing promises to be an inexpensive and efficient technology for $NO_X$ removal. However, while $SO_2$ and $NO_2$ are quite easily removed by wet scrubbing mechanisms, NO is much more difficult to remove due to the fact that it is very sparingly soluble in aqueous solutions, which greatly increases the liquid phase resistance to mass transfer.

## 1.2 Biofuel Production

Biofuels are the liquid and gaseous products obtained from the biomass. Biofuels do not produced larger amount of $CO_2$ emission than the quantity consumed by photosynthesis. For this reason, biofuels are omitted from the $CO_2$ balance of the Kyoto protocol from the United Nation's climate panel. Replacing fossil fuels with biofuels is considered to advance desirable objectives such as energy security, climate protection and growth of energy usage in rural areas. Governments around the world have adopted policies to support advance and exploitation of biofuel technologies to harvest some of these benefits. In the United States, renewable energy standard was legislated as part of the Energy Independence and Security Act of 2007 that requires $1.36 \times 10^8 \ m^3$ of biofuels in transportation fuel mix by 2022 (US-Congress, 2007).

Biofuels have been generally devided into three different category or 'generations' depending upon the feedstock they are prepared from and the level of their technical development in manufacturing processes (IEA, 2008, 2009). The 1st generation includes the biofuels that have their production technology well understood and have already developed commercial markets such as the biodiesel produced from oil crops and animal fats, bioethanol

prepared from sugar and starch crops, and renewable diesel prepared using biomethane from anaerobic digestion of wet biomass. The 2$^{nd}$ generation biofuels have undeveloped biochemical or thermochemical technologies including the biodiesel and bioethanol produced by using novel feedstocks of oil, starch and sugars; and ethanol, butanol and syndiesel produced from lignocellulosic. Finally, the 3$^{rd}$ generation or advanced biofuels include biofuels such as biodiesel and bioethanol from algae and hydrogen from biomass. The manufacturing routes for these biofuels are at the infant stages of research and are noticeably away from commercialization (IEA, 2009; Stocker, 2008). Biofuels from waste material such as agricultural and animal wastes is in considerable interest and is the main topic in this work.

      **1.2.1 Biodiesel.** Biodiesel is also called fatty acid methyl ester (FAME). It is a clean-burning, renewable fuel normally obtained from vegetable oils, animal fats, recycled cooking oil and waste greases and virtually every waste material from animal and agricultural origin. It is biodegradable and non-toxic and free of sulfur compounds making it more clean burning fuel than petroleum diesel with lesser emission of smoke, un-burnt carbon and particulate matter, sulfur oxides ($SO_x$), and carbon monoxide (CO). It has excellent lubricating properties that extend engine life, superior cetane number, flash point compared to conventional diesel and acceptable cold filter plugging point (CFPP) makes it very attractive alternative (Graboski & McCormick, 1998) (Boehman, 2005; Demirbas, 2005). Currently, there are modifications needed in the existing diesel engines to use biodiesel only but when as a blend with petroleum diesel fuel is used no such modifications require. The use of biodiesel is recommended by governments across the world to (i) improve energy supply security, (ii) reduce greenhouse gas emissions, and (iii) boost rural incomes and employments (Bozbas, 2008). Table 1 shows various properties of biodiesel in compared to petroleum diesel. From this data it can be deduced that the biodiesel

viscosity and specific gravity is higher than the petroleum. The boiling points are almost same but the flash point and cetane number (ignition quality) is higher than the petroleum. The presence of extra oxygen in the bio-oil yield unconverted hydrocarbon and less CO emissions in bio-oil combustion. Except viscosity, cloud and pour points all the property in bio-oil is rather good compared to petroleum fuels. That is why; biodiesel is always preferable to petroleum as a fuel.

Table 1

*Comparison between Petroleum Diesel and Biodiesel*

| Fuel Property | Petroleum Diesel | Biodiesel |
|---|---|---|
| Fuel Standard | ASTM D975 | ASTM D6751 |
| Fuel Composition | $C_{10}$-$C_{21}$ HC[a] | $C_{10}$-$C_{21}$ FAME[b] |
| Kinetic Viscosity,mm$^2$/s (at 40 $^0$C) | 1.3-4.1 | 1.9-6.0 |
| Specific Gravity, kg/L | 0.85 | 0.88 |
| Boiling Point, $^0$C | 188-343 | 182-338 |
| Flash point, $^0$C | 60-80 | 100-170 |
| Cloud point, $^0$C | -15 to 5 | -3 to 12 |
| Pour point, $^0$C | -35 to -15 | -15 to 10 |
| Cetane number (ignition quality) | 40-55 | 48-65 |
| Stoichiometric air/fuel ratio (AFR) | 15 | 13.8 |
| Life-cycle energy balance | 0.83/1 | 3.2/1 |

[a]HC-hydrocarbon; [b]FAME-fatty acid methyl esters

**1.2.2 Life cycle analysis and current trend.** The main advantage of bio based fuels is that they are environmental friendly because they have positive life cycle energy balance (3.2

units of energy produced per unit of energy consumed) compared to the petroleum diesel (0.83 unit of energy produced per unit energy consumed). The biodiesel has less CO & $CO_2$ emissions as well as other emissions. It has all the properties similar to petroleum diesel (table-5) and can be used as a blend with petroleum diesel in the engines and also directly (100%) with minor engine modification (A. Kiss, F. Omota, A. Dimian, & G. Rothenberg, 2006).
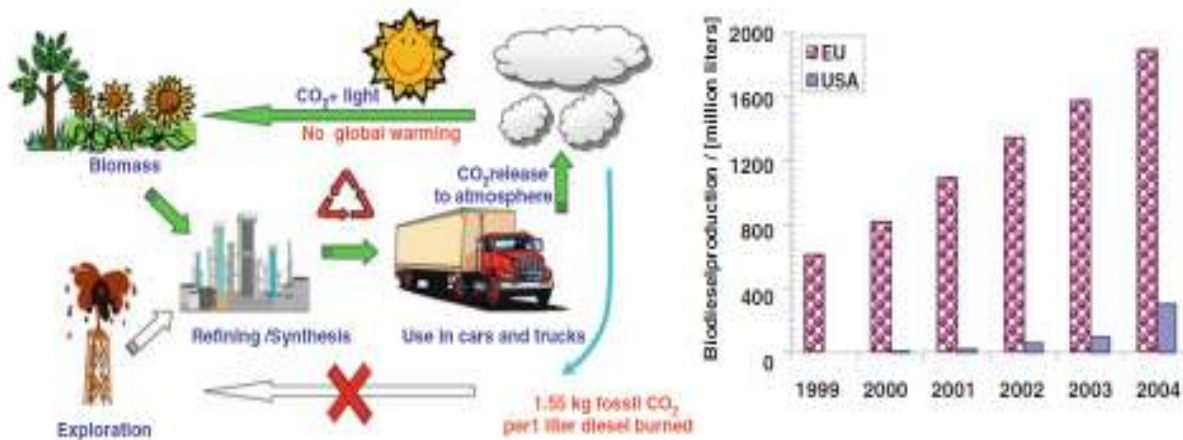


*Figure 1.* Life cycle diagram of biodiesel compared to petroleum and US biodiesel production compared to European Union (EU) countries.

1st part of Figure 1 clearly shows that bio fuels are renewable source of energy while the petroleum is non-renewable and non-sustainable because of no replenishment of petroleum fuels. Also, biofuels emit lot less greenhouse gases and thus mitigating the increase of greenhouse gases in Earth's Biosphere. Despite all the advantages the US and world's movement toward a bio-based renewable and sustainable energy system is rather slow. 2nd part of the Figure 1 shows US slow progress compared to the EU counterpart to bio-oil production.

**1.2.3 Bio-oil production from agricultural and animal waste.** To make biodiesel from various sources, one can follow these primary ways: (Kiss et al., 2007)

1. Vegetable oil direct blending

2. Use of micro-emulsions with short chain alcohols

3. Thermal Pyrolysis of agricultural wastes

4. Hydrothermal Liquefaction of animal waste

5. Trans-esterification of triglycerides by catalytic reaction

6. Esterification of fatty acids with alcohols using liquid and solid acid catalysts

The simplified block diagram of the whole process of biodiesel generation from agricultural and animal waste is given in Figure 2.
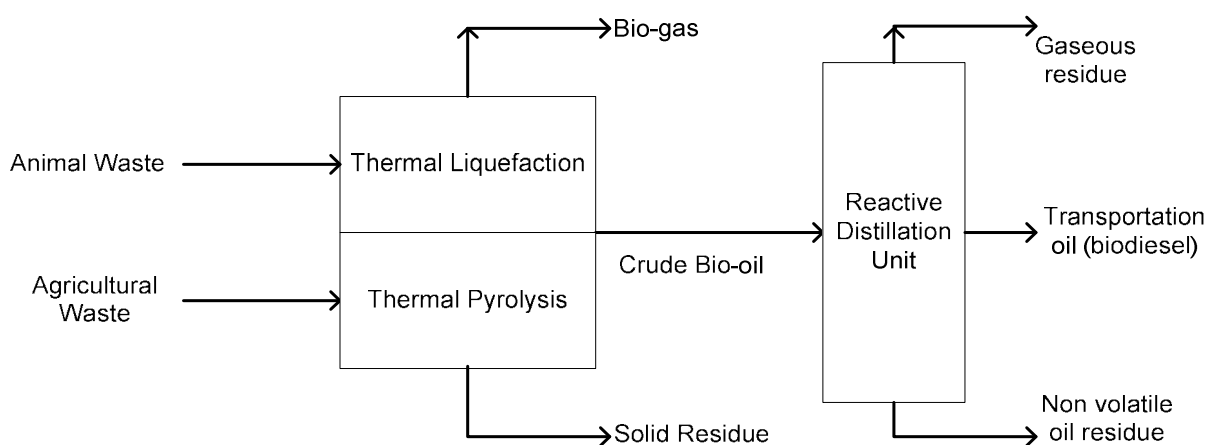


*Figure 2.* Process flow-sheet for producing transportation oil (biodiesel) from agricultural and animal waste.

   ***1.2.3.1 Thermal liquefaction and thermal pyrolysis of animal waste.*** Animal waste from animal farms are huge source of renewable energy as potential energy from only swine manure is equivalent to almost 2.1% of US annual petroleum energy consumption. In additional, animal waste polluts environment and it is required to treat the animal wastes for a clean environment. (Theegala & Midgett, 2012; Xiu, Shahbazi, Shirley, & Cheng, 2010). Figure 3 includes a block diagram for hydrothermal liquefaction and the temperature effect on product yield.
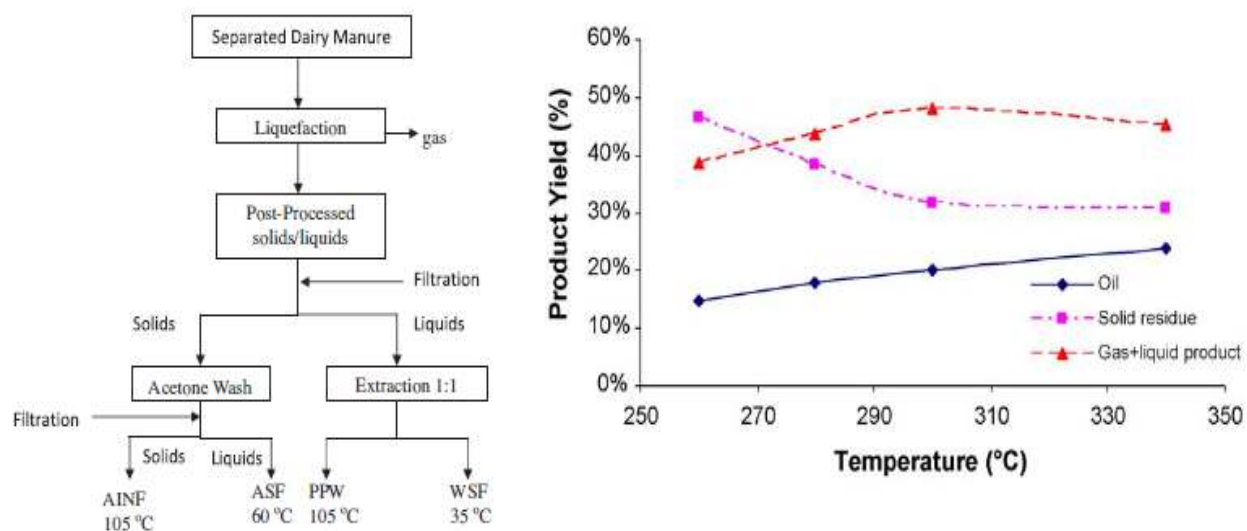
*Figure 3*. Conceptual diagram for the separation and quantification of the hydrothermal liquefaction product and effect of temperature on product yield.

The bio-oil derived from hydrothermal liquefaction is almost similar property as petroleum diesel. But the oil has very high viscosity and the liquid also has significant corossiveness. That is why further upgradation is required to use it as transportation oil which will be discussed later.

***1.2.3.2 Liquefaction of biomass and thermal pyrolysis of agricultural waste.*** There are lots of ways to get bio-oil from agricultural waste residues. The thermal methods includes: direct combustion, pyrolysis, gasification and one of thermochemical methods is the hydrothermal liquefaction of wet biomass (Toor, Rosendahl, & Rudolf, 2011). Before processing the agricultural residues are dried and after treatment they produced bio-mass. The biomass is then processed via hydrothermal liquefaction where hemicellulose, cellulose and lignin of the biomass is broken down under heat treatment to produce thick crude bio-oil and some solid residue and biogas. The carbohydrade and lignin breakdown scheme is given in Figure 4.
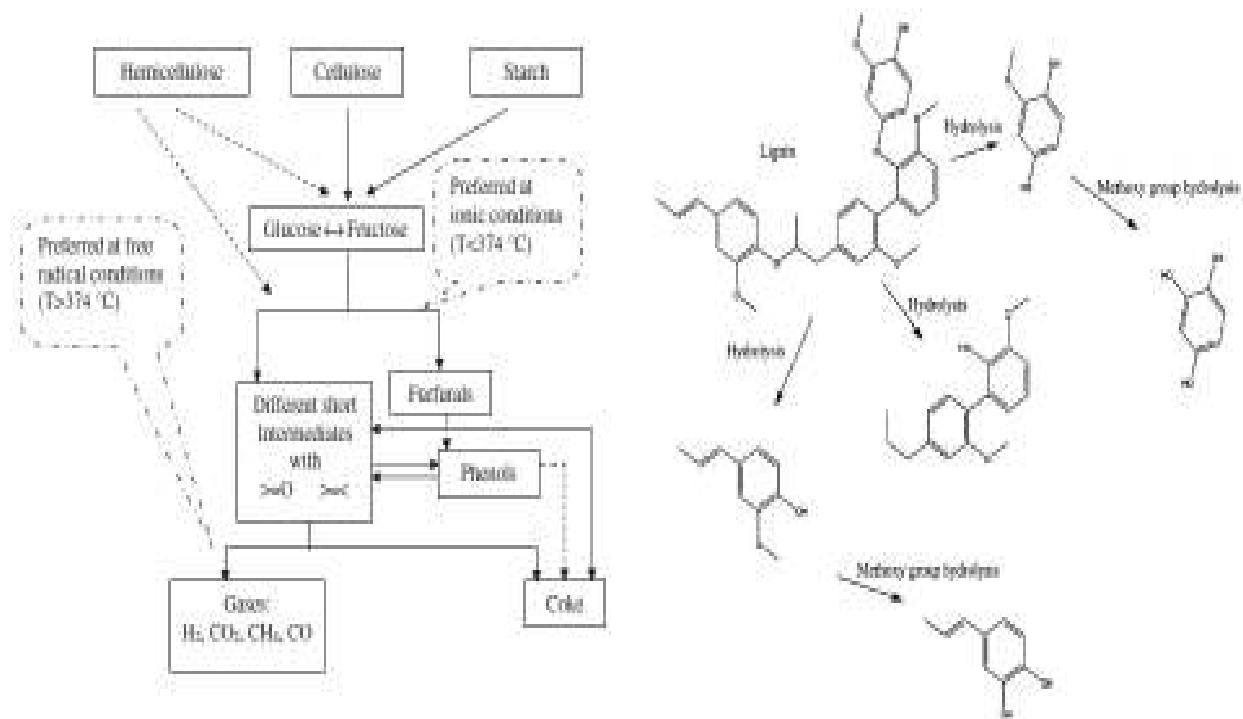
*Figure 4.* Carbohydrate and lignin degradation in liquefaction of biomass.

In Figure 5 products (cradle to grave) from thermal biomass conversion is given as well as fast

pyrolysis upgrading methods is also shown.
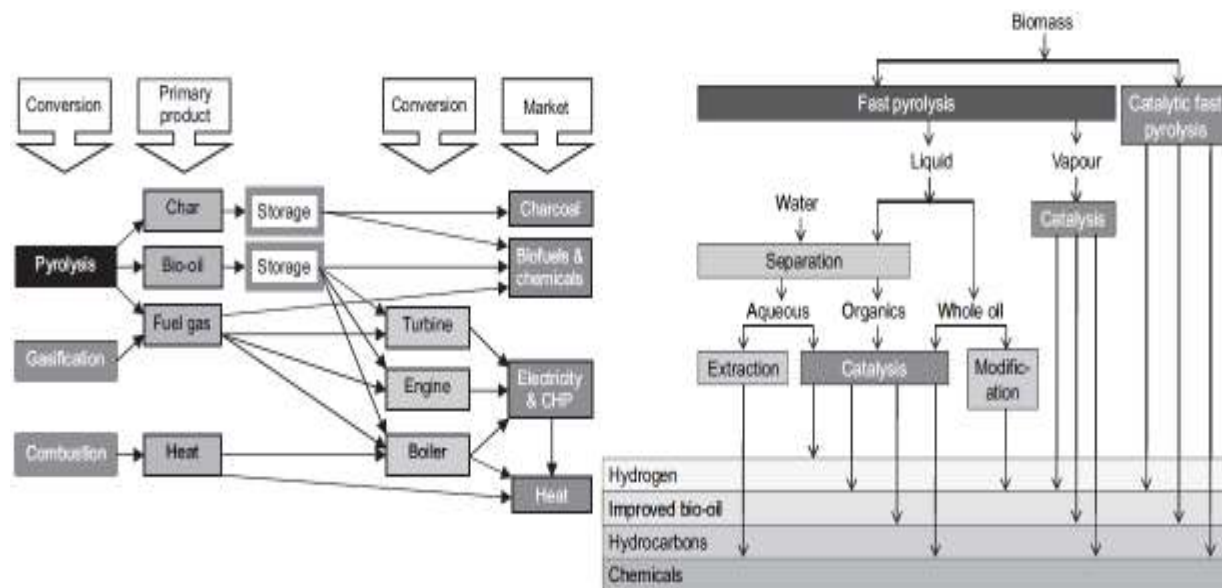


*Figure 5.* Products from thermal biomass conversion and fast pyrolysis upgrading methods.

The end products distribution (liquid oil, solid residue and gaseous products) can vary with the pyrolysis methods and the temperature of the process selected.

      **1.2.4 The emissions from bio-oil combustion.** The emissions (except $NO_x$) from the biodiesel (B100) and biodiesel blends (B20 & B80) with conventionsl petroleum diesel is much less than the direct petroleum fuels and the Figure 6 shows the comparison between them (A. Kiss et al., 2006; Kiss, 2011; Kiss et al., 2007). Also, Table 2 shows the percentage change of emissions from petroleum diesel to biodiesel. In a typical analysis of the emissions of biodiesel as compared to petroleum diesel it can be seen that all the emissions except $NO_x$ is less in biodiesel emission. Thus, the study of $NO_x$ removal especially nitric oxide (NO) removal from the combustion exhaust is very important for the successful implementation of biodiesel instead of petroleum diesel. Also, biodiesel has virtually no Sulfur oxides ($SO_x$) emission (100% less in Table 2). That is why, biodiesel and biofuels have the potential capability of replacing coal fired power plants if implemented in near future.
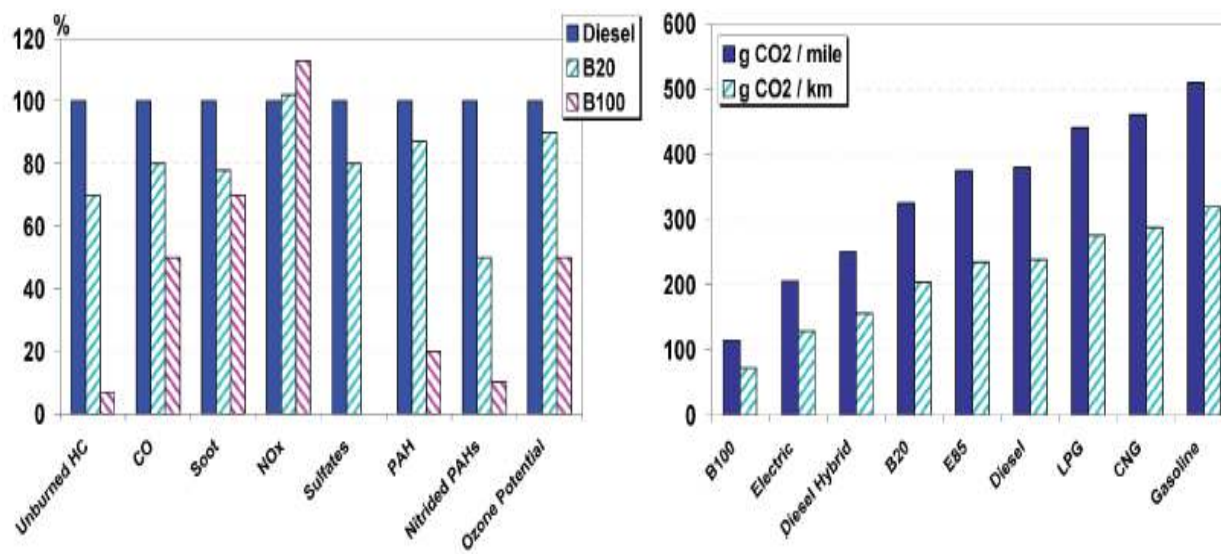


*Figure 6.* Comparison of biodiesel combustion with petroleum diesel.

Table 2

*Comparison between Various Emissions of Biodiesel and Petroleum Diesel*

| Emission Type | B20 | B100 |
|---|---|---|
| Total Unburned Hydrocarbons | -20% | -67% |
| Carbon monoxide (CO) | -12% | -48% |
| $CO_2$ (life cycle production) | -16% | -79% |
| Particulate Matter | -12% | -47% |
| Nitrogen Oxides ($NO_x$) | +2% | +10% |
| Sulfur Oxides ($SO_x$) | -20% | -100% |
| Polycyclic Aromatics (PAH) | -13% | -80% |
| Nitrated PAH's (nPAH) | -50% | -90% |

**1.2.5 Production of biodiesel from crude bio-oil.** Biodiesel is a mixture of mono-alkyl esters of fatty acids that can be produced from viscous and corrosive crude bio-oil by several ways. Biodiesel is produced via transesterification reactions where triglycerides react with alcohol in the presence of acid catalysts, base catalysts or enzymes or by esterification reaction of organic acids with alcohols in presence of acid catalysts. The chemical composition of biodiesel depends on the feedstock from which it is produced, as feedstocks of different origin have different fatty acid composition (Pinto et al., 2005).

1. Trans-esterification of triglycerides with short chain alcohols using liquid catalyst: This can be done by using acid, base or enzyme based catalysts and the composition of biodiesel depend on the content of raw fatty materials (fatty acid groups building triglycerides). But the method has significant disadvantages including the corrosiveness of the liquid catalysts. Also,

the liquid catalysts must be neutralized which produce waste salt stream and the presence of free

fatty acids tend to produce soap as a unwanted byproduct that require expensive separation.

Typical trans-esterification reaction scheme (Gómez-Castro, Rico-Ramírez, Segovia-Hernández,

& Hernández-Castro, 2011):

$$n\text{-butanol} + \text{methyl acetate} \rightleftharpoons n\text{-butyl acetate} + \text{methanol}$$
$$\text{(}n\text{-BuOH)} \qquad \text{(MeOAc)} \qquad \text{(}n\text{-BuOHc)} \qquad \text{(MeOH)}$$
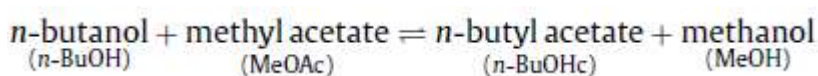
2. Batch wise Esterification of fatty acids using $H_2SO_4$ as catalyst: This process is very

suitable to control the esters with specific carbon content and has uses in cosmetics,

pharmaceuticals and food industries. But batch process cannot handle very large-scale

production and this also need very costly neutralization and separation and presence of sulfuric

acid in biodiesel increase the sulfur emission.
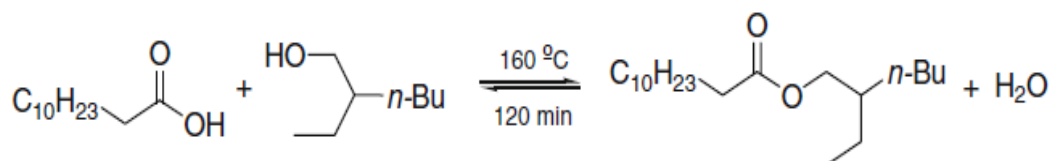


3. Continuous Reactive Distillation (RD) process using solid acid catalysts: The RD

combines the reaction and separation in one unit and one can shift the reaction equilibrium to the

desired point by the continuous removal of the products. This process does not produce any

waste salt stream as all the reactions and separation can be done inside one single unit. Two-step

reaction scheme for biodiesel production is shown in the following reaction (Gomez-Castro,

Rico-Ramirez, Segovia-Hernandez, & Hernandez, 2010).

The reaction equations:

$$\begin{array}{l} CH_2-OCOR^1 \\ | \\ CH-OCOR^2 \\ | \\ CH_2-OCOR^3 \\ \text{Triglyceride} \end{array} + 3H_2O \rightleftharpoons \begin{array}{l} R^1COOH \\ R^2COOH \\ R^3COOH \\ \text{Fatty acids} \end{array} + \begin{array}{l} CH_2-OH \\ | \\ CH-OH \\ | \\ CH_2-OH \\ \text{Glycerol} \end{array}$$

$$R^4COOH + CH_3OH \rightleftharpoons R^4COOCH_3 + H_2O$$

Fatty acid → Biodiesel
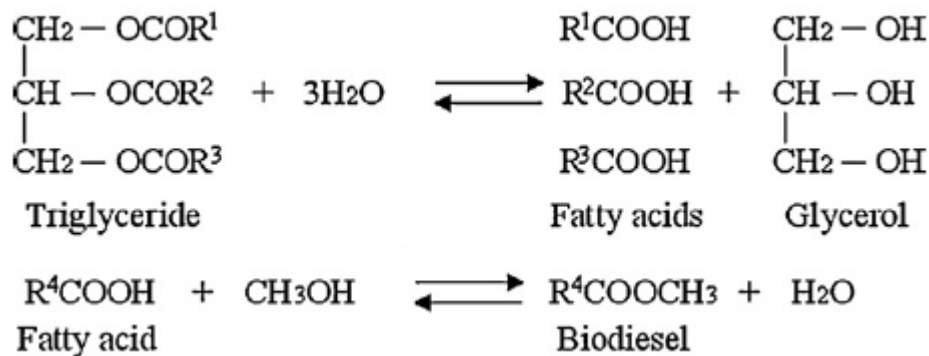
As the residence time in Reactive Distillation column is low due to the hydraulic constraints, the solid acid catalysts should be very strong acid and they are characterized by their Bronsted or Lewis Acidity. Production of biodiesel using solid acid catalysts are not well established in industries yet because it is difficult to find a suitable solid acid catalyst and the non-ideality of the mixture in reactive distillation column may result in the segregation of the mixture into aqueous and organic layer because of the absence of any agitating device in RD column.
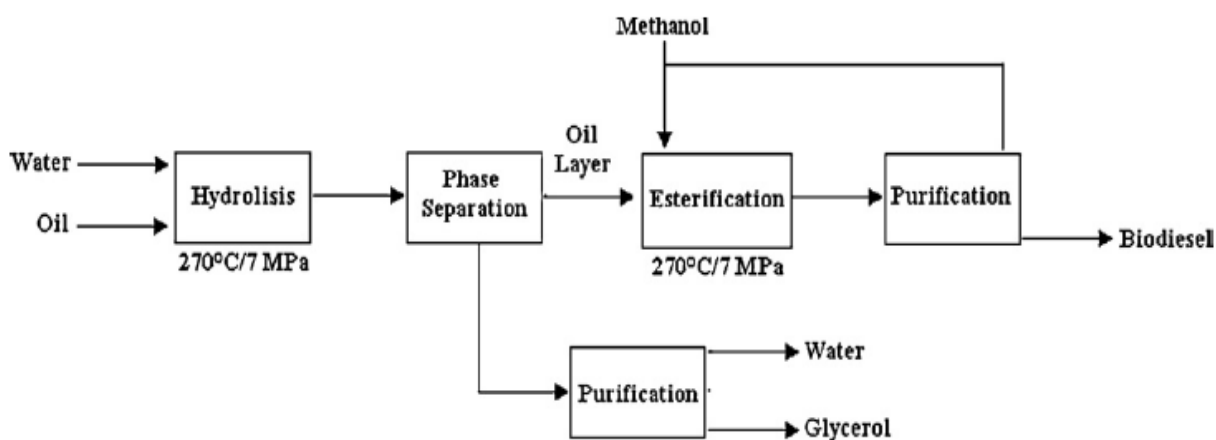


*Figure 7.* Schematic diagram for the production of biodiesel in RD column.

***1.2.5.1 Catalysts for reactive distillation (RD).*** The catalysts investigated till today for the solid acid catalyzed reactive distillation is given in Figure 8.

| Catalyst sample | Surface area ($m^2/g$) | Pore volume ($cm^3/g$) | Pore diameter max./mean/calc. [nm] | Sulfur content (% |
|---|---|---|---|---|
| $Cs_{2.5}H_{0.5}PW_{12}O_{40}$ | 163 | 0.135 | 2/5.5/3 | N/A |
| $ZrO_2/SO_4^{2-}/650\ °C$ | 118 | 0.098 | 4.8/7.8/7.5 | 2.3 |
| $TiO_2/SO_4^{2-}/550\ °C$ | 129 | 0.134 | 4.1/4.3/4.2 | 2.1 |
| $SnO_2/SO_4^{2-}/650\ °C$ | 100 | 0.102 | 3.8/4.1/4.1 | 2.6 |

| | Acidity (meq $g^{-1}$) |
|---|---|
| $H_2SO_4$ | 20.4 |
| $H_3PW_{12}O_{40}$ | 1.0 |
| $Cs_{2.5}H_{0.5}PW_{12}O_{40}$ | 0.15 |
| Zeolites (Y, β, ZSM5) | 0.52–1.12 (depending on Si/Al ratio) |
| Amberlyst-15 | 4.70 |
| Nafion-50 | 0.80 |
| $Nb_2O_5 \cdot 5H_2O$ | 0.31 |
| $SO_4^{2-}/ZrO_2$ | 0.20 |

*Figure 8.* Major catalysts investigated and their effects on RD of esterification reaction.

In the literature different solid acid catalysts including zeolites, ion exchange resins, sulfated carbon based catalysts, heteropoly compounds and mixed metal oxides were studied (A. Kiss et al., 2006). Zeolites gave lower conversion compared to non-catalyzed reaction. The ion-exchange resins gave good fractional conversion but resins are not stable at high temperature. The tungstophosphoric acid shows high activity but the acid is soluble in water and that is why they are not good choices as catalysts. Sulfated Zirconia (SZ) shows comparative high reaction rate and conversion and they are thermally stable and not soluble in water. Also SZ has large pore and does not limit the diffusion of fatty acid in the pore. Thus, sulfated zirconia is the most suitable candidate for this process. Another crucially important catalyst characteristic is its hydrophobicity. If the catalyst is hydrophilic it will gradually dissolve in water and we will lose

costly produced catalysts. Due to this reason, tungstophosphoric acid is not a good catalysts even if the conversion is better than the sulfated zirconia catalysts.

   *1.2.5.2 Reactive distillation (RD) design.* The reactive distillation design for solid acid catalyzed reactions is very complicated because of the simultaneous presence of the following (A. Kiss et al., 2006):

1.  Chemical and Phase Equilibrium (CPE)

2.  Vapor-Liquid Equilibrium (VLE)

3.  Vapor-Liquid-Liquid Equilibrium (VLLE)

4.  Catalysts Activity and kinetics

5.  Mass Transfer in Gas-Liquid and Solid-Liquid

6.  Adsorption of The Reactants and Desorption of The Products on Catalysts Surface

Figure 9 shows CPE diagram for esterification reaction in reactive distillation and how complicated the design could be. In reactive distillation of bio-oil two phase exists below $100^0$C and that is why the operating temperature is always selected over $100^0$C for the RD column (A. Kiss et al., 2006).
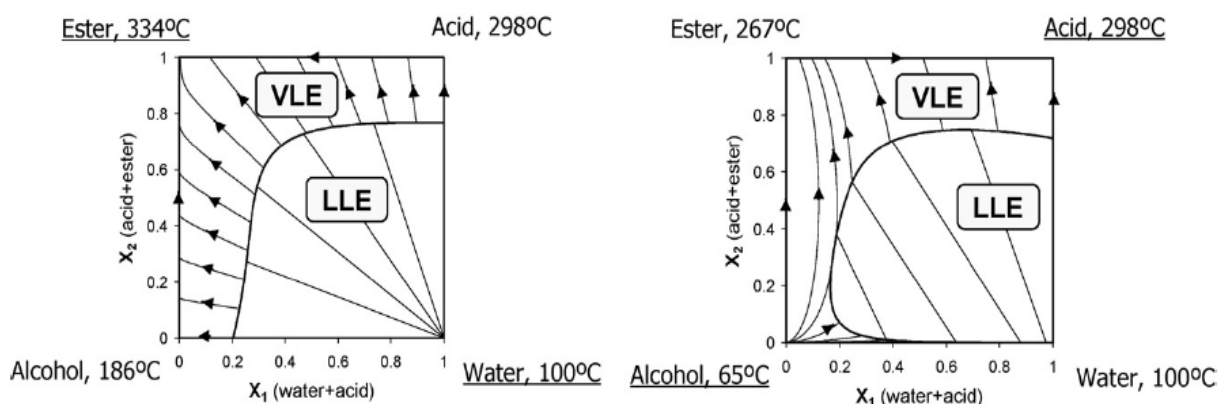


*Figure 9.* Equilibrium diagram for dodecanoic acid with 2-ethylhexanol and methanol.

Figure 10 shows a conceptual diagram for the FAME production. The flowchart is drawn using ASPENPLUS for the purpose of rigorous simulation (Kiss et al., 2007).
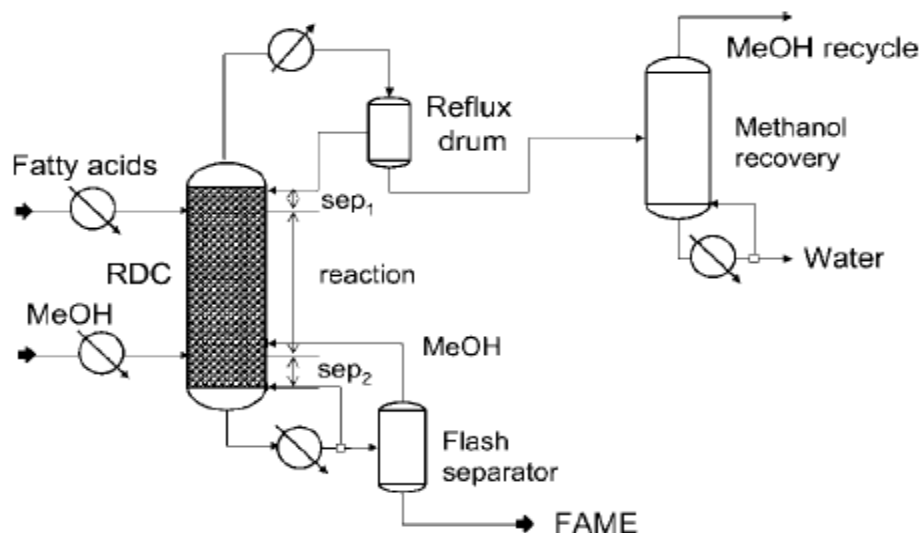


*Figure 10.* FAME production by reactive distillation of esterification reaction.

UNIQUAC property model is used to combate the non-ideality of the solution. The ester produced and the biproduct water and unreacted alcohol is taken away continuously as the bottom and top products respectively to shift the reaction equilibrium towards ester formation. The reactants (acid and alcohol) is fed at stoichiometric ratio. The reaction takes place in the homogeneous phase if the mixture split into two phases. To prevent the formation of two phase the inlet feed ratio and the operating temperature of RD column is selected very carefully using the information from Chemical and Phase Equilibrium (CPE) diagram.

The plot found from ASPEN simulation is given in Figure 11. ASPEN permits us to perform stage-by-stage calculation and the results can be plotted.
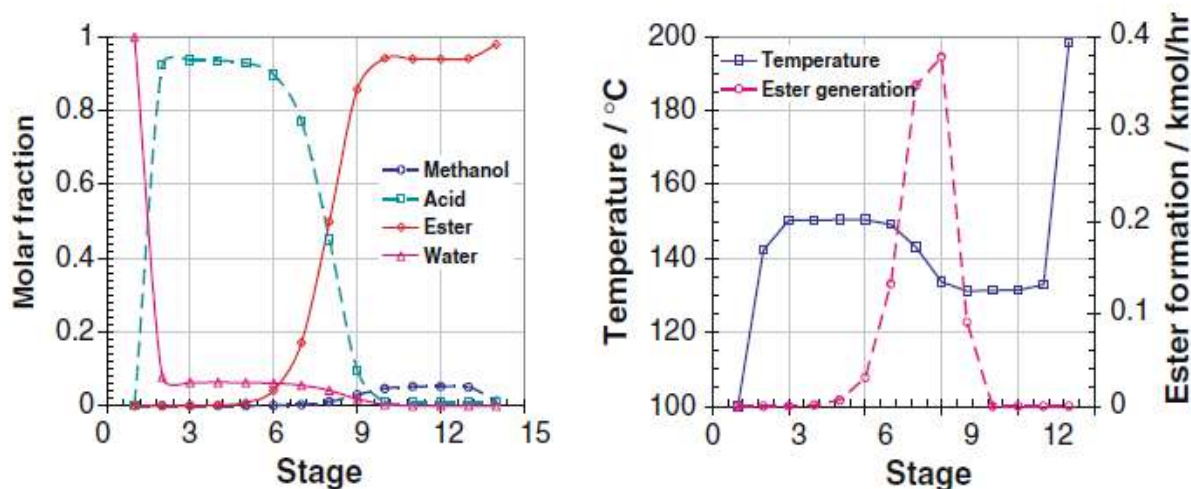
*Figure 11. Liquid composition, temperature and ester formation profile in a RD column.*

For the kinetic based design bio-oil is considered composed of Tri-, Di-, and Mono-glycerides (TG, DG, MG resp.) and the following reactions are considered and the kinetic constants are given (Noshadi, Amin, & Parnas, 2012):

$$TG + MeOH \overset{catalyst}{\leftrightarrow} DG + FAME \qquad\qquad (R1)$$

$$DG + MeOH \overset{catalyst}{\leftrightarrow} MG + FAME \qquad\qquad (R2)$$

$$MG + MeOH \overset{catalyst}{\leftrightarrow} G + FAME \qquad\qquad (R3)$$

With this kinetic data the simulated results can be compared to the expermental data. Then the effects of various distillation parameter on conversion can be observed for both experimental data and simulated data. Steinigeweg, S. et al. observed such plots and in figure-plot of fractional conversion vs. reflux ratio is given for the comparison of experimental data and the simulated data (Steinigeweg & Gmehling, 2004).

Table 3

*Kinetic Constants in Reactive Distillation for* $k_i = A_i \exp(-\dfrac{E_{a_i}}{RT})$

| Kinetic constants | Conventional | Reactive Distillation |
|---|---|---|
| $A_1$ | $1.52 \times 10^8$ | $7.46 \times 10^{16}$ |
| $A_2$ | $1.47 \times 10^8$ | $1.00 \times 10^{15}$ |
| $A_3$ | 2614.24 | $6.17 \times 10^8$ |
| $E_{a1}$ | 14700 | 33870 |
| $E_{a2}$ | 14200 | 29850 |
| $E_{a3}$ | 6400 | 19470 |
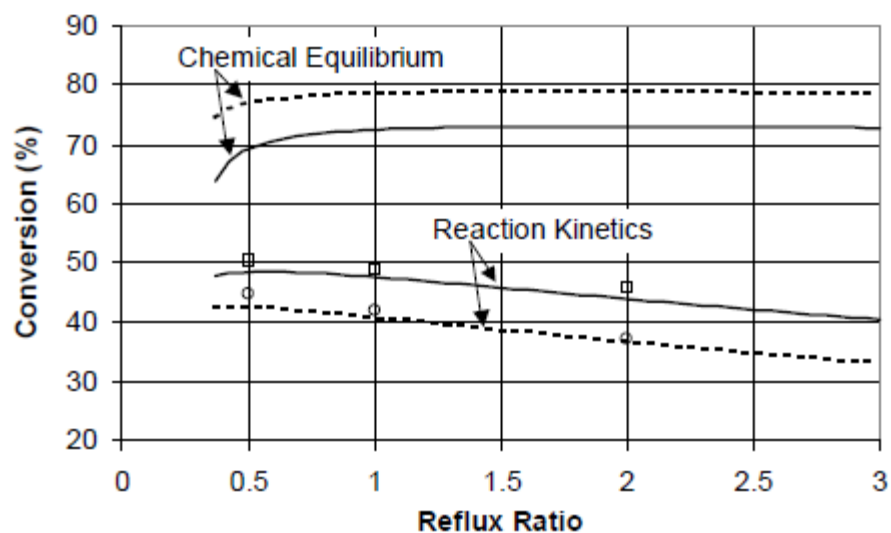


*Figure 12.* Effect of reflux ratio on conversion for both equilibrium and kinetic-based model.

   ***1.2.5.3 Key benefits of reactive distillation (RD).*** From the above discussions, it is clear that biodiesel can be produced from crude bio-oil by reactive distillation in presence of solid acid catalysts. The main advantages of Reactive Distillation process over other trans-esterification

and esterification can be summarized below: (Gomez-Castro et al., 2010; Jantharasuk, Gani, Górak, & Assabumrungrat, 2011; A. Kiss et al., 2006; Kiss et al., 2007)

1. The RD process uses solid acid catalysts. So, sulfur contamination in product and subsequent extra $SO_x$ emission is free unlike other liquid acid catalyzed methods.

2. Lower excess alcohol requirement.

3. Capital investments and operating costs are very low compared to other processes due to less unit operation and lower energy consumption.

4. High productivity (6-10 times of the other processes).

5. No waste salt stream is generated.

6. Higher reaction rate and selectivity and avoidance of azeotrope.

**1.3 Nitrogen Oxides ($NO_x$) Control**

$NO_X$ is a term ascribed to seven oxides of nitrogen ($N_2O$, $NO$, $N_2O_2$, $N_2O_3$, $NO_2$, $N_2O_4$, $N_2O_5$) in combined. $NO_2$ is most prevalent and anthropogenic representative of $NO_x$ family and actually regulated by Environmental Protection Agency (EPA). Nitric oxide ($NO$) is also very closely related to $NO_2$, as reaction between $NO$ and $O_2$ produces $NO_2$ and $NO_2$ reacts with oxygen in the air in presence of UV radiation (from sunlight) to produce ozone and $NO$, thus the two compounds often exist interchangeably in the troposphere. $NO$ can also react with the free radicals produced by Volatile Organic Compounds (VOC's) in presence of UV in the higher atmosphere. Although $NO_2$ is the species that is regulated by EPA, emissions of $NO_X$ from combustion are primarily in the form of $NO$.

$$N_2 + O^{\bullet} \rightarrow NO + N^{\bullet} \tag{1.1}$$

$$N^{\bullet} + O_2 \rightarrow NO + O^{\bullet} \tag{1.2}$$

$$N^{\bullet} + OH^{\bullet} \rightarrow NO + H \tag{1.3}$$

In the atmosphere, the species' of $NO_x$ family are all interconvertible in gaseous, liquid and interfacial phase and exists as a mixture of components determined by the reversibility of complex interspecies reaction scheme (Owusu & Adewuyi, 2006). NO is rapidly converted to $NO_2$ and hence, it is used as the representative for the $NO_X$ family and regulated by EPA. However, NO should be emphasized equally for the environmental protection measure as it is the most sparingly soluble among the species' of the $NO_x$ family and has widespread detrimental environmental and health effects.

**1.3.1 Sources of $NO_x$.** Although majority of $NO_x$ is emitted from automobiles and other mobile sources, substantial emissions are also added by such anthropogenic industrial sources as electric power plant boilers, industrial boilers, incinerators, gas turbines, reciprocating spark ignition and Diesel engines in stationary sources, iron and steel mills, cement manufacture, glass manufacture, petroleum refineries, and nitric acid manufacture. Natural sources of nitrogen oxides include lightning, forest fires, grass fires, trees, bushes, grasses, and yeasts. From Figure 6, it is also evident that bio-oil and biodiesel combustion produces higher $NO_x$ emission compared to petroleum fuel. So, successful implementation of biodiesel as an alternative energy also requires successful $NO_x$ emission control techniques. Figure 13 shows a graphic portrayal of the emissions from $NO_X$ sources.

$NO_x$ are produced mainly by three methods in all combustion processes. These are:

- Thermal $NO_X$: Thermal $NO_x$ is produced when oxygen reacts with nitrogen present in the combustion environment and the amount of thermal $NO_x$ produced is related to the nitrogen and oxygen molar concentrations and the temperature of combustion. At lower temperature (less than 1300 $^0$C) nitrogen is quite inert and does not react with oxygen in

the environment. But higher temperature pave the way for the reaction between nitrogen and oxygen and small amount of thermal $NO_x$ is produced.

- Fuel $NO_X$: In fossil fuels and bio-fuels, nitrogen molecules are embedded as a building block of several compounds. Upon combustion, this molecular nitrogen is released and forms "fuel $NO_X$" when reacts with oxygen.

- Prompt $NO_X$: Prompt $NO_X$ is formed from molecular nitrogen in the air combining with fuel in fuel-rich conditions which exist, to some extent, in all combustion. This nitrogen then oxidizes along with the fuel and becomes $NO_X$ during combustion, just like fuel $NO_X$.



| | Total Emissions |
|---|---|
| On Road Vehicles | 6,491,821 |
| Non Road Equipment | 4,162,872 |
| Electricity Generation | 3,783,659 |
| Fossil Fuel Combustion | 2,384,297 |
| Industrial Processes | 1,163,635 |
| Waste Disposal | 155,415 |
| Fires | 94,372 |
| Residential Wood Combustion | 38,324 |
| Solvent Use | 6,400 |
| Miscellaneous | 3,644 |
| Fertilizer & Livestock | 2,098 |
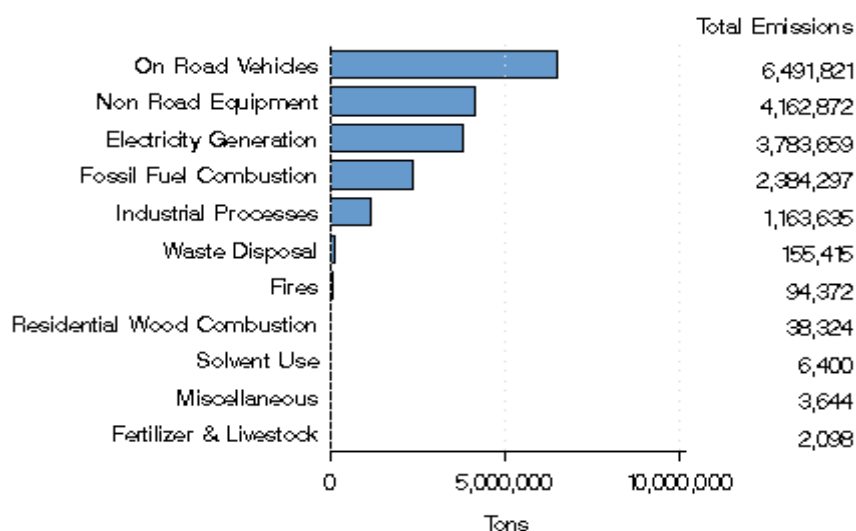
*Figure 13. National $NO_x$ emissions by source sectors in 2005.*

**1.3.2 Environmental and health effects of $NO_x$.** $NO_X$ has multiple adverse public health and environmental effects. Among them are increasing ground level (tropospheric) ozone concentration, acid deposition, drinking water nitrate levels, eutrophication, smog, global warming, and respiratory and heart diseases etc. The major environmental and health effects are discussed shortly.

- **Ground level ozone formation:** With the help of atmospheric VOC's, NO and $NO_2$ form a cycle which increases the ozone concentration in the troposphere. The interaction between $NO_X$, $O_3$ and VOC's in the atmosphere involves complex non-linear processes and is influenced by complex meteorological processes such as temperature, wind direction and speed. Thus, it is not a local problem and effects of $NO_X$ can be felt in areas hundreds of miles away from the emission source.

- **Acid deposition:** $NO_X$ and $SO_2$ in the atmosphere react with the water present to form acids which are carried down to earth by rain and are deposited in water bodies. This has adverse effects on aquatic and terrestrial ecosystems, materials, visibility, and public health. Nitric acid deposition plays a dominant role in fish kills observed in sensitive water bodies. In addition, the increased amount of nitrates in stream water has adverse health effects, especially for infants. The added nitrate can remain in water and be transported long distance downstream.

- **Eutrophication:** is the process in which a particular aquatic system is overloaded with nutrients to the point that it increases the primary productivity of the ecosystem. Nitrogen is the limiting nutrient for the growth of algae in most coastal waters and estuaries in United States. When excessive nitrogen is added accelerated algal growth causes severe reduction in water quality causing variety of problems including depletion of oxygen needed for fish to survive. Eutrophication decreases the resource value of rivers, lakes, and estuaries such that recreation, fishing, hunting, and aesthetic enjoyment are hindered. Health-related problems can occur where eutrophic conditions interfere with drinking water treatment.

- **Particulate matter, PM:** $NO_X$ react with VOC's in the atmosphere in presence of sunlight to form nitrate particles and acid aerosols. Because of their small size nitrate particles have a relatively long atmospheric lifetime; these small particles can also penetrate deeply into the lungs. In large cities where pollutant emission is high the particulate matter and ozone in the atmosphere create a haze which causes visibility impairment and a range of other adverse health effects. This is termed as smog which is a combination of the words "smoke" and "fog". It can cause shortness of breath, pain when deeply inhaled, wheezing, and coughing. It can cause eye and nose irritation and it dries out the protective membranes of the nose and throat and interferes with the body's ability to fight infection, increasing susceptibility to illness.

**1.3.3 Government regulations.** The United State government has introduced several regulatory drivers to reduce $NO_X$ concentration in the atmosphere time to time. The Title IV acid rain program, established through the 1990 Clean Air Act Amendments (CAAA) was the first federal regulatory driver for $NO_X$ control. This program involved two phases – Phase I started on January 1, 1996 and Phase II started on January 1, 2000. The implementation of this program was unit specific - the $NO_X$ emission rate limits ranging from 0.40 to 0.86 lb/MMBtu depending on the type of boiler/burner configuration and based on application of LNB technology. The Clean Air Act requires EPA to set National Ambient Air Quality Standards (NAAQS) for pollutants considered harmful to public health and the environment. The Clean Air Act established two types of national air quality standards.

Primary standards set limits to protect public health, including the health of "sensitive" populations such as asthmatics, children, and the elderly. Secondary standards set limits to protect public welfare, including protection against decreased visibility, damage to animals,

crops, vegetation, and buildings. The second driver was the EPA's $NO_X$ State Implementation Plan (SIP) Call Rule in 1998 emanate from the Title I National Ambient Air Quality Standards (NAAQS) for ozone. This regulation required 21 eastern states and the District of Columbia to participate in a regional cap-and-trade program based on an equivalent $NO_X$ emission rate of 0.15 lb/MMBtu beginning in 2003-04. Under a cap-and-trade system, a government authority first sets a *cap*, deciding how much pollution in total will be allowed. Next, companies are issued credits, essentially licenses to pollute, based on how large they are, what industries they work in. If a company comes in below its cap, it has extra credits which it may *trade* with other companies.

A third regulatory driver is the Clean Air Interstate Rule (CAIR) finalized in May 2005. It resulted from EPA's revision to the fine particulate matter (PM) and ozone NAAQS in 1997. This regulation will set $NO_X$ emission caps of 0.15 lb/MMBtu for 2010 and 0.125 lb/MMBtu for 2015 for the 28 eastern states and District of Columbia. It will take effect in two phases, with Phase I compliance date of January 1, 2009 and a Phase II compliance date of January 1, 2015.

New coal-fired power plants are required to meet both New Source Performance Standard (NSPS) and New Source Review (NSR) $NO_X$ emission requirements. Under NSR, a new plant is required to install either Best Available Control Technology (BACT) if located in ozone NAAQS attainment area, or Lowest Achievable Emission Rate (LAER) technology if located in an ozone NAAQS nonattainment area. Recent state BACT/LAER determinations have established $NO_X$ emission rate limits for new coal-fired plants between 0.05 and 0.10 lb/MMBtu and required the installation of LNB and SCR.

**1.3.4 Removal of nitric oxide (NO).** Numerous chemical oxidants have been studied for their effectiveness in the case of $NO_X$ removal by wet scrubbing. The various chemicals that

have been studied include water-soluble ferrous-chelating agents, hydrogen peroxide ($H_2O_2$) and peracids, yellow phosphorous, organic hydroperoxides, sodium chlorite ($NaClO_2$), potassium permanganate ($KMnO_4$), sodium hypochlorite, peroxymonosulfate (oxone) etc. (Y. Adewuyi, X. He, H. Shaw, & W. Lolertpihop, 1999; Y. Adewuyi & S. Owusu, 2003). Adewuyi and Owusu (Y. Adewuyi & S. Owusu, 2003) previously reported the absorption and oxidation of $NO_X$ in aqueous solutions of peroxymonosulfate or oxone (with active ingredient, $HSO_5^-$) in a bubble column reactor using NO feed concentrations of about 500 or 1000 ppm. This work completed in our lab at North Carolina Agricultural and Technical State University (NCATSU) showed that (1) the fractional removal ranged from 60 to 86%; (2) the highest removal of NO occurred at the lowest gas flow rate of 0.1 standard liter per minute (slpm) for the range of flow rates (0.1-1.0 slpm) tested; (3) the NO removal efficiency was not significantly affected by temperature in the range of 22-55 °C; (4) the presence of $SO_2$ increased the overall fractional conversion of nitric oxide (NO); and (5) the optimal fractional conversion occurred with 0.02 M oxone in the pH range of 6.5 to 8.5. The rate of reaction was found to be first order with respect to NO and zero order with respect to $HSO_5^-$. The results demonstrated the feasibility of removing $NO_X$ and $SO_x$ simultaneously by low-temperature aqueous scrubbing using oxone.

One of the most successful remediation methods in nitric oxide removal from exhaust gaseous stream is advanced oxidation process (AOP) which involves the oxidation of nitric oxide by free radical reactions mainly hydroxyl radical ($OH^\bullet$) and sulfate radical ($SO_4^{\bullet-}$). The various methods of producing hydroxyl radical ($OH^\bullet$) include sonolysis, use of $H_2O_2$/UV radiation or by using Fenton's reagent ($H_2O_2$/$Fe^{2+}$). The complete sonochemical reactions involving $OH^\bullet$ were investigated and discussed in detail by Adewuyi (2005) (Adewuyi, 2005a, 2005b). Owusu and Adewuyi (2006) investigated simultaneous absorption and oxidation of nitric oxide (NO) and

sulfur dioxide ($SO_2$) in water in presence of ultrasonic irradiation at room temperature in a bubble column reactor. The results show a 65-80% removal of NO with the complete removal of $SO_2$ (Owusu & Adewuyi, 2006).

In spite of the various research efforts, the industrial use of wet scrubbing for $NO_X$ removal has been slow due the added cost of chemicals, disposal of the spent solution and the complexity of some scrubbing systems. Therefore, an inexpensive, efficient and environmentally benign chemical needs to be found. Sodium persulfate could be one such compound. It is a strong oxidant, has an excellent shelf life when stored properly and is very inexpensive; thus it has many of the criteria for being a candidate for the chemical oxidant in the wet scrubbing of $NO_X$. Also, in the presence of impurities in the aqueous phase, such as bicarbonates, persulfate is far more chemically stable compared to hydrogen peroxide, which is a more widely used oxidant. This makes persulfate an even more attractive oxidant of choice.

The persulfate anion is one of the strongest oxidizing agents in aqueous solutions. The standard oxidation-reduction potential (E°) (eq 1.4) for the half-cell persulfate reaction is 2.01 V (Latimer, 1952), comparable to ozone and hydrogen peroxide, both of which are widely used in wastewater treatment.

$$S_2O_8^{2-} + 2e^- \rightarrow 2SO_4^{2-}, \quad E° = 2.01 \text{ V} \tag{1.4}$$

Although persulfate anion is a strong oxidizing agent it is kinetically slow at ordinary conditions.(Osgerby, 2006) Persulfate can be activated by heat, photo or metal catalysts. It has been established that when activated it generates intermediate sulfate free radical ($SO_4^-$) (House, 1962).

$$S_2O_8^{2-} \xrightarrow{heat \text{ } or \text{ } h\nu} 2SO_4^- \tag{1.5}$$

$$S_2O_8^{2-} + Fe^{2+} \xrightarrow{chemical \text{ } activation} 2SO_4^- + SO_4^{2-} + Fe^{3+} \tag{1.6}$$
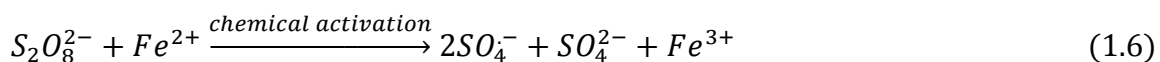
The sulfate free radical is very reactive and has a high oxidation potential and actively scavenges any oxidizable substance in the solution. It also reacts with water to form the OH radical, which is even more reactive (in fact, the most reactive oxidant other than fluorine). Both of these reactive radicals, therefore, lead to rapid destruction of any pollutant in solution.

**1.4 Scope of the Work**

Two different studies were carried out in the present thesis toward chemical reactive separations in energy and environmental processes.

- In the first part (CHAPTER 3), the Aspen PLUS simulation for reactive distillation for esterification of pyrolysis bio-oil was done using RADFRAC module using UNIQUAC property model for property estimation for phase equilibrium and minimization of Gibbs free energy for chemical reactions. Firstly, the simulation was attempted considering bio-oil to be the mixture of simplest components (70% acetic acid and 30% water) for esterification reaction with n-butanol. The simulation was then expanded for other acids, phenol and other complex components. Finally, rate based simulation was performed using RATEFRAC module. Advanced simulation tools Design Specification and Sensitivity Analysis were performed on each simulations to optimize the reactive distillation operations and to design a completely energy cost minimized reactive distillation unit.

- In the second part (CHAPTER 4), studies on nitric oxide (NO) removal by combined aqueous persulfate and ferrous-EDTA systems were carried out in a bubble column reactor as bio-fuel combustion produces higher NO compared to petroleum fuel and also significant amount of NO is released from coal fired power plants and other industrial combustions. Studies were performed at different inlet concentrations, for different

oxidant concentrations and for different temperature and pH. The results were compared to the nitric oxide removal by only persulfate systems and also $Fe^{2+}$ activated persulfate systems.

**CHAPTER 2**

**Instruments, Materials and Methods**

**2.1 Materials**

Sodium persulfate ($Na_2S_2O_8$, powder, >98%), iron (II) sulfate heptahydrate

($FeSO_4.7H_2O$, >99%), concentrated sulfuric acid (95-98%) and 1.0 N sodium hydroxide solution

were obtained from Acros Organics, Morris Plains, NJ; disodium ethylenediamine tetraacetate

($Na_2$-EDTA, reagent grade), 1, 10-phenanthroline monohydrate, hydroxylamine hydrochloride

(96%), acetic acid (99.7%), anhydrous sodium acetate (99%), fuming nitric acid (90%) and

sodium hydroxide (solid) were obtained from Fisher Chemical, Fair Lawn, NJ; and 5.0 N

sulfuric acid from LabChem Inc., Pittsburg, PA. Extra-dry nitrogen ($N_2$) and standard mixtures

of NO in ultrapure nitrogen were obtained from Airgas National Welders, Charlotte, NC.

Deionized water was obtained by using a Milli-Q Advantage A 10 purifier with Elix 5 system

from Millipore Corporation, Bedford, MA. The resistivity of the water was always greater than

18.2 MΩ.cm and total organic contents (TOC), silicates and heavy metals contents were

minimized to a very low parts per billion (ppb) levels.

**2.2 Experimental Setup**

The schematic diagram for the NO absorption, consisting of a thermally jacketed bubble

column reactor made of pyrex glass (5.1 cm i.d. × 61-cm length; Ace Glass, Inc., Vineland, NJ),

flue gas blending system consisting of a Dynablender mass flow controller (Matheson Tri-gas,

Montgomeryville, PA)  with two flow transducer calibrated to allow a maximum flow of 5

standard liters per minute (SLPM) gas, and analytical train of Fourier Transform Infrared (FTIR)

spectrometer (Tensor 27; Bruker Optics, Billerica, MA), and shown in Figure 14. The scrubber

was operated in semibatch mode in the experiments; simulated gas at a flow rate of 0.1 SLPM

flowed upward continuously through 1 L total volume of stationary scrubbing solution (corresponding liquid height ~0.5 m). The experiments were performed at 23-70 $^0$C and each temperature set was maintained through jacketed cooling by means of cooling/heating water from a refrigerated bath (Neslab RTE 7D1, Thermo Scientific, Newington, NH).
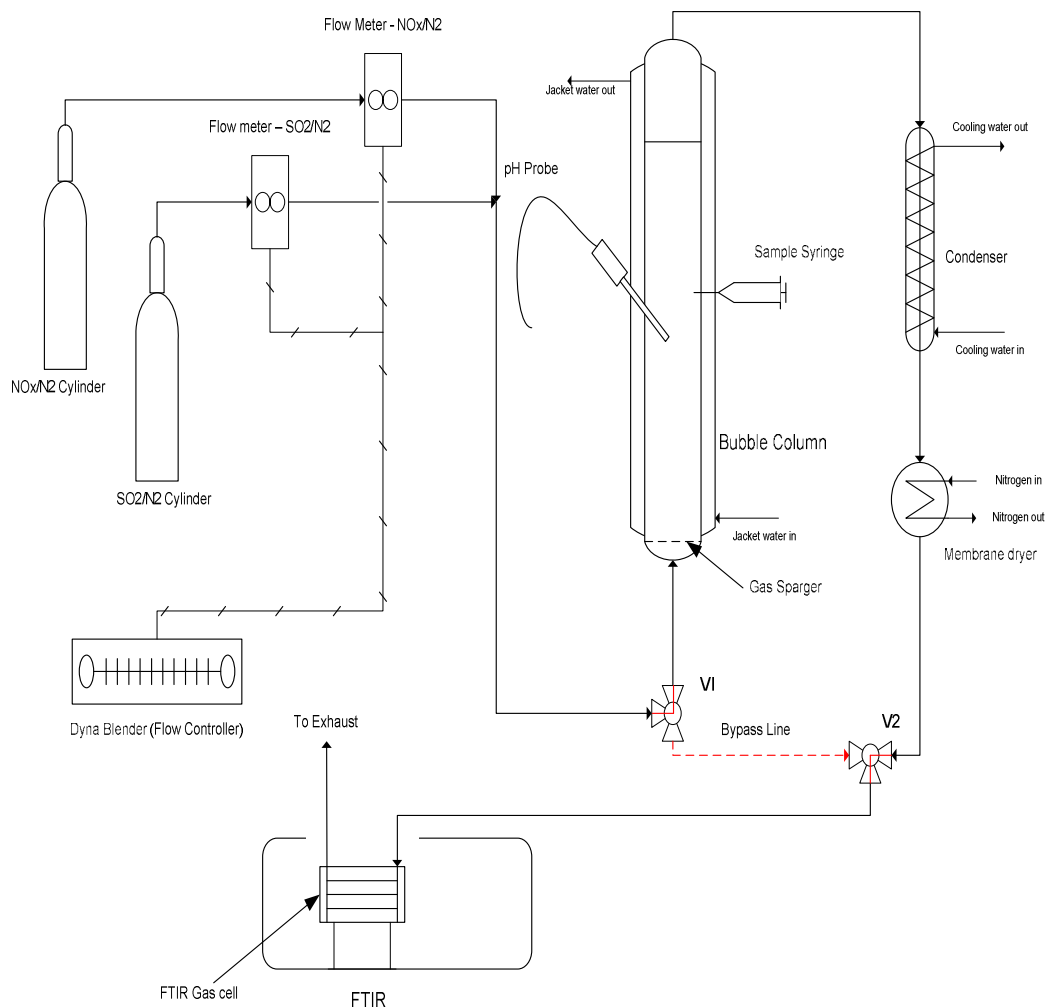


*Figure 14.* Schematic diagram of the experimental setup.

The exit gas from the reactor passed through a membrane dryer (MD-050-48P, Perma Pure, Inc.) to remove moisture prior to analysis with the Fourier transform infrared (FTIR) spectrometer equipped with a custom gas cell made by FTIR.com. Both the FTIR and membrane dryer were purged with dry, $CO_2$ free air from laboratory gas generator (Parker Balston,

Haverhill, MA) to continuously remove the moisture. $NO_x$ concentration in the outlet gas was continuously monitored and recorded by proprietary software, Enformatic FTIR Collection Manager (EFCM) from FTIR.com, calibrated with standards of different gas species obtained from Airgas National Welders. The scrubbing solution may be analyzed before and after the experiment using a Dionex ICS 3000 ion chromatographic system (Dionex Corporation, Sunnyvale, CA) for anions. The solution pH was monitored continuously using Accumet pH meter 50. Initial and Final pH were recorded for each of the experiments. The details of the analytical procedures, including the analysis of gas-phase $NO_x$ and anions in solution are reported in previous studies (Khan & Adewuyi, 2010, 2011).

**2.3 Analytical Equipment and Instrumentation**

**2.3.1 Fourier transform infrared spectrophotometer (FTIR).** Fourier transform infrared (FTIR) spectrometer (Tensor 27; Bruker Optics, Billerica, MA) was used to analyze the inlet and outlet gas composition. The picture of the instrument and the schematic diagram are shown in Figure 15 and 16, respectively.



*Figure 15.* Image of Fourier transform infrared spectroscopy (FTIR).
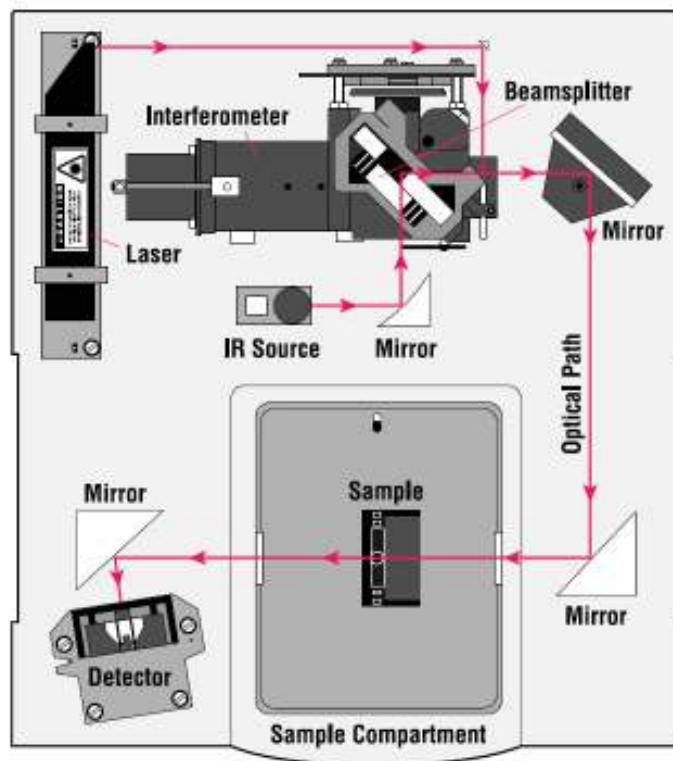
*Figure 16.* Schematic diagram of an FTIR.

The instruments consist of an interferometer, a sample compartment, a beam source and a detector. The interferometer consists of a beamsplitter which divides the incoming infrared beam into two optical beams. One beam reflects off of a flat mirror which is fixed in place. The other beam reflects off of a flat mirror which can move to a very short distance (a few millimeters) away from the beamsplitter. The two beams reflect off of their respective mirrors and are recombined when they meet back at the beamsplitter. Because the path that one beam travels is a fixed length and the other is constantly changing as its mirror moves, the signal which exits the interferometer is the result of these two beams interfering with each other. The resulting signal is called an interferogram which has the unique property that every data point (a function of the moving mirror position) has information about every infrared frequency which comes from the source. However, the information in the interferogram must be decoded. This can be

accomplished via the Fourier transformation. This transformation is performed by the computer which then presents the user with the desired spectral information for analysis. The collection and analysis of the data were performed by the proprietary software called Enformatic FTIR Collection Manager (EFCM) from FTIR.com. Once the software is calibrated with standard gases it is able to perform online monitoring of the different species in the gas phase. Figure 17 shows the calibration spectrums used for calibrating EFCM (Khan & Adewuyi, 2010).
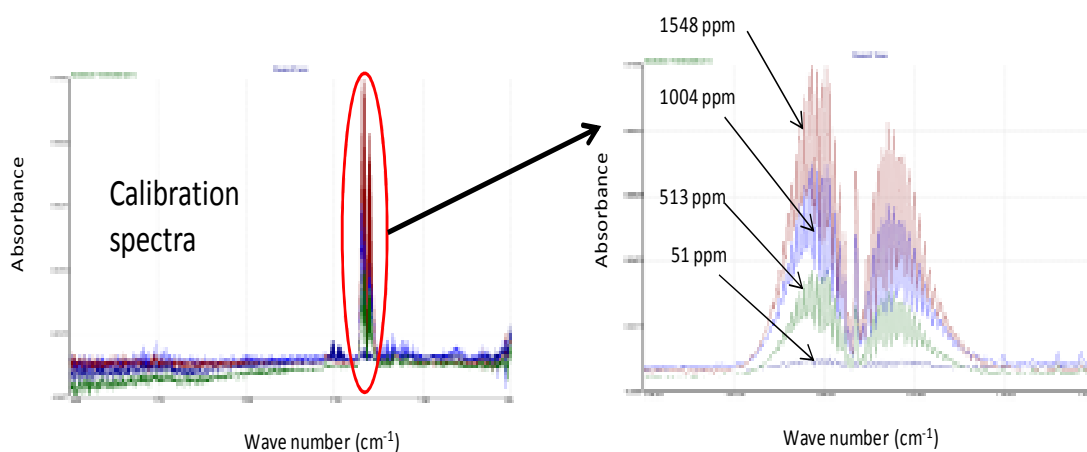


*Figure 17.* Calibration spectra for the standard concentration of NO.

**2.3.2 UV-Vis spectrophotometer.** The concentration of iron species' ($Fe^{2+}$, $Fe^{3+}$ and $Fe^{II}$-EDTA) was determined by measuring the absorbance using Beckman DU 7500 UV-Vis spectrophotometer. The photograph of the instrument is given in Figure 18.

The DU Series 7500 spectrophotometer is a flat field spectrograph. Undispersed light form the source passes through the sample and is dispersed by the concave holographic grating onto the diode array. The diode array consists of 512 elements; each diode reads 1.25 nm. Readings at a particular wavelength are obtained by interpolating the readings at the two bracketing diodes. The focal point of the beam is on the right side of the sample compartment, not in the middle. All sampling accessories will position the sample at the focal point. The

entrance slit selectively discriminates against light from sources other than the ones in the instruments.



*Figure 18.* Photograph of the UV-Vis spectrophotometer.

## 2.4 Aspen Simulation Frameworks

Steps taken to carry out Aspen PLUS simulation of reactive distillation for esterification of pyrolysis bio-oil includes:

- The binary and ternary interactions between the components were studied by using Aspen Property PLUS to understand whether and where the binary and ternary azeotropes present in the reaction mixtures.

- The flow diagram (Figure 22 and 33) in Aspen for reactive distillation was drawn by using Aspen process flow sheet with RADFRAC Module because RADFRAC is a tool in Aspen that best suited with distillation and other stage separation processes and reactions can be easily added to the separation for a reactive distillation process.

- UNIQUAC property method was used as the base method for property estimation because a group contribution activity coefficient method is the best suitable

method to represent highly non-ideal multicomponent mixtures and interaction

parameters are readily available in Aspen.

- The reaction equilibrium was determined by specifying Aspen to calculate it by

  minimizing Gibbs free energy.

- The process was optimized using the Design Specification and Sensitivity

  Analysis tools by varying several parameters to obtain a minimized energy costs.

- The fractional conversion and separation efficiency was maximized for a specific

  feed composition.

- The temperature and composition profile was drawn along the column for

  different feed mixtures.

- Ester flow rate and fractional conversion were drawn with alcohol and water feed

  rate.

- All the distillation column parameters such as condenser and reboiler heat duty,

  number of stages, and reflux ratio with different inlet conditions were studied.

**CHAPTER 3**

**Simulation of Reactive Distillation for Esterification of Pyrolysis Bio-oil**

**3.1 Backgrounds**

Pyrolysis bio-oil is a very complex mixture of different organic compounds mainly different fatty acids, water, phenols and alcohols (Junming, Jianchun, Yunjuan, & Yanju, 2008). The Aspen simulation considering all the components present in bio-oil is a complex task but it is the overall objective of this project. Our goal is to first carry out reactive distillation considering only one acid at first for the simulation and then expand the components to incorporate another short chain and long chain fatty acids. Finally, since pyrolysis bio-oil also consists of alcohols and phenols, alcohols and phenols will be considered part of bio-oil in appropriate amount and the n-butanol feed will be reduced accordingly. Also, since bio-oil consists of water we will consider water in bio-oil that will be separated from esterification products.

A typical analysis of pyrolysis bio-oil reveals the following chemical compounds (Mohan, Pittman, & Steele, 2006; Mullen & Boateng, 2008):

(i)      Carboxylic acids (mainly acetic 5-15% and formic 3-5%)
(ii)     Alcohols
(iii)    Aldehydes 1-2%
(iv)     Esters
(v)      Ketones 1-2%
(vi)     Phenols and phenolic compounds 5-20%
(vii)    Guaiacols
(viii)   Syringols
(ix)     Sugars 5%
(x)      Furans 1-5%
(xi)     Alkenes
(xii)    Aromatics
(xiii)   Nitrogen compounds 0-1%
(xiv)    Miscellaneous oxygenates 3-20%

Water content varies between 15% to 40% and a mid range values of 30% was selected for all the simulation but the sensitivity analysis by varying water content was accomplished to see the effect of water content on other parameters.

**3.2 Results and Discussion**

The reactive distillation design for solid acid catalyzed reactions are very complicated issue because of the simultaneous presence of the following (A. Kiss et al., 2006):

1.  Chemical and Phase Equilibrium (CPE)

2.  Vapor-Liquid Equilibrium (VLE)

3.  Vapor-Liquid-Liquid Equilibrium (VLLE)

4.  Catalysts Activity and kinetics

5.  Mass Transfer in Gas-Liquid and Solid-Liquid

6.  Adsorption of The Reactants and Desorption of The Products on Catalysts Surface

Because of many complicated interactions between the components first the binary and ternary interactions between the components can provide simple guide-step for the initial clue. Aspen Property PLUS can be used to observe the binary and ternary interactions between the two or three compounds. These interactive diagrams can provide the valuable foresight about the azeotropes present in the reactive distillation operations. Then Chemical and Phase equilibria should be observed to understand the liquid phase separation into two and the region in which a homogeneous region of mixture is present that is vital to the healthy RD operations because liquid phase splitting stopped the mass transfer that is very important for both reaction and separation.

As an initial attempt, the bio-oil is considered to consist of acetic acid, one of the simplest acids, diluted in water. Since the pyrolysis bio-oil always have some amount of water in it, we

considered water in our simulation. The bio-oil (acetic acid with water) is reacted with n-butanol in esterification reaction to produce n-butyl acetate and water.

**3.2.1 Aspen simulation using Property PLUS.** Binary and Ternary interection between the four components in the reactive distillation is studied using Aspen Property Plus. The binary plots for all the pairs of chemicals are plotted at average column temperature 200 $^0$C and column pressure 1 MPa. For the property analysis and the simulation UNIQUAC property method is used as the base property estimation method.

From the binary y-x diagram in Figure 19, it can be seen that, the final two product water and ester form a binary azeotrope as well as two reactants acetic acid and n-butanol. Acetic acid does not form any azeotrope with either water or ester and that is why it is easy to separate unreacted acid either from water and ester. N-butanol also forms a binary azeotrope with water. Since the reaction is equilibrium controlled, unreacted acid and alcohol are present in some amount with the product and the whole reaction and separation phenomena in Reactive Distillation unit is quite complex. In Figure 19, six binary interactions are provided at 200 $^0$C and 1MPa. The relatively high temperature and pressure is chosen to comply with the previous step pyrolysis and we expect the bio-oil entered the Reactive Distillation from pyrolysis unit will maintain high temperature and pressure, thus avoid any intermediate cooling or heating operation.

The ternary interaction plots or the residue plots are provided in Figure 20. From the four ternary plots it can be seen that no ternary azeotrope is present.
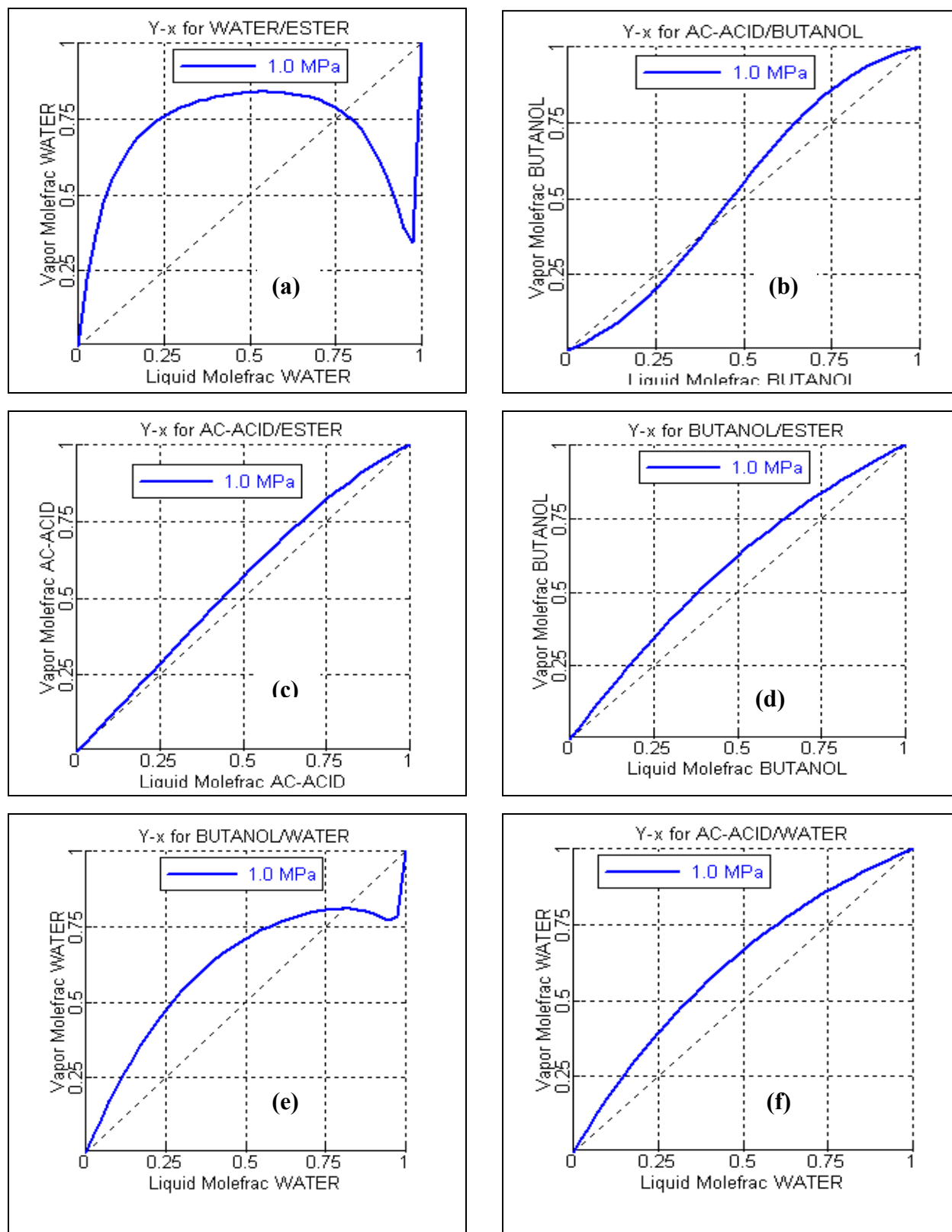
*Figure 19.* Binary interaction between the components determined by Aspen Property PLUS.
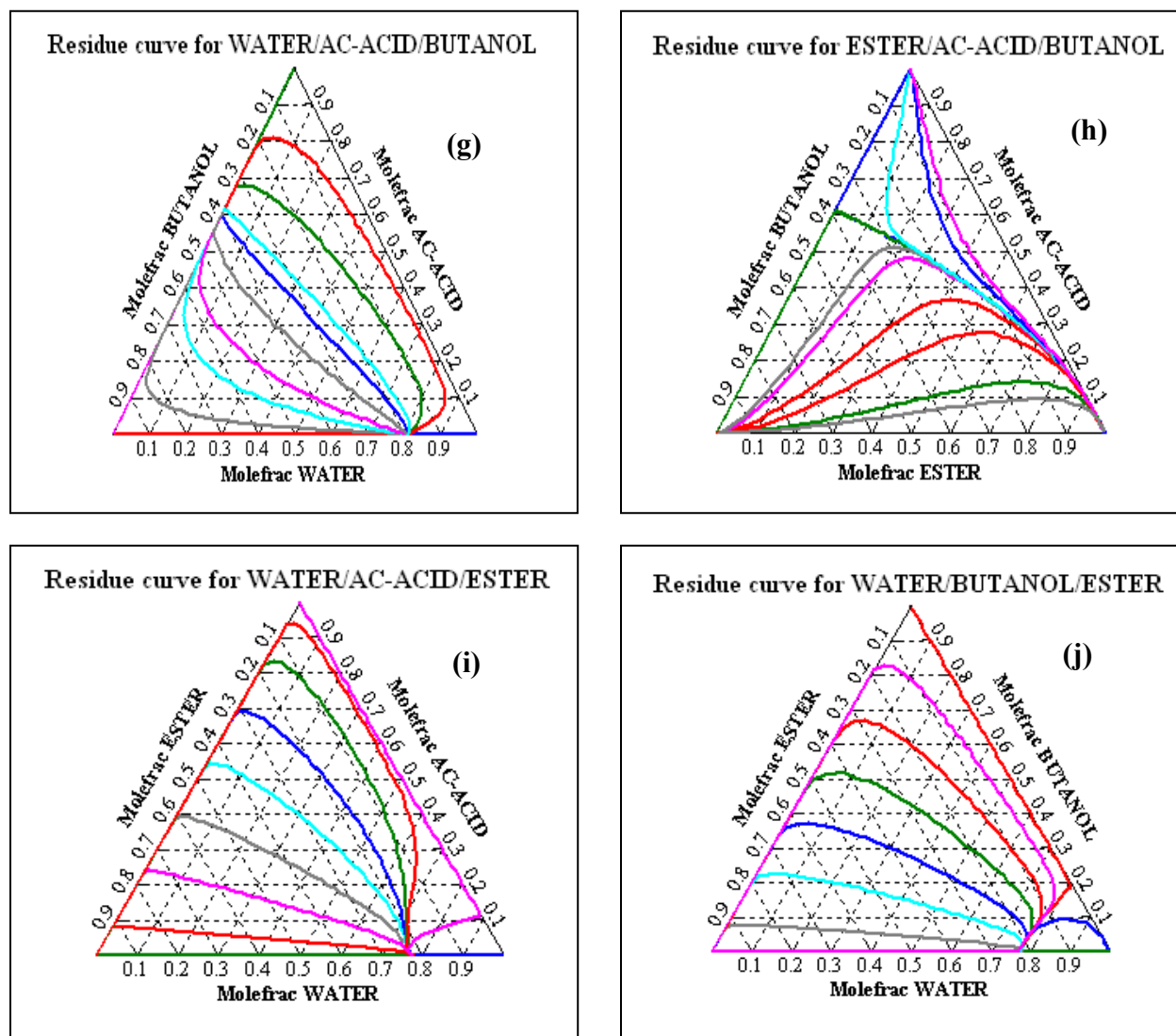
*Figure 20.* Ternary interaction between the components determined by Aspen Property PLUS.

Normally, in terms of reactive distillation the organic compounds are sparingly soluble in water. That is why sometimes the liquid mixture can be splitted into two phases (aqueous and organic) in the reactive distillation column, this is detrimental to our cause as the liquid phase splitting could stop further reaction and separation. The molar feed ratio is chosen by carefully observing the chemical and phase equilibrium (CPE) diagram so that the mixture in the column always stays in the single liquid phase region.

Following is a CPE diagram of methanol and lauric acid reactive distillation (Dimian, Bildea, Omota, & Kiss, 2009):
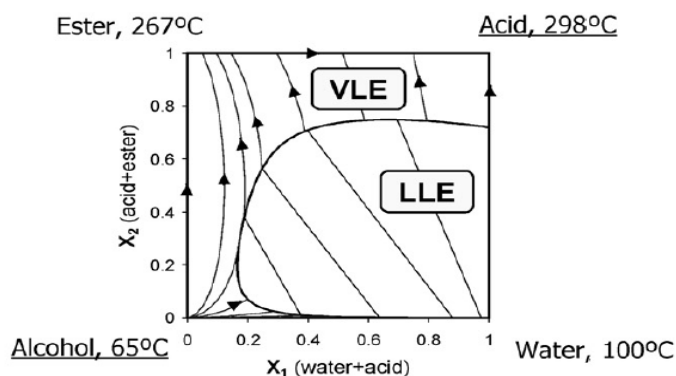


*Figure 21.* CPE diagram for lauric acid-methanol reactive distillation system.

From this diagram it can be clearly seen that bottom right part is the region where liquid-liquid equilibrium region occur and the liquid phase split into two. That is why the system is operated in the single liquid phase region (left and upper region of the Figure 21).

**3.2.2 Aspen PLUS simulation for reactive distillation of simplest bio-oil.** The reaction is simulated in a Reactive Distillation unit (RADFRAC module) in Aspen PLUS. All the components were present in Aspen data-bank. The reaction is incorporated with the RADFRAC distillation unit in equilibrium form (where Aspen will calculate the equilibrium constant by minimizing the Gibbs free energy).

The flow diagram in Aspen for reactive distillation is drawn by using aspen process flow diagram with the RADFRAC Module acting as the column performing both reaction and separation. In the RADFRAC besides conventional distillation input parameters the reaction input parameters can also be given and the reactive stages can be specified. For the simulation, UNIQUAC property method is used as the base method for property estimation. The reaction equilibrium is determined by specifying Aspen to calculate it by minimizing Gibbs free energy.

In case of a known reaction equilibrium constants, the known parameters can be also be given as input to calculate the reaction products.
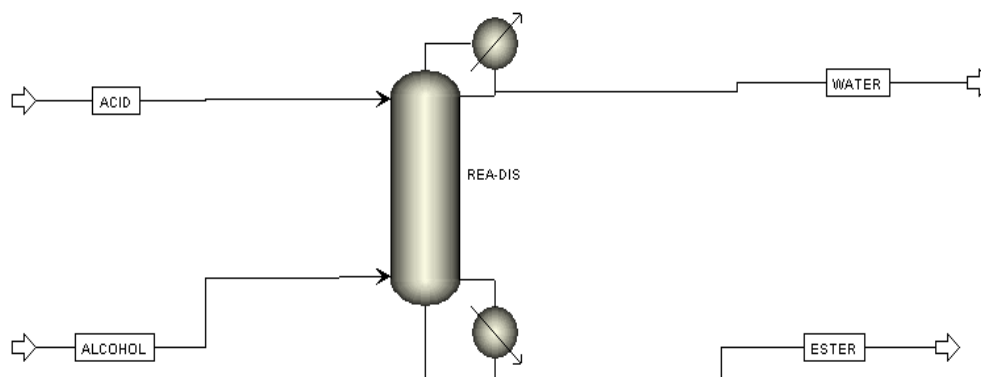


*Figure 22.* Flow-diagram for the RD in Aspen PLUS using RADFRAC module.

At first 1 kmol/hr of bio-oil is considered as 70% acetic acid and 30% water. The simulated bio-oil is simulated with stoichiometric amount of n-butanol (0.7 kmol/hr). The feeds are considered at 200 $^0$C temperature and 1MPa pressure. The system is simulated using UNIQUAC as the base property method. The optimum distillate rate and the reflux ratio were found by using sensitivity analysis for the highest conversion and separation. The stream result is given below in Figure 23.

*Figure 23.* Stream results for the acetic acid-butanol RD column.

From this stream result we can see the conversion was 76.7% and all the water was separated from the ester product. But some ester was carried away with water due to the presence of azeotrope as well as the unreacted n-butanol with ester. Unreacted acetic acid split between two streams almost equally. The temperature profile in the column is given in Figure 24.
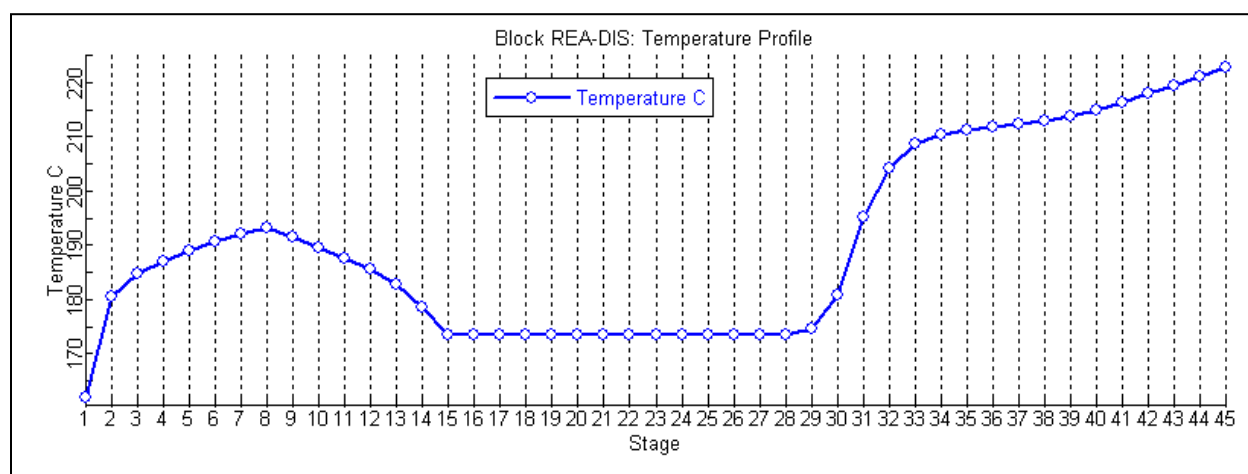


*Figure 24.* Temperature profile for the acetic acid-butanol RD column

The composition profile is given in Figure 25. We can see in the reactive stages (6-30) the composition remains almost constant as the composition is determined by the reaction

equilibrium. In the stripping section (stage 31-45) composition of water decreases to zero and in the enriching section (stage 1-6) amount of ester remains low. The abrupt change of composition in stage-8 and stage-15 is due to the introduction of two feed stream.
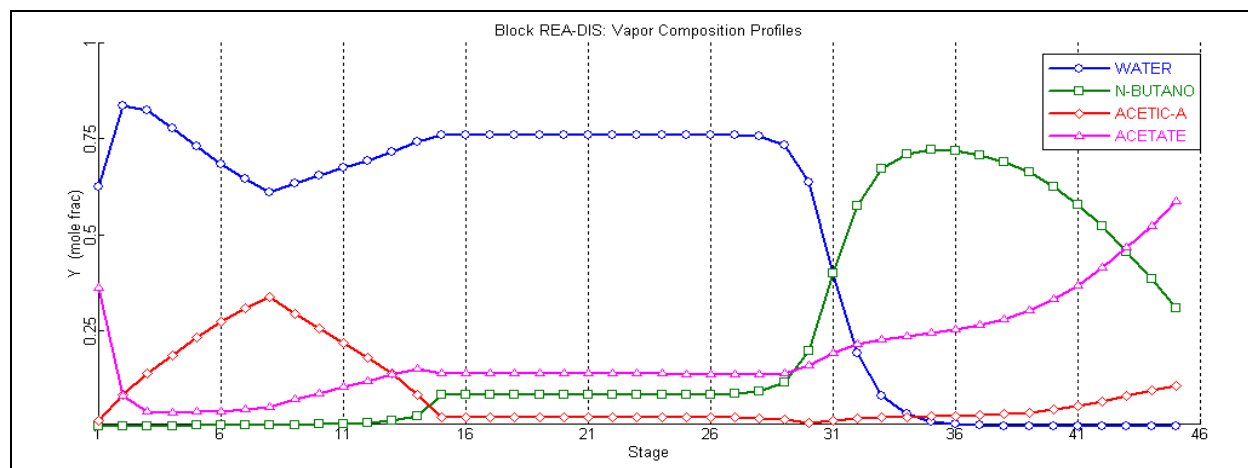


*Figure 25.* Composition profile for the acetic acid-butanol RD column.

Now, sensitivity analysis can be carried out to observe the effect of changing one variable on other variable. The following two plots give the effect of alcohol flow rate and presence of water in the bio oil on reaction conversion.
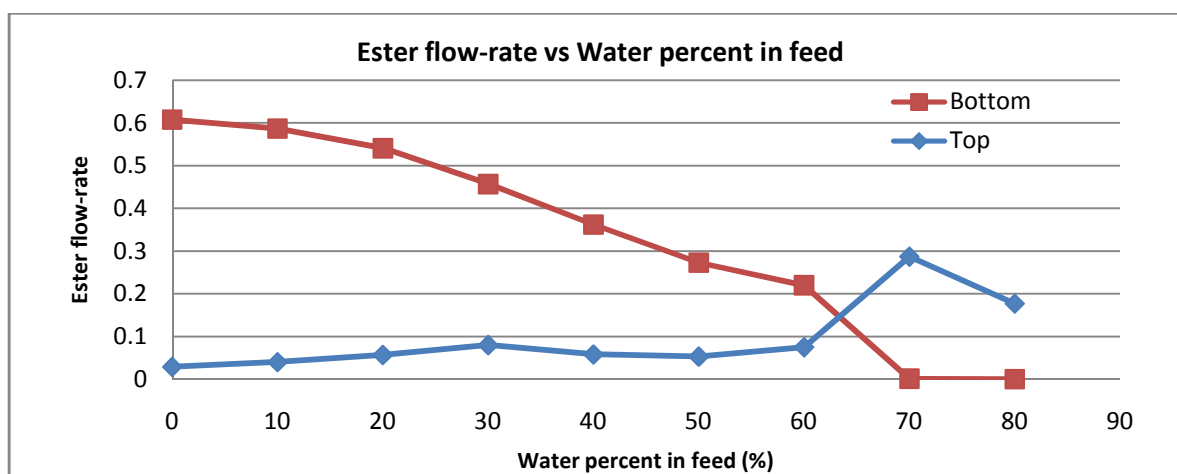


*Figure 26.* Effect of water percent in bio-oil on ester flow rate.

**Conv. of acid vs Water percent in feed**
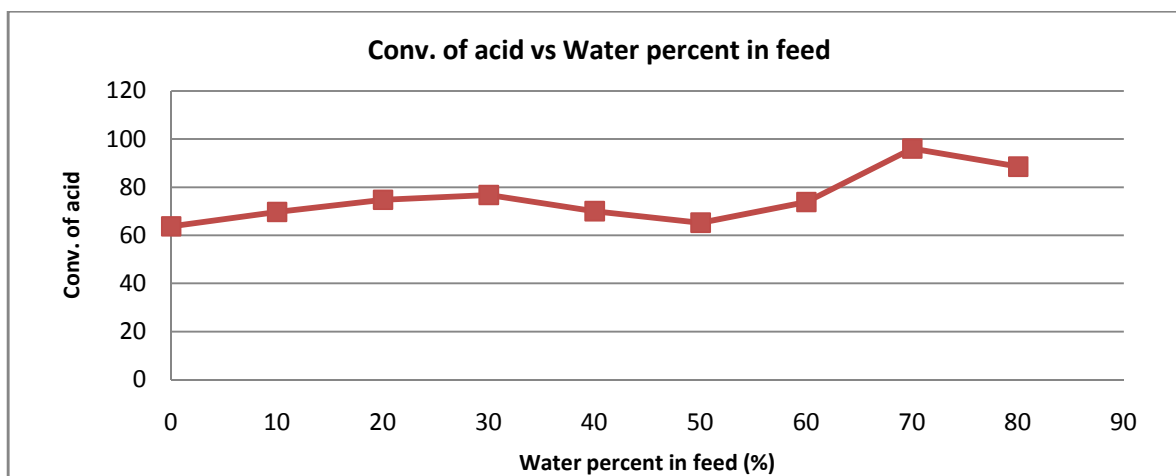
*Figure 27.* Effect of water percent in bio-oil on conversion of acid.

Like these two sensitivity analysis any other can be carried out to observe the effect of any input variable to any output variables. Using the sensitivity analysis and design spec. the simulation was optimized further for the condenser heat duty, reboiler heat duty, and number of stages (reactive, enriching and stripping section) and a cost effective Reactive Distillation unit for the esterification of acetic acid can be achieved. The condenser heat duty was -19.32 kW and reboiler heat duty was 17.12 kW.

**3.2.3 Aspen PLUS simulation for reactive distillation of complex bio-oil.** For this simulation bio-oil is considered is composed of formic acid, acetic acid, propionic acid with water. For the simulation purpose 30% water, 30% acetic acid, 20% formic acid, 20% propionic acid is considered our simulated bio-oil. The feed is simulated first with stoichimetric amount of n-butanol with the optimized parameters from the previous simulation and then further optimized in terms of ester flow rate in bottom and top products, conversion of acids etc to produce n-butyl acetate, n-butyl formate, n-butyl propionate. The stream results are given in Figure 28.

| | ACID | ALCOHOL | ESTER | WATER |
|---|---|---|---|---|
| Temperature C | 180.0 | 180.0 | 224.4 | 161.5 |
| Pressure bar | 10.000 | 10.000 | 10.000 | 10.000 |
| Vapor Frac | 0.000 | 0.000 | 0.000 | 0.000 |
| Mole Flow kmol/hr | 1.000 | 0.700 | 0.650 | 1.050 |
| Mass Flow kg/hr | 47.441 | 51.886 | 71.274 | 28.053 |
| Volume Flow cum/hr | 0.061 | 0.081 | 0.115 | 0.036 |
| Enthalpy   MMkcal/hr | -0.093 | -0.048 | -0.068 | -0.075 |
| Mole Flow | | | | |
| WATER | 0.300 | | TRACE | 0.910 |
| N-BUTANO | | 0.700 | 0.087 | 0.003 |
| ACETIC-A | 0.300 | | 0.001 | 0.035 |
| ACETATE | | | 0.217 | 0.048 |
| FORMIC-A | 0.200 | | 0.007 | 0.021 |
| PROPI-A | 0.200 | | 0.001 | 0.026 |
| FORMATE | | | 0.167 | 0.005 |
| PROPIONA | | | 0.169 | 0.004 |

*Figure 28.* Stream results for mix acid-butanol RD column.

From these results we can see that conversion of acid (bio-oil) is 87.1%. The conversion is higher from the previous simulation can be attributed to the high reaction was achieved using acid mixture and may be optimization was done to a superior degree. As like the previous simulation, water was completely separated from the ester. But the unreacted acids and tiny amount of ester goes with water for the presence of binary azeotrope in water-este mixture. But, in overall this simulation result is very good compared to the one presented in Figure 23. The stage by stage composition profile is given in Figure 29.
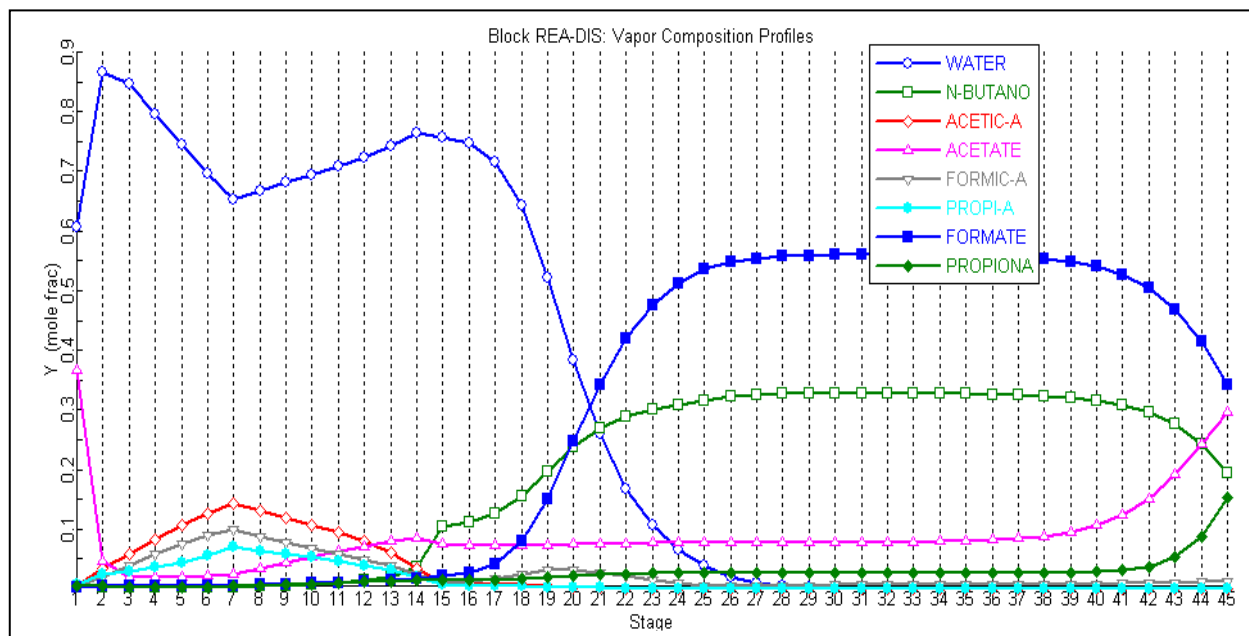
*Figure 29*. Composition profile for mix acid-butanol RD column.

Again, the effect of the change in different input parameters on the output parameters can be observed by carrying out sensitivity analysis and a specific value of any output variable can be achieved using Design Spec. by varying any related input variables. Though this simulation is a very good one and the ester production is almost optimized there are more scope in optimization in the reboiler and condenser heat duty and subsequently reducing the cost of operation. The optimum reboiler and condenser heat duty were 23.18 and -24.90 kW respectively. Sensitivity analysis showing the effect of alcohol flow rate on acid conversion is given in Figure 30.

**Conv of acid vs. Alcohol flow-rate**
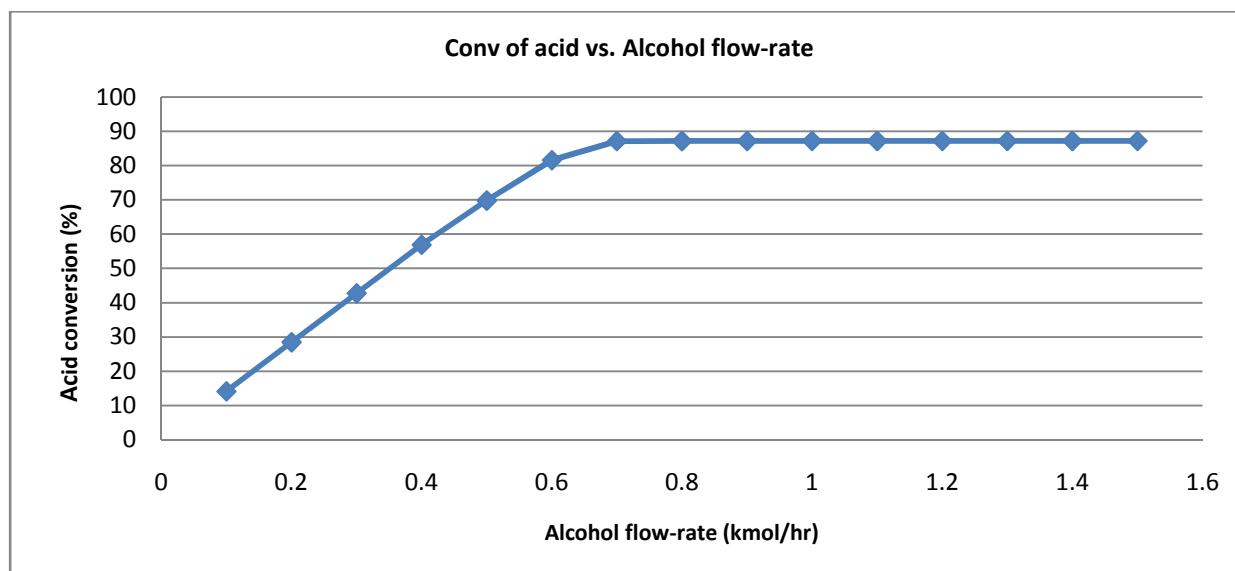


*Figure 30.* Effect of alcohol flow rate on acid conversion.

**3.2.4 Aspen PLUS simulation for reactive distillation of complex bio-oil including phenol and other alcohol.** Phenol and phenolic compounds (lignin derived) present in small amount in the pyrolysis bio-oil. Phenol reacts with acids to form ester also. The reactions of phenol with formic acid, acetic acid and propanoic acid produce phenyl formate, phenyl acetate and phenyl propanoate respectively. Since, phenol reacts same way butanol reacts with acids total butanol feed rate was reduced. The amount of phenolic and other alcoholic compound typically varies 5-20% resulting in a 5-20% of the butanol feed.

First the simulation was run including 10% phenol. It can be seen from the stream result that almost all the phenol reacts with formic acid to form phenyl formate. The amount of butanol feed is reduced accordingly and the fractional conversion of esterification reaction is 94%.

| | BIO-OIL | BUTANOL | ESTER | WATER |
|---|---|---|---|---|
| Temperature C | 180.0 | 180.0 | 231.7 | 163.2 |
| Pressure bar | 10.000 | 10.000 | 10.000 | 10.000 |
| Vapor Frac | 0.000 | 0.000 | 0.000 | 0.000 |
| Mole Flow kmol/hr | 1.000 | 0.600 | 0.550 | 1.050 |
| Mass Flow kg/hr | 49.445 | 44.474 | 59.444 | 34.474 |
| Volume Flow cum/hr | 0.059 | 0.070 | 0.089 | 0.045 |
| Enthalpy    MMkcal/hr | -0.084 | -0.041 | -0.052 | -0.077 |
| Mole Flow kmol/hr | | | | |
| WATER | 0.300 | | TRACE | 0.864 |
| N-BUTANO | | 0.600 | 0.122 | 0.014 |
| ACETIC-A | 0.300 | | TRACE | 0.016 |
| ACETATE | | | 0.168 | 0.116 |
| FORMIC-A | 0.200 | | TRACE | 0.010 |
| PROPI-A | 0.100 | | TRACE | 0.010 |
| FORMATE | | | 0.076 | 0.014 |
| PROPIONA | | | 0.083 | 0.006 |
| PHENO-01 | 0.100 | | TRACE | TRACE |
| PHE-FOR | | | 0.100 | TRACE |
| PHE-ACE | | | TRACE | TRACE |
| PHE-PRO | | | TRACE | TRACE |

*Figure 31.* Stream results for mix acid with phenol-butanol RD column.
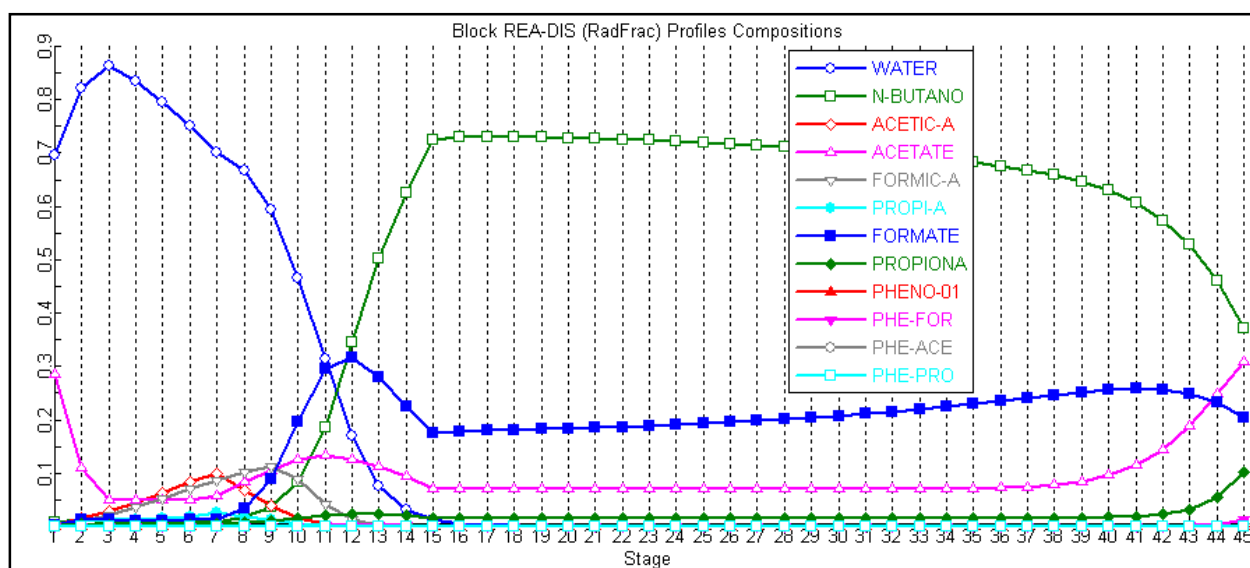


*Figure 32.* Composition profile for mix acid with phenol-butanol RD column.

The simulation was then carried out including 5% other alcohols in the bio-oil feed with other previous compounds. The butanol feed was reduced 5% and the simulation results were similar entirely except the product includes other esters. The fractional conversion of the esterification reaction was 95%. The optimized reboiler and condenser heat duty were 20.84 and -24.15 kW respectively.

**3.2.5 Rate-based simulation of pyrolysis bio-oil.** The reactive distillation unit was simulated using RadFrac module with equilibrium based reactions in the reactive zone of the column. The RadFrac module simulates the separation process based on the assumption that there is complete equilibrium between the liquid and vapor in every stage. On the other hand the RateFrac module handles the separation process in a more realistic rate-based manner considering actual non-equilibrium between vapor-liquid interphase. RateFrac simulates actual tray and packed columns rather than idealized representation of equilibrium stages by accounting the heat and mass transfer to determine the degree of separation.

The previous simulation for the simple bio-oil (70% acetic acid and 30% water) was carried out using RadFrac module. Now, our goal is to produce a more realistic simulation using RateFrac module in the Aspen Plus.
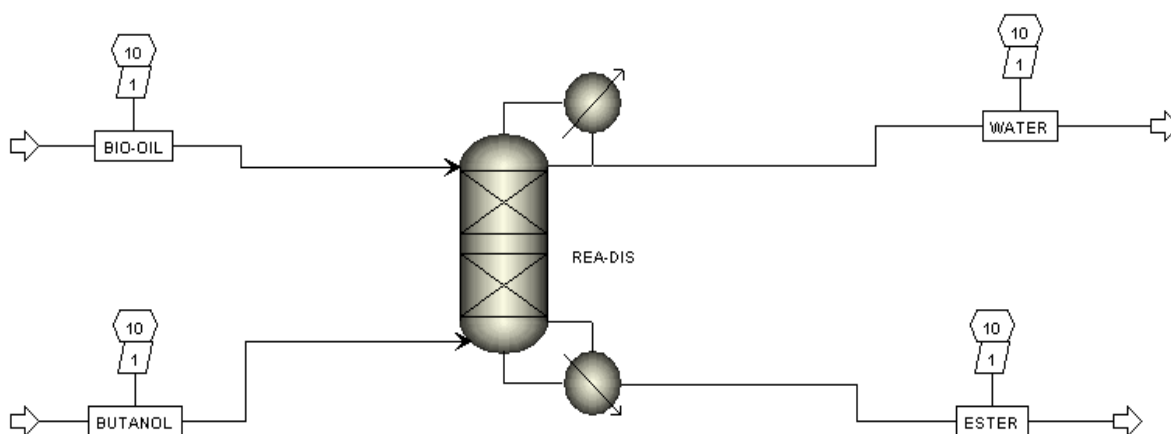
*Figure 33.* Flow-diagram for the RD in Aspen PLUS using RATEFRAC module.

In the RateFrac simulation the tray specification and packing specification was included as well as column diameter calculation. The RateFrac simulation is not typical stage by stage calculation rather it calculates separation on a segment by segment basis. The reactions were included in the RateFrac reactive distillation module. When using non-equilibrium realistic concept the percent conversion and degree of separation in reactive distillation column both dropped 1-2% compared to the idealized stage by stage calculation. The column diameter was calculated using 80% flooding in the trays.

The Rate based RateFrac operation is very complex and I am still trying to further optimization of the process. It can be seen that the optimum number of segment also increased for using idealized situation using non-equilibrium with 80% flooding.

| Display: Streams ▼ | Format: GEN_M ▼ | Stream Table | | |
|---|---|---|---|---|
| | ACID ▼ | ALCOHOL ▼ | WATER ▼ | ESTER ▼ |
| Temperature C | 180.0 | 180.0 | 159.8 | 224.9 |
| Pressure bar | 10.000 | 10.000 | 10.000 | 10.000 |
| Vapor Frac | 0.000 | 0.000 | 0.000 | 0.000 |
| Mole Flow kmol/hr | 1.000 | 0.700 | 1.050 | 0.650 |
| Mass Flow kg/hr | 47.441 | 51.886 | 28.445 | 70.882 |
| Volume Flow cum/hr | 0.061 | 0.081 | 0.036 | 0.113 |
| Enthalpy MMkcal/hr | -0.093 | -0.048 | -0.075 | -0.068 |
| Mole Flow | | | | |
| WATER | 0.300 | | 0.921 | TRACE |
| N-BUTANO | | 0.700 | 0.005 | 0.074 |
| ACETIC-A | 0.300 | | 0.020 | 0.002 |
| ACETATE | | | 0.058 | 0.220 |
| FORMIC-A | 0.200 | | 0.010 | 0.019 |
| PROPI-A | 0.200 | | 0.025 | 0.002 |
| FORMATE | | | 0.005 | 0.165 |
| PROPIONA | | | 0.006 | 0.167 |

*Figure 34.* Stream results for mix acid-butanol RD column using RATEFRAC.

**CHAPTER 4**

**Nitric Oxide Removal by Combined Persulfate and Ferrous-EDTA Systems**

**4.1 Backgrounds**

Nitrogen oxides (NOx – mainly $NO_2$ and NO) and sulfur oxides ($SO_x$ – mainly $SO_2$) are the most prominent acid gases emitted from the burning of fossil fuel, especially from the coal fired power plants, and are responsible for widespread problems of air pollution, health hazards, acid rains etc.(Adewuyi, Khan, & Sakyi, 2013; Yusuf Gbadebo Adewuyi & Nana Yaw Sakyi, 2013; Yusuf G. Adewuyi & Nana Y. Sakyi, 2013). Of these oxides, $NO_2$ and $SO_2$ are very soluble in water and can be separated easily from the exhaust stream by simple scrubbing, but nitric oxide (NO) is sparingly soluble and cannot be separated easily (Yusuf Gbadebo Adewuyi & Nana Yaw Sakyi, 2013; Yusuf G. Adewuyi & Nana Y. Sakyi, 2013; Khan & Adewuyi, 2010). It is well known that the commonly practiced methods of removing NO such as selective catalytic and non-catalytic processes have high capital costs and undesirable problems with high temperatures and handling of harmful chemicals. Therefore, alternative cost-effective and environmentally friendlier processes, such as scrubbing suitable oxidizing agents capable of increasing the solubility of NO in water significantly, are of ardent interest (Y. G. Adewuyi & S. O. Owusu, 2003; Yusuf Gbadebo Adewuyi & Nana Yaw Sakyi, 2013; Yusuf G. Adewuyi & Nana Y. Sakyi, 2013; Khan & Adewuyi, 2010; Sweeney & Liu, 2001). Hence, the use of aqueous $H_2O_2$, aqueous $H_2O_2$ with $HNO_3$, NaCl solutions, NaClO solutions, $Na_2SO_3$ solutions with $FeSO_4$ , acidic/alkaline $NaClO_2$ solutions, aqueous $NaClO_2$ solutions with $Na_2CO_3$ , $NaClO_2$ powder, alkaline $NaClO_3$ solutions, aqueous $ClO_2$ solution, alkaline $KMnO_4$ solutions, $KMnO_4$ solutions with $(NH_4)_2CO_3$, aqueous $Na_2S$ solutions and iron/cobalt chelate compounds in presence or absence of $SO_2$ is widespread in the literature (Y. G. Adewuyi, X. He, H. Shaw, &

W. Lolertpihop, 1999; Baveja, Rao, & Sarkar, 1979; Brogren, Karlsson, & Bjerle, 1997; Byun et al., 2009; Chen, Hsu, & Yang, 2005; Chen, Lin, & Yang, 2011; T.-W. Chien & Chu, 2000; T. W. C. H. H. H. T. Chien, 2003; Hsin Chu, Chien, & Twu, 2001; H. Chu, Chien, & Li, 2001; H. Chu, Li, & Chien, 1998; Deshwal, Lee, Jung, Shon, & Lee, 2008; Guo et al., 2010; Hutson, Krzyzynska, & Srivastava, 2008; Jin, Deshwal, Park, & Lee, 2006; Pan et al., 2013; Sada, Kumazawa, Hayakawa, Kudo, & Kondo, 1977; Thomas & Vanderschuren, 1996, 1997; Wei, Yu, Cai, Luo, & Tan, 2009). Recently a comparative study of NO removal by $[Co(NH_3)_6]Cl_2$, $Fe^{II}$-EDTA and $H_2O_2$ is investigated (Yu, Zhu, & Tan, 2012). The experimental data suggest higher removal by $[Co(NH_3)_6]Cl_2$ but higher pH requirement (pH 10.5) can derail its implication. In a previous study, oxone or potassium hydrogen peroxymonosulfate ($2KHSO_5.KHSO_4.K_2SO4$) was used in the removal of NO in absence or presence of $SO_2$ and detailed experimental and kinetic aspects of this process, including feasibility, stoichiometry, reaction pathways and the effects of various process parameters reported (Y. G. Adewuyi & S. O. Owusu, 2003). Owusu and Adewuyi (2006) investigated simultaneous absorption and oxidation of nitric oxide (NO) and sulfur dioxide ($SO_2$) in water in presence of ultrasonic irradiation at room temperature in a bubble column reactor. The results show a 65-80% removal of NO with the complete removal of $SO_2$ (Owusu & Adewuyi, 2006).

This was followed by work on NO absorption by aqueous sodium persulfate ($Na_2S_2O_8$) activated by temperature. The use of persulfate in NO removal was first in this kind and suggested to reduce the process costs as persulfate is comparatively cheaper than oxone and also, significant amount of NO removal could be achieved (up to 90% at 90 $^0$C) (Khan & Adewuyi, 2010). In a recent study involving the removal of NO in presence of $SO_2$ by the aqueous persulfate systems, it was demonstrated that the absorption of NO was greatly enhanced in the

presence of $SO_2$ (70-80% NO removal at 23-70 $^0$C), while the $SO_2$ itself was completely

removed (Yusuf G. Adewuyi & Nana Y. Sakyi, 2013). The most recent study on the removal of

NO using persulfate systems simultaneously activated by temperature and $Fe^{2+}$ ion, showed that

NO removal further increased by almost 10% in presence of $Fe^{2+}$ at all temperatures compared to

temperature-only activation (Yusuf Gbadebo Adewuyi & Nana Yaw Sakyi, 2013). It was

proposed that the thermal and $Fe^{2+}$ ion activation of the persulfate anion leads to the production

of the sulfate radicals ($SO_4^{\bullet-}$), which is responsible for the production of hydroxyl radical ($OH^{\bullet-}$)

that acts as the main oxidant for the conversion of NO in the aqueous solution (Yusuf Gbadebo

Adewuyi & Nana Yaw Sakyi, 2013; Khan & Adewuyi, 2010). The use of sodium persulfate as

the oxidizing agents creates the necessary $OH^{\bullet}$ radical for NO absorption-oxidation that obviates

any ultra-violet or ultrasonic assistant as described in some advanced oxidation literatures

(Adewuyi & Khan, 2012; Adewuyi & Owusu, 2006; Y. Liu, Zhang, & Sheng, 2011). Also, the

safe and environmentally benign nature, water solubility, chemical stability and excellent shelf

life in storage give sodium persulfate comparative edge over other reagents (Yusuf Gbadebo

Adewuyi & Nana Yaw Sakyi, 2013; Yusuf G. Adewuyi & Nana Y. Sakyi, 2013; Khan &

Adewuyi, 2010).

It was shown that almost 100% NO removal is attainable by this system but only at very

high temperature (90 $^0$C). Hence, the energy required for the higher temperature process could be

the main stumbling block that impedes further development. A number of reports have suggested

NO removal by iron chelating agent, such as Ferrous NTA, HEDTA, DPTA, cobalt

ethylenediamine solutions (Demmink & Beenackers, 1998; Demmink, van Gils, & Beenackers,

1997; Hofele, van Velzen, Langenkamp, & Schaber, 1996; Long, Xiao, & Yuan, 2005; Long,

Xin, Chen, Xiao, & Yuan, 2007; Wubs & Beenackers, 1993). But the use of chelated ferrous

ethylenediamine tetraacetic acid ($Fe^{II}$-EDTA) with or without some other reagents ($Fe^{II}$-citrate,

$Na_2SO_3$, $MgSO_3$, $Na_2S_2O_4$) is the most widespread and prevalent in liturature, where NO is

combined with $Fe^{II}$-EDTA by reversible binding and separated from the solution (T. W. Chien,

Hsueh, Chu, & Chu, 2009; Demmink et al., 1997; Francesca Gambardella, Alberts, Winkelman,

& Heeres, 2005; N. Liu et al., 2012; Narita, Sato, Shioya, Ikari, & Okabe, 1984; Sada,

Kumazawa, & Hikosaka, 1986; Sada, Kumazawa, Kudo, & Kondo, 1980; Sada, Kumazawa, &

Takada, 1984; Suchecki, Mathews, & Kumazawa, 2005; Teramoto, Hiramine, Shimada,

Sugimoto, & Teranishi, 1977; Wang, Zhao, & Wu, 2007). The main drawbacks of this process

include removal of the $Fe^{II}$-EDTA(NO) complex, fast oxidation of $Fe^{II}$-EDTA to the inert $Fe^{III}$-

EDTA and high cost of EDTA. The problems can be somewhat overcome in BioDeNOx process

where $Fe^{II}$-EDTA(NO) is broken down by denitrifying bacteria and $Fe^{III}$-EDTA is reduced by

iron reducing bacteria and resultant $Fe^{II}$-EDTA is recycled back to the reactor (W. Li, Wu, &

Shi, 2006; W. Li, Wu, Zhang, Shao, & Shi, 2007; van der Maas, Harmsen, Weelink, Klapwijk, &

Lens, 2004; van der Maas, Peng, Klapwijk, & Lens, 2005; van der Maas, van den Bosch,

Klapwijk, & Lens, 2005; Zhang, Mi, Cai, Jiang, & Li, 2008). But the process was impeded by

the slow action of the biological process, uncertainty involving bacteria culture, detrimental

effect of sulfur compounds present in flue gas and the costs of installing additional unit (N. Liu

et al., 2012; Maas, Brink, Klapwijk, & Lens, 2009; Manconi, van der Maas, & Lens, 2006).

Recently, some researchers have suggested denitrification and/or reduction by the catalytic

activity of activated carbon, direct electrochemical process or bio-film electrode reactor but the

requirement for additional complex unit still persists (Gao, Mi, Zhou, & Li, 2011; Long, Yang,

Chou, Li, & Yuan, 2013; Mi, Gao, Zhang, Cai, & Li, 2009; Wu, Wang, & Zhao, 2008; Yang,

Chou, Li, Long, & Yuan, 2013; Zhu et al., 2010). It is widely reported in the literature that

denitrification and/or reduction can also be enhanced by sulfur derived ions, from $Na_2SO_3$, $MgSO_3$, $Na_2S_2O_4$ etc. in a combined process with $Fe^{II}$-EDTA (David Littlejohn & Chang, 1990; Narita et al., 1984; Sada et al., 1986; Sada, Kumazawa, & Yoshikawa, 1988; Suchecki et al., 2005; Wang et al., 2007). It has also been suggested that both $Fe^{II}$-EDTA and $Fe^{III}$-EDTA can also activate persulfate anion, like ferrous ion, thus producing a complete synergistic relationship with the persulfate in NO removal process (Liang, Bruell, Marley, & Sperry, 2004a, 2004b; Liang & Lee, 2008; Liang, Lee, Hsu, Liang, & Lin, 2008; Liang, Liang, & Chen, 2009). Ahmad et al. (2012) investigated extensively the iron-EDTA activated persulfate systems using reactant-specific probes and electron spin resonance (ESR) and concluded that both $Fe^{II}$-EDTA and $Fe^{III}$-EDTA decompose persulfate more rapidly than only $Na_2$-EDTA (Ahmad, Teel, Furman, Reed, & Watts, 2012). Additionally, Li et al. (2007) by measuring hydroxyl radical formation, suggests that Fenton and Fenton like reactions were never suppressed by iron-chelating agents (L. Li et al., 2007). However, to the best of our knowledge the simultaneous and synergistic application of $S_2O_8^{2-}$ and $Fe^{II}$-EDTA for NO removal has never been studied although it has the potential to be a solution in the decade long struggle against NO pollution.

**4.2 Experimental Procedure**

**4.2.1 Experimental procedure for NO removal.** Initially, the column was filed with around 750 ml of de-ionized water and temperature was allowed to reach the desired level and stabilize. Pure, dry nitrogen gas was passed through it for at least 15 min to purge it of all dissolved oxygen and then through a bypass line until a stable reading was obtained. Freshly prepared $Fe^{2+}$, $Na_2EDTA$ and persulfate solutions of appropriate quantity to make $1.0 \pm 0.05$ L solution of desired concentration were added to the water one after another, respectively. To maintain the solution pH at neutral level, NaOH and/or $H_2SO_4$ solution were used. Additional

water was added to make the total volume of solution $1.0 \pm 0.05$ L and few drops of NaOH or $H_2SO_4$ were added to adjust the pH again before the bubbling of the gas through the solution was started. This additional volume of NaOH/ $H_2SO_4$ solution is insignificant compared to total volume and does not affect the total liquid volume or height. Once all the reagents dissolved completely, the solution has become greenish. The simulated flue gas was switched to the inlet of the reactor and bubbling through the solution. The dissolution of persulfate seemed rapid and even vigorous at higher temperature aided by the gas mixing action. The outlet gas reached the FTIR almost instantaneously and data acquisition started.

**4.2.2 Spectrophotometric determination of iron species'.** Iron species' ($Fe^{2+}$, $Fe^{3+}$ and $Fe^{II}$-EDTA) were determined spectrophotometrically using Beckman DU-7500 spectrophotometer (Beckman Coulter, Inc., Fullerton, CA). $Fe^{2+}$ and ($Fe^{2+} + Fe^{3+}$) ion concentration was determined at peak absorbance of 506-512 nm and 393-399 nm wavelength UV-vis spectra, respectively, by a modified 1, 10-phenanthroline colorimetric method for better accuracy and $Fe^{3+}$ concentration was determined from the difference (Yusuf Gbadebo Adewuyi & Nana Yaw Sakyi, 2013; Harvey, Smart, & Amis, 1955; W. Li et al., 2006; W. Li et al., 2007; N. Liu et al., 2012). Also, at low wavelength $Fe^{II}$-EDTA compound shows higher absorbance and the concentration can be determined spectrophotometrically (D. Littlejohn & Chang, 1982; Zang, Kotowski, & Van Eldik, 1988; Zhang, Li, Wu, Chen, & Shi, 2007). From the UV-vis spectrum of $Fe^{II}$-EDTA it can be seen that there is no clear absorbance peak and a wide range of wavelength (270-300 nm) is selected for absorbance measurement.

*4.2.2.1 Determination of calibration curves.* Standard $Fe^{2+}$ and $Na_2EDTA$ solutions were prepared in different concentrations and dilutions. Previously prepared hydroxylamine hydrochloride and 1,10-phenanthroline solutions were added with standard $Fe^{2+}$ solutions and pH

4.5 was obtained by using acetic acid-sodium acetate buffer. The standard solutions were taken to sampling compartment of spectrophotometer, quartz cuvettes (Spectrocell Corporation, Oreland, PA) after the spectrophometer is "Blanked" using blank solution (same solution except $Fe^{2+}$). Absorbance was measured and recorded multiple times for each of the dilutions and concentrations at seven different wavelengths (506-512 nm). The corresponding absorbance of a particular concentration is found by discarding outlier data and then averaging the retentions. The calibration curves of $Fe^{2+}$ were drawn at different wavelengths by plotting absorbance with their respective concentrations. Same procedure was followed to determine $(Fe^{2+} + Fe^{3+})$ calibration curves except the addition of hydroxylamine hydrochloride, as it is used to regenerate $Fe^{2+}$ oxidized to $Fe^{3+}$. In this case, pH was kept at 3.9 and the wavelength range was 393-399 nm. $Fe^{II}$-EDTA was prepared by mixing standard $Fe^{2+}$ and $Na_2EDTA$ solutions (molar ratio 1:1) and adding few drops of concentrated sulfuric acid. The calibration curves of $Fe^{II}$-EDTA were obtained by repeating same spectrophotometric procedure at 270-330 nm wavelength range.

*4.2.2.2 Determination of iron species concentrations.* The samples were taken from the reactor by the side syringe as quickly as 30 s up to 3980 s in a series of test tubes. The withdrawn sample total volume was small compared to total liquid volume and did not affect NO absorption process. Each of the samples is then diluted from one-half up to one-128th of the original strength. For the $Fe^{2+}$ and $(Fe^{2+} + Fe^{3+})$ determination 1, 10-phenanthroline is addedd to this samples and absorbance was measured in spectrophotometer in ranges 506-512 nm and 393-399 nm respectively. For $Fe^{II}$-EDTA determination absorbance was directly measured from the spectrophometer in the range of 270-330 nm. The "Blank" solution in these cases was prepared by using all the ingredients present in bubble column reactor except $Fe^{2+}$. From these absorbance data using the calibration curves, the concentration of $Fe^{2+}$, $Fe^{3+}$ and Fe-EDTA was measured.

Finally, the respective concentrations were multiplied by their dilution factors, and then averaged to find the concentration of a particular sample. The concentrations were plotted against time to find iron species' concentration profiles.

## 4.3 Results and Discussion

Simulated NO gas of 753 ppm (initial gas-phase) absorption-oxidation experiments were carried out at several temperatures (23, 30, 40, 50, 60 and 70 (±1) $^0$C) in 0.1 M persulfate solution in absence/presence of 0.05-0.02 M Fe$^{2+}$ and 0.05-0.03 M Na$_2$-EDTA. The pH of the solution was always kept near neutral acidic region (pH 6.0-7.0). The detail criteria for the selection of gas-phase NO and liquid-phase reagent concentrations will be discussed later in preliminary investigation. From the EFCM, outlet gas species concentrations were obtained as a profile with time and the percent conversion of NO is calculated using the initial and final steady state value of NO concentration from eq 4.1.

$$X_{NO} = \frac{[NO]_{in} - [NO]_{out}}{[NO]_{in}} \times 100\% \tag{4.1}$$

where [NO]$_{in}$ and [NO]$_{out}$ are the steady state concentration in ppm of NO at the inlet and outlet of the reactor, respectively. The steady state outlet concentrations of NO were calculated by averaging the values of the outlet concentration after 3000 s.

### 4.3.1 Preliminary investigation and determination of optimum Fe$^{2+}$:EDTA ratio.

Because of the complex and multifarious chemical behavior of both persulfate and and Fe$^{II}$-EDTA oxidation, determination of appropriate concentration of persulfate, Fe$^{2+}$ and Na$_2$-EDTA is very important in NO removal process by simultaneous persulfate and Fe$^{II}$-EDTA processes.

From previous studies on oxidation of various contaminants by temperature and Fe$^{2+}$ activated persulfate systems, severance of persulfate ion (E$^0$ = 2.01 V) into sulfate free radicals ($SO_4^{\bullet-}$) is quite slow in ordinary conditions, but achievable by using heat, light, ultrasound and/or

transition metal ions ($Fe^{2+}$ in this case) as represented by eqs 4.2 and 4.3, respectively, can provide the necessary initiation stage for the chain of reactions (Adewuyi, 2005a, 2005b; Yusuf Gbadebo Adewuyi & Nana Yaw Sakyi, 2013; Khan & Adewuyi, 2010; H. Kusic, Peternel, Koprivanac, & Loncaric Bozic, 2010; Liang & Bruell, 2008).

$$S_2O_8^{2-} \xrightarrow{heat} 2\ SO_4^{\bullet-};\ k_2 = 1.0\ \times 10^{-7}\ (25°C)\ or\ 5.7\ \times 10^{-7}s^{-1}(70°C) \tag{4.2}$$

$$S_2O_8^{2-} + Fe^{2+} \xrightarrow{k_3} SO_4^{2-} + SO_4^{\bullet-} + Fe^{3+};\ k_3 = 1.7 - 2.7\ or\ 2.0\ \times 10^1 M^{-1}s^{-1} \tag{4.3}$$
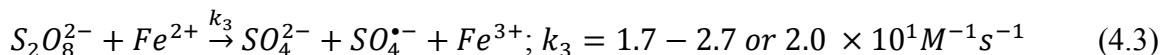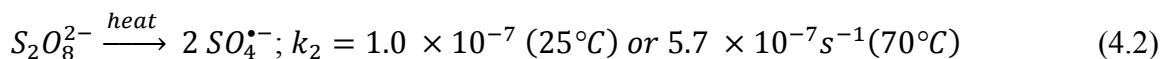
Generation of reactive sulfate free radical ($E^0$ = 2.6 V) followed by the split of the water molecule to produce even more reactive $OH^\bullet$ radical ($E^0$ = 2.8 V) shown in eq 4.4 (Yusuf Gbadebo Adewuyi & Nana Yaw Sakyi, 2013; Yusuf G. Adewuyi & Nana Y. Sakyi, 2013; Khan & Adewuyi, 2010).

$$SO_4^{\bullet-} + H_2O \xrightarrow{k_4} HSO_4^- + OH^\bullet\ ;\ k_4 = 6.6 \times 10^2 s^{-1} \tag{4.4}$$
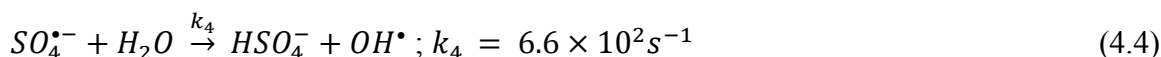
It is quite obvious that majority of NO absorption takes place by reacting with $OH^\bullet$ radical to produce $NO_2^-$ (Adewuyi & Khan, 2012; Yusuf Gbadebo Adewuyi & Nana Yaw Sakyi, 2013; Yusuf G. Adewuyi & Nana Y. Sakyi, 2013; Khan & Adewuyi, 2010).

$$OH^\bullet + NO \xrightarrow{k_5} H^+ + NO_2^-;\ k_5 = 2 \times 10^{10} M^{-1}s^{-1} \tag{4.5}$$
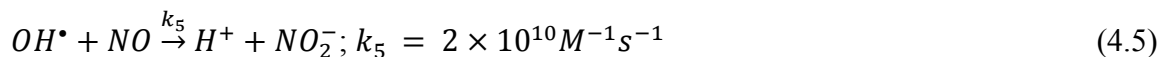
In their latest work Adewuyi and Sakyi speculate the possibility of direct oxidation of NO by persulfate ion to $NO_2$ gas (Yusuf Gbadebo Adewuyi & Nana Yaw Sakyi, 2013).

$$S_2O_8^{2-} + NO + H_2O \xrightarrow{k_6} 2\ HSO_4^- + NO_2 \tag{4.6}$$

It is quite understandable that if $S_2O_8^{2-}$ ion with a standard reduction potential 2.01 V can react with NO, with 2.6 V potential $SO_4^{\bullet-}$ can also react with NO.

$$SO_4^{\bullet-} + NO + H_2O \xrightarrow{k_7} HSO_4^- + NO_2^- + H^+ \tag{4.7}$$
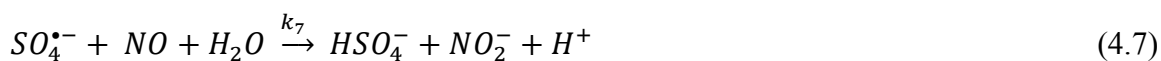
The intermediate $NO_2^-$ is responsible for further asymmetric cleavage of $S_2O_8^{2-}$ ion

producing one $SO_4^{\bullet-}$ ion but it can potentially attach sulfate radical to convert it to relatively inert

$SO_4^{2-}$ ion (Yusuf Gbadebo Adewuyi & Nana Yaw Sakyi, 2013; Yusuf G. Adewuyi & Nana Y.

Sakyi, 2013).

$$S_2O_8^{2-} + NO_2^- \xrightarrow{k_8} SO_4^{2-} + SO_4^{\bullet-} + NO_2 \tag{4.8}$$

$$NO_2^- + SO_4^{\bullet-} \xrightarrow{k_9} SO_4^{2-} + NO_2 \,; k_9 \; = \; 9.8 \times 10^8 M^{-1} s^{-1} \tag{4.9}$$
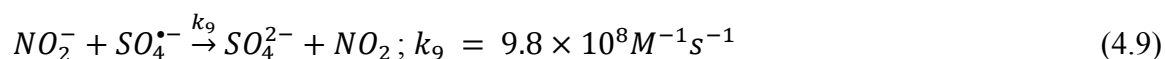
$NO_2$ gas produced in Reaction 4.8 and 4.9 is readily soluble in water and reacts with

active $OH^\bullet$ radical producing $NO_3^-$ (Yusuf Gbadebo Adewuyi & Nana Yaw Sakyi, 2013; Yusuf

G. Adewuyi & Nana Y. Sakyi, 2013).

$$NO_2 + OH^\bullet \xrightarrow{k_{10}} H^+ + NO_3^- \,; k_{10} \; = \; 4.5 \times 10^9 M^{-1} s^{-1} \tag{4.10}$$
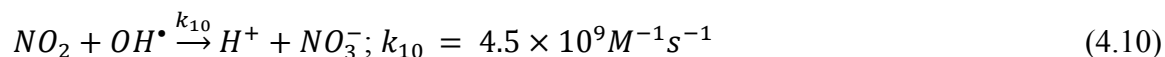
Eqs 4.9 and 4.10 provides the termination steps after the successive propagation through

reaction (4.4) to (4.8) from initiation Reaction (4.2) and (4.3). Khan and Adewuyi (2010) in their

persulfate only systems, and subsequently Adewuyi and Sakyi (2013) in their persulfate and Fe^{2+}

systems took great care in determining the optimum persulfate and Fe^{2+} concentration in NO

removal experiments. NO conversions (%) were determined for different persulfate

concentration at various temperatures and it was concluded that 0.1 M persulfate concentration is

optimum at all temperatures based on NO removal efficiency. The corresponding costs of

chemicals associated with increase in persulfate concentration beyond 0.1 M cannot be justified

since improvement in the removal efficiency is minimal. The inability of persulfate solution to

further increase the removal efficiency at higher temperature and persulfate concentration was

attributed to the radical-radical scavenging reactions such as self-recombination and inter-

combination presented in eqs 4.11, 4.12 and 4.13 (Yusuf Gbadebo Adewuyi & Nana Yaw Sakyi,

2013; Yusuf G. Adewuyi & Nana Y. Sakyi, 2013; Khan & Adewuyi, 2010; Lee, Lo, Kuo, & Lin, 2012).

$$SO_4^{\bullet-} + OH^{\bullet} \xrightarrow{k_{11}} HSO_4^- + \frac{1}{2}O_2; k_{11} = 1 \times 10^{10} M^{-1}s^{-1} \qquad (4.11)$$

$$SO_4^{\bullet-} + SO_4^{\bullet-} \xrightarrow{k_{12}} S_2O_8^{2-}; k_{12} = 7.6 \times 10^8 M^{-1}s^{-1} \qquad (4.12)$$

$$SO_4^{\bullet-} + S_2O_8^{2-} \xrightarrow{k_{13}} S_2O_8^{\bullet-} + SO_4^{2-}; k_{13} = 7.6 \times 10^8 M^{-1}s^{-1} \qquad (4.13)$$
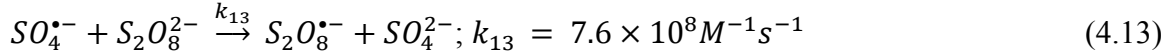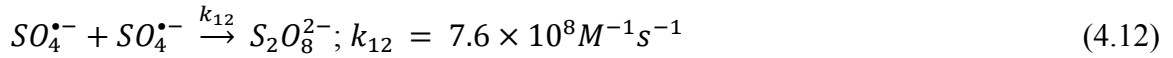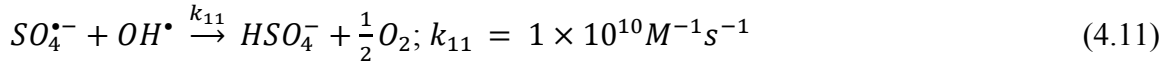
They also performed detailed analysis on studies for the optimization of $Fe^{2+}$ concentration. NO removal was determined by varying $Fe^{2+}$ concentration for different persulfate concentration. Based on the observation they concluded that the optimum concentration of $Fe^{2+}$ was 0.01 M with all persulfate concentration. The possible explanation they pointed out was that, as the $Fe^{2+}$ concentration becomes too high, excess $Fe^{2+}$ starts consuming $SO_4^{\bullet-}$ and $OH^{\bullet}$ radicals through the reaction given in eqs 4.14 and 4.15 (Yusuf Gbadebo Adewuyi & Nana Yaw Sakyi, 2013; H. Kusic et al., 2010).

$$Fe^{2+} + OH^{\bullet} \xrightarrow{k_{14}} Fe^{3+} + OH^-; k_{14} = 3.2 \times 10^8 M^{-1}s^{-1} \qquad (4.14)$$

$$SO_4^{\bullet-} + Fe^{2+} \xrightarrow{k_{15}} Fe^{3+} + SO_4^{2-}; k_{15} = 4.6 \times 10^9 or\ 3.0 \times 10^8 M^{-1}s^{-1} \qquad (4.15)$$
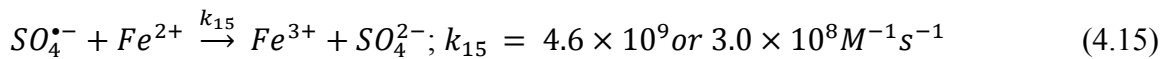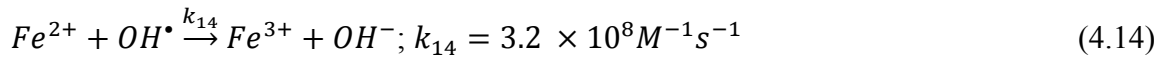
Khan and Adewuyi (2010) studied pH effects on NO absorption in persulfate only system and found that pH effect is not that significant on NO removal at all temperatures. The possible reaction kinetics was studied to understand this behavior although alkaline pH was found to be effective in the removal of ground water contamination (Block, Brown, & Robinson, 2004; Khan & Adewuyi, 2010; Liang, Wang, & Bruell, 2007). Adewuyi and Sakyi (2013) expanded the work by introducing $SO_2$ simultaneously with NO and found that neutral pH shows considerably higher removal efficiency compared to acidic and alkaline region (Yusuf G. Adewuyi & Nana Y. Sakyi, 2013). When $Fe^{2+}$ activation was added, the solution pH was kept 2.5-3.0 to prevent $Fe^{2+}$

oxidation to $Fe^{3+}$ and the precipitation as $Fe(OH)_3$ (Yusuf Gbadebo Adewuyi & Nana Yaw Sakyi, 2013; Block et al., 2004). One of the main drawbacks of this Fenton-like process is the low pH requirement, creating severe acidic environment and possible equipment erosion and corrosion. Most of the literature on NO removal by $Fe^{II}$-EDTA suggests a neutral pH as $Fe^{II}$-EDTA exists as $Fe^{II}$-$H_2$EDTA in acidic and $Fe^{II}$-(OH)EDTA and $Fe^{II}$-$(OH)_2$EDTA in alkaline solution (Liang et al., 2009). A pH value in a near neutral acidic region (6.0-7.0) is desirable for a combined persulfate $Fe^{II}$-EDTA system to counteract the lower pH requirement in Fenton-like process and facilitate NO removal by $Fe^{II}$-EDTA simultaneously working with persulfate.

Also, the main objective of this study is to understand and quantify the simultaneous and synergistic NO removal by persulfate and $Fe^{II}$-EDTA. For this reason, persulfate and $Fe^{2+}$ concentration and pH for all experiments were kept at 0.1 M, 0.01 M and 6.5 respectively based on the aforementioned investigation. Obviously, the detailed study of the effect of persulfate, $Fe^{2+}$, EDTA concentration and pH on NO removal and their interdependency warrants an interest and will be presented in a follow-up paper. Previous studies involving the effect of NO inlet concentration (500-1000 ppm) at various conditions were done in detail and it can be deduced that NO removal efficiency does not change significantly with different inlet NO concentration (Khan & Adewuyi, 2010). As a result, 753 ppm inlet NO concentration was selected as it is the average NO concentration in typical industrial flue gases.

The optimum molar ratio for $Fe^{2+}$:EDTA has been investigated and widely reported in the literature to be around 1:1 in the removal of organic and inorganic pollutants (Francesca Gambardella et al., 2005; N. Liu et al., 2012; Wang et al., 2007; Wu et al., 2008; Zhu et al., 2010). $Fe^{2+}$ and EDTA react with one another according to the reversible reaction presented in eq 4.16.

$$Fe^{2+} + \text{EDTA}^{2-} \overset{K_{16}}{\Longleftrightarrow} Fe^{II}\text{-}EDTA \qquad (4.16)$$

The kinetics of this reversible reaction fixes the amount of Fe[II]-EDTA produced in the solution. The Fe$^{2+}$:EDTA molar ratio of 1:1 is desirable according to the stoichiometry of this reaction, but, a different molar ratio other than 1:1 also observed, when Fe[II]-EDTA is used with other reagents in a combined NO absorption process (N. Liu et al., 2012). Since, to the best of our knowledge Fe[II]-EDTA is being used with persulfate for the very first time in NO absorption, the optimum molar ratio of Fe$^{2+}$ and EDTA should be determined experimentally.

Figure 35 shows the NO concentration profiles at (a) 40, (b) 50 and (c) 60 $^0$C for 0.1 M persulfate and 0.01 M Fe$^{2+}$ solution with different EDTA concentration (0, 0.005, 0.01, 0.015, 0.02, 0.025 and 0.03 M). At 40 $^0$C (Figure 35a) the concentration profiles were smooth and steady but at 50 and 60 $^0$C (Figure 35b and 35c, respectively) were more chaotic, which can be understood by the higher activation and greater interaction between reaction species. For a better understanding of the effect of EDTA concentration (Fe$^{2+}$:EDTA ratio) Table 4 and Figure 36 is constructed  showing the respective NO conversion (%) with EDTA concentration at 40, 50 and 60 $^0$C. At all three different temperatures, the NO conversion values suggested an increase in NO conversion up to 0.01M EDTA concentration. But after 0.01M EDTA the NO conversion values start to decrease steadily with the increase in EDTA concentration. These plots clearly demonstrate that NO conversion peaks at 0.01M EDTA and the ratio for ferrous ion and EDTA concentration 1:1 is optimum at all temperature.

The main observation in this work is that when we use EDTA solution with persulfate and ferrous ion solution for NO removal from flue gas the NO conversion efficiency improves, compared to use of only persulfate and ferrous ion.
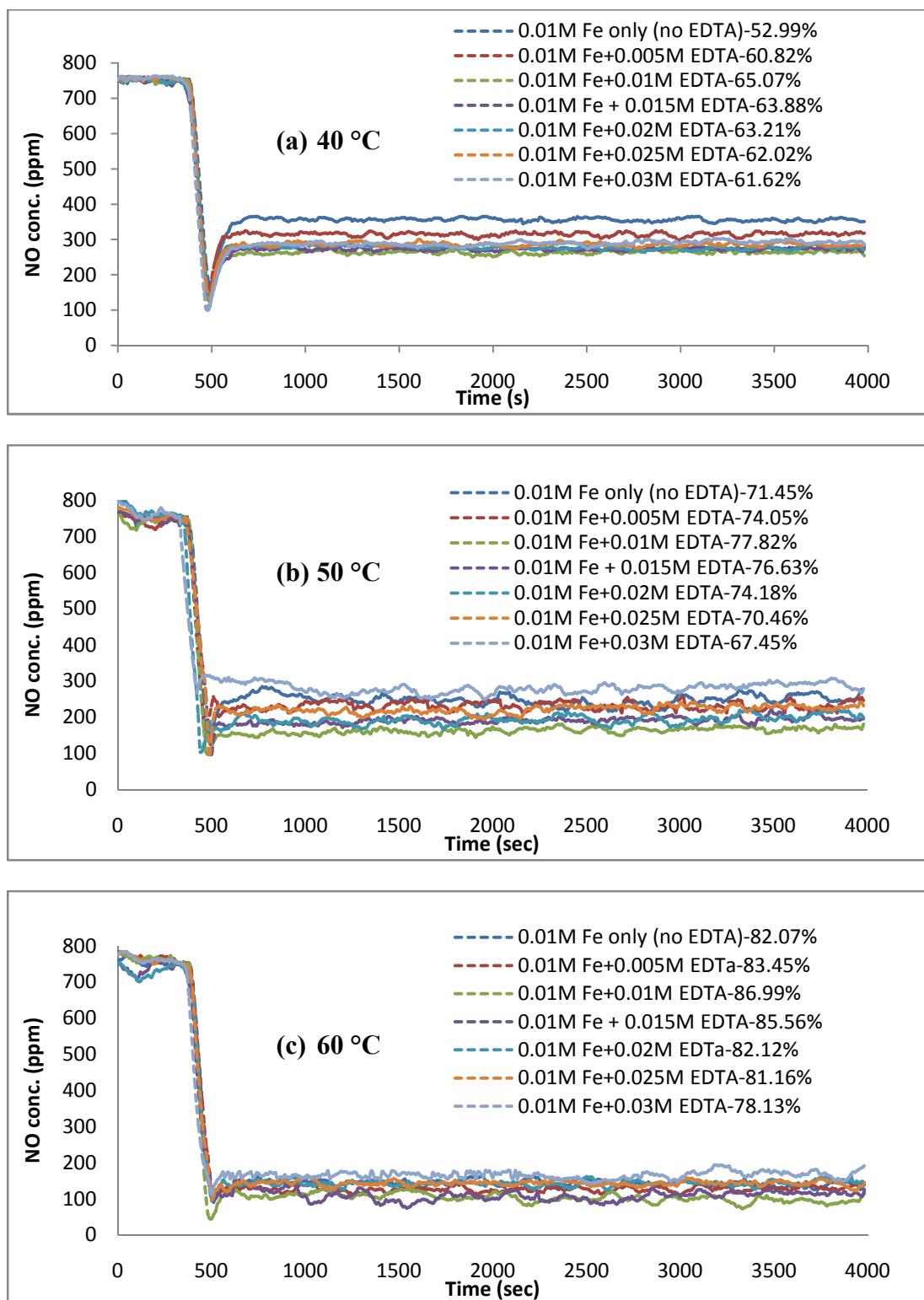
*Figure 35.* NO concentration profiles at 40, 50 and 60 $^0$C for $Na_2S_2O_8$ concentration of 0.1 M

and $Fe^{2+}$ concentration of 0.01 M for different $Na_2$-EDTA concentration (0-0.03 M).

Table 4

*NO Conversion for Different EDTA Concentration for 0.01 M Fe$^{2+}$ and 0.1 M Persulfate*

| Temperature ($^0$C) | NO conversion (%) | | | | | | |
|---|---|---|---|---|---|---|---|
| | 0 M EDTA | 0.005 M EDTA | 0.01 M EDTA | 0.015 M EDTA | 0.02 M EDTA | 0.025 M EDTA | 0.03 M EDTA |
| 40 | 52.99 | 58.17 | 65.28 | 64.10 | 63.21 | 61.52 | 60.62 |
| 50 | 71.45 | 74.05 | 77.82 | 76.63 | 74.18 | 71.46 | 67.45 |
| 60 | 82.07 | 83.45 | 86.99 | 85.56 | 82.12 | 81.16 | 78.13 |
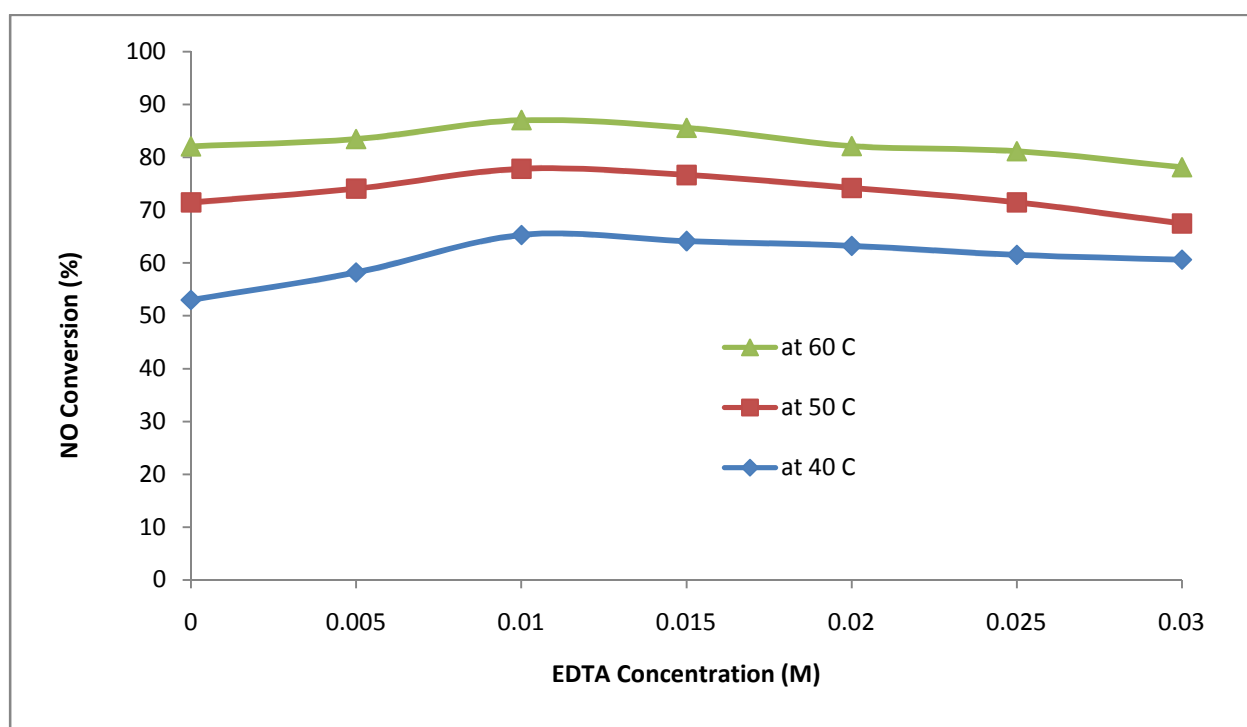


*Figure 36.* NO fractional conversion at 40, 50 and 60 $^0$C for Na$_2$S$_2$O$_8$ concentration of 0.1 M and Fe$^{2+}$ concentration of 0.01 M for different Na$_2$-EDTA concentration (0-0.03 M).

Adewuyi and Sakyi (2013) demonstrated that adding 0.01M Fe$^{2+}$ ion with 0.1M persulfate can improve the NO conversion efficiency 10% further (Yusuf Gbadebo Adewuyi & Nana Yaw Sakyi, 2013). These graphs clearly show that the optimum molar ratio for Fe$^{2+}$ and EDTA that will be added to 0.1M persulfate is 1:1. As 0.01 M Fe$^{2+}$ is already established optimum with 0.1 M persulfate for the future investigation for NO removal will be carried out

for 0.01 M $Fe^{2+}$ and 0.01 M $Na_2$-EDTA with 0.1 M persulfate. Also, 0.005 and 0.02 M

$Fe^{2+}$/EDTA was used in iron speciation experiments, as speciation and material balance of iron

species' gives us opportunity to delve into the chemical kinetics. From Figure 36 and Table 4, we

can see NO conversion increases with additional EDTA concentration up to 0.01M and then start

decreasing with the further addition of $Na_2$EDTA. At 40 $^0$C it can be seen that even for 0.03 M

EDTA the NO conversion (61.62%) does not drop below the conversion of 0 M EDTA (0.01 M

$Fe^{2+}$ only, no EDTA) that is 52.99%. But at 50 and 60 $^0$C and with 0.03M EDTA NO

conversions are 67.45% and 78.13% respectively, which are much lower than the case without

EDTA, that is 71.45% and 82.07% respectively, suggesting at higher temperature excess EDTA

is more detrimental. According to the literature studies, as pointed out before, $Fe^{II}$-EDTA

absorbs NO by a reversible binding producing nitrosyl compound as presented in eq 17 (T. W.

Chien et al., 2009; Demmink et al., 1997; Francesca Gambardella et al., 2005; N. Liu et al.,

2012; Narita et al., 1984; Sada et al., 1986; Sada et al., 1980; Sada et al., 1984; Suchecki et al.,

2005; Teramoto et al., 1977; Wang et al., 2007).

$$Fe^{II}\text{-}EDTA + \text{NO} \overset{K_{17}}{\Longleftrightarrow} Fe^{II}\text{-}EDTA(NO); K_{17} = 3.6 \times 10^6 \ (25°C) \ or \ 6 \times 10^5 M^{-1}$$

$$(50°C) \tag{4.17}$$
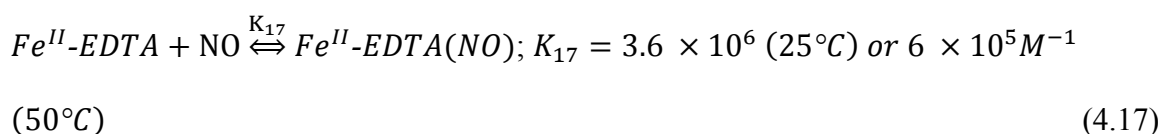
$Fe^{2+}$ not only reacts with EDTA according to Reaction 4.16 to produce $Fe^{II}$-EDTA, which

is then used to combine with NO in eq 4.17, but $Fe^{2+}$ also activates persulfate in the solution

according to Reaction 4.3. At higher EDTA doses, EDTA combined with too much $Fe^{2+}$, thus

lowering the amount of $Fe^{2+}$ available for persulfate activation. From Figure 36 and Table 4, it

can be seen that NO absorption capability of the solution did not drop drastically but a gradual

decrease was observed, indicating that excess EDTA only affects iron activation of persulfate by

scavenging $Fe^{2+}$ required, but not the temperature activation of persulfate.

**4.3.2 Synergistic effect of Fe$^{II}$-EDTA with persulfate.** Once the optimum concentration of persulfate and Fe$^{2+}$ was established, and the molar ratio Fe$^{2+}$:EDTA corresponds to the highest absorption of NO investigated, using the optimum initial Fe$^{2+}$ and EDTA concentrations established with 0.1 M persulfate solution, the effect of Fe$^{II}$-EDTA addition was compared to the temperature only and Fe$^{2+}$ activated persulfate systems.

Adewuyi and Sakyi (2013) investigated the different injection methods of Fe$^{2+}$ and persulfate, and concluded that both persulfate and Fe$^{2+}$ simultaneously introduced at the top of the reactor at the beginning of reaction gives best NO removal. Since EDTA reacts with Fe$^{2+}$ by Reaction 4.16, Fe$^{2+}$ solution was first added to the de-oxygenated water followed by Na$_2$-EDTA reaction. After the reaction between Fe$^{2+}$ and EDTA is completed persulfate is added from the top of the reactor. The reversible nature of the reaction presented in eq 4.16, dictate the presence of Fe$^{2+}$, EDTA and Fe$^{II}$-EDTA in the solution, and enough Fe$^{2+}$ remains in the solution for persulfate activation. The graphs in Figure 37 demonstrate the NO concentration profile at 30 $^0$C for 0.1M persulfate with 0.01M Fe$^{2+}$/EDTA compared to the profiles for 0.1M persulfate only and for 0.1M persulfate with 0.01M Fe$^{2+}$.
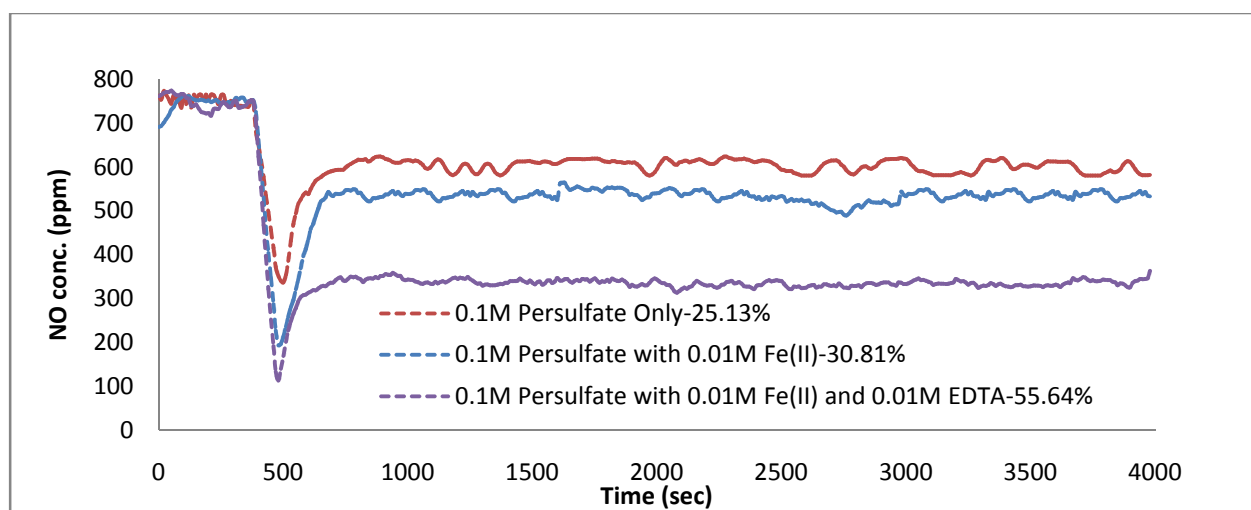


*Figure 37.* Comparative NO concentration profiles at 30 $^0$C.
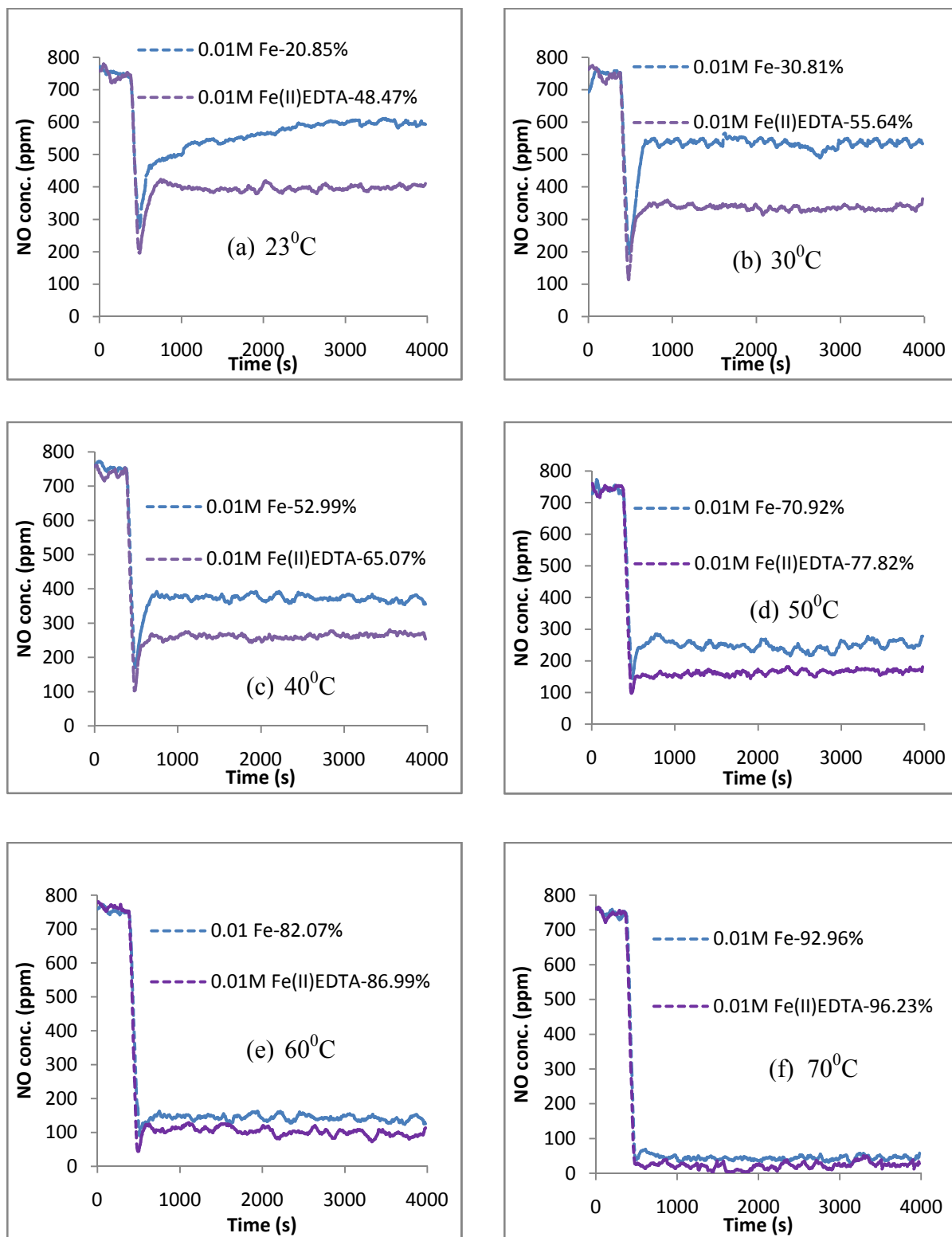
*Figure 38.* Comparative NO concentration profiles at various temperatures (23-70 $^0$C).

The conversion for 0.1M persulfate only at 30 $^0$C is about 25.13%. Adding 0.01M $Fe^{2+}$ the conversion increases up tp 30.81%, a 5.68% increase in the NO removal efficiency. When 0.01 M $Fe^{2+}$ and 0.01 M EDTA is added to 0.1 M persulfate solution the conversion is 55.64%, an additional 24.83% increase in NO removal efficiency. The plots in Figure 38 show the comparative NO concentration profiles at six different temperatures (23, 30, 40, 50, 60 and 70 $^0$C) between 0.1M persulfate activated by 0.1M $Fe^{2+}$ ion and 0.1M persulfate with 0.01M Fe(II) and 0.01M EDTA. NO removal experiments for 0.1 M persulfate only system was not carried out at all temperature except 23 $^0$C because NO conversion value can be found from Khan and Adewuyi (2010) and also, Adewuyi and Sakyi (2013) have already established the comparative advantage of $Fe^{2+}$ activated persulfate system over persulfate only system (10 % more NO removal at all temperatures) (Yusuf Gbadebo Adewuyi & Nana Yaw Sakyi, 2013; Khan & Adewuyi, 2010). Addition of 0.01 M EDTA increases NO conversion efficiency by almost 28% at 23 $^0$C, where at 30 $^0$C the conversion increases by almost 25%. At 40, 50, 60 and 70 $^0$C the conversion increases about 13%, 7%, 5% and 4%, respectively, as presented in figure 38. In Figure 39, NO conversion at 23-70 $^0$C is compared for the three systems, where NO conversion values for persulfate only system were taken from Khan and Adewuyi (2013) (Khan & Adewuyi, 2010). At higher temperature increase in NO removal efficiency by adding 0.01 M EDTA become less significant but maintains a higher value always. As a result, close to 100% removal is found at 70 $^0$C by adding EDTA whereas, for the $Fe^{2+}$ activated persulfate system 90 $^0$C is required to obtain about 100% removal. This higher removal gives a remarkable advantage in the industrial flue gas treatment, as flue gas is generally obtained at 50-70 $^0$C in the effluent treatment plant. But the fact is undeniable that comparative advantage gradually diminishes from lower temperature (28% at 23 $^0$C) to higher temperature (4% at 70 $^0$C). This may be attributed to

the reversible binding of NO with $Fe^{II}$-EDTA in Reaction 4.17. As the literature values suggest, the forward reaction constant, $k_{17}$ ($6 \times 10^7$ $M^{-1}s^{-1}$ at 25 $^0C$) is higher in the lower temperature. At higher temperature $k_{17}$ becomes lower ($3.7 \times 10^7$ $M^{-1}s^{-1}$ at 50 $^0C$) where the backward reaction constant, $k_{-17}$ increases (6 to 60 $s^{-1}$), resulting in a lower value of equilibrium constant $K_{17}$ at higher temperature (T. W. Chien et al., 2009; N. Liu et al., 2012). But the comparative advantage still holds (around 5% higher NO conversion at 70 $^0C$) due to the synergistic effect of $Fe^{II}$-EDTA on persulfate oxidation of NO.
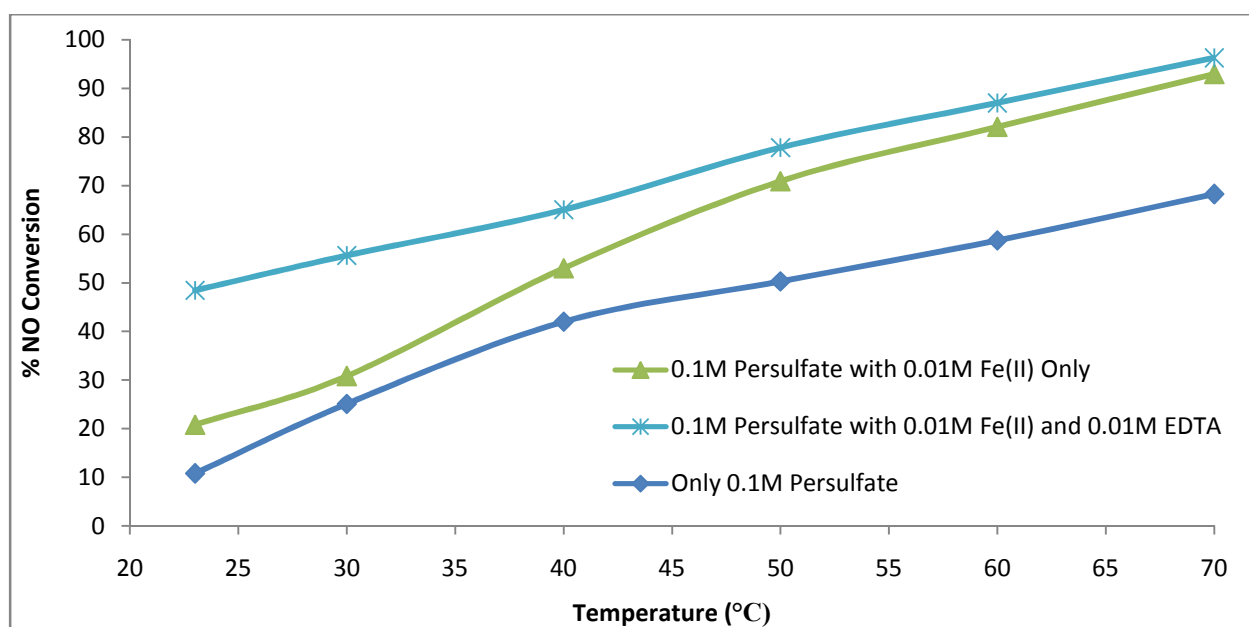


*Figure 39.* Dependence of NO fractional conversions on temperature.

Since, at 23 $^0C$ NO removal increased by almost 30% and at 70 $^0C$ by 4-5% (Figure 39) and $Fe^{II}$-EDTA reversible binding with NO by Reaction 4.17 is slower at higher temperature as backward reaction rate increases, we should see little or no increase in NO removal. But, NO removal increased almost 4% instead. This can be explained by the comparative activation of persulfate by $Fe^{2+}$ only and $Fe^{II}$-EDTA. It was reported in the literature that iron chelate never attacks hydroxyl radical and does not suppress Fenton or Fenton-like reactions (L. Li et al., 2007). Thus in Reaction 4.14 and 4.15, where $Fe^{2+}$ was responsible for the scavenging of

hydroxyl and sulfate radicals, chances of this occurring is less when $Fe^{II}$-EDTA is used instead. Liang et al. (2004) also worked on persulfate activation by chelated ferrous ion to destruct TCE and concluded that chelated iron compound is far superior to unchelated $Fe^{2+}$ in persulfate activation (Liang et al., 2004b). The superiority of $Fe^{II}$-EDTA over $Fe^{2+}$ as a persulfte activator was also confirmed by ESR spectroscopy and probe compounds investigation to track different free radicals (Ahmad et al., 2012). It can be seen from Figure 5 that $Fe^{2+}$ activated persulfate system gives higher NO removal at higher temperature compared to persulfate only system, which is due to the higher activation of persulfate at higher temperature. The difference between NO removals of $Fe^{II}$-EDTA activated persulfate system and only persulfate system is almost equal at every temperature (35-40%). It can be said that $Fe^{II}$-EDTA activation of persulfate is about 5% and the remaining 22-25% increase is due to the direct absorption of $Fe^{II}$-EDTA. It was also reported in the literature that NO can be bound to $FeSO_4$ solution by reaction in eq 4.18 but the order of magnitude of the reaction constant is four times less than that of Reaction 4.17 (Sada et al., 1980).

$$FeSO_4 + \text{NO} \overset{K_{18}}{\Longleftrightarrow} Fe(NO)SO_4 \tag{4.18}$$

Reaction 4.18 is thus very slow compared to Reaction 4.17 and considered insignificant for NO removal by only $Fe^{II}$-EDTA, but can play a significant role in combined persulfate and $Fe^{II}$-EDTA systems nonetheless. In $Fe^{2+}$ activated persulfate system, all the $Fe^{2+}$ reacts very quickly and remains virtually non-existent in the solution the possibility of Reaction 4.18 is almost none. But, in combined persulfate and $Fe^{II}$-EDTA systems the concentration of $Fe^{2+}$ is determined by the equilibrium reaction in eq 4.17 (measured by spectrophotometric method) and the possibility of Reaction 4.18 reinvigorates and can aid the NO removal efficiency.

Oxygen is considered very detrimental in NO absorption process by Fe$^{II}$-EDTA solution as it reacts with Fe$^{II}$-EDTA producing inert Fe$^{III}$-EDTA by reaction in eq 4.19 (Francesca Gambardella et al., 2005; N. Liu et al., 2012; Maas et al., 2009; Mi et al., 2009; Piché, Ribeiro, Bacaoui, & Larachi, 2005; Sada, Kumazawa, & Machida, 1987; van der Maas, van den Brink, Utomo, Klapwijk, & Lens, 2006; Zhang et al., 2007).

$$4Fe^{II}\text{-}EDTA + O_2 + H_2O \xrightarrow{k_{19}} 4Fe^{III}\text{-}EDTA + 4OH^-; \quad k_{19} = 1.09 \times 10^4 \times$$

$$\exp\left(-\frac{2.33 \times 10^4}{RT}\right) \tag{4.19}$$
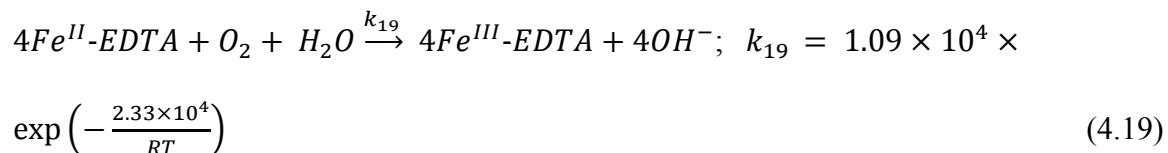
The reaction is studied by Sada et al. (1988) and found to be first order in $O_2$ and half order in Fe$^{II}$-EDTA, and only to suppress this reaction as much as 20% excess Fe$^{II}$-EDTA is added in the system (Sada et al., 1988). In our experiment water was de-aerated completely by purging with dry nitrogen before starting the NO absorption and also $Fe^{2+}$ and Na$_2$-EDTA was added to the system separately without producing Fe$^{II}$-EDTA outside the reactor. So, the system remained completely oxygen free throughout the experiments. There is a possibility of small amount oxygen production according to Reaction 4.11, but this reaction is only radical-radical scavenging occurs in higher persulfate doses. Also, there was no $O_2$ could be determined in FTIR and no Fe$^{III}$-EDTA found in spectrophotometric determination of iron species'. Thus, the systems were operated in almost completely oxygen free environment and detrimental effects of oxygen via Reaction 4.19 were avoided. Of course, studies of NO removal in presence of $O_2$ and effect of its concentration has immense interest, but it is outside the scope of this work and will be reported in future publication.

It was also reported in the literature that Fe$^{II}$-EDTA also reacts with $NO_2^-$ and $NO_2$ by reaction presented in eqs 4.20 and 4.21, respectively, producing both Fe$^{II}$-EDTA(NO) and Fe$^{III}$-EDTA (H. Li & Fang, 1988; N. Liu et al., 2012; van der Maas et al., 2004).

$$2Fe^{II}\text{-}EDTA + NO_2^- + 2H^+ \overset{K_{20}}{\Longleftrightarrow} Fe^{II}\text{-}EDTA(NO) + Fe^{III}\text{-}EDTA + H_2O \qquad (4.20)$$

$$2Fe^{II}\text{-}EDTA + 2NO_2 \overset{K_{21}}{\Longleftrightarrow} Fe^{II}\text{-}EDTA(NO) + Fe^{III}\text{-}EDTA + NO_3^- \qquad (4.21)$$
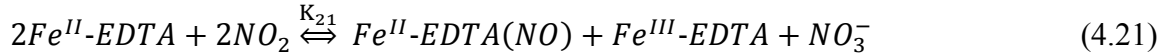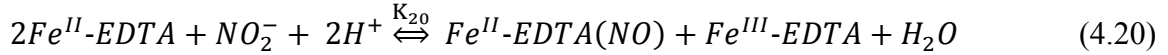
The denitrification of $Fe^{II}$-EDTA(NO) can be done in biological processes where ethanol acts as a electron donor compound (F. Gambardella, Winkelman, & Heeres, 2006; W. Li et al., 2006)

$$6Fe^{II}\text{-}EDTA(NO) + C_2H_5OH \overset{k_{22}}{\longrightarrow} 6Fe^{II}\text{-}EDTA + 3N_2 + 3H_2O + 2CO_2 \qquad (4.22)$$

$Fe^{II}$-EDTA can also act an electron donor. It was reported that denitrification using $Fe^{II}$-EDTA as an electron donor is chemical reaction rather than biological in nature, thus probable in our system (W. Li et al., 2006; W. Li et al., 2007; N. Liu et al., 2012; Manconi et al., 2006; van der Maas et al., 2004; van der Maas, van den Bosch, et al., 2005; Zhang et al., 2007).

$$2Fe^{II}\text{-}EDTA(NO) + 2Fe^{II}\text{-}EDTA + 4H^+ \overset{k_{23}}{\longrightarrow} 4Fe^{III}\text{-}EDTA + N_2 + 2H_2O \qquad (4.23)$$
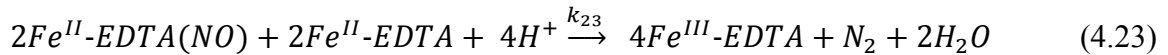
As a result of these reactions $Fe^{II}$-EDTA(NO) and $Fe^{III}$-EDTA are produced in the system, and the absorption capability of the solution decreases with the progression of time. The success of an effective NO removal process by $Fe^{II}$-EDTA lies in the efficient reduction of $Fe^{II}$-EDTA(NO) and $Fe^{III}$-EDTA, and regeneration of $Fe^{II}$-EDTA in the system. Sulfate and other persulfate derived ions in our system can effectively accomplish this task. It was reported in the literature that $HSO_3^-$ and/or $SO_3^{2-}$ can be used to reduce $Fe^{II}$-EDTA(NO) and $Fe^{III}$-EDTA in NO removal process (T. W. Chien et al., 2009; Narita et al., 1984; Sada et al., 1986; Sada et al., 1980; Sada et al., 1984; Teramoto et al., 1977; Wang et al., 2007). According to these studies the following reactions are proposed in our system for the reduction of $Fe^{II}$-EDTA(NO) and $Fe^{III}$-EDTA back to $Fe^{II}$-EDTA.

$$Fe^{III}\text{-}EDTA + HSO_4^- \overset{k_{24}}{\longrightarrow} Fe^{II}\text{-}EDTA + \tfrac{1}{2}S_2O_8^{2-} + H^+ \qquad (4.24)$$

$$Fe^{II}\text{-}EDTA(NO) + SO_4^{2-} \overset{K_{25}}{\Longleftrightarrow} Fe^{II}\text{-}EDTA(NO)SO_4^{2-} \tag{4.25}$$

$$2Fe^{II}\text{-}EDTA(NO) + 2HSO_4^{-} \overset{K_{26}}{\Longleftrightarrow} 2Fe^{II}\text{-}EDTA + N_2O + 2SO_4^{2-} + H_2O \tag{4.26}$$
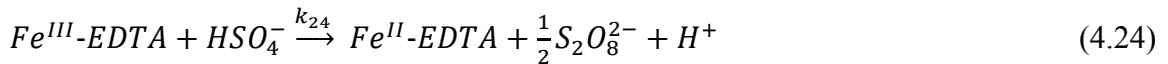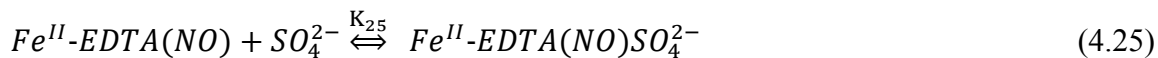
With this reduction reaction scheme persulfate system also helps $Fe^{II}$-EDTA chemistry producing a complete synergistic and simultaneous relationship. The literature studies for NO removal by $Fe^{II}$-EDTA solution show that with the passage of time $Fe^{II}$-EDTA solution losses NO removal capability and the NO conversion drops significantly as early as 2-3 hours (W. Li et al., 2006; N. Liu et al., 2012; Wang et al., 2007; Zhu et al., 2010). The long time viability of the absorbent solution was tested at 30 $^0$C for both 0.01 M $Fe^{2+}$ activated 0.1 M persulfate and combined 0.1 M persulfate and 0.01 M $Fe^{II}$-EDTA processes. For the long period of time (6 h) NO removal efficiency was found to be 28.07% for $Fe^{2+}$ activated persulfate sytem and 56.88% for the combined persulfate and $Fe^{2+}$-EDTA system. The long time viability of the combined solution to sustain absorption-oxidation capability indicates the continuous reduction of $Fe^{II}$-EDTA(NO) to $Fe^{II}$-EDTA by reactions in eqs 4.23, 4.24 and 4.25 for a long time, further confirming the beneficial action of persulfate and persulfate derived radicals and ions on $Fe^{II}$-EDTA.

**4.3.3 Iron speciation and material balance.** The iron species' present in the solution ($Fe^{2+}$, $Fe^{3+}$ and $Fe^{II}$-EDTA) is determined spectrophotometrically at 50 $^0$C using 0.1 M persulfate concentration and three different $Fe^{2+}$ and EDTA ($Fe^{2+}$:EDTA = 1:1) concentrations, as discussed earlier.

Samples were taken by the side syringe very quickly starting as early as 30 s to the end of the experiment after certain time intervals. The samples were then analyzed using spectrophotometer. $Fe^{2+}$ and $Fe^{3+}$ concentrations were analyzed by using standard 1, 10-phenanthroline colorimetric method and $Fe^{II}$-EDTA concentration were determined using their

absorbances in 270-330 nm. Total measured Fe is the sum of $Fe^{2+}$, $Fe^{3+}$ and $Fe^{II}$-EDTA and undetermined Fe is the difference between initial iron concentration and total measured iron.
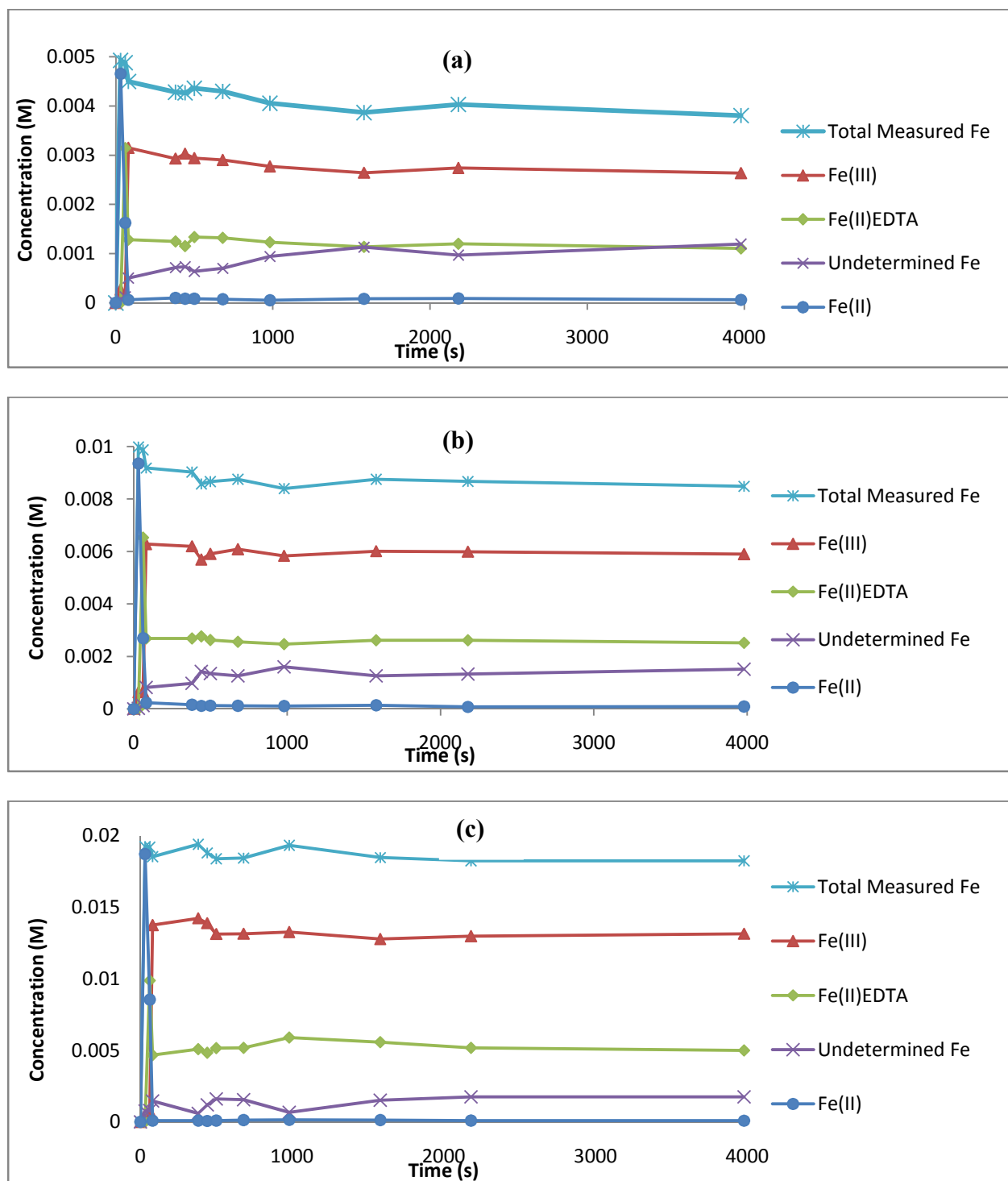


*Figure 40.* Iron species' profiles at 50 $^0$C for 0.1 M persulfate solution.
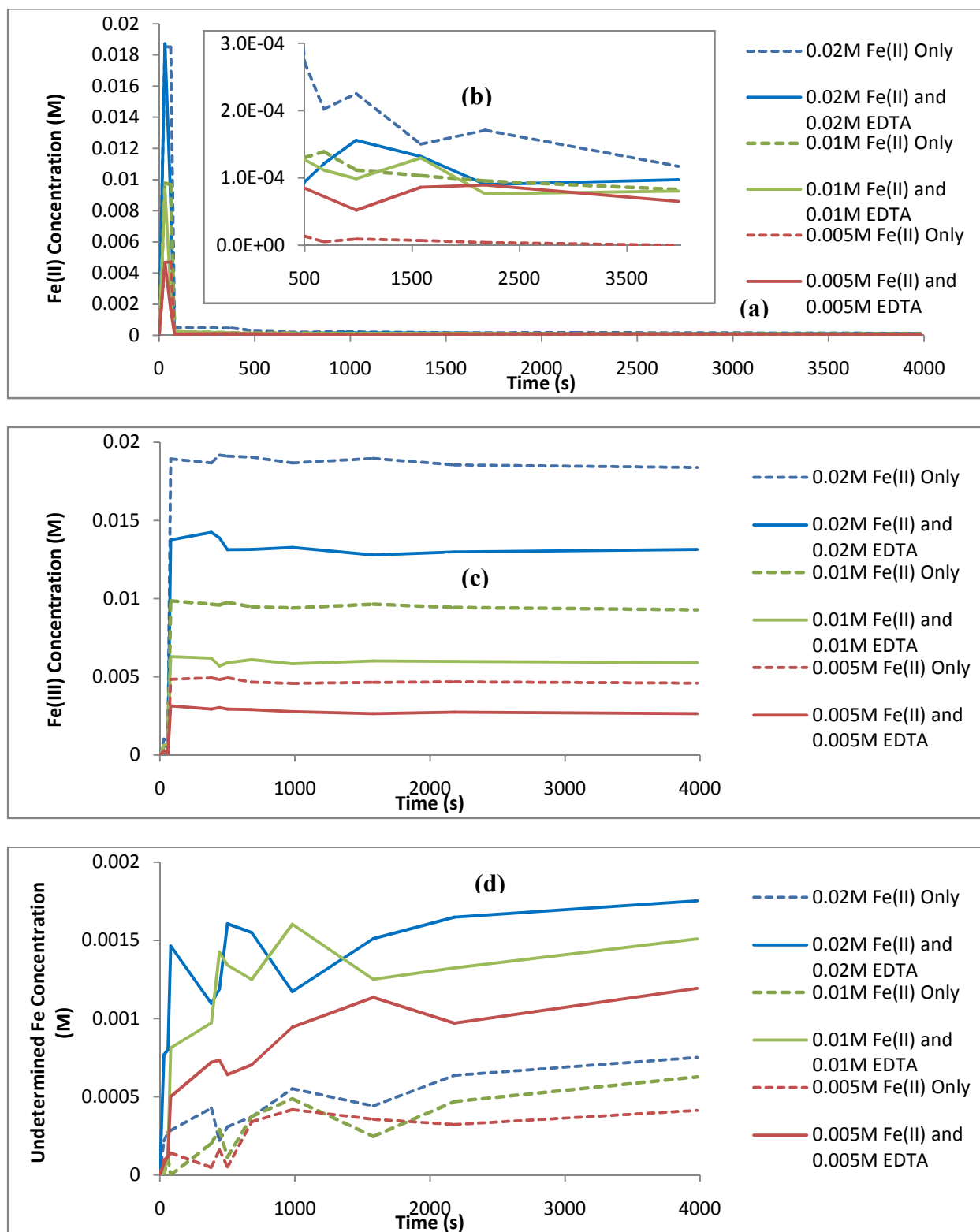
*Figure 41.* Comparative iron species' profiles in presence and absence of EDTA.

Figure 40 shows the profiles of all the iron species at 50 $^0$C. It can be seen from Figure 40 that $Fe^{2+}$ concentration remains close to zero throughout the experiment suggesting near complete reaction with both persulfate and EDTA. The undetermined Fe consists of non-labile iron hydroxides, $Fe^{II}$-EDTA(NO) and other non-labile iron species presents in very small amounts. Since all other non-labile species except $Fe^{II}$-EDTA(NO) remain constant throughout the experiment, the increase in the undetermined Fe suggests increase in $Fe^{II}$-EDTA(NO) concentration, resulting from Reaction (4.17) progression. Since, $Fe^{II}$-EDTA(NO) concentration increases very slightly and slowly throughout the experiment, it can be said that its accumulation in the solution is very small indicating its reduction back to $Fe^{II}$-EDTA by persulfate and radicals in the system, thus confirming the synergistic action of persulfate on $Fe^{II}$-EDTA.

Figure 41 shows the comparison between the iron species' concentration in $Fe^{2+}$ activated persulfate system and combined persulfate and $Fe^{II}$-EDTA system. In Figure 41a, $Fe^{2+}$ ion concentration is plotted for both of $Fe^{2+}$ activated 0.1M persulfate system and 0.1M persulfate with both $Fe^{2+}$ and EDTA for 0.005M, 0.01M and 0.02M. Ferrous ion concentration for both systems is similar, upon addition of oxidant $Fe^{2+}$ concentration quickly diminished to very low level indicating it has been oxidized to $Fe^{3+}$ ion. To observe the difference between the $Fe^{2+}$ concentration profiles of two processes more closely, Figure 41b is drawn. Figure 41b is truncation of figure 41a from 500 s to 4000 s to show the comparative $Fe^{2+}$ concentration more clearly. We can see $Fe^{2+}$ ion increases ($1 \times 10^{-5}$ to $2.8 \times 10^{-4}$ M on average) with the initial Fe(II) concentration (0.005 to 0.02M) for $Fe^{2+}$ activated persulfate systems. But for combined persulfate and $Fe^{II}$-EDTA system the concentration of Fe(II) ion remains the same ($1 \times 10^{-4}$ M on average) for 0.005M, 0.01M and 0.02M initial concentration. This can be explained by the reversible reaction in eq 4.16, where, the forward and backward reactions stabilize $Fe^{2+}$

concentration in the system that facilitates the $Fe^{2+}$ activation of persulfate. Figure 41c shows the $Fe^{3+}$ ion concentration profiles determined by 1,10-phenanthroline method. As compared to $Fe^{2+}$ activated persulfate system $Fe^{3+}$ ion concentration decreases significantly during the absorption process. The concentration of $Fe^{3+}$ in $Fe^{2+}$ activated persulfate systems is almost equal to sum of the concentration of $Fe^{3+}$ and $Fe^{II}$-EDTA in combined persulfate and $Fe^{II}$-EDTA systems. This implies that the addition of EDTA actually formed $Fe^{II}$-EDTA by consuming $Fe^{2+}$ ion that are supposed to be converted into $Fe^{3+}$ anyway, thus increasing the NO removal without affecting the temperature and $Fe^{2+}$ activation of persulfate, and further confirming that $Fe^{II}$-EDTA does not suppress persulfate activation as discussed earlier. Figure 41d shows the concentration profile for undetermined Fe species'. In the persulfate systems with only $Fe^{2+}$ the undetermined Fe consists of only non-labile iron species'. In combined persulfate and $Fe^{II}$-EDTA systems undetermined Fe also consists of $Fe^{II}$-EDTA(NO) and $Fe^{III}$-EDTA. Since in spectrophotometric determination significant amount of $Fe^{III}$-EDTA was never found, the difference between undetermined Fe concentaion in two systems is $Fe^{II}$-EDTA(NO) assuming that the non-labile iron species' concentration remain same for the same initial $Fe^{2+}$ concentration. It can be seen that $Fe^{II}$-EDTA(NO) concentration (difference between two systems) is 0.001 M. $Fe^{II}$-EDTA(NO) does not change when $Fe^{II}$-EDTA increased from 0.01 to 0.02 M, suggesting no further NO removal occurred for the increase in initial $Fe^{2+}$ concentration from 0.01 to 0.02 M, thus confirming previously chosen optimum $Fe^{2+}$ concentration of 0.01 M. Again, presence of only 10% of initial $Fe^{2+}$ as $Fe^{II}$-EDTA(NO) and absence of $Fe^{III}$-EDTA indicates $Fe^{II}$-EDTA(NO) and $Fe^{III}$-EDTA reduction by sulfate ions in the combined system is significant.

**4.3.4 Effect of initial persulfate concentration on NO removal.** NO concentration profiles were drawn for three different persulfate concentration (0.05, 0.10 and 0.20 M) at

different temperature (23 to 70 $^0$C). As we can see from Figure 42, when 0.05M persulfate is used the NO conversion rate is quite low compared to 0.1M persulfate and there was almost 6-7% increase in NO conversion from 0.05 to 0.1 M persulfate concentration. Adewuyi and Nana (2013) established 0.1M persulfate as optimum concentration of persulfate. In their work, Adewuyi and Nana also showed that, after 0.1M persulfate there is no considerable advantage adding more persulfate as at 0.2M persulfate concentration there were negligible or no improvement in NO conversion. From Figure 42, it also can be said that at 23, 30 and 40 $^0$C there was only 2-3% improvement in NO conversion on average upon increasing the persulfate concentration from 0.1 to 0.2M. However, at 50, 60 and 70 $^0$C there was almost no visible improvement. But when persulfate is activated by only iron the improvement in NO conversion holds throughout the temperature range (23 to 70 $^0$C). This can also be explained by the temperature activation of reversible reaction. At higher temperature the backward reaction started to influence more in the reaction equilibrium and reversible binding of NO with Fe(II)EDTA starts to reverse. So, considering the cost of double amount of persulfate and the subsequent NO removal it can be concluded that the optimum concentration of persulfate in this process should be 0.01M. This observation is completely relevant with the studies of Adewuyi and Nana (2013), who found the optimum persulfate concentration at 0.1M in the case of Fe$^{2+}$ activated persulfate. In the persulfate only absorption studied by Khan and Adewuyi (2010), it was shown that after 0.1M persulfate NO removal rate slows down considerably and steadied.
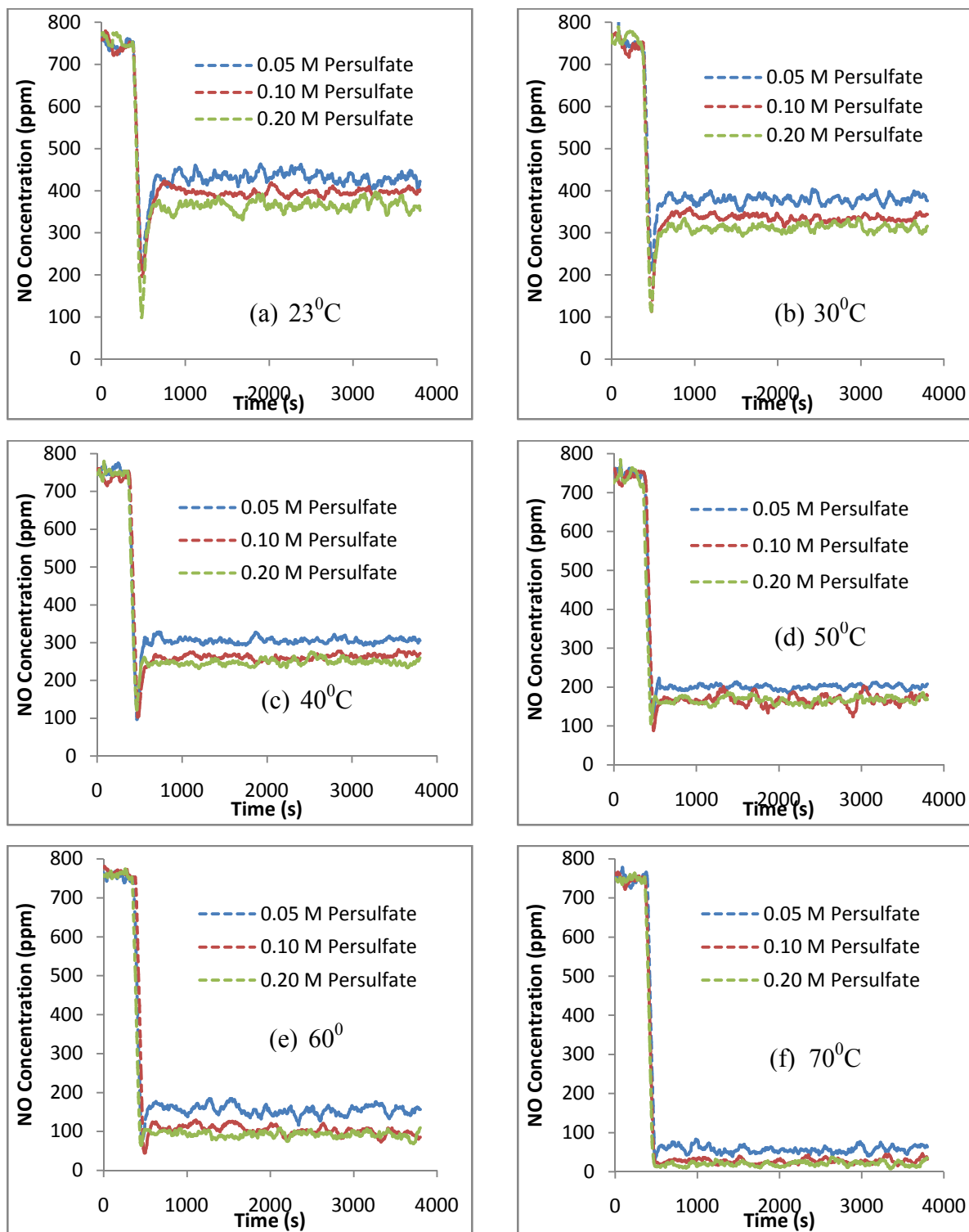
*Figure 42.* NO concentration plots for different initial persulfate concentration (0.05-0.20 M) at different temperatures (23-70 $^0$C).
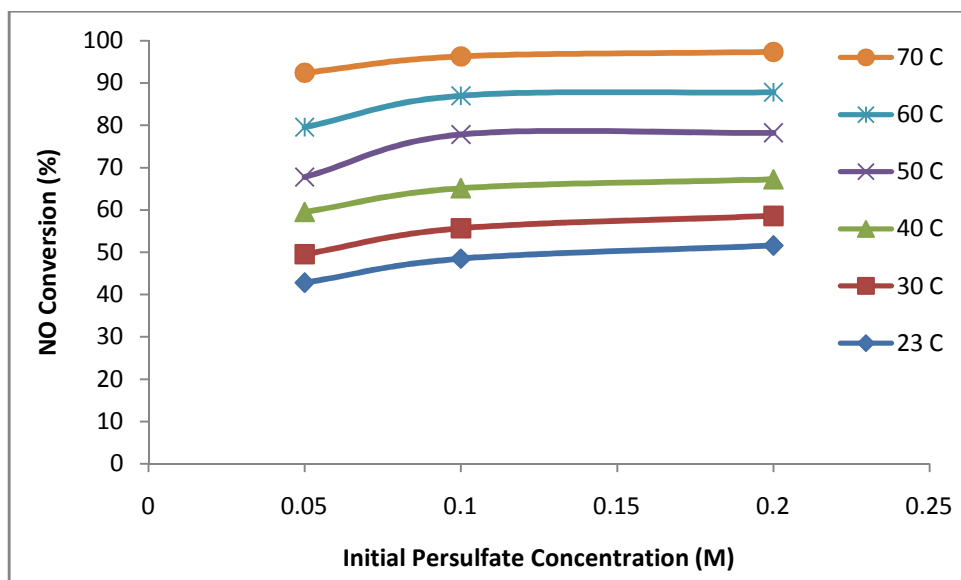
*Figure 43.* NO conversion with initial persulfate concentration for different temperatures.
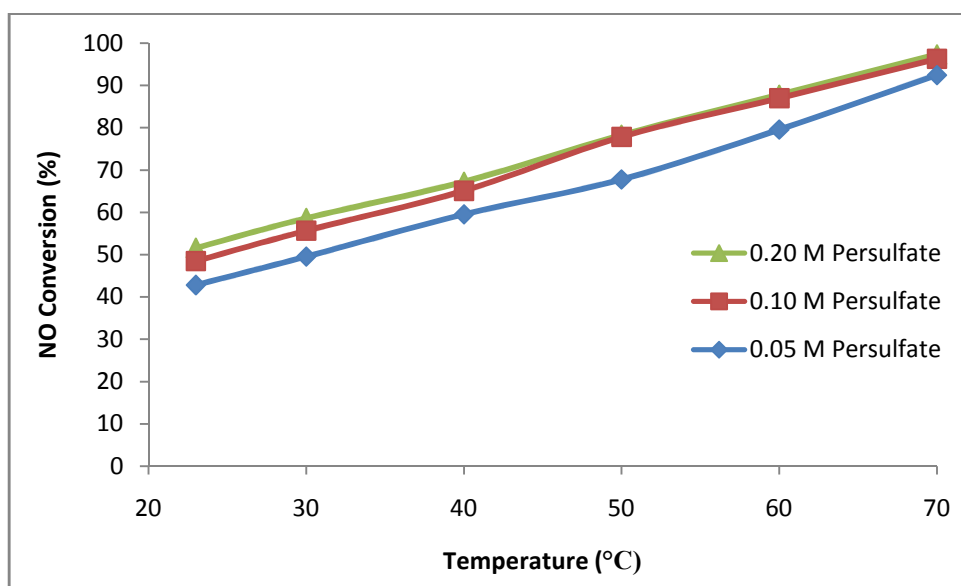


*Figure 44.* NO conversion with temperature for different initial persulfate concentrations.

This fact can be explained by the following radical-radical scavenging reactions. With high persulfate concentration more $SO_4^{\bullet-}$ and $OH^{\bullet}$ radicals forms, although vital for the NO oxidation and absorption with higher concentration radicals starts to consume themselves by the radical-radical interaction in eqs 4.11 and 4.12.

That is why, after a certain optimum level, the increase in persulfate concentration does not guarantee any further increase in NO removal. In this case, as well as previous studies by Khan and Adewuyi and Adewuyi and Nana the optimum level is demonstrably 0.1M. This clearly demonstrates that for every temperature from 0.05 to 0.10M persulfate concentration NO conversion increases and after 0.10 M NO conversion stabilizes as shown in Figure 42. Figure 44 is identical as Figure 43, but NO conversion plotted with temperature for different persulfate concentration. It can be seen from the graph that from 0.10M persulfate to 0.20M persulfate there is no improvement in NO conversion at higher temperature whereas at low temperature there is small improvement that can be deemed insignificant establishing the optimum concentration as 0.10M persulfate.

**4.3.5 Effect of initial $Fe^{2+}$/EDTA (1:1) concentration on NO removal.** The graphs in Figure 45 show the effect of different $Fe^{2+}$/EDTA concentration (0.005 to 0.05M) on NO concentration profiles and NO removal at different temperature. At 23 $^0$C the removal of NO shows significant increase from 0.005 to 0.01M EDTA (37.98% to 48.47%). But from 0.01 to 0.02M Fe/EDTA it only increase up to 52.59% and at 0.05M Fe/EDTA the conversion actually decrease to 51.26%. At 30 $^0$C, from 0.005 to 0.01M Fe/EDTA NO removal increase from 48.74% to 55.64%, where at 0.02M Fe/EDTA it increases up to 61.75%. At 0.05M Fe/EDTA it decreases slightly to 61.15%. At 40 $^0$C, NO removal increases from 60.69% to 65.07% when Fe/EDTA concentration is increases from 0.005M to 0.01M. At 0.02M Fe/EDTA it increases slightly to 66.14%. But at 0.05M Fe/EDTA the solution losses almost all its absorption capacity and NO profile goes upward sharply after sometime and the final NO removal was found to be only 19.12%. This behavior also observed at 50, 60 and 70 $^0$C.
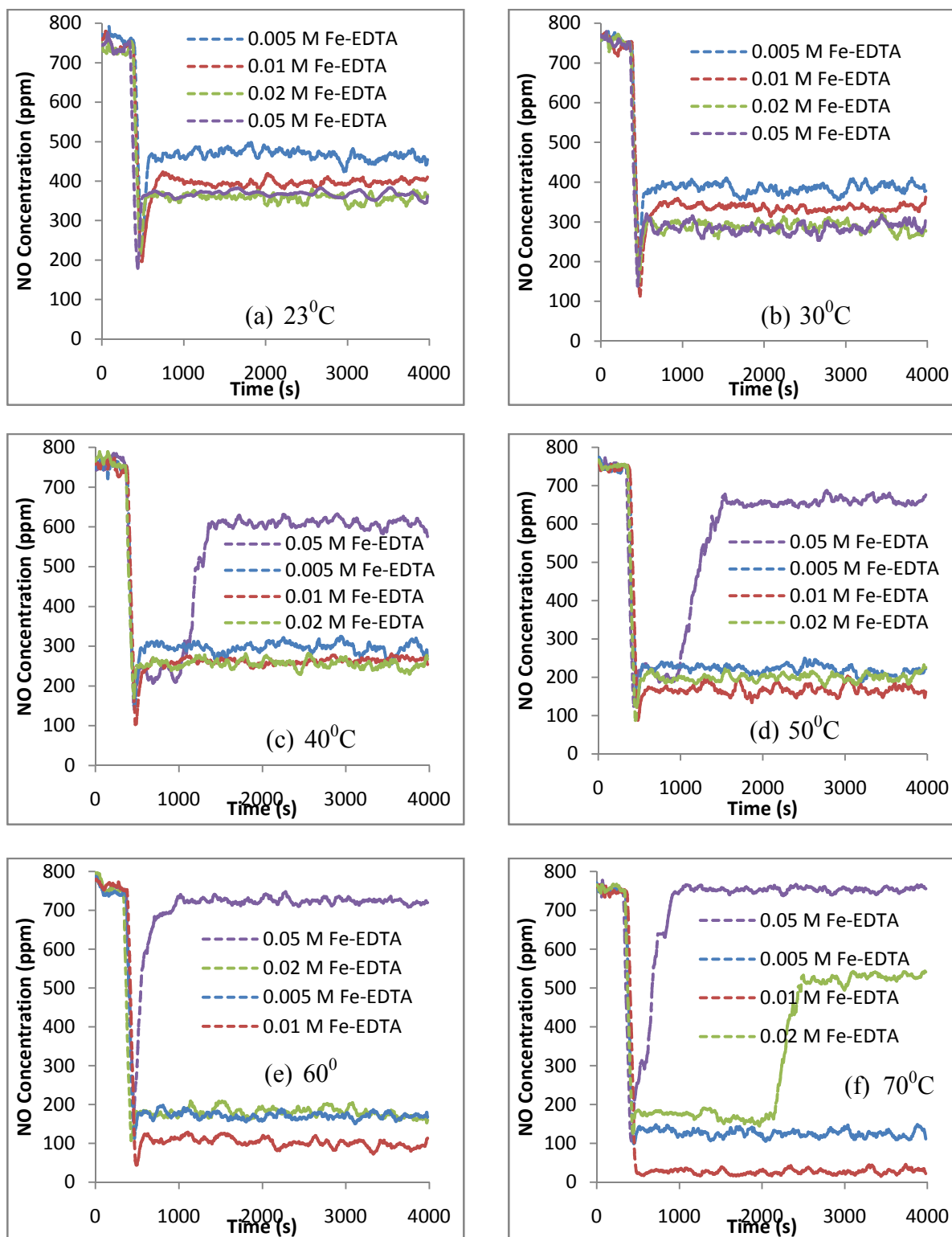
*Figure 45.* NO concentration plots for different initial $Fe^{2+}$/EDTA concentrations.

At 50 $^0$C, NO removal increases from 70.65% to 77.82% when Fe/EDTA concentration is increases from 0.005M to 0.01M. At 0.02M Fe/EDTA NO removal actually decreases to73.57%. But at 0.05M Fe/EDTA the solution losses almost all its absorption capacity and NO profile goes upward sharply after sometime and the final NO removal was found to be only 13.28%. At 60 $^0$C, the NO absorption profile behaves similarly like at 50 $^0$C and the final NO removal was found to be 77.29%, 86.99%, 76.0% and 3.85% at 0.005, 0.01, 0.02 and 0.05M Fe/EDTA, respectively. At 70 $^0$C, NO removal increases from 83.4% to 96.28% from 0.005 to 0.01M Fe/EDTA. At 0.02M Fe/EDTA initially the removal was found to be 78.0%. But after around 2200 s the solution losses its absorption capacity significantly and suddenly NO profile started to go upward until it stabilizes at NO removal of 29.22%. At 0.05M Fe/EDTA only after the mixing effect, the solution losses its absorption capacity and NO conversion is almost zero (0.4%).

From Figure 45, it can be clearly inferred that Fe$^{II}$-EDTA has antagonistic effect on persulfate solution at higher concentration similar to the antagonistic effect by Fe(II) ion shown in the work of Adewuyi and Sakyi (2013). The reasons given are probably similar, that is, at high Fe/EDTA concentration Fe(II) and Fe(II)EDTA may start to scavenge the $SO_4^{\bullet-}$ and/or $OH^{\bullet}$ radicals. Also, the sulfate/bisulfate ions and radicals that was helping the reversible binding of NO by reduced back the Fe(III)EDTA to Fe(II)EDTA also start to break down the iron-chelate compound entirely. That is why, whereas, at lower Fe/EDTA concentration persulfate and Fe(II)EDTA act synergistically to boost the NO removal to an unprecedented level, at higher Fe/EDTA concentration and higher temperature they act completely antagonistically to each other to destroy the absorption capacity of the solution.
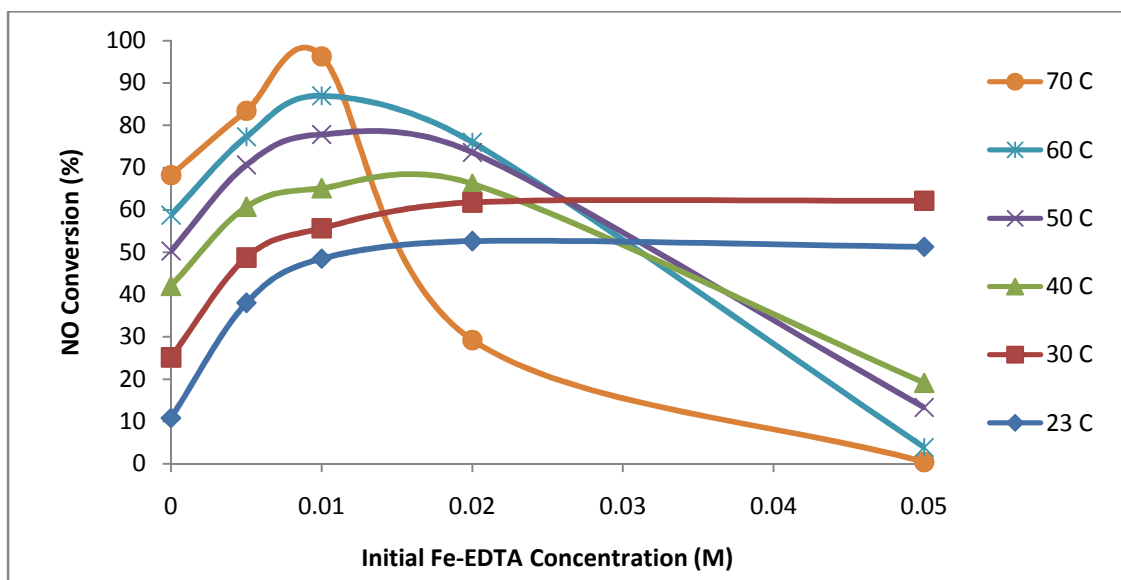
*Figure 46.* NO conversion with initial $Fe^{2+}$/EDTA concentration for different temperatures.
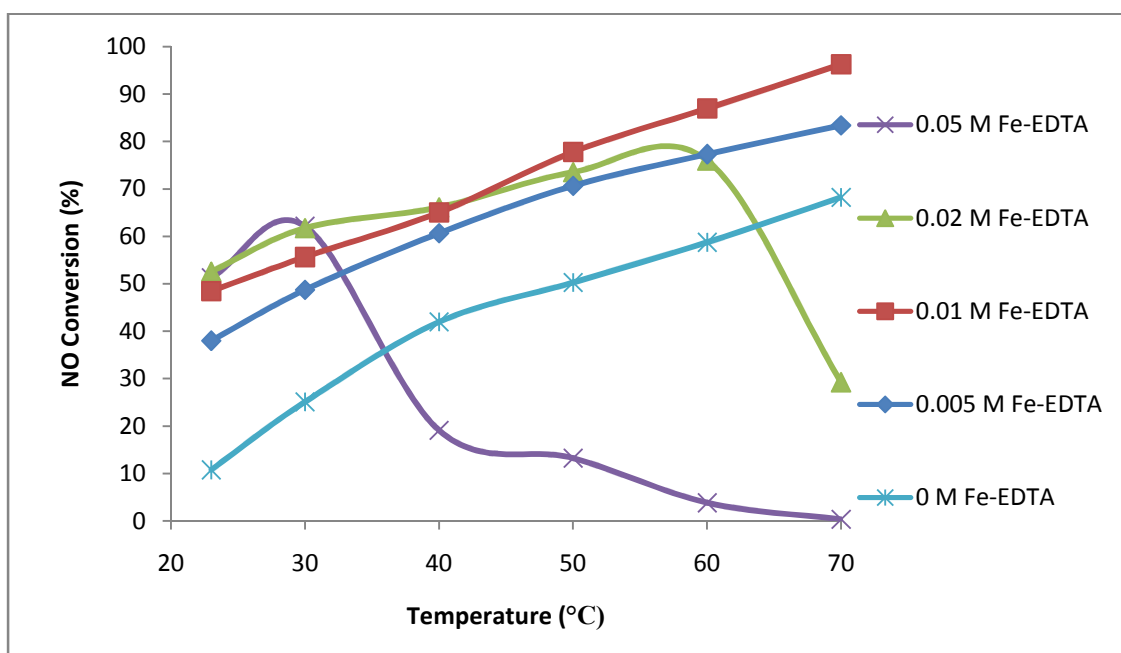


*Figure 47.* NO conversion with temperature for different initial $Fe^{2+}$/EDTA concentrations.

In Figure 46, NO conversion from the NO concentration profiles of Figure 45 is plotted against initial Fe/EDTA concentration (0 to 0.05M) for different temperature (23 to 70 $^0$C). The data for 0M Fe/EDTA (persulfate only system) is taken from the work of Khan and Adewuyi (2010). It is evident that NO conversion rises from 0 to 0.01M Fe/EDTA for all temperature.

After that NO conversion rises or stabilizes only at lower temperature where for higher

temperature NO conversion decreases at 0.02M Fe/EDTA. At 0.05M Fe/EDTA and higher

temperature NO conversion falls drastically as the solution losses its absorption capacity

completely.

In Figure 47, NO conversion is plotted against temperature (23 to 70 $^0$C) for different

initial Fe/EDTA concentration (0 to 0.05M). It can be assumed that the excess Fe/EDTA at

higher temperature started to consume the free radicals responsible for the persulfate absorption

and oxidation and rendered the whole persulfate chemistry ineffective. Also, at higher

temperature the sulfate/bi-sulfate ions that used to aid reversible binding of NO with Fe$^{II}$EDTA

by converting back Fe$^{III}$EDTA to Fe$^{III}$EDTA may destroy the ability of Fe-EDTA complex to

bind NO by separating iron from chelate. It can be concluded safely that optimum Fe/EDTA

concentration for 0.1M persulfate is 0.01M.

**4.3.6 Effect of pH on NO removal.** NO conversion profile is obtained for different pH

(2.0 to 12.0) for 0.1M persulfate and 0.01M Fe/EDTA concentration (optimum condition) at 40

and 50 $^0$C. It can be seen from both figure NO concentration behavior behave differently at

acidic and alkaline pH. At neutral and slightly below neutral range (~6.5) NO removal shows its

best efficiency. The concentration profile is almost perfectly flat after initial mixing effect

dipping and the solution sustain its absorption capability throughout the experiment.

It is worth saying that pH of the solution was stabilized by phosphate buffer solution for

pH 4.0, 8.0 and 10.0. The pH of the solution was around 6.0 after the addition of persulfate and

Fe/EDTA and few drops of 1.0N NaOH is enough to bring it near 7.0. After the experiment

(4000 s) the pH falls by 0.2-0.3 and the average persulfate was around 6.5. For pH 2.0 and 12.0

H$_2$SO$_4$ and NaOH solution were used respectively until the pH reach the desired pH. Apart from

the near neutral pH, the NO absorption profiles showed different behavior in acidic and alkaline region. In the acidic region (pH 2.0 and 4.0) after the initial dip for the mixing effect the removal was close to the near neutral NO removal. As time progressed, NO profiles went upward almost linearly and NO conversion falls accordingly. This effect was more conspicuous for pH 2.0 than pH 4.0.

In the alkaline region (pH 8.0, 10.0 and 12.0) NO conversion profiles showed different kind of behavior. After the initial dip NO profile rose to a very high value and then dropped as the time progressed but always stays over the profile at neutral pH. At pH 12.0 NO concentration profile never came back to close to near neutral level and NO conversion is very low for pH 12.0. Another important point is that at pH 12.0 NO conversion at 50 $^{0}$C is actually low compared to that of at 40 $^{0}$C.

Figure 49 is plotted from the NO concentration profiles shown in Figure 48 at 40 and 50 $^{0}$C and clearly illustrates behavior discussed in Figure 48. At pH 2.0 NO removal is quite low and at pH 4.0 it rises but best NO conversion is found at pH 6.5 (near neutral pH). After pH 6.5 in the alkaline region NO conversion started to decrease again and falls sharply after pH 10.0. At pH 12.0 NO removal for 50 $^{0}$C is actually below that of 40 $^{0}$C. This NO conversion graph clearly demonstrates that neutral of near neutral acidic pH (6.5) shows the best removal for a persulfate/Fe$^{2+}$/EDTA system.
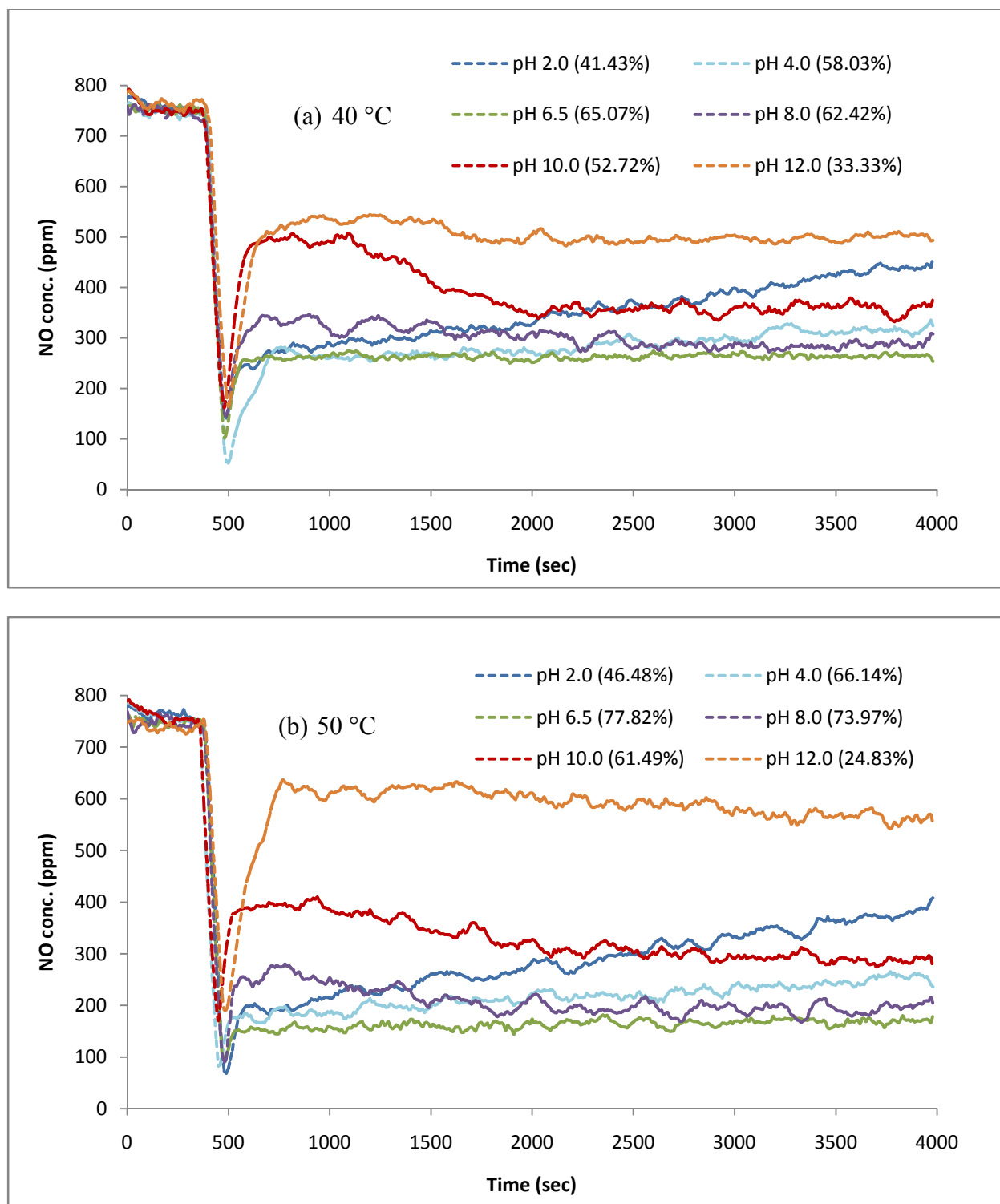
*Figure 48.* NO concentration profile for different starting pH (2.0-12.0) of the solution.
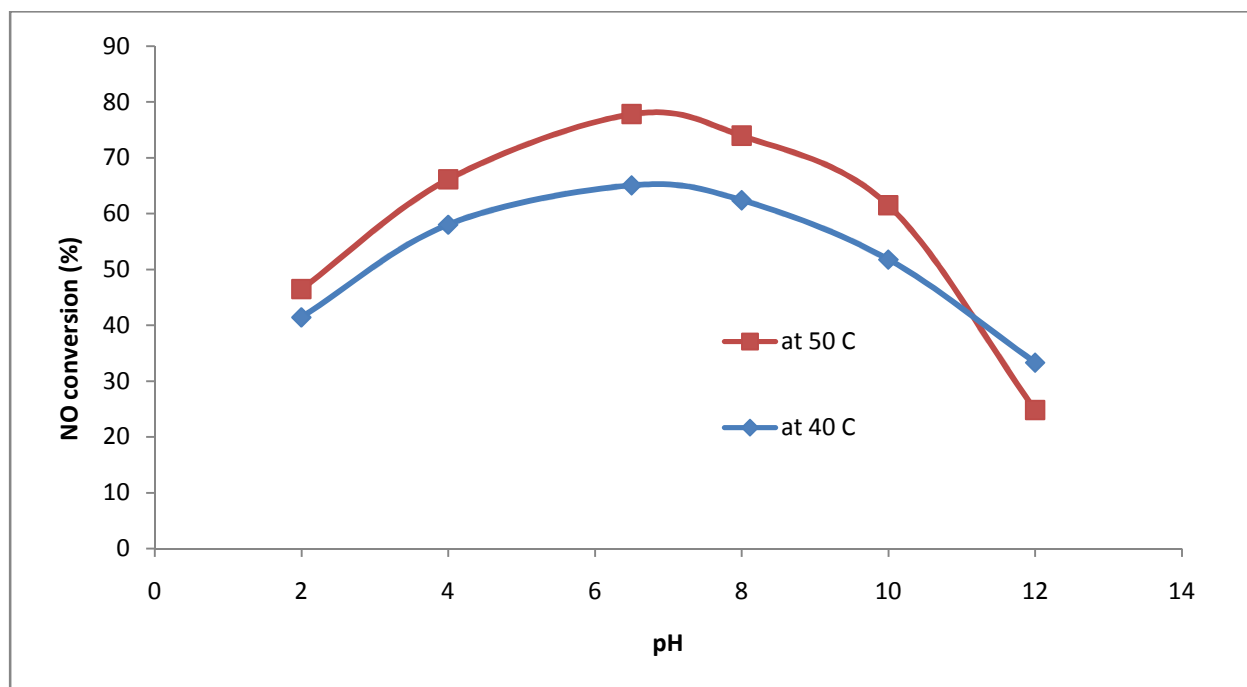
*Figure 49.* NO conversion for different pH (2.0-12.0).
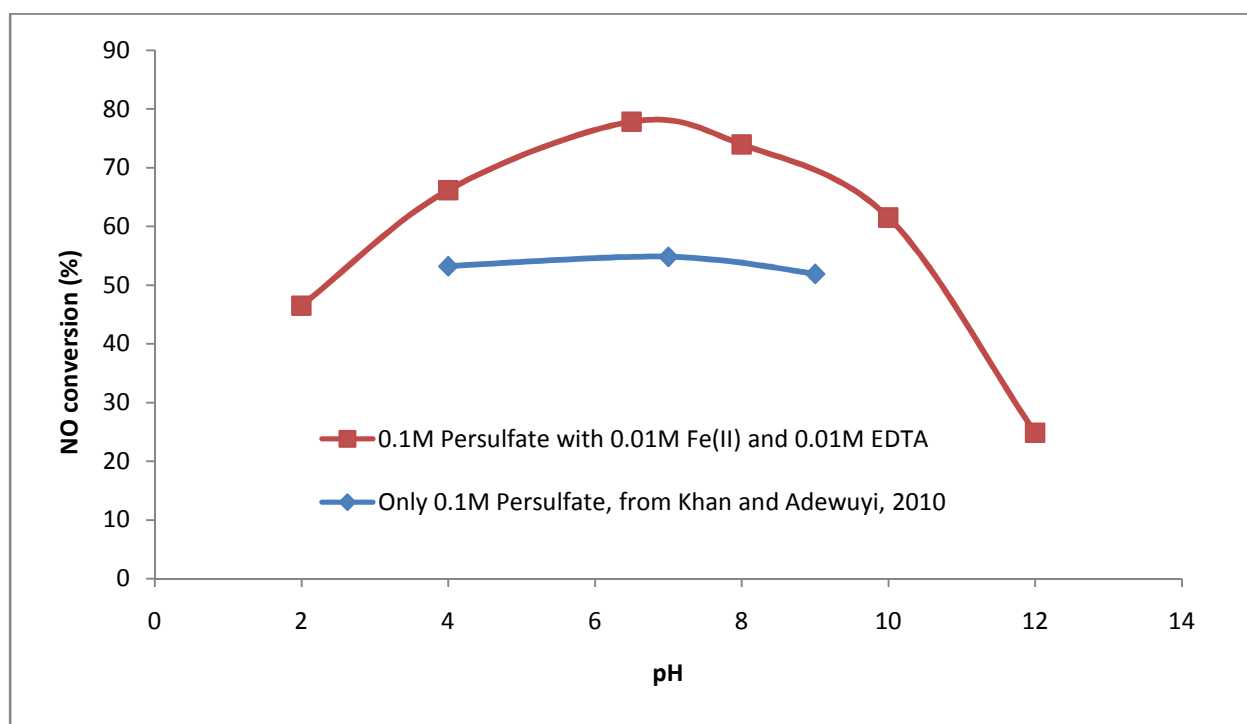


*Figure 50.* Comparative NO conversion for different pH with/without $Fe^{2+}$/EDTA.

The pH effect of this system is also compared to the pH effect for only persulfate system in Figure 50. It can be seen from Figure 50 that persulfate only system shows little variation in NO removal with the variation in pH but persulfate with Fe(II) and EDTA is very sensitive to pH change and shows the best removal at near neutral pH (~6.5).

**CHAPTER 5**

**Conclusion and Future Research**

**5.1 Conclusions**

The Aspen simulation for reactive distillation of bio oil was carried out and about 90%

conversions were found for some compositions of bio-oil. The binary and ternary interection

between the components were studied by using Aspen Property PLUS to observe the possible

location of azeotropes. Design specification and sensitivity analysis were also performed to

establish the effect of various parameters and to optimize the reactive distillation process.

Initially, 1 kmol/h of bio-oil is considered as only 70% acetic acid and 30 % water at 200 $^0$C and

1 MPa and the esterification reaction with stoichiometric amount of n-butanol was simulated and

the optimized reaction conversion was found to be 76.7%. Then, the composition of bio-oil was

considered 30% acetic acid, 20% formic acid, 20% propanoic acid and 30% water and overall

reaction conversion rose to 87.1%. When 10% phenol was added to the bio-oil as a constituent

overall reaction conversion saw another surge to 94% and the alcohol feed reduced considerably

due to the acid-phenol reaction that reduce the alcohol requirement for the esterification reaction.

The optimized number of stages was found to be around 45. Finally, a rate-based simulation was

performed using RATEFRAC module with bubble cap trays and structured packing and

considering 80% flooding in the trays. The overall reaction conversion and degree of separation

dropped by about 5% in this simulation as rate-based simulation is more complex and requires

additional constraints. The temperature and composition profiles for each of the simulation are

drawn along the column length. Sensitivity Analysis was done to optimize various input

parameters including ester flow-rate and water percent in the feed. The Aspen based simulation

done in this work could provide valuable insight in lab-scaled and industrial reactive distillation

column design and the reaction parameters calculated could play a vital role in catalyst design for reactive distillation of pyrolysis bio-oil.

The chemistry and removal rates of NO by combined aqueous solution of persulfate and Fe$^{II}$-EDTA were studied extensively and major reaction pathways proposed. The simultaneous and synergistic action of persulfate and Fe$^{II}$-EDTA for the removal of NO is demonstrated along with the temperature effects (23-70 $^{0}$C) in a bubble column reactor operated in semi-batch mode. The ratio at which Fe$^{2+}$ and EDTA should be added to the system prior to the beginning of the reaction was determined to be 1:1, and confirmed with most of the existing literature values. The optimum persulfate and Fe$^{2+}$/EDTA concentration were used 0.1 M and 0.01 M, respectively, and the removal of NO by combined persulfate and Fe$^{II}$-EDTA system was found to boost the NO conversion by almost 30% over Fe$^{2+}$ activated persulfate system at lower temperature and by 5% at the highest temperature. Thus, the combined persulfate and Fe$^{II}$-EDTA system results in a close to 100% removal efficiency at 70 $^{0}$C (inlet temperature for most flue gas system) where Fe$^{2+}$ activated persulfate system requires 90 $^{0}$C, thus significantly reducing the energy costs. Spectrophotometric determination of cationic species' (iron) was carried out to comprehend and develop the reaction mechanism very clearly and precisely. The presence of Fe$^{II}$-EDTA, was able to enhance persulfate activation at any temperature without suppressing the oxidation chemistry of persulfate resulting in a significant higher NO removal. Persulfate and other sulfur based ions were also able to boost Fe$^{II}$-EDTA chemistry by reducing back reaction products Fe$^{II}$-EDTA(NO) and Fe$^{III}$-EDTA to Fe$^{II}$-EDTA and driving the forward reaction in the reversible binding with NO. The combined persulfate and Fe$^{II}$-EDTA process also operated more effectively at near neutral pH region (pH 6.0-7.0). It can be considered a significant improvement over the operational and process difficulties associated in Fe$^{2+}$ activated persulfate

system where the operating pH was 2.5-3.5. In practical industrial processes, oxygen presents in the flue gases create a major obstacle in NO treatment by $Fe^{II}$-EDTA, as oxygen reacts with $Fe^{II}$-EDTA to produce inert $Fe^{III}$-EDTA. In presence of considerable amount of oxygen the process can slowed down or even halt. But the synergistic effects of persulfate over $Fe^{II}$-EDTA may be enough to remove oxygen enriched flue NO gases, as combined persulfate and $Fe^{II}$-EDTA solution can retain separation capability longer than $Fe^{II}$-EDTA silution. However, this needs to be verified by further follow up experiments.

## 5.2 Recommendations for Future Research

### 5.2.1 Recommendation of reactive distillation for esterification of pyrolysis bio-oil.

Future research for the reactive distillation for esterification of pyrolysis bio-oil is summarized below.

- Pyrolysis bio-oil includes significant amount of miscellaneous oxygenates (mainly hydroxyl-acetaldehyde). Since both hydroxyl and aldehyde functional group present in this compound the reaction scheme is quite complex for this compound. A simulation can be carried out including 10% hydroxyl-acetaldehyde with all other compounds already included in the simulation.

- Detail stage by stage mathematical modeling can be carried out for one or two compounds in simulated bio-oil. The mathematical equations can be solved by MATLAB using known values of reaction constants and thermodynamic constants and the result can be compared to the Aspen results.

- The short-cut RD modeling methods like ($\infty$-$\infty$)-analysis, ($\infty$-$N_{min}$)-analysis, bifurcation analysis can be carried out for a complete mathematical modeling to meet the ultimate

target of developing a simulation and model that can be readily applied in industries for reactive distillation of bio-oil.

**5.2.2 Recommendation of nitric oxide removal by combined aqueous persulfate and ferrous-EDTA systems.** Future works on nitric oxide removal by combined aqueous persulfate and ferrous-EDTA systems includes:

- A rigorous model can be developed with reaction kinetics and mass transfer phenomena based on proposed reaction scheme can be solved simultaneously by numerical method by predicting the kinetic and mass transfer parameters for that the model fits the experimental data by adjusting the parameters either Monte Carlo objective function or root mean square deviation (RMSD) (Cabrera Reina, Santos-Juanes Jordá, García Sánchez, Casas López, & Sánchez Pérez, 2012; Hrvoje Kusic et al., 2011). The estimated reaction constants and mass transfer coefficients will be pivotal in designing industrial scale NO removal by combined persulfate and ferrous-EDTA systems.

- NO gas concentration used in these experiments was 753 ppm. The experiments can be carried out at different NO concentrations to perform a kinetic analysis based on film theory of gas absorption to determine the enhancement factors, $E_i$ and Hatta number, $H\alpha$ to finally determine the overall pseudo reaction order and overall reaction constants.

- Industrial NO is often associated with $SO_2$ gas. Thus NO removal studies in presence of $SO_2$ are of immense importance. Previous studies suggested that presence of $SO_2$ actually enhance NO removal efficiency in NO removal by aqueous persulfate systems (Yusuf G. Adewuyi & Nana Y. Sakyi, 2013). Since, combined action of persulfate and ferrous-EDTA systems is being used for NO removal for the first time the experiments

should be perform in presence of $SO_2$ gas to observe the beneficial or detrimental effects of $SO_2$ on NO removal.

- Effects of other flue gas constituents, especially $O_2$ on the persulfate-$Fe^{II}$-EDTA-NO and persulfate-$Fe^{II}$-EDTA-NO-$SO_2$ systems can be observed and results can be compared to the similar studies available in the literature for other NO removal reagents.

- Design of Experimental studies can be performed using Taguchi statistical methods to observe the effects of different experimental parameters such as inlet gas concentrations, persulfate concentrations, ferrous-EDTA concentrations, temperature and pH on NO removal efficiency and finally to optimize the process parameters for optimum NO removal.

## References

Adewuyi, Y., He, X., Shaw, H., & Lolertpihop, W. (1999). Simultaneous absorption and oxidation of NO and $SO_2$ by aqueous solutions of sodium chlorite. Chem. Eng. Commun., 174(1), 21-51.

Adewuyi, Y., & Owusu, S. (2003). Aqueous absorption and oxidation of nitric oxide with oxone for the treatment of tail gases: Process feasibility, stoichiometry, reaction pathways, and absorption rate. Ind. Eng. Chem. Res, 42(17), 4084-4100.

Adewuyi, Y. G. (2005a). Sonochemistry in Environmental Remediation. 1. Combinative and Hybrid Sonophotochemical Oxidation Processes for the Treatment of Pollutants in Water. Environmental Science & Technology, 39(10), 3409-3420. doi: 10.1021/es049138y

Adewuyi, Y. G. (2005b). Sonochemistry in Environmental Remediation. 2. Heterogeneous Sonophotocatalytic Oxidation Processes for the Treatment of Pollutants in Water. Environmental Science & Technology, 39(22), 8557-8570. doi: 10.1021/es0509127

Adewuyi, Y. G., Khan, M. A., & Sakyi, N. Y. (2013). Kinetics and Modeling of the Removal of Nitric Oxide by Aqueous Sodium Persulfate Simultaneously Activated by Temperature and Fe2+. Industrial & Engineering Chemistry Research, 53(2), 828-839. doi: 10.1021/ie402801b

Adewuyi, Y. G., & Khan, N. E. (2012). Modeling the ultrasonic cavitation-enhanced removal of nitrogen oxide in a bubble column reactor. AIChE Journal, 58(8), 2397-2411. doi: 10.1002/aic.12751

Adewuyi, Y. G., & Owusu, S. O. (2006). Ultrasound-Induced Aqueous Removal of Nitric Oxide from Flue Gases: Effects of Sulfur Dioxide, Chloride, and Chemical Oxidant. The Journal of Physical Chemistry A, 110(38), 11098-11107. doi: 10.1021/jp0631634

Adewuyi, Y. G., & Sakyi, N. Y. (2013). Removal of Nitric Oxide by Aqueous Sodium Persulfate Simultaneously Activated by Temperature and Fe2+ in a Lab-scale Bubble Reactor. Industrial & Engineering Chemistry Research. doi: 10.1021/ie4025177

Adewuyi, Y. G., & Sakyi, N. Y. (2013). Simultaneous Absorption and Oxidation of Nitric Oxide and Sulfur Dioxide by Aqueous Solutions of Sodium Persulfate Activated by Temperature. Industrial & Engineering Chemistry Research, 52(33), 11702-11711. doi: 10.1021/ie401649s

Ahmad, M., Teel, A., Furman, O., Reed, J., & Watts, R. (2012). Oxidative and Reductive Pathways in Iron-Ethylenediaminetetraacetic Acid–Activated Persulfate Systems. Journal of Environmental Engineering, 138(4), 411-418. doi: doi:10.1061/(ASCE)EE.1943-7870.0000496

Bauen, A., Berndes, G., Junginger, M., Londo, M., Vuille, F., Ball, R., . . . Mozaffarian, H. (2009). Bioenergy–A Sustainable and Reliable Energy Source: A Review of Status and Prospects: International Energy Agency, Paris, France.

Baveja, K. K., Rao, D. S., & Sarkar, M. K. (1979). KINETICS OF ABSORPTION OF NITRIC OXIDE IN HYDROGEN PEROXIDE SOLUTIONS. Journal of Chemical Engineering of Japan, 12(4), 322-325.

Block, P. A., Brown, R. C., & Robinson, D. (2004). Novel Activation Technologies for Sodium Persulfate In Situ Chemical Oxidation. Fourth International Conference on the Remediation of Chlorinated and Recalcitrant Compounds, Monterey,CA.

Boehman, A. L. (2005). Biodiesel production and processing. [doi: 10.1016/j.fuproc.2004.11.001]. Fuel processing technology, 86(10), 1057-1058.

Bozbas, K. (2008). Biodiesel as an alternative motor fuel: Production and policies in the European Union. [doi: 10.1016/j.rser.2005.06.001]. Renewable and Sustainable Energy Reviews, 12(2), 542-552.

Brogren, C., Karlsson, H. T., & Bjerle, I. (1997). Absorption of NO in an alkaline solution of KMnO4. Chemical Engineering & Technology, 20(6), 396-402. doi: 10.1002/ceat.270200607

Byun, Y., Ko, K. B., Cho, M., Namkung, W., Lee, K., Shin, D. N., & Koh, D. J. (2009). Reaction Pathways of NO Oxidation by Sodium Chlorite Powder. Environmental Science & Technology, 43(13), 5054-5059. doi: 10.1021/es900152b

Cabrera Reina, A., Santos-Juanes Jordá, L., García Sánchez, J. L., Casas López, J. L., & Sánchez Pérez, J. A. (2012). Modelling photo-Fenton process for organic matter mineralization, hydrogen peroxide consumption and dissolved oxygen evolution. Applied Catalysis B: Environmental, 119–120(0), 132-138. doi: http://dx.doi.org/10.1016/j.apcatb.2012.02.021

Chen, L., Hsu, C.-H., & Yang, C.-L. (2005). Oxidation and absorption of nitric oxide in a packed tower with sodium hypochlorite aqueous solutions. Environmental Progress, 24(3), 279-288. doi: 10.1002/ep.10075

Chen, L., Lin, K.-F., & Yang, C.-L. (2011). Pilot study of absorption of NO2 with Na2S aqueous solutions. Environmental Progress & Sustainable Energy, 30(4), 632-639. doi: 10.1002/ep.10551

Chien, T.-W., & Chu, H. (2000). Removal of SO2 and NO from flue gas by wet scrubbing using an aqueous NaClO2 solution. Journal of Hazardous Materials, 80(1–3), 43-57. doi: http://dx.doi.org/10.1016/S0304-3894(00)00274-0

Chien, T. W., Hsueh, H. T., Chu, B. Y., & Chu, H. (2009). Absorption kinetics of NO from simulated flue gas using Fe(II)EDTA solutions. Process Safety and Environmental Protection, 87(5), 300-306. doi: http://dx.doi.org/10.1016/j.psep.2009.06.002

Chien, T. W. C. H. H. H. T. (2003). Kinetic Study on Absorption of SO[sub 2] and NO[sub X] with Acidic NaClO[sub 2] Solutions Using the Spraying Column. [Article]. Journal of Environmental Engineering, 129(11), 967. doi: 10.1061/(asce)0733-9372(2003)129:11(967)

Chu, H., Chien, T.-W., & Twu, B.-W. (2001). The absorption kinetics of NO in NaClO2/NaOH solutions. Journal of Hazardous Materials, 84(2–3), 241-252. doi: http://dx.doi.org/10.1016/S0304-3894(01)00215-1

Chu, H., Chien, T. W., & Li, S. Y. (2001). Simultaneous absorption of SO2 and NO from flue gas with KMnO4/NaOH solutions. Science of The Total Environment, 275(1–3), 127-135. doi: http://dx.doi.org/10.1016/S0048-9697(00)00860-3

Chu, H., Li, S. Y., & Chien, T. W. (1998). The absorption kinetics of no from flue gas in a stirred tank reactor with KMnO4/NaOH solutions. Journal of Environmental Science and Health, Part A, 33(5), 801-827. doi: 10.1080/10934529809376763

Demirbas, A. (2005). Biodiesel production from vegetable oils via catalytic and non-catalytic supercritical methanol transesterification methods. [doi: 10.1016/j.pecs.2005.09.001]. Progress in Energy and Combustion Science, 31(5–6), 466-487.

Demmink, J. F., & Beenackers, A. A. C. M. (1998). Gas Desulfurization with Ferric Chelates of EDTA and HEDTA: New Model for the Oxidative Absorption of Hydrogen Sulfide. Industrial & Engineering Chemistry Research, 37(4), 1444-1453. doi: 10.1021/ie970427n

Demmink, J. F., van Gils, I. C. F., & Beenackers, A. A. C. M. (1997). Absorption of Nitric Oxide into Aqueous Solutions of Ferrous Chelates Accompanied by Instantaneous Reaction. Industrial & Engineering Chemistry Research, 36(11), 4914-4927. doi: 10.1021/ie9702800

Deshwal, B. R., Lee, S. H., Jung, J. H., Shon, B. H., & Lee, H. K. (2008). Study on the removal of NOx from simulated flue gas using acidic NaClO2 solution. Journal of Environmental Sciences, 20(1), 33-38. doi: http://dx.doi.org/10.1016/S1001-0742(08)60004-2

Dimian, A. C., Bildea, C. S., Omota, F., & Kiss, A. A. (2009). Innovative process for fatty acid esters by dual reactive distillation. Computers & Chemical Engineering, 33(3), 743-750. doi: 10.1016/j.compchemeng.2008.09.020

Environmental Defense Fund. (2010) Retrieved 20 May, 2010, from http://www.edf.org/page.cfm?tagID=78

Gambardella, F., Alberts, M. S., Winkelman, J. G. M., & Heeres, E. J. (2005). Experimental and Modeling Studies on the Absorption of NO in Aqueous Ferrous EDTA Solutions. Industrial & Engineering Chemistry Research, 44(12), 4234-4242. doi: 10.1021/ie048767d

Gambardella, F., Winkelman, J. G. M., & Heeres, H. J. (2006). Experimental and modelling studies on the simultaneous absorption of NO and in aqueous iron chelate solutions. Chemical Engineering Science, 61(21), 6880-6891. doi: http://dx.doi.org/10.1016/j.ces.2006.07.003

Gao, L., Mi, X.-H., Zhou, Y., & Li, W. (2011). A pilot study on the regeneration of ferrous chelate complex in NOx scrubber solution by a biofilm electrode reactor. Bioresour Technol, 102(3), 2605-2609. doi: http://dx.doi.org/10.1016/j.biortech.2010.10.012

Gómez-Castro, F. I., Rico-Ramírez, V., Segovia-Hernández, J. G., & Hernández-Castro, S. (2011). Esterification of fatty acids in a thermally coupled reactive distillation column by the two-step supercritical methanol method. Chemical Engineering Research and Design, 89(4), 480-490. doi: 10.1016/j.cherd.2010.08.009

Gomez-Castro, F. I., Rico-Ramirez, V., Segovia-Hernandez, J. G., & Hernandez, S. (2010). Feasibility study of a thermally coupled reactive distillation process for biodiesel production. Chemical Engineering and Processing: Process Intensification, 49(3), 262-269. doi: 10.1016/j.cep.2010.02.002

Graboski, M. S., & McCormick, R. L. (1998). Combustion of fat and vegetable oil derived fuels in diesel engines. Progress in Energy and Combustion Science, 24(2), 125-164.

Guo, R.-t., Gao, X., Pan, W.-g., Ren, J.-x., Wu, J., & Zhang, X.-b. (2010). Absorption of NO into NaClO3/NaOH solutions in a stirred tank reactor. Fuel, 89(11), 3431-3435. doi: http://dx.doi.org/10.1016/j.fuel.2010.03.020

Harvey, A. E., Smart, J. A., & Amis, E. S. (1955). Simultaneous Spectrophotometric Determination of Iron(II) and Total Iron with 1,10-Phenanthroline. Analytical Chemistry, 27(1), 26-29. doi: 10.1021/ac60097a009

Hofele, J., van Velzen, D., Langenkamp, H., & Schaber, K. (1996). Absorption of NO in aqueous solutions of FeIINTA: determination of the equilibrium constant. Chemical Engineering and Processing: Process Intensification, 35(4), 295-300. doi: http://dx.doi.org/10.1016/0255-2701(95)04134-6

House, D. A. (1962). Kinetics and Mechanism of Oxidations by Peroxydisulfate. Chemical Reviews, 62(3), 185-203. doi: 10.1021/cr60217a001

Hutson, N. D., Krzyzynska, R., & Srivastava, R. K. (2008). Simultaneous Removal of SO2, NOX, and Hg from Coal Flue Gas Using a NaClO2-Enhanced Wet Scrubber. Industrial & Engineering Chemistry Research, 47(16), 5825-5831. doi: 10.1021/ie800339p

IEA. (2007). Potential Contribution of Bioenergy to the World's Future Energy Demand: International Energy Agency, Paris, France.

IEA. (2008). From 1st-to 2nd-Generation BioFuel Technologies. An Overview of Current Industry and R & D Activities.: International Energy Agency, Paris, France.

IEA. (2009). Bioenergy–A Sustainable and Reliable Energy Source: International Energy Agency, Paris, France.

IEA. (2010). World Energy Outlook 2010: International Energy Agency, Paris, France.

IPCC. (2007). IPCC Fourth Assessment Report. Cambridge, United Kingdom and New York, USA: IPCC.

IPCC. (2011). IPCC Special Report on Renewable Energy Sources and Climate Change Mitigation. Cambridge, United Kingdom and New York, NY, USA: IPCC.

Jantharasuk, A., Gani, R., Górak, A., & Assabumrungrat, S. (2011). Methodology for design and analysis of reactive distillation involving multielement systems. Chemical Engineering Research and Design, 89(8), 1295-1307. doi: http://dx.doi.org/10.1016/j.cherd.2011.04.016

Jin, D.-S., Deshwal, B.-R., Park, Y.-S., & Lee, H.-K. (2006). Simultaneous removal of SO2 and NO by wet scrubbing using aqueous chlorine dioxide solution. Journal of Hazardous Materials, 135(1–3), 412-417. doi: http://dx.doi.org/10.1016/j.jhazmat.2005.12.001

Junming, X., Jianchun, J., Yunjuan, S., & Yanju, L. (2008). Bio-oil upgrading by means of ethyl ester production in reactive distillation to remove water and to improve storage and fuel characteristics. Biomass and Bioenergy, 32(11), 1056-1061. doi: 10.1016/j.biombioe.2008.02.002

Khan, N. E., & Adewuyi, Y. G. (2010). Absorption and Oxidation of Nitric Oxide (NO) by Aqueous Solutions of Sodium Persulfate in a Bubble Column Reactor. Industrial & Engineering Chemistry Research, 49(18), 8749-8760. doi: 10.1021/ie100607u

Khan, N. E., & Adewuyi, Y. G. (2011). A new method of analysis of peroxydisulfate using ion chromatography and its application to the simultaneous determination of peroxydisulfate and other common inorganic ions in a peroxydisulfate matrix. Journal of Chromatography A, 1218(3), 392-397. doi: http://dx.doi.org/10.1016/j.chroma.2010.11.038

Kiss, A., Omota, F., Dimian, A., & Rothenberg, G. (2006). The heterogeneous advantage: biodiesel by catalytic reactive distillation. Topics in Catalysis, 40(1), 141-150. doi: 10.1007/s11244-006-0116-4

Kiss, A. A. (2011). Heat-integrated reactive distillation process for synthesis of fatty esters. Fuel Processing Technology, 92(7), 1288-1296. doi: 10.1016/j.fuproc.2011.02.003

Kiss, A. A., Dimian, A. C., & Rothenberg, G. (2007). Biodiesel by Catalytic Reactive Distillation Powered by Metal Oxides. Energy & Fuels, 22(1), 598-604. doi: 10.1021/ef700265y

Kiss, A. A., Omota, F., Dimian, A. C., & Rothenberg, G. (2006). The heterogeneous advantage: biodiesel by catalytic reactive distillation. Topics in Catalysis, 40(1-4), 141-150. doi: 10.1007/s11244-006-0116-4

Kusic, H., Peternel, I., Koprivanac, N., & Loncaric Bozic, A. (2010). Iron-Activated Persulfate Oxidation of an Azo Dye in Model Wastewater: Influence of Iron Activator Type on Process Optimization. Journal of Environmental Engineering, 137(6), 454-463. doi: 10.1061/(asce)ee.1943-7870.0000347

Kusic, H., Peternel, I., Ukic, S., Koprivanac, N., Bolanca, T., Papic, S., & Bozic, A. L. (2011). Modeling of iron activated persulfate oxidation treating reactive azo dye in water matrix. Chemical Engineering Journal, 172(1), 109-121. doi: http://dx.doi.org/10.1016/j.cej.2011.05.076

Latimer, W. M. (1952). The oxidation states of the elements and their potentials in aqueous solution (2nd Ed. ed.). New York, N.Y.: Prentice Hall.

Lee, Y.-C., Lo, S.-L., Kuo, J., & Lin, Y.-L. (2012). Persulfate oxidation of perfluorooctanoic acid under the temperatures of 20–40 °C. Chemical Engineering Journal, 198–199(0), 27-32. doi: http://dx.doi.org/10.1016/j.cej.2012.05.073

Li, H., & Fang, W. (1988). Kinetics of absorption of nitric oxide in aqueous iron(II)-EDTA solution. Industrial & Engineering Chemistry Research, 27(5), 770-774. doi: 10.1021/ie00077a009

Li, L., Abe, Y., Kanagawa, K., Shoji, T., Mashino, T., Mochizuki, M., . . . Miyata, N. (2007). Iron-chelating agents never suppress Fenton reaction but participate in quenching spin-trapped radicals. Analytica Chimica Acta, 599(2), 315-319. doi: http://dx.doi.org/10.1016/j.aca.2007.08.008

Li, W., Wu, C.-Z., & Shi, Y. (2006). Metal chelate absorption coupled with microbial reduction for the removal of NOx from flue gas. Journal of Chemical Technology & Biotechnology, 81(3), 306-311. doi: 10.1002/jctb.1394

Li, W., Wu, C.-Z., Zhang, S.-H., Shao, K., & Shi, Y. (2007). Evaluation of Microbial Reduction of Fe(III)EDTA in a Chemical Absorption-Biological Reduction Integrated NOx Removal System. Environmental Science & Technology, 41(2), 639-644. doi: 10.1021/es061757e

Liang, C., & Bruell, C. J. (2008). Thermally Activated Persulfate Oxidation of Trichloroethylene: Experimental Investigation of Reaction Orders. Industrial & Engineering Chemistry Research, 47(9), 2912-2918. doi: 10.1021/ie070820l

Liang, C., Bruell, C. J., Marley, M. C., & Sperry, K. L. (2004a). Persulfate oxidation for in situ remediation of TCE. I. Activated by ferrous ion with and without a persulfate–thiosulfate redox couple. Chemosphere, 55(9), 1213-1223. doi: http://dx.doi.org/10.1016/j.chemosphere.2004.01.029

Liang, C., Bruell, C. J., Marley, M. C., & Sperry, K. L. (2004b). Persulfate oxidation for in situ remediation of TCE. II. Activated by chelated ferrous ion. Chemosphere, 55(9), 1225-1233. doi: http://dx.doi.org/10.1016/j.chemosphere.2004.01.030

Liang, C., & Lee, I. L. (2008). In situ iron activated persulfate oxidative fluid sparging treatment of TCE contamination — A proof of concept study. Journal of Contaminant Hydrology, 100(3–4), 91-100. doi: http://dx.doi.org/10.1016/j.jconhyd.2008.05.012

Liang, C., Lee, I. L., Hsu, I. Y., Liang, C.-P., & Lin, Y.-L. (2008). Persulfate oxidation of trichloroethylene with and without iron activation in porous media. Chemosphere, 70(3), 426-435. doi: http://dx.doi.org/10.1016/j.chemosphere.2007.06.077

Liang, C., Liang, C.-P., & Chen, C.-C. (2009). pH dependence of persulfate activation by EDTA/Fe(III) for degradation of trichloroethylene. Journal of Contaminant Hydrology, 106(3–4), 173-182. doi: http://dx.doi.org/10.1016/j.jconhyd.2009.02.008

Liang, C., Wang, Z.-S., & Bruell, C. J. (2007). Influence of pH on persulfate oxidation of TCE at ambient temperatures. Chemosphere, 66(1), 106-113. doi: http://dx.doi.org/10.1016/j.chemosphere.2006.05.026

Littlejohn, D., & Chang, S. G. (1982). Kinetic study of ferrous nitrosyl complexes. The Journal of Physical Chemistry, 86(4), 537-540. doi: 10.1021/j100393a024

Littlejohn, D., & Chang, S. G. (1990). Reaction of ferrous chelate nitrosyl complexes with sulfite and bisulfite ions. Industrial & Engineering Chemistry Research, 29(1), 10-14. doi: 10.1021/ie00097a002

Liu, N., Lu, B.-H., Zhang, S.-H., Jiang, J.-L., Cai, L.-L., Li, W., & He, Y. (2012). Evaluation of Nitric Oxide Removal from Simulated Flue Gas by Fe(II)EDTA/Fe(II)citrate Mixed Absorbents. Energy & Fuels, 26(8), 4910-4916. doi: 10.1021/ef300538x

Liu, Y., Zhang, J., & Sheng, C. (2011). Study on the Kinetics of NO Removal from Simulated Flue Gas by a Wet Ultraviolet/H2O2 Advanced Oxidation Process. Energy & Fuels, 25(4), 1547-1552. doi: 10.1021/ef200086f

Long, X.-l., Xiao, W.-d., & Yuan, W.-k. (2005). Removal of Sulfur Dioxide and Nitric Oxide Using Cobalt Ethylenediamine Solution. Industrial & Engineering Chemistry Research, 44(4), 686-691. doi: 10.1021/ie049513v

Long, X.-l., Xin, Z.-l., Chen, M.-b., Xiao, W.-d., & Yuan, W.-k. (2007). Nitric oxide absorption into cobalt ethylenediamine solution. Separation and Purification Technology, 55(2), 226-231. doi: http://dx.doi.org/10.1016/j.seppur.2006.12.018

Long, X.-L., Yang, L., Chou, X.-w., Li, C., & Yuan, W.-k. (2013). Reduction of [Fe(III)EDTA]− catalyzed by activated carbon modified with ammonia solution. Environmental Progress & Sustainable Energy, n/a-n/a. doi: 10.1002/ep.11758

Maas, P. v. d., Brink, P. v. d., Klapwijk, B., & Lens, P. (2009). Acceleration of the Fe(III)EDTA− reduction rate in BioDeNOx reactors by dosing electron mediating compounds. Chemosphere, 75(2), 243-249. doi: http://dx.doi.org/10.1016/j.chemosphere.2008.04.043

Manconi, I., van der Maas, P., & Lens, P. N. L. (2006). Effect of sulfur compounds on biological reduction of nitric oxide in aqueous Fe(II)EDTA2− solutions. Nitric Oxide, 15(1), 40-49. doi: http://dx.doi.org/10.1016/j.niox.2005.11.012

Mi, X.-H., Gao, L., Zhang, S.-H., Cai, L.-L., & Li, W. (2009). A new approach for Fe(III)EDTA reduction in NOx scrubber solution using bio-electro reactor. Bioresour Technol, 100(12), 2940-2944. doi: http://dx.doi.org/10.1016/j.biortech.2009.01.046

Mohan, D., Pittman, C. U., & Steele, P. H. (2006). Pyrolysis of Wood/Biomass for Bio-oil:  A Critical Review. Energy & Fuels, 20(3), 848-889. doi: 10.1021/ef0502397

Mullen, C. A., & Boateng, A. A. (2008). Chemical Composition of Bio-oils Produced by Fast Pyrolysis of Two Energy Crops†. Energy & Fuels, 22(3), 2104-2109. doi: 10.1021/ef700776w

Narita, E., Sato, T., Shioya, T., Ikari, M., & Okabe, T. (1984). Formation of hydroxylamidobis(sulfate) ion by the absorption of nitric oxide in aqueous solutions of sodium sulfite containing iron(II)-EDTA complex. Industrial & Engineering Chemistry Product Research and Development, 23(2), 262-265. doi: 10.1021/i300014a018

Noshadi, I., Amin, N. A. S., & Parnas, R. S. (2012). Continuous production of biodiesel from waste cooking oil in a reactive distillation column catalyzed by solid heteropolyacid: Optimization using response surface methodology (RSM). Fuel, 94, 156-164. doi: 10.1016/j.fuel.2011.10.018

Osgerby, I. T. (2006). ISCO technology overview: Do you really understand the chemistry? In E. J. Calabrese, P. T. Kostecki & J. Dragun (Eds.), Contaminated soils, sediments and water (Vol. 10, pp. 287-308). New York, USA: Springer.

Owusu, S. O., & Adewuyi, Y. G. (2006). Sonochemical Removal of Nitric Oxide from Flue Gases. Industrial & Engineering Chemistry Research, 45(13), 4475-4485. doi: 10.1021/ie0509692

Pan, W.-g., Guo, R.-t., Zhang, X.-b., Ren, J.-x., Jin, Q., & Xu, H.-j. (2013). Absorption of NO by using aqueous KMnO4/(NH4)2CO3 solutions. Environmental Progress & Sustainable Energy, 32(3), 564-568. doi: 10.1002/ep.11658

Piché, S., Ribeiro, N., Bacaoui, A., & Larachi, F. ı. (2005). Assessment of a redox alkaline/iron-chelate absorption process for the removal of dilute hydrogen sulfide in air emissions. Chemical Engineering Science, 60(22), 6452-6461. doi: http://dx.doi.org/10.1016/j.ces.2005.04.065

Pinto, A. C., Guarieiro, L. L. N., Rezende, M. J. C., Ribeiro, N. M., Torres, E. A., Lopes, W. A., . . . Andrade, J. B. (2005). Biodiesel: An overview. Journal of the Brazilian Chemical Society, 16(6B), 1313-1330.

Ragauskas, A. J., Williams, C. K., Davison, B. H., Britovsek, G., Cairney, J., Eckert, C. A., . . . Tschaplinski, T. (2006). The path forward for biofuels and biomaterials. Science, 311(5760), 484-489. doi: 10.1126/science.1114736

Sada, E., Kumazawa, H., Hayakawa, N., Kudo, I., & Kondo, T. (1977). Absorption of NO in aqueous solutions of KMnO4. Chemical Engineering Science, 32(10), 1171-1175. doi: http://dx.doi.org/10.1016/0009-2509(77)80049-3

Sada, E., Kumazawa, H., & Hikosaka, H. (1986). A kinetic study of absorption of nitrogen oxide (NO) into aqueous solutions of sodium sulfite with added iron(II)-EDTA chelate. Industrial & Engineering Chemistry Fundamentals, 25(3), 386-390. doi: 10.1021/i100023a014

Sada, E., Kumazawa, H., Kudo, I., & Kondo, T. (1980). Individual and Simultaneous Absorption of Dilute NO and SO2 in Aqueous Slurries of MgSO3 with FeII-EDTA. Industrial & Engineering Chemistry Process Design and Development, 19(3), 377-382. doi: 10.1021/i260075a008

Sada, E., Kumazawa, H., & Machida, H. (1987). Oxidation kinetics of FeII-EDTA and FeII-NTA chelates by dissolved oxygen. Industrial & Engineering Chemistry Research, 26(7), 1468-1472. doi: 10.1021/ie00067a033

Sada, E., Kumazawa, H., & Takada, Y. (1984). Chemical reactions accompanying absorption of nitric oxide into aqueous mixed solutions of iron(II)-EDTA and sodium sulfite. Industrial & Engineering Chemistry Fundamentals, 23(1), 60-64. doi: 10.1021/i100013a012

Sada, E., Kumazawa, H., & Yoshikawa, Y. (1988). Simultaneous removal of NO and SO2 by absorption into aqueous mixed solutions. AIChE Journal, 34(7), 1215-1220. doi: 10.1002/aic.690340719

Steinigeweg, S., & Gmehling, J. (2004). Transesterification processes by combination of reactive distillation and pervaporation. Chemical Engineering and Processing: Process Intensification, 43(3), 447-456. doi: 10.1016/s0255-2701(03)00129-6

Stocker, M. (2008). Biofuels and biomass-to-liquid fuels in the biorefinery: Catalytic conversion of lignocellulosic biomass using porous materials. Angewandte Chemie International Edition, 47(48), 9200-9211. doi: 10.1002/anie.200801476

Suchecki, T. T., Mathews, B., & Kumazawa, H. (2005). Kinetic Study of Ambient-Temperature Reduction of FeIIIedta by Na2S2O4. Industrial & Engineering Chemistry Research, 44(12), 4249-4253. doi: 10.1021/ie0493006

Sweeney, A. J., & Liu, Y. A. (2001). Use of Simulation To Optimize NOx Abatement by Absorption and Selective Catalytic Reduction. Industrial & Engineering Chemistry Research, 40(12), 2618-2627. doi: 10.1021/ie0005295

Teramoto, M., Hiramine, S.-i., Shimada, Y., Sugimoto, Y., & Teranishi, H. (1977). Absorption of dilute nitric monoxide in aqueous solutions of Fe(II)-EDTA and mixed solutions of Fe(II)-EDTA and Na2SO3. Journal of Chemical Engineering of Japan, 11(6), 450-457.

Theegala, C. S., & Midgett, J. S. (2012). Hydrothermal liquefaction of separated dairy manure for production of bio-oils with simultaneous waste treatment. [Research Support, Non-U.S. Gov't

Research Support, U.S. Gov't, Non-P.H.S.]. Bioresour Technol, 107, 456-463. doi: 10.1016/j.biortech.2011.12.061

Thomas, D., & Vanderschuren, J. (1996). The absorption-oxidation of NOx with hydrogen peroxide for the treatment of tail gases. Chemical Engineering Science, 51(11), 2649-2654. doi: http://dx.doi.org/10.1016/0009-2509(96)00131-5

Thomas, D., & Vanderschuren, J. (1997). Modeling of NOx Absorption into Nitric Acid Solutions Containing Hydrogen Peroxide. Industrial & Engineering Chemistry Research, 36(8), 3315-3322. doi: 10.1021/ie960436g

Toor, S. S., Rosendahl, L., & Rudolf, A. (2011). Hydrothermal liquefaction of biomass: A review of subcritical water technologies. Energy, 36(5), 2328-2342. doi: 10.1016/j.energy.2011.03.013

Energy Independence and Security Act of 2007 (2007).

van der Maas, P., Harmsen, L., Weelink, S., Klapwijk, B., & Lens, P. (2004). Denitrification in aqueous FeEDTA solutions. Journal of Chemical Technology & Biotechnology, 79(8), 835-841. doi: 10.1002/jctb.1057

van der Maas, P., Peng, S., Klapwijk, B., & Lens, P. (2005). Enzymatic versus Nonenzymatic Conversions during the Reduction of EDTA-Chelated Fe(III) in BioDeNOx Reactors. Environmental Science & Technology, 39(8), 2616-2623. doi: 10.1021/es049222d

van der Maas, P., van den Bosch, P., Klapwijk, B., & Lens, P. (2005). NOx removal from flue gas by an integrated physicochemical absorption and biological denitrification process. Biotechnology and Bioengineering, 90(4), 433-441. doi: 10.1002/bit.20420

van der Maas, P., van den Brink, P., Utomo, S., Klapwijk, B., & Lens, P. (2006). NO removal in continuous BioDeNOx reactors: Fe(II)EDTA2− regeneration, biomass growth, and EDTA degradation. Biotechnology and Bioengineering, 94(3), 575-584. doi: 10.1002/bit.20859

Wang, L., Zhao, W., & Wu, Z. (2007). Simultaneous absorption of NO and SO2 by FeIIEDTA combined with Na2SO3 solution. Chemical Engineering Journal, 132(1−3), 227-232. doi: http://dx.doi.org/10.1016/j.cej.2006.12.030

Wei, J. C., Yu, P., Cai, B., Luo, Y. B., & Tan, H. Z. (2009). Absorption of NO in Aqueous NaClO2/Na2CO3 Solutions. Chemical Engineering & Technology, 32(1), 114-119. doi: 10.1002/ceat.200800479

Wu, Z. B., Wang, L., & Zhao, W. R. (2008). Kinetic study on regeneration of FeIIEDTA in the wet process of NO removal. Chemical Engineering Journal, 140(1−3), 130-135. doi: http://dx.doi.org/10.1016/j.cej.2007.09.025

Wubs, H. J., & Beenackers, A. A. C. M. (1993). Kinetics of the oxidation of ferrous chelates of EDTA and HEDTA in aqueous solution. Industrial & Engineering Chemistry Research, 32(11), 2580-2594. doi: 10.1021/ie00023a022

Xiu, S., Shahbazi, A., Shirley, V., & Cheng, D. (2010). Hydrothermal pyrolysis of swine manure to bio-oil: Effects of operating parameters on products yield and characterization of bio-oil. Journal of Analytical and Applied Pyrolysis, 88(1), 73-79. doi: 10.1016/j.jaap.2010.02.011

Yang, L., Chou, X.-w., Li, C., Long, X.-l., & Yuan, W.-k. (2013). Reduction of [Fe(III)EDTA]− catalyzed by activated carbon modified with KOH solution. Journal of Industrial and Engineering Chemistry, 19(3), 784-790. doi: http://dx.doi.org/10.1016/j.jiec.2012.10.017

Yu, H., Zhu, Q., & Tan, Z. (2012). Absorption of nitric oxide from simulated flue gas using different absorbents at room temperature and atmospheric pressure. Applied Energy, 93(0), 53-58. doi: http://dx.doi.org/10.1016/j.apenergy.2011.03.039

Zang, V., Kotowski, M., & Van Eldik, R. (1988). Kinetics and mechanism of the formation of FeII(edta)NO in the system FeII(edta)/NO/HONO/NO2- in aqueous solutions. Inorganic Chemistry, 27(19), 3279-3283. doi: 10.1021/ic00292a007

Zhang, S.-H., Li, W., Wu, C.-Z., Chen, H., & Shi, Y. (2007). Reduction of Fe(II)EDTA-NO by a newly isolated Pseudomonas sp. strain DN-2 in NO x scrubber solution. Applied Microbiology and Biotechnology, 76(5), 1181-1187. doi: 10.1007/s00253-007-1078-6

Zhang, S.-H., Mi, X.-H., Cai, L.-L., Jiang, J.-L., & Li, W. (2008). Evaluation of complexed NO reduction mechanism in a chemical absorption–biological reduction integrated NO x removal system. Applied Microbiology and Biotechnology, 79(4), 537-544. doi: 10.1007/s00253-008-1469-3

Zhu, H.-s., Mao, Y.-p., Yang, X.-j., Chen, Y., Long, X.-l., & Yuan, W.-k. (2010). Simultaneous absorption of NO and SO2 into FeII–EDTA solution coupled with the FeII–EDTA regeneration catalyzed by activated carbon. Separation and Purification Technology, 74(1), 1-6. doi: http://dx.doi.org/10.1016/j.seppur.2010.04.012

Speciation for Different Fe$^{2+}$/EDTA Concentration
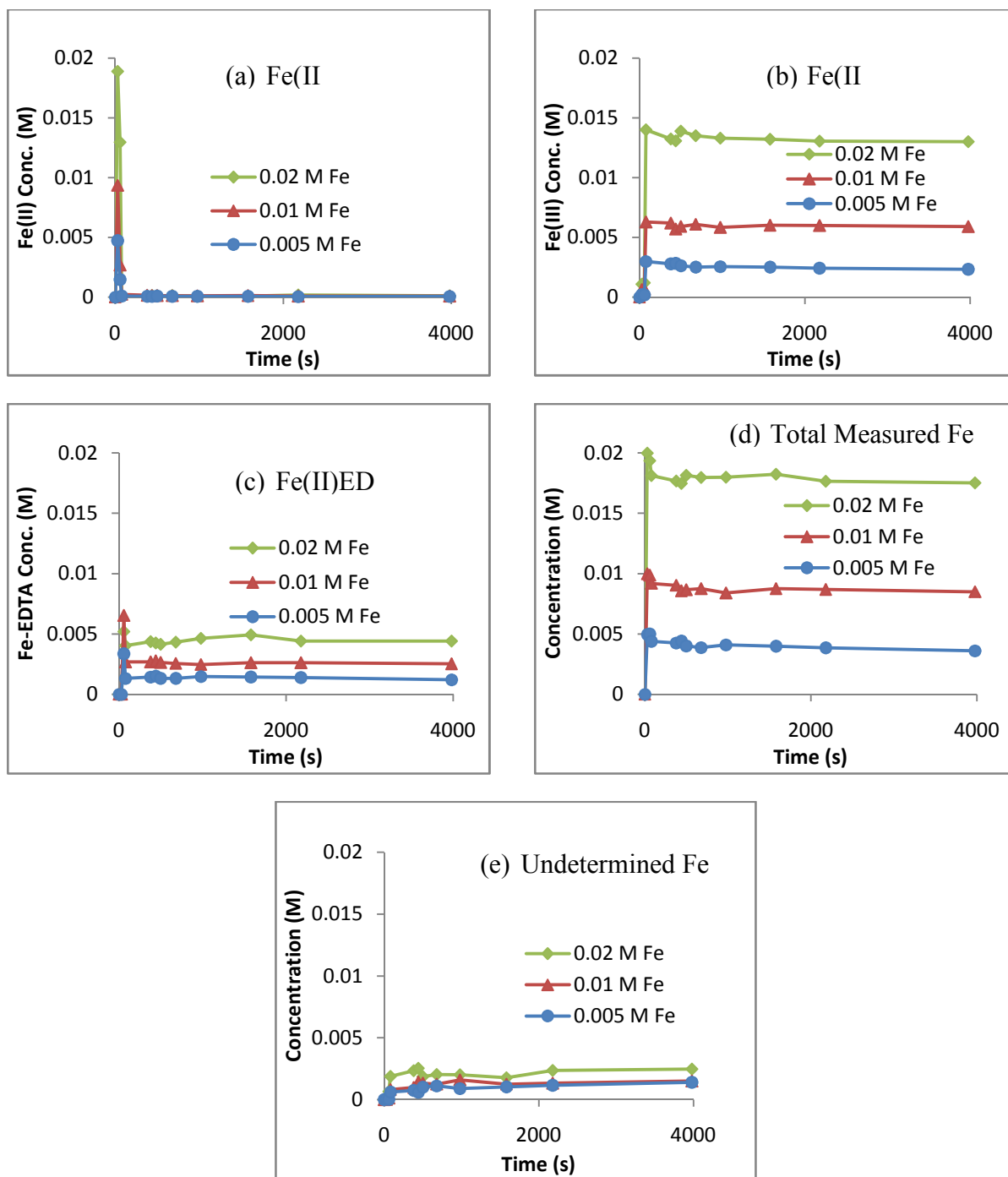


*Figure A.1.* Speciation plots for different iron components for different initial Fe$^{2+}$ concentration.
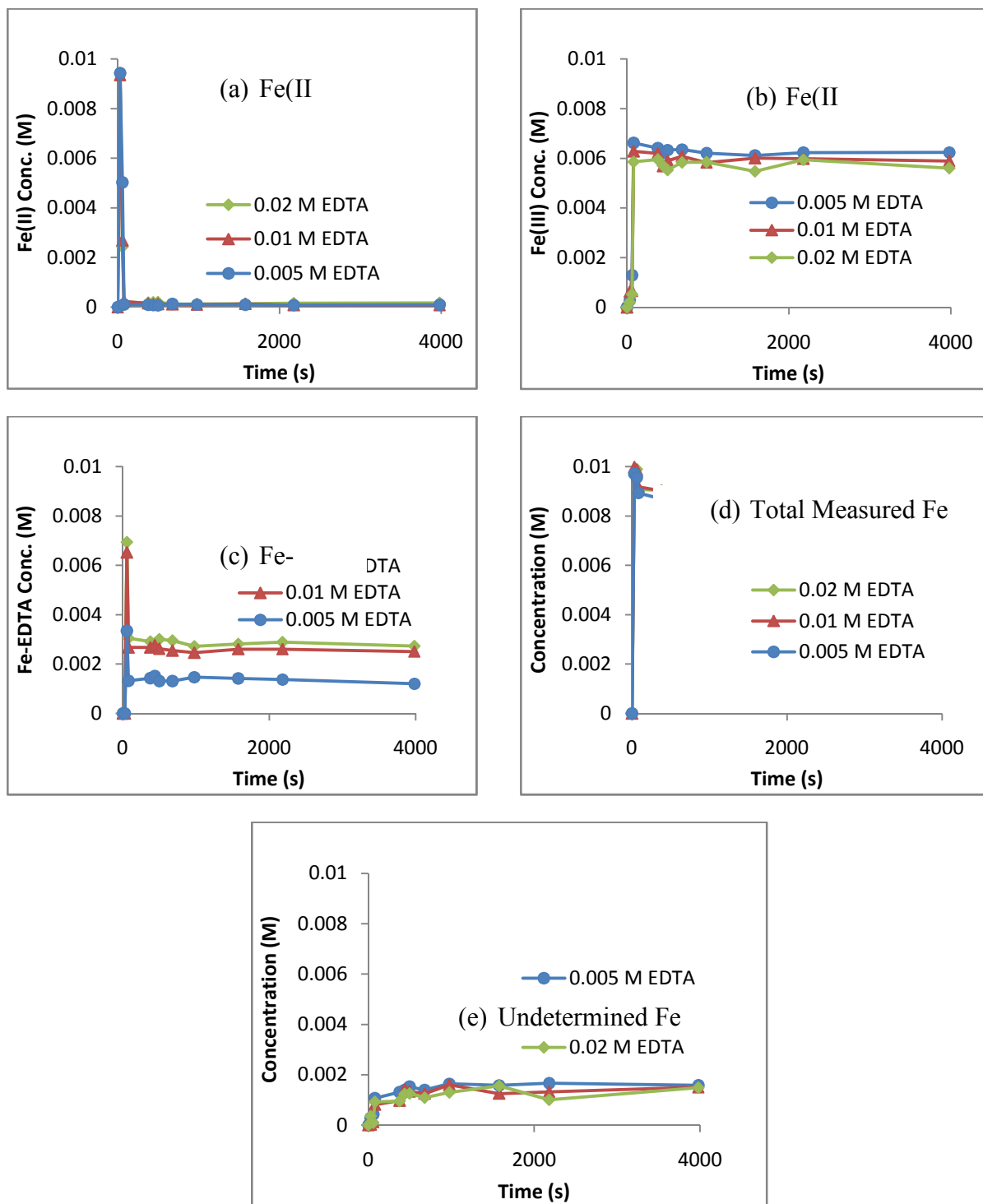
*Figure A.2.* Speciation plots for different iron components for different initial EDTA concentration.

Table A.1

*Iron Species Concentration for Different Initial $Fe^{2+}$ and/or EDTA Concentration at 50 $^0C$*

| Iron Species' | Types of Values | | Concentration (M) | | | | | |
|---|---|---|---|---|---|---|---|---|
| | | | $Fe^{2+}$ Only | $Fe^{2+}$ / EDTA | $Fe^{2+}$ Only | $Fe^{2+}$ / EDTA | $Fe^{2+}$ Only | $Fe^{2+}$ / EDTA |
| Initial Concentration | | | 0.005 | | 0.01 | | 0.02 | |
| $Fe^{2+}$ | Range | Minimum | 0 | 0.000052 | 0.00008 | 0.000076 | 0.00012 | 0.000081 |
| | | Maximum | $2.20 \times 10^{-5}$ | 0.000099 | 0.00022 | 0.00023 | 0.0005 | 0.00016 |
| | Steady State Average | | $1.05 \times 10^{-5}$ | 0.000078 | 0.00013 | 0.00012 | 0.00028 | 0.00011 |
| $Fe^{3+}$ | Range | Minimum | 0.00457 | 0.00264 | 0.00929 | 0.00569 | 0.01838 | 0.01279 |
| | | Maximum | 0.00494 | 0.00315 | 0.00986 | 0.00628 | 0.01918 | 0.01423 |
| | Steady State Average | | 0.00474 | 0.00286 | 0.00957 | 0.00599 | 0.01884 | 0.01337 |
| $Fe^{II}$-EDTA | Range | Minimum | - | 0.00111 | - | 0.00247 | - | 0.00468 |
| | | Maximum | | 0.00132 | | 0.00277 | | 0.0059 |
| | Steady State Average | | | 0.00123 | | 0.00261 | | 0.00518 |
| Total Measured Fe | Range | Minimum | 0.00458 | 0.00381 | 0.00937 | 0.0084 | 0.0185 | 0.01825 |
| | | Maximum | 0.00495 | 0.0045 | 0.01 | 0.00919 | 0.01956 | 0.0194 |
| | Steady State Average | | 0.00475 | 0.00416 | 0.00969 | 0.00872 | 0.01911 | 0.01866 |
| Undetermined Fe | Range | Minimum | 0.00005 | 0.005 | 0 | 0.00031 | 0.00022 | 0.0011 |
| | | Maximum | 0.00042 | 0.00119 | 0.00063 | 0.00151 | 0.00075 | 0.00175 |
| | Steady State Average | | 0.00025 | 0.00084 | 0.00031 | 0.00128 | 0.00044 | 0.00144 |

*Appendix B*

Concentration Profile for Long Period of Time
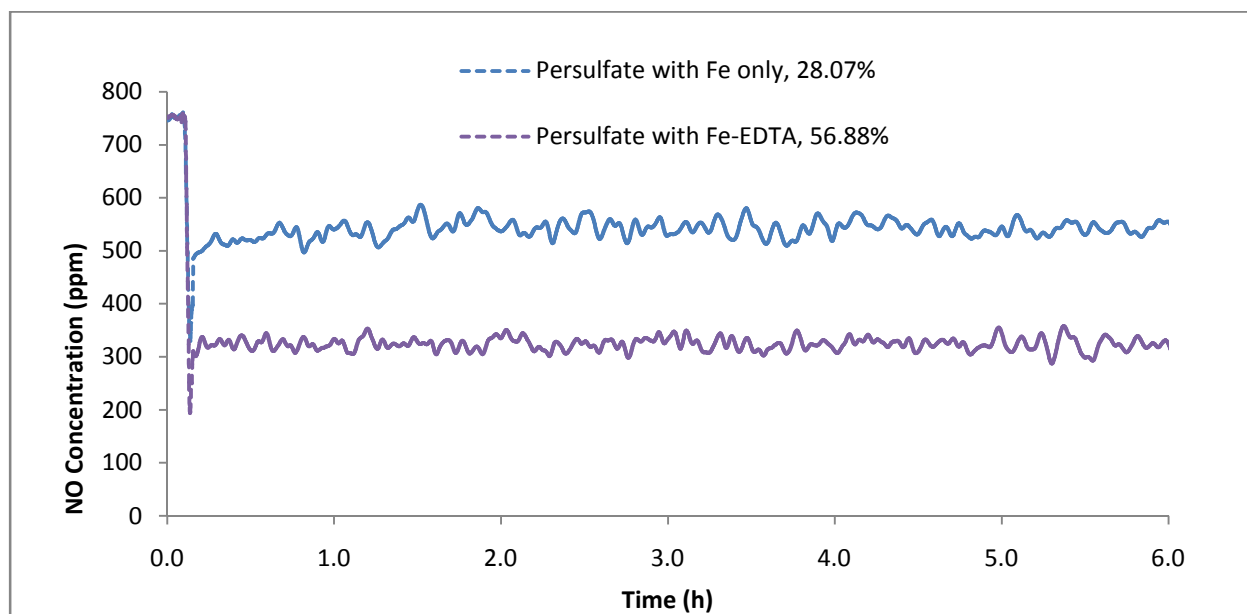


*Figure B.1.* NO concentration profile for 6.0 h for 0.1 M persulfate and 0.01 M $Fe^{2+}$ (with or without 0.01 M EDTA) at 30 $^0$C.

*Appendix C*

Complete Proposed Reaction Scheme

Table C.1

*Proposed Reaction Scheme for NO Removal by Combined Persulfate/Fe$^{II}$-EDTA Systems*

| # | Reaction | Kinetic Constant |
|---|----------|------------------|

**Persulfate Degradation and NO Consumption by Radicals**

1. $S_2O_8^{2-} + heat \xrightarrow{k_1} 2\ SO_4^{\bullet-}$
   $1.0 \times 10^{-7}\ (25°C)\ or\ 5.7$
   $\times 10^{-7} s^{-1} (70°C)$

2. $S_2O_8^{2-} + Fe^{2+} \xrightarrow{k_2} SO_4^{2-} + SO_4^{\bullet-} + Fe^{3+}$
   $1.7 - 2.7\ or\ 2.0$
   $\times 10^1\ M^{-1}s^{-1}\ (70°C)$

3. $SO_4^{\bullet-} + H_2O \xrightarrow{k_3} HSO_4^- + OH^\bullet$
   $6.6 \times 10^2 s^{-1}$

4. $OH^\bullet + NO \xrightarrow{k_4} H^+ + NO_2^-$
   $2 \times 10^{10}\ M^{-1}s^{-1}$

5. $S_2O_8^{2-} + NO_2^- \xrightarrow{k_5} SO_4^{2-} + SO_4^{\bullet-} + NO_2$

6. $NO_2^- + SO_4^{\bullet-} \xrightarrow{k_6} SO_4^{2-} + NO_2$
   $9.8 \times 10^8\ M^{-1}s^{-1}$

7. $NO_2 + OH^\bullet \xrightarrow{k_7} H^+ + NO_3^-$
   $4.5 \times 10^9\ M^{-1}s^{-1}$

**Direct Consumption of NO by Persulfate**

8. $S_2O_8^{2-} + NO + H_2O \xrightarrow{k_8} 2\ HSO_4^- + NO_2$

**Reaction of Ferrous Ion with Radicals**

9. $Fe^{2+} + OH^\bullet \xrightarrow{k_9} Fe^{3+} + OH^-$
   $3.2 \times 10^8\ M^{-1}s^{-1}$

10. $SO_4^{\bullet-} + Fe^{2+} \xrightarrow{k_{10}} Fe^{3+} + SO_4^{2-}$
    $4.6 \times 10^9\ or\ 3.0 \times 10^8\ M^{-1}s^{-1}$

Radical-Radical Interaction

11 $SO_4^{\bullet-} + OH^\bullet \xrightarrow{k_{11}} HSO_4^- + \dfrac{1}{2}O_2$ $\qquad$ $1 \times 10^{10}\ M^{-1}s^{-1}$

12 $SO_4^{\bullet-} + SO_4^{\bullet-} \xrightarrow{k_{12}} S_2O_8^{2-}$ $\qquad$ $7.6 \times 10^8\ M^{-1}s^{-1}$

13 $SO_4^{\bullet-} + S_2O_8^{2-} \xrightarrow{k_{13}} S_2O_8^{\bullet-} + SO_4^{2-}$ $\qquad$ $7.6 \times 10^8\ M^{-1}s^{-1}$
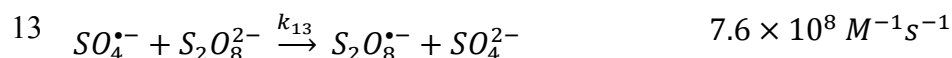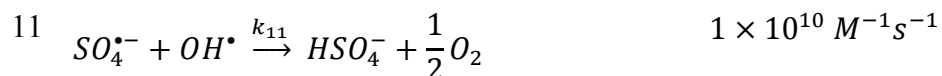
NO Absorption Reaction by $FeSO_4$

14 $FeSO_4 + NO \underset{}{\overset{K_{14}}{\Longleftrightarrow}} Fe(NO)SO_4$

Reaction of $Fe^{II}$-EDTA

15 $Fe^{2+} + EDTA^{2-} \overset{K_{15}}{\Longleftrightarrow} Fe^{II}\text{-}EDTA$

16 $Fe^{II}\text{-}EDTA + NO \overset{K_{16}}{\Longleftrightarrow} Fe^{II}\text{-}EDTA(NO)$ $\qquad$ $3.6 \times 10^6\ M^{-1}(25°C)$

17 $4Fe^{II}\text{-}EDTA + O_2 + H_2O \xrightarrow{k_{17}} 4Fe^{III}\text{-}EDTA$

$\qquad + 4OH^-$

18 $2Fe^{II}\text{-}EDTA + NO_2^- + 2H^+$

$\qquad \overset{K_{18}}{\Longleftrightarrow} Fe^{II}\text{-}EDTA(NO)$

$\qquad + Fe^{III}\text{-}EDTA + H_2O$

19 $2Fe^{II}\text{-}EDTA(NO) + 2Fe^{II}\text{-}EDTA + 4H^+$

$\qquad \xrightarrow{k_{19}} 4Fe^{III}\text{-}EDTA + N_2$

$\qquad + 2H_2O$

20 $2Fe^{II}\text{-}EDTA + 2NO_2 \overset{K_{20}}{\Longleftrightarrow} Fe^{II}\text{-}EDTA(NO)$
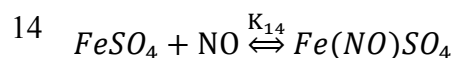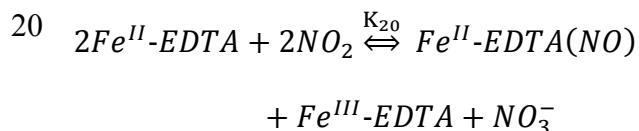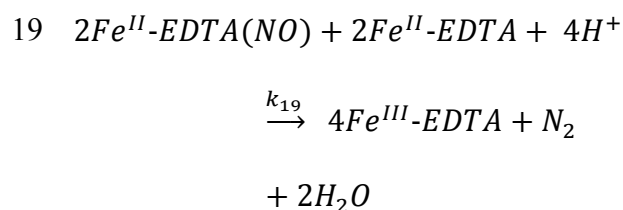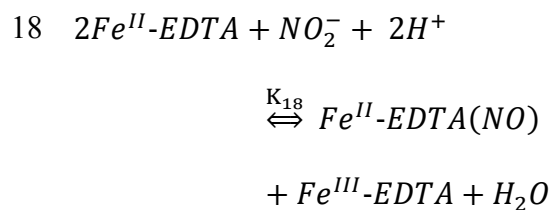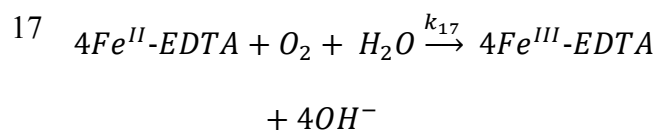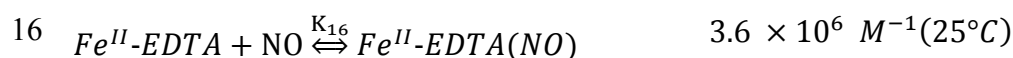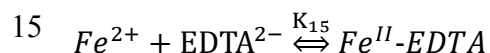
$\qquad + Fe^{III}\text{-}EDTA + NO_3^-$

Reaction Under Alkaline Condition

21 $\quad 2NO + 4OH^- \xrightarrow{k_{21}} 2NO_2^- + 2H_2O + 2e^-$

22 $\quad SO_4^{\bullet-} + OH^- \xrightarrow{k_{22}} SO_4^{2-} + OH^{\bullet}$ $\qquad\qquad\qquad\qquad 1.4 \times 10^7\ M^{-1}s^{-1}$

23 $\quad OH^{\bullet} + OH^- \overset{K_{23}}{\Leftrightarrow} O^{\bullet-} + H_2O$ (at very high pH)
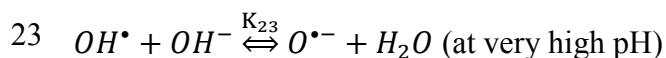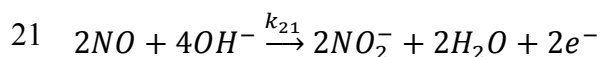
Reaction Under Acidic Condition

24 $\quad 2NO + 2H_2O \xrightarrow{k_{24}} 2HNO_2 + 2H^+ + 2e^-$

25 $\quad 3HNO_2 \overset{K_{25}}{\Leftrightarrow} NO_3^- + 2NO + H^+ + H_2O$

26 $\quad 3NO_2 + H_2O \xrightarrow{k_{26}} 2HNO_3 + NO$

27 $\quad NO + NO_2 + H_2O \overset{K_{27}}{\Leftrightarrow} 2HNO_2$

28 $\quad 2NO_2 + H_2O \overset{K_{28}}{\Leftrightarrow} 2H^+ + NO_3^- + NO_2^-$

29 $\quad S_2O_8^{2-} + H^+ \xrightarrow{k_{29}} HS_2O_8^-$

30 $\quad HS_2O_8^- \xrightarrow{k_{30}} SO_4 + HSO_4^-$

31 $\quad SO_4 \xrightarrow{k_{31}} SO_3 + \dfrac{1}{2}O_2$

32 $\quad S_2O_8^{2-} + H_2O \xrightarrow{H^+,k_{32}} H_2SO_5 + SO_4^{2-}$ (at very low pH)

Reduction of Fe$^{II}$-EDTA(NO) and Fe$^{III}$-EDTA

33 $\quad Fe^{III}\text{-}EDTA + SO_4^{\bullet-} \xrightarrow{k_{33}} Fe^{II}\text{-}EDTA + \dfrac{1}{2}S_2O_8^{2-}$

34 $\quad 3Fe^{II}\text{-}EDTA(NO) + 4HSO_4^- \xrightarrow{k_{34}} 3Fe^{II}\text{-}EDTA$

$$+ 2HON(SO_4)_2^{2-} + \dfrac{1}{2}N_2 + H_2O$$

35    $4Fe^{II}\text{-}EDTA(NO) + 4HSO_4^- \xrightarrow{k_{35}} 4Fe^{II}\text{-}EDTA$

$$+ \, 2HON(SO_4)_2^{2-} + N_2 + H_2N_2O_2$$

36    $H_2N_2O_2 \xrightarrow{k_{36}} N_2O + H_2O$

37    $2Fe^{II}\text{-}EDTA(NO) + SO_4^{\bullet-} \overset{K_{37}}{\Longleftrightarrow} 2Fe^{II}\text{-}EDTA$

$$+ \, (NO)_2SO_4^{2-}$$

38    $(NO)_2SO_4{}^{2-} \overset{K_{38}}{\Longleftrightarrow} N_2O + SO_4^{2-}$

39    $Fe^{II}\text{-}EDTA(NO) + SO_4^{\bullet-} \overset{K_{39}}{\Longleftrightarrow} Fe^{II}\text{-}EDTA(NO)SO_4^{2-}$

*Appendix D*

Modeling Formulation and Solution Approach

The rate of consumption of any species i in the bulk phase can be written as,

$$\frac{d(C_i)}{dt} = -r_i = -\sum_{m=1}^{n} r_m \tag{D.1}$$

Where $C_i$ and $r_i$ is the concentration and the sum of rates of reactions including the species i, respectively.

The rate of individual reaction $r_m$ is,

$$r_m = k_m \prod_{q=1}^{p} C_q{}^{a_q} \tag{D.2}$$

Where $k_m$ is the rate constant of the reaction and $a_q$ is the stoichiometric coefficient of species q.

According to the film theory, the rate of transfer of gaseous species *j* from gas to liquid is,

$$R_{A,j} = K_L a_j (\frac{P_j}{H_j} - C_j) \tag{D.3}$$

Where $K_L a$ is the mass-transfer coefficient, H is the Henry's law coefficient, $P_j$ is the partial pressure of j at the outlet. $P_j$ is calculated as $P_i = ppm_i \times 10^{-6} \times P_{total}$ where $P_{total}$ is 1 atm and $ppm_i$ is molar ppm. The material balance of j in the gas phase yields

$$\frac{V_G}{RT}\frac{dP_j}{dt} = \frac{Q}{RT}\left(P_j^{in} - P_j\right) - R_{A,j}V_L \tag{D.4}$$

Where $V_G$ is the gas holdup volume, R is the gas constant, T is the temperature, Q is the gas flow rate, $P_j^{in}$ is the partial pressure of j at the inlet, $V_L$ is the liquid volume. Therefore,

$$\frac{dP_j}{dt} = \frac{Q}{V_G}\left(P_j^{in} - P_j\right) - \frac{V_L RT}{V_G}K_L a_j(\frac{P_j}{H_j} - C_j) \tag{D.5}$$

The material balance for aqueous *i* yields the equation

$$\frac{dC_j}{dt} = K_L a_j \left(\frac{P_j}{H_j} - C_j\right) - r_j \tag{D.6}$$

The equations found in eqs D.1, D.5 and D.6 arise a system of equation that perfectly represents the absorption system. The equations can be solved simultaneously by numerical method by predicting the kinetic and mass transfer parameters for that the model fits the experimental data. The parameters can be adjusted by minimizing either Monte Carlo objective function given in equation D.7 or root mean square deviation (RMSD) in eq D.8.

$$J = \sum_{i=1}^{n} i \cdot \left(\sum_{k=1}^{m} \left|\frac{y_{exp,ki} - y_{mod,ki}}{y_{exp,ki}}\right|\right) \tag{D.7}$$

$$RMSD = \sqrt{\frac{1}{n}\sum_{i=1}^{n}(y_{exp,i} - y_{mod,i})^2} \tag{D.8}$$

*Appendix E*

MATLAB Code for Modeling Work

## E.1 Modeling with PSS Approach

### E.1.1 Code for 23 $^0$C

```matlab
function persulfate_mak_23_13rxn()

clc

 conc1=xlsread('\23deg.xls','e1','C:C');

 time30deg=xlsread('\23deg.xls','e1','D:D');

 conc2=xlsread('\23deg.xls','e1','F:F');

%   time50deg=xlsread('\70deg.xls','e1','D:D');

 conc3=xlsread('\23deg.xls','e1','G:G');

%  time60deg=xlsread('\70deg.xls','e1','D:D');

 conc4=xlsread('\23deg.xls','e1','I:I');

%  time40deg=xlsread('\70deg.xls','e1','D:D');

 figure(1)

 plot(time30deg, conc3,'r');

 hold on

%legend ('Experimental');

figure(1)

 hold on

 plot(time30deg, conc4,'r');

 figure(1)

 hold on
```

```matlab
plot(time30deg, conc2,'r');

figure(1)

 hold on

E1=plot(time30deg, conc1,'r');

%Constants

 R = 8.314;      %universal gas constant, J/mol.K

 H = 5.223e4*1;    %henry's law constant, Pa/(mol/m^3)

 %Parameters

 q = 1.667e-6*1;   %gas flow rate, m^3/s

 V_gas = 1.96e-5*1; %gas holdup, m^3, based on 1 cm height increase

 V_liq = 1e-3;   %liquid volume, m^3

 T = 296;       %temperature, K

 P = 101325;     %pressure, Pa

 y_NO_in = 1010e-6; %mol fraction of NO, converted from mol fraction of 0.105%

 V_1 = 1e-4*1;   %head space

 V_2 = 1e-4*0;

 %parameters to be determined

 kLa = 1.96e-2;  %mass transfer coefficient, s^-1 1.6, .48

 k_1 = 1.18e-8;

 k_2 = 2.59e-4;

 k_3 = 1.46e-2;

 k_4 = 2.53e-3;

 k_5 = 1.22e-8;
```

```matlab
k_6 = 1.36e-7;

k_7 = 5.23e-2;

k_sr= 6.24e-5;

function dydt=odefun(t, y)

    dydt = zeros(3,1);

    dydt(1) = kLa*P/H*y(2) – kLa*y(1) – 2*y(4)*k_1-k_2*y(1)*y(4)-

k_3*y(4)*y(5)+k_4*y(5)+k_5+k_6+k_sr*y(1);  %C_NO_liq

    dydt(2) = q/V_gas*y_NO_in – y(2)*(q/V_gas)  -

(y(2)+y_NO_in)*0.5*(kLa*V_liq*R*T/(H*V_gas)) …

        + kLa*V_liq*R*T/(P*V_gas)*y(1)*1; %y_NO_gas

    dydt(3) = q/V_1*(y(2) – y(3));

    dydt(4) = -k_1*y(4)-k_2*y(1)*y(4)-k_3*y(4)*y(5)+k_6;

    dydt(5) = -k_3*y(4)*y(5)-(k_4+k_7)*y(5); %ferrous ion

    dydt(6) = 2*k_1*y(4);   %product of reaction 3

    %dydt(7) = 8*(y_S2O8_ini – y(4)) + q/V_liq*(y_NO_in – y(2))/(R*T);   %oxygen balance

%       dydt(8) = 2*(y_S2O8_ini – y(4)) – 2*y(5) – y(6);   %sulfate balance

    %dydt(5) = q/V_1*(y(2)-y(5));    %volume effect

end

tspan = [0 3200];

M = [1 0 0 0 0 0% 0 0

    0 1 0 0 0 0% 0 0

    0 0 1 0 0 0% 0 0

    0 0 0 1 0 0% 0 0
```

```
        0 0 0 0 1 0% 0 0

        0 0 0 0 0 1];% 0 0

        %0 0 0 0 0 0 0 0

        %0 0 0 0 0 0 0 1];

    options = odeset('Refine', 1, 'NonNegative', [1]);

%    y_S2O8_ini = 0.01*1e3;  %concentration of persulfate, mol/m^3

%    y0 = [0 y_NO_in y_NO_in y_S2O8_ini 0 0];% 0 0];

%    [t, y]=ode45(@odefun, tspan, y0, options);

%    figure(1);

%    t = t + 600;

%    plot(t,y(:,2)*1e6);

% %   plot(t,y(:,4)/y_S2O8_ini);

%    hold on

    y_Fe_ini = 0.01*1e3;  %concentration of persulfate, mol/m^3

    y_S2O8_ini = 0.02*1e3;  %concentration of persulfate, mol/m^3

    y0 = [0 y_NO_in y_NO_in y_S2O8_ini y_Fe_ini 0];% 0 0];

    [t, y]=ode45(@odefun, tspan, y0, options);

    figure(1);

    t = t + 600;

    E2=plot(t,y(:,2)*1e6);

%   plot(t,y(:,4)/y_S2O8_ini);

    y(end,2)*1e6

    y_S2O8_ini = 0.05*1e3;  %concentration of persulfate, mol/m^3
```

```matlab
y0 = [0 y_NO_in y_NO_in y_S2O8_ini y_Fe_ini 0];% 0 0];

[t, y]=ode45(@odefun, tspan, y0, options);

figure(1);

t = t + 600;

plot(t,y(:,2)*1e6);
%   plot(t,y(:,4)/y_S2O8_ini);

y(end,2)*1e6

y_S2O8_ini = 0.1*1e3;  %concentration of persulfate, mol/m^3

y0 = [0 y_NO_in y_NO_in y_S2O8_ini y_Fe_ini 0];% 0 0];

[t, y]=ode45(@odefun, tspan, y0, options);

figure(1);

t = t + 600;

plot(t,y(:,2)*1e6);
%   plot(t,y(:,4)/y_S2O8_ini);

y(end,2)*1e6

y_S2O8_ini = 0.2*1e3;  %concentration of persulfate, mol/m^3

y0 = [0 y_NO_in y_NO_in y_S2O8_ini y_Fe_ini 0];% 0 0];

[t, y]=ode45(@odefun, tspan, y0, options);

figure(1);

t = t + 600;

plot(t,y(:,2)*1e6);
%   plot(t,y(:,4)/y_S2O8_ini);

y(end,2)*1e6
```

```matlab
  xlabel('Time(s)')

  ylabel('NO Concentration (ppm)')

  legend([E1 E2],'Experimental', 'Model')

end
```

### E.1.2 Code for 30 $^0$C

```matlab
    function persulfate_mak_30_13rxn()

  clc

   conc1=xlsread('\30deg.xls','e1','C:C');

    time30deg=xlsread('\30deg.xls','e1','D:D');

   conc2=xlsread('\30deg.xls','e1','F:F');

%    time50deg=xlsread('\30deg.xls','e1','D:D');

   conc3=xlsread('\30deg.xls','e1','G:G');

%   time60deg=xlsread('\30deg.xls','e1','D:D');

   conc4=xlsread('\30deg.xls','e1','I:I');

%    time40deg=xlsread('\40deg.xls','e1','D:D');

   figure(1)

   plot(time30deg, conc3,'r');

    hold on

figure(1)

  hold on

 plot(time30deg, conc4,'r');

 figure(1)

  hold on
```

```matlab
plot(time30deg, conc2,'r');

figure(1)

 hold on

E1=plot(time30deg, conc1,'r');

%Constants

 R = 8.314;     %universal gas constant, J/mol.K

 H = 5.223e4*1;   %henry's law constant, Pa/(mol/m^3)

 %Parameters

 q = 1.667e-6*1;   %gas flow rate, m^3/s

 V_gas = 1.96e-5*1; %gas holdup, m^3, based on 1 cm height increase

 V_liq = 1e-3;   %liquid volume, m^3

 T = 303;       %temperature, K

 P = 101325;     %pressure, Pa

 y_NO_in = 1010e-6; %mol fraction of NO, converted from mol fraction of 0.105%

 V_1 = 1e-4*1;   %head space

 V_2 = 1e-4*0;

 %parameters to be determined

 kLa = 2.12e-2;  %mass transfer coefficient, s^-1 1.6, .48

 k_1 = 1.32e-8;

 k_2 = 3.89e-4;

 k_3 = 3.05e-2;

 k_4 = 3.96e-3;

 k_5 = 1.92e-8;
```

```matlab
k_6 = 2.12e-7;

k_7 = 7.65e-2;

k_sr= 8.40e-5;

function dydt=odefun(t, y)

    dydt = zeros(3,1);

        dydt(1) = kLa*P/H*y(2) - kLa*y(1) - 2*y(4)*k_1-k_2*y(1)*y(4)-
k_3*y(4)*y(5)+k_4*y(5)+k_5+k_6+k_sr*y(1);  %C_NO_liq


        dydt(2) = q/V_gas*y_NO_in - y(2)*(q/V_gas)  -
(y(2)+y_NO_in)*0.5*(kLa*V_liq*R*T/(H*V_gas)) ...

        + kLa*V_liq*R*T/(P*V_gas)*y(1)*1; %y_NO_gas

    dydt(3) = q/V_1*(y(2) - y(3));

    dydt(4) = -k_1*y(4)-k_2*y(1)*y(4)-k_3*y(4)*y(5)+k_6;

    dydt(5) = -k_3*y(4)*y(5)-(k_4+k_7)*y(5); %ferrous ion

    dydt(6) = 2*k_1*y(4);   %product of reaction 3

    %dydt(7) = 8*(y_S2O8_ini - y(4)) + q/V_liq*(y_NO_in - y(2))/(R*T);   %oxygen balance

%      dydt(8) = 2*(y_S2O8_ini - y(4)) - 2*y(5) - y(6);   %sulfate balance

    %dydt(5) = q/V_1*(y(2)-y(5));    %volume effect

end

tspan = [0 3200];

M = [1 0 0 0 0 0% 0 0

    0 1 0 0 0 0% 0 0

    0 0 1 0 0 0% 0 0
```

```matlab
        0 0 0 1 0 0%0 0

        0 0 0 0 1 0%0 0

        0 0 0 0 0 1];%0 0

        %0 0 0 0 0 0 0 0

        %0 0 0 0 0 0 0 1];

    options = odeset('Refine', 1, 'NonNegative', [1]);
%    y_S2O8_ini = 0.01*1e3;  %concentration of persulfate, mol/m^3

%    y0 = [0 y_NO_in y_NO_in y_S2O8_ini 0 0];% 0 0];

%    [t, y]=ode45(@odefun, tspan, y0, options);

%    figure(1);

%    t = t + 600;

%    plot(t,y(:,2)*1e6);

% %    plot(t,y(:,4)/y_S2O8_ini);

%    hold on

    y_Fe_ini = 0.01*1e3;  %concentration of persulfate, mol/m^3

    y_S2O8_ini = 0.02*1e3;  %concentration of persulfate, mol/m^3

    y0 = [0 y_NO_in y_NO_in y_S2O8_ini y_Fe_ini 0];% 0 0];

    [t, y]=ode45(@odefun, tspan, y0, options);

    figure(1);

    t = t + 600;

    E2=plot(t,y(:,2)*1e6);

%    plot(t,y(:,4)/y_S2O8_ini);

    y(end,2)*1e6
```

```
y_S2O8_ini = 0.05*1e3;  %concentration of persulfate, mol/m^3

y0 = [0 y_NO_in y_NO_in y_S2O8_ini y_Fe_ini 0];% 0 0];

[t, y]=ode45(@odefun, tspan, y0, options);

figure(1);

t = t + 600;

plot(t,y(:,2)*1e6);
%    plot(t,y(:,4)/y_S2O8_ini);

y(end,2)*1e6

y_S2O8_ini = 0.1*1e3;  %concentration of persulfate, mol/m^3

y0 = [0 y_NO_in y_NO_in y_S2O8_ini y_Fe_ini 0];% 0 0];

[t, y]=ode45(@odefun, tspan, y0, options);

figure(1);

t = t + 600;

plot(t,y(:,2)*1e6);
%    plot(t,y(:,4)/y_S2O8_ini);

y(end,2)*1e6

y_S2O8_ini = 0.2*1e3;  %concentration of persulfate, mol/m^3

y0 = [0 y_NO_in y_NO_in y_S2O8_ini y_Fe_ini 0];% 0 0];


[t, y]=ode45(@odefun, tspan, y0, options);

figure(1);

t = t + 600;

plot(t,y(:,2)*1e6);
```

```
%    plot(t,y(:,4)/y_S2O8_ini);

    y(end,2)*1e6

    xlabel('Time(s)')

    ylabel('NO Concentration (ppm)')

  legend([E1 E2],'Experimental', 'Model')

end
```

### E.1.3 Code for 40 $^0$C

```
        function persulfate_mak_40_13rxn()

    clc

     conc1=xlsread('\40deg.xls','e1','C:C');

     time30deg=xlsread('\40deg.xls','e1','D:D');

    conc2=xlsread('\40deg.xls','e1','F:F');

%    time50deg=xlsread('\40deg.xls','e1','D:D');

    conc3=xlsread('\40deg.xls','e1','G:G');

%   time60deg=xlsread('\40deg.xls','e1','D:D');

    conc4=xlsread('\40deg.xls','e1','I:I');

%    time40deg=xlsread('\40deg.xls','e1','D:D');

    figure(1)

    plot(time30deg, conc3,'r');

    hold on

%length (time30deg),length(conc3)

figure(1)

    hold on
```

```matlab
plot(time30deg, conc4,'r');

figure(1)

 hold on

plot(time30deg, conc2,'r');

figure(1)

 hold on

E1=plot(time30deg, conc1,'r');

%Constants

 R = 8.314;      %universal gas constant, J/mol.K

 H = 5.223e4*1;    %henry's law constant, Pa/(mol/m^3)

 %Parameters

 q = 1.667e-6*1;   %gas flow rate, m^3/s

 V_gas = 1.96e-5*1; %gas holdup, m^3, based on 1 cm height increase

 V_liq = 1e-3;   %liquid volume, m^3

 T = 313;       %temperature, K

 P = 101325;     %pressure, Pa

 y_NO_in = 1010e-6; %mol fraction of NO, converted from mol fraction of 0.105%

 V_1 = 1e-4*1;   %head space

 V_2 = 1e-4*0;

 %parameters to be determined

 kLa = 2.67e-2;  %mass transfer coefficient, s^-1 1.6, .48

 k_1 = 2.79e-8;

 k_2 = 4.58e-4;
```

```matlab
    k_3 = 6.15e-2;

    k_4 = 8.89e-3;

    k_5 = 2.75e-8;

    k_6 = 3.81e-7;

    k_7 = 1.75e-1;

    k_sr= 2.23e-4;

    function dydt=odefun(t, y)

        dydt = zeros(3,1);

            dydt(1) = kLa*P/H*y(2) – kLa*y(1) – 2*y(4)*k_1-k_2*y(1)*y(4)-
k_3*y(4)*y(5)+k_4*y(5)+k_5+k_6+k_sr*y(1);  %C_NO_liq

            dydt(2) = q/V_gas*y_NO_in – y(2)*(q/V_gas)  -
(y(2)+y_NO_in)*0.5*(kLa*V_liq*R*T/(H*V_gas)) …

                + kLa*V_liq*R*T/(P*V_gas)*y(1)*1; %y_NO_gas

        dydt(3) = q/V_1*(y(2) – y(3));

        dydt(4) = -k_1*y(4)-k_2*y(1)*y(4)-k_3*y(4)*y(5)+k_6;

        dydt(5) = -k_3*y(4)*y(5)-(k_4+k_7)*y(5); %ferrous ion

        dydt(6) = 2*k_1*y(4);   %product of reaction 3

        %dydt(7) = 8*(y_S2O8_ini – y(4)) + q/V_liq*(y_NO_in – y(2))/(R*T);   %oxygen balance

%      dydt(8) = 2*(y_S2O8_ini – y(4)) – 2*y(5) – y(6);   %sulfate balance

        %dydt(5) = q/V_1*(y(2)-y(5));    %volume effect

    end

    tspan = [0 3200];

    M = [1 0 0 0 0 0% 0 0
```

```matlab
       0 1 0 0 0 0% 0 0

       0 0 1 0 0 0% 0 0

       0 0 0 1 0 0% 0 0

       0 0 0 0 1 0% 0 0

       0 0 0 0 0 1];% 0 0

       %0 0 0 0 0 0 0 0

       %0 0 0 0 0 0 0 1];

    options = odeset('Refine', 1, 'NonNegative', [1]);

%    y_S2O8_ini = 0.01*1e3;  %concentration of persulfate, mol/m^3

%    y0 = [0 y_NO_in y_NO_in y_S2O8_ini 0 0];% 0 0];

%    [t, y]=ode45(@odefun, tspan, y0, options);

%    figure(1);

%    t = t + 600;

%    plot(t,y(:,2)*1e6);

% %    plot(t,y(:,4)/y_S2O8_ini);

%    hold on

    y_Fe_ini = 0.01*1e3;  %concentration of persulfate, mol/m^3

    y_S2O8_ini = 0.022*1e3;  %concentration of persulfate, mol/m^3

    y0 = [0 y_NO_in y_NO_in y_S2O8_ini y_Fe_ini 0];% 0 0];

    [t, y]=ode45(@odefun, tspan, y0, options);

    figure(1);

    t = t + 600;

    E2=plot(t,y(:,2)*1e6);
```

```matlab
%    plot(t,y(:,4)/y_S2O8_ini);

    y(end,2)*1e6

    y_S2O8_ini = 0.05*1e3;  %concentration of persulfate, mol/m^3

    y0 = [0 y_NO_in y_NO_in y_S2O8_ini y_Fe_ini 0];% 0 0];

    [t, y]=ode45(@odefun, tspan, y0, options);

    figure(1);

    t = t + 600;

    plot(t,y(:,2)*1e6);

%    plot(t,y(:,4)/y_S2O8_ini);

    y(end,2)*1e6

    y_S2O8_ini = 0.1*1e3;  %concentration of persulfate, mol/m^3

    y0 = [0 y_NO_in y_NO_in y_S2O8_ini y_Fe_ini 0];% 0 0];

    [t, y]=ode45(@odefun, tspan, y0, options);

    figure(1);

    t = t + 600;

    plot(t,y(:,2)*1e6);

%    plot(t,y(:,4)/y_S2O8_ini);

    y(end,2)*1e6

    y_S2O8_ini = 0.22*1e3;  %concentration of persulfate, mol/m^3

    y0 = [0 y_NO_in y_NO_in y_S2O8_ini y_Fe_ini 0];% 0 0];

    [t, y]=ode45(@odefun, tspan, y0, options);

    figure(1);

    t = t + 600;
```

```matlab
    plot(t,y(:,2)*1e6);
%   plot(t,y(:,4)/y_S2O8_ini);

    y(end,2)*1e6

    xlabel('Time(s)')

    ylabel('NO Concentration (ppm)')

   legend([E1 E2],'Experimental', 'Model')

end
```

### E.1.4 Code for 50 $^0$C

```matlab
        function persulfate_mak_50_13rxn()

    clc

    clear all

    conc1=xlsread('\50deg.xls','e1','C:C');

     time30deg=xlsread('\50deg.xls','e1','D:D');

    conc2=xlsread('\50deg.xls','e1','F:F');

%    time50deg=xlsread('\50deg.xls','e1','D:D');

    conc3=xlsread('\50deg.xls','e1','G:G');

%   time60deg=xlsread('\50deg.xls','e1','D:D');

    conc4=xlsread('\50deg.xls','e1','I:I');

 %  time40deg=xlsread('\40deg.xls','e1','D:D');

    figure(1)

     plot(time30deg, conc3,'r');

    hold on

figure(1)
```

```matlab
hold on

plot(time30deg, conc4,'r');

 figure(1)

 hold on

plot(time30deg, conc2,'r');

figure(1)

 hold on

E1=plot(time30deg, conc1,'r');

%Constants

 R = 8.314;      %universal gas constant, J/mol.K

 H = 5.223e4*1;    %henry's law constant, Pa/(mol/m^3)

 %Parameters

 q = 1.667e-6*1;   %gas flow rate, m^3/s

 V_gas = 1.96e-5*1; %gas holdup, m^3, based on 1 cm height increase

 V_liq = 1e-3;   %liquid volume, m^3

 T = 323;        %temperature, K

 P = 101325;     %pressure, Pa

 y_NO_in = 1010e-6; %mol fraction of NO, converted from mol fraction of 0.105%

 V_1 = 1e-4*1;   %head space

 V_2 = 1e-4*0;

 %parameters to be determined

 kLa = 3.36e-2;  %mass transfer coefficient, s^-1 1.6, .48

 k_1 = 4.44e-8;
```

```matlab
k_2 = 6.11e-4;

k_3 = 1.26e-1;

k_4 = 1.60e-2;

k_5 = 3.99e-8;

k_6 = 6.48e-7;

k_7 = 3.46e-1;

k_sr= 3.92e-4;

function dydt=odefun(t, y)

    dydt = zeros(3,1);

    dydt(1) = kLa*P/H*y(2) - kLa*y(1) - 2*y(4)*k_1-k_2*y(1)*y(4)-
k_3*y(4)*y(5)+k_4*y(5)+k_5+k_6+k_sr*y(1);  %C_NO_liq

    dydt(2) = q/V_gas*y_NO_in - y(2)*(q/V_gas)  -
(y(2)+y_NO_in)*0.5*(kLa*V_liq*R*T/(H*V_gas)) ...

        + kLa*V_liq*R*T/(P*V_gas)*y(1)*1; %y_NO_gas

    dydt(3) = q/V_1*(y(2) - y(3));

    dydt(4) = -k_1*y(4)-k_2*y(1)*y(4)-k_3*y(4)*y(5)+k_6;

    dydt(5) = -k_3*y(4)*y(5)-(k_4+k_7)*y(5); %ferrous ion

    dydt(6) = 2*k_1*y(4);   %product of reaction 3

    %dydt(7) = 8*(y_S2O8_ini - y(4)) + q/V_liq*(y_NO_in - y(2))/(R*T);   %oxygen balance

%     dydt(8) = 2*(y_S2O8_ini - y(4)) - 2*y(5) - y(6);   %sulfate balance

    %dydt(5) = q/V_1*(y(2)-y(5));    %volume effect

end

tspan = [0 3200];
```

```matlab
M = [1 0 0 0 0 0% 0 0

     0 1 0 0 0 0% 0 0

     0 0 1 0 0 0% 0 0

     0 0 0 1 0 0% 0 0

     0 0 0 0 1 0% 0 0

     0 0 0 0 0 1];% 0 0

     %0 0 0 0 0 0 0 0

     %0 0 0 0 0 0 0 1];

     options = odeset('Refine', 1, 'NonNegative', [1]);

%    y_S2O8_ini = 0.01*1e3;  %concentration of persulfate, mol/m^3

%    y0 = [0 y_NO_in y_NO_in y_S2O8_ini 0 0];% 0 0];

%    [t, y]=ode45(@odefun, tspan, y0, options);

%    figure(1);

%    t = t + 600;

%    plot(t,y(:,2)*1e6);

% %   plot(t,y(:,4)/y_S2O8_ini);

%    hold on

     y_Fe_ini = 0.01*1e3;  %concentration of persulfate, mol/m^3

     y_S2O8_ini = 0.02*1e3;  %concentration of persulfate, mol/m^3

     y0 = [0 y_NO_in y_NO_in y_S2O8_ini y_Fe_ini 0];% 0 0];

     [t, y]=ode45(@odefun, tspan, y0, options);

     figure(1);

     t = t + 600;
```

```matlab
    E2=plot(t,y(:,2)*1e6);
%   plot(t,y(:,4)/y_S2O8_ini);

    y(end,2)*1e6

    y_S2O8_ini = 0.05*1e3;  %concentration of persulfate, mol/m^3

    y0 = [0 y_NO_in y_NO_in y_S2O8_ini y_Fe_ini 0];% 0 0];

    [t, y]=ode45(@odefun, tspan, y0, options);

    figure(1);

    t = t + 600;

    plot(t,y(:,2)*1e6);
%   plot(t,y(:,4)/y_S2O8_ini);

    y(end,2)*1e6

    y_S2O8_ini = 0.1*1e3;  %concentration of persulfate, mol/m^3

    y0 = [0 y_NO_in y_NO_in y_S2O8_ini y_Fe_ini 0];% 0 0];

    [t, y]=ode45(@odefun, tspan, y0, options);

    figure(1);

    t = t + 600;

    plot(t,y(:,2)*1e6);
%   plot(t,y(:,4)/y_S2O8_ini);

    y(end,2)*1e6

    y_S2O8_ini = 0.2*1e3;  %concentration of persulfate, mol/m^3

    y0 = [0 y_NO_in y_NO_in y_S2O8_ini y_Fe_ini 0];% 0 0];

    [t, y]=ode45(@odefun, tspan, y0, options);

    figure(1);
```

```matlab
   t = t + 600;

   plot(t,y(:,2)*1e6);
%   plot(t,y(:,4)/y_S2O8_ini);

   y(end,2)*1e6

   xlabel('Time(s)')

   ylabel('NO Concentration (ppm)')

  legend([E1 E2],'Experimental', 'Model')
end
```

### E.1.5 Code for 60 $^0$C

```matlab
       function persulfate_mak_60_13rxn()

   clc

    conc1=xlsread('\60deg.xls','e1','C:C');

    time30deg=xlsread('\60deg.xls','e1','D:D');

   conc2=xlsread('\60deg.xls','e1','F:F');
%    time50deg=xlsread('\60deg.xls','e1','D:D');

   conc3=xlsread('\60deg.xls','e1','G:G');
%   time60deg=xlsread('\60deg.xls','e1','D:D');

   conc4=xlsread('\60deg.xls','e1','I:I');
%   time40deg=xlsread('\40deg.xls','e1','D:D');

   figure(1)

    plot(time30deg, conc3,'r');

    hold on

figure(1)
```

```matlab
hold on

plot(time30deg, conc4,'r');

figure(1)

hold on

plot(time30deg, conc2,'r');

figure(1)

hold on

E1=plot(time30deg, conc1,'r');

%Constants

R = 8.314;      %universal gas constant, J/mol.K

H = 5.223e4*1;    %henry's law constant, Pa/(mol/m^3)

%Parameters

q = 1.667e-6*1;   %gas flow rate, m^3/s

V_gas = 1.96e-5*1; %gas holdup, m^3, based on 1 cm height increase

V_liq = 1e-3;   %liquid volume, m^3

T = 333;        %temperature, K

P = 101325;     %pressure, Pa

y_NO_in = 1010e-6; %mol fraction of NO, converted from mol fraction of 0.105%

V_1 = 1e-4*1;   %head space

V_2 = 1e-4*0;

%parameters to be determined

kLa = 4.06e-2;  %mass transfer coefficient, s^-1 1.6, .48

k_1 = 5.57e-8;
```

```
k_2 = 6.85e-4;

k_3 = 2.52e-1;

k_4 = 3.02e-2;

k_5 = 5.82e-8;

k_6 = 9.53e-7;

k_7 = 5.69e-1;

k_sr= 5.72e-4;

function dydt=odefun(t, y)

    dydt = zeros(3,1);

    dydt(1) = kLa*P/H*y(2) - kLa*y(1) - 2*y(4)*k_1-k_2*y(1)*y(4)-
k_3*y(4)*y(5)+k_4*y(5)+k_5+k_6+k_sr*y(1);  %C_NO_liq

    dydt(2) = q/V_gas*y_NO_in - y(2)*(q/V_gas)  -
(y(2)+y_NO_in)*0.5*(kLa*V_liq*R*T/(H*V_gas)) ...

        + kLa*V_liq*R*T/(P*V_gas)*y(1)*1; %y_NO_gas

    dydt(3) = q/V_1*(y(2) - y(3));

    dydt(4) = -k_1*y(4)-k_2*y(1)*y(4)-k_3*y(4)*y(5)+k_6;

    dydt(5) = -k_3*y(4)*y(5)-(k_4+k_7)*y(5); %ferrous ion

    dydt(6) = 2*k_1*y(4);   %product of reaction 3

    %dydt(7) = 8*(y_S2O8_ini - y(4)) + q/V_liq*(y_NO_in - y(2))/(R*T);   %oxygen balance

%     dydt(8) = 2*(y_S2O8_ini - y(4)) - 2*y(5) - y(6);   %sulfate balance

    %dydt(5) = q/V_1*(y(2)-y(5));    %volume effect

end

tspan = [0 3200];
```

```
M = [1 0 0 0 0 0% 0 0

    0 1 0 0 0 0% 0 0

    0 0 1 0 0 0% 0 0

    0 0 0 1 0 0% 0 0

    0 0 0 0 1 0% 0 0

    0 0 0 0 0 1];% 0 0

    %0 0 0 0 0 0 0 0

    %0 0 0 0 0 0 0 1];

   options = odeset('Refine', 1, 'NonNegative', [1]);

%    y_S2O8_ini = 0.01*1e3;  %concentration of persulfate, mol/m^3

%    y0 = [0 y_NO_in y_NO_in y_S2O8_ini 0 0];% 0 0];

%    [t, y]=ode45(@odefun, tspan, y0, options);

%    figure(1);

%    t = t + 600;

%    plot(t,y(:,2)*1e6);

% %    plot(t,y(:,4)/y_S2O8_ini);

%    hold on

   y_Fe_ini = 0.01*1e3;  %concentration of persulfate, mol/m^3

   y_S2O8_ini = 0.02*1e3*.95;  %concentration of persulfate, mol/m^3

   y0 = [0 y_NO_in y_NO_in y_S2O8_ini y_Fe_ini 0];% 0 0];

   [t, y]=ode45(@odefun, tspan, y0, options);

   figure(1);

   t = t + 600;
```

```
    E2=plot(t,y(:,2)*1e6);
%   plot(t,y(:,4)/y_S2O8_ini);

    y(end,2)*1e6

    y_S2O8_ini = 0.04*1e3;  %concentration of persulfate, mol/m^3

    y0 = [0 y_NO_in y_NO_in y_S2O8_ini y_Fe_ini 0];% 0 0];

    [t, y]=ode45(@odefun, tspan, y0, options);

    figure(1);

    t = t + 600;

    plot(t,y(:,2)*1e6);
%   plot(t,y(:,4)/y_S2O8_ini);

    y(end,2)*1e6

    y_S2O8_ini = 0.1*1e3;  %concentration of persulfate, mol/m^3

    y0 = [0 y_NO_in y_NO_in y_S2O8_ini y_Fe_ini 0];% 0 0];

    [t, y]=ode45(@odefun, tspan, y0, options);

    figure(1);

    t = t + 600;

    plot(t,y(:,2)*1e6);
%   plot(t,y(:,4)/y_S2O8_ini);

    y(end,2)*1e6

    y_S2O8_ini = 0.2*1e3;  %concentration of persulfate, mol/m^3

    y0 = [0 y_NO_in y_NO_in y_S2O8_ini y_Fe_ini 0];% 0 0];

    [t, y]=ode45(@odefun, tspan, y0, options);

    figure(1);
```

```matlab
    t = t + 600;

    plot(t,y(:,2)*1e6);
%   plot(t,y(:,4)/y_S2O8_ini);

    y(end,2)*1e6

    xlabel('Time(s)')

    ylabel('NO Concentration (ppm)')

   legend([E1 E2],'Experimental', 'Model')
end
```

### E.1.6 Code for 70 $^0$C

```matlab
        function persulfate_mak_70_13rxn()

    clc

     conc1=xlsread('\70deg.xls','e1','C:C');

      time30deg=xlsread('\70deg.xls','e1','D:D');

     conc2=xlsread('\70deg.xls','e1','F:F');
%     time50deg=xlsread('\70deg.xls','e1','D:D');

    conc3=xlsread('\70deg.xls','e1','G:G');
%    time60deg=xlsread('\70deg.xls','e1','D:D');

    conc4=xlsread('\70deg.xls','e1','I:I');
%    time40deg=xlsread('\70deg.xls','e1','D:D');

    figure(1)

     plot(time30deg, conc3,'r');

     hold on

figure(1)
```

```matlab
hold on

plot(time30deg, conc4,'r');

figure(1)

 hold on

plot(time30deg, conc2,'r');

figure(1)

 hold on

E1=plot(time30deg, conc1,'r');

%Constants

 R = 8.314;      %universal gas constant, J/mol.K

 H = 5.223e4*1;    %henry's law constant, Pa/(mol/m^3)

 %Parameters

 q = 1.667e-6*1;   %gas flow rate, m^3/s

 V_gas = 1.96e-5*1; %gas holdup, m^3, based on 1 cm height increase

 V_liq = 1e-3;   %liquid volume, m^3

 T = 343;       %temperature, K

 P = 101325;     %pressure, Pa

 y_NO_in = 1010e-6; %mol fraction of NO, converted from mol fraction of 0.105%

 V_1 = 1e-4*1;   %head space

 V_2 = 1e-4*0;

 %parameters to be determined

 kLa = 4.35e-2;  %mass transfer coefficient, s^-1 1.6, .48

 k_1 = 6.99e-8;
```

```matlab
k_2 = 8.57e-4;

k_3 = 6.00e-1;

k_4 = 6.71e-2;

k_5 = 8.49e-8;

k_6 = 1.40e-6;

k_7 = 1.09e-0;

k_sr= 1.15e-3;

function dydt=odefun(t, y)

    dydt = zeros(3,1);

    dydt(1) = kLa*P/H*y(2) - kLa*y(1) - 2*y(4)*k_1-k_2*y(1)*y(4)-
k_3*y(4)*y(5)+k_4*y(5)+k_5+k_6+k_sr*y(1);  %C_NO_liq

    dydt(2) = q/V_gas*y_NO_in - y(2)*(q/V_gas)  -
(y(2)+y_NO_in)*0.5*(kLa*V_liq*R*T/(H*V_gas)) ...

        + kLa*V_liq*R*T/(P*V_gas)*y(1)*1; %y_NO_gas

    dydt(3) = q/V_1*(y(2) - y(3));

    dydt(4) = -k_1*y(4)-k_2*y(1)*y(4)-k_3*y(4)*y(5)+k_6;

    dydt(5) = -k_3*y(4)*y(5)-(k_4+k_7)*y(5); %ferrous ion

    dydt(6) = 2*k_1*y(4);   %product of reaction 3

    %dydt(7) = 8*(y_S2O8_ini - y(4)) + q/V_liq*(y_NO_in - y(2))/(R*T);   %oxygen balance

%     dydt(8) = 2*(y_S2O8_ini - y(4)) - 2*y(5) - y(6);   %sulfate balance

    %dydt(5) = q/V_1*(y(2)-y(5));    %volume effect

end

tspan = [0 3200];
```

```
    M = [1 0 0 0 0 0% 0 0

       0 1 0 0 0 0% 0 0

       0 0 1 0 0 0% 0 0

       0 0 0 1 0 0% 0 0

       0 0 0 0 1 0% 0 0

       0 0 0 0 0 1];% 0 0

       %0 0 0 0 0 0 0 0

       %0 0 0 0 0 0 0 1];

    options = odeset('Refine', 1, 'NonNegative', [1]);

%    y_S2O8_ini = 0.01*1e3;  %concentration of persulfate, mol/m^3

%    y0 = [0 y_NO_in y_NO_in y_S2O8_ini 0 0];% 0 0];

%    [t, y]=ode45(@odefun, tspan, y0, options);

%    figure(1);

%    t = t + 600;

%    plot(t,y(:,2)*1e6);

% %    plot(t,y(:,4)/y_S2O8_ini);

%    hold on

    y_Fe_ini = 0.01*1e3;  %concentration of persulfate, mol/m^3

    y_S2O8_ini = 0.02*1e3;  %concentration of persulfate, mol/m^3

    y0 = [0 y_NO_in y_NO_in y_S2O8_ini y_Fe_ini 0];% 0 0];

    [t, y]=ode45(@odefun, tspan, y0, options);

    figure(1);

    t = t + 600;
```

```
E2=plot(t,y(:,2)*1e6);
%   plot(t,y(:,4)/y_S2O8_ini);

    y(end,2)*1e6

    y_S2O8_ini = 0.05*1e3;  %concentration of persulfate, mol/m^3

    y0 = [0 y_NO_in y_NO_in y_S2O8_ini y_Fe_ini 0];% 0 0];

    [t, y]=ode45(@odefun, tspan, y0, options);

    figure(1);

    t = t + 600;

    plot(t,y(:,2)*1e6);
%   plot(t,y(:,4)/y_S2O8_ini);

    y(end,2)*1e6

    y_S2O8_ini = 0.1*1e3;  %concentration of persulfate, mol/m^3

    y0 = [0 y_NO_in y_NO_in y_S2O8_ini y_Fe_ini 0];% 0 0];

    [t, y]=ode45(@odefun, tspan, y0, options);

    figure(1);

    t = t + 600;

    plot(t,y(:,2)*1e6);
%   plot(t,y(:,4)/y_S2O8_ini);

    y(end,2)*1e6

    y_S2O8_ini = 0.4*1e3;  %concentration of persulfate, mol/m^3

    y0 = [0 y_NO_in y_NO_in y_S2O8_ini y_Fe_ini 0];% 0 0];

    [t, y]=ode45(@odefun, tspan, y0, options);

    figure(1);
```

```matlab
    t = t + 600;

    plot(t,y(:,2)*1e6);
%   plot(t,y(:,4)/y_S2O8_ini);

    y(end,2)*1e6

    xlabel('Time(s)')

    ylabel('NO Concentration (ppm)')

   legend([E1 E2],'Experimental', 'Model')
end
```

### E.1.7 Code for 23-70 $^0$C

```matlab
    function persulfate_mak_23to90_13rxn()

    clc

     conc1=xlsread('\23to90deg.xls','Sheet6','D4:D402');

     %time30deg=xlsread('\23deg.xls','e1','C4:C402');

     time30deg=0:10:3980;

     conc2=xlsread('\23to90deg.xls','Sheet6','E4:E402');

%     time50deg=xlsread('\70deg.xls','e1','D:D');

     conc3=xlsread('\23to90deg.xls','Sheet6','F4:F402');

%    time60deg=xlsread('\70deg.xls','e1','D:D');

     conc4=xlsread('\23to90deg.xls','Sheet6','G4:G402');

%    time40deg=xlsread('\70deg.xls','e1','D:D');

conc5=xlsread('\23to90deg.xls','Sheet6','H4:H402');

conc6=xlsread('\23to90deg.xls','Sheet6','I4:I402');

conc7=xlsread('\23to90deg.xls','Sheet6','J4:J402');
```

```
conc8=xlsread('\23to90deg.xls','Sheet6','K4:K402');

  figure(1)

   plot(time30deg, conc3,'r');

    hold on

%legend ('Experimental');

figure(1)

  hold on

 plot(time30deg, conc4,'r');

 figure(1)

  hold on

 plot(time30deg, conc2,'r');

 figure(1)

  hold on

 E1=plot(time30deg, conc5,'r');

 figure(1)

  hold on

 plot(time30deg, conc6,'r');

 figure(1)

  hold on

 plot(time30deg, conc7,'r');

 figure(1)

  hold on

 plot(time30deg, conc8,'r');
```

```matlab
figure(1)

hold on

plot(time30deg, conc1,'r');

%Constants

   R = 8.314;      %universal gas constant, J/mol.K

   H = 5.223e4*1;    %henry's law constant, Pa/(mol/m^3)

   %Parameters

   q = 1.667e-6*1;   %gas flow rate, m^3/s

   V_gas = 1.96e-5*1; %gas holdup, m^3, based on 1 cm height increase

   V_liq = 1e-3;   %liquid volume, m^3

   P = 101325;     %pressure, Pa

   y_NO_in = 1010e-6; %mol fraction of NO, converted from mol fraction of 0.105%

   V_1 = 1e-4*1;   %head space

   V_2 = 1e-4*0;

    y_Fe_ini = 0.01*1e3;  %concentration of persulfate, mol/m^3

   y_S2O8_ini = 0.1*1e3;  %concentration of persulfate, mol/m^3

   y0 = [0 y_NO_in y_NO_in y_S2O8_ini y_Fe_ini 0];% 0 0];

   function dydt=odefun(t, y)

      dydt = zeros(3,1);

        dydt(1) = kLa*P/H*y(2) - kLa*y(1) - 2*y(4)*k_1-k_2*y(1)*y(4)-
k_3*y(4)*y(5)+k_4*y(5)+k_5+k_6+k_sr*y(1);  %C_NO_liq

        dydt(2) = q/V_gas*y_NO_in - y(2)*(q/V_gas)  -
(y(2)+y_NO_in)*0.5*(kLa*V_liq*R*T/(H*V_gas)) ...
```

```matlab
        + kLa*V_liq*R*T/(P*V_gas)*y(1)*1; %y_NO_gas

    dydt(3) = q/V_1*(y(2) - y(3));

    dydt(4) = -k_1*y(4)-k_2*y(1)*y(4)-k_3*y(4)*y(5)+k_6;

    dydt(5) = -k_3*y(4)*y(5)-(k_4+k_7)*y(5); %ferrous ion

    dydt(6) = 2*k_1*y(4);   %product of reaction 3

    %dydt(7) = 8*(y_S2O8_ini - y(4)) + q/V_liq*(y_NO_in - y(2))/(R*T);   %oxygen balance
%      dydt(8) = 2*(y_S2O8_ini - y(4)) - 2*y(5) - y(6);   %sulfate balance

    %dydt(5) = q/V_1*(y(2)-y(5));    %volume effect

end

tspan = [0 3380];

M = [1 0 0 0 0 0% 0 0

   0 1 0 0 0 0% 0 0

   0 0 1 0 0 0% 0 0

   0 0 0 1 0 0% 0 0

   0 0 0 0 1 0% 0 0

   0 0 0 0 0 1];% 0 0

   %0 0 0 0 0 0 0 0

   %0 0 0 0 0 0 0 1];

options = odeset('Refine', 1, 'NonNegative', [1]);

T = 296;       %temperature, K

%parameters to be determined

kLa = 1.96e-2;  %mass transfer coefficient, s^-1 1.6, .48

k_1 = 1.18e-8;
```

```matlab
k_2 = 2.59e-4;

k_3 = 1.46e-2;

k_4 = 2.53e-3;

k_5 = 1.22e-8;

k_6 = 1.36e-7;

k_7 = 5.23e-2;

k_sr= 6.24e-5;

[t, y]=ode45(@odefun, tspan, y0, options);

figure(1);

t = t + 600;

E2=plot(t,y(:,2)*1e6);
%   plot(t,y(:,4)/y_S2O8_ini);

y(end,2)*1e6

hold on

T = 303;       %temperature, K

%parameters to be determined

kLa = 2.12e-2;  %mass transfer coefficient, s^-1 1.6, .48

k_1 = 1.32e-8;

k_2 = 3.89e-4;

k_3 = 3.05e-2;

k_4 = 3.96e-3;

k_5 = 1.92e-8;

k_6 = 2.12e-7;
```

```matlab
    k_7 = 7.65e-2;

    k_sr= 8.40e-5;

    [t, y]=ode45(@odefun, tspan, y0, options);

    figure(1);

    t = t + 600;

    E2=plot(t,y(:,2)*1e6);
%   plot(t,y(:,4)/y_S2O8_ini);

    y(end,2)*1e6

    hold on

    T = 313;      %temperature, K

    %parameters to be determined

    kLa = 2.67e-2;  %mass transfer coefficient, s^-1 1.6, .48

    k_1 = 2.79e-8;

    k_2 = 4.58e-4;

    k_3 = 6.15e-2;

    k_4 = 8.89e-3;

    k_5 = 2.75e-8;

    k_6 = 3.81e-7;

    k_7 = 1.75e-1;

    k_sr= 2.23e-4;

    [t, y]=ode45(@odefun, tspan, y0, options);

    figure(1);

    t = t + 600;
```

```matlab
E2=plot(t,y(:,2)*1e6);
%    plot(t,y(:,4)/y_S2O8_ini);
y(end,2)*1e6
hold on
T = 323;        %temperature, K
%parameters to be determined
kLa = 3.36e-2;  %mass transfer coefficient, s^-1 1.6, .48
k_1 = 4.44e-8;
k_2 = 6.11e-4;
k_3 = 1.26e-1;
k_4 = 1.60e-2;
k_5 = 3.99e-8;
k_6 = 6.48e-7;
k_7 = 3.46e-1;
k_sr= 3.92e-4;
[t, y]=ode45(@odefun, tspan, y0, options);
figure(1);
t = t + 600;
E2=plot(t,y(:,2)*1e6);
%    plot(t,y(:,4)/y_S2O8_ini);
y(end,2)*1e6
hold on
T = 333;        %temperature, K
```

```matlab
%parameters to be determined

kLa = 4.06e-2;  %mass transfer coefficient, s^-1 1.6, .48

k_1 = 5.57e-8;

k_2 = 6.85e-4;

k_3 = 2.52e-1;

k_4 = 3.02e-2;

k_5 = 5.82e-8;

k_6 = 9.53e-7;

k_7 = 5.69e-1;

k_sr= 5.72e-4;

[t, y]=ode45(@odefun, tspan, y0, options);

figure(1);

t = t + 600;

E2=plot(t,y(:,2)*1e6);

%   plot(t,y(:,4)/y_S2O8_ini);

y(end,2)*1e6

hold on

T = 343;      %temperature, K

%parameters to be determined

kLa = 4.35e-2;  %mass transfer coefficient, s^-1 1.6, .48

k_1 = 6.99e-8;

k_2 = 8.57e-4;

k_3 = 6.00e-1;
```

```matlab
k_4 = 6.71e-2;

k_5 = 8.49e-8;

k_6 = 1.40e-6;

k_7 = 1.09e-0;

k_sr= 1.15e-3;

[t, y]=ode45(@odefun, tspan, y0, options);

figure(1);

t = t + 600;

E2=plot(t,y(:,2)*1e6);

%   plot(t,y(:,4)/y_S2O8_ini);

y(end,2)*1e6

hold on

T = 353;        %temperature, K

%parameters to be determined

kLa = 4.64e-2;  %mass transfer coefficient, s^-1 1.6, .48

k_1 = 8.77e-8;

k_2 = 1.22e-3;

k_3 = 1.42e-0;

k_4 = 1.18e-1;

k_5 = 1.44e-7;

k_6 = 2.25e-6;

k_7 = 1.73e-0;

k_sr= 1.71e-3;
```

```matlab
[t, y]=ode45(@odefun, tspan, y0, options);

figure(1);

t = t + 600;

E2=plot(t,y(:,2)*1e6);
%   plot(t,y(:,4)/y_S2O8_ini);

y(end,2)*1e6

hold on

 T = 363;       %temperature, K

%parameters to be determined

kLa = 5.37e-2;  %mass transfer coefficient, s^-1 1.6, .48

k_1 = 1.29e-7;

k_2 = 1.59e-3;

k_3 = 2.45e-0;

k_4 = 2.12e-1;

k_5 = 2.11e-7;

k_6 = 3.30e-6;

k_7 = 3.25e-0;

k_sr= 2.54e-3;

[t, y]=ode45(@odefun, tspan, y0, options);

figure(1);

t = t + 600;

E2=plot(t,y(:,2)*1e6);
%   plot(t,y(:,4)/y_S2O8_ini);
```

```matlab
    y(end,2)*1e6

    xlabel('Time(s)')

    ylabel('NO Concentration (ppm)')

   legend([E1 E2],'Experimental','Model')

%

 end
```

**E.1.8 Code for iron with different temperature**

```matlab
     function iron_01M_difftemp_13rxn

    clc

    clear all

%Constants

    R = 8.314;      %universal gas constant, J/mol.K

    H = 5.223e4*1;    %henry's law constant, Pa/(mol/m^3)

    %Parameters

    q = 1.667e-6*1;   %gas flow rate, m^3/s

    V_gas = 1.96e-5*1; %gas holdup, m^3, based on 1 cm height increase

    V_liq = 1e-3;   %liquid volume, m^3

    P = 101325;     %pressure, Pa

    y_NO_in = 1010e-6; %mol fraction of NO, converted from mol fraction of 0.105%

    V_1 = 1e-4*1;   %head space

    V_2 = 1e-4*0;

     y_Fe_ini = 0.01*1e3;  %concentration of persulfate, mol/m^3

    y_S2O8_ini = 0.1*1e3;  %concentration of persulfate, mol/m^3
```

```
y0 = [0 y_NO_in y_NO_in y_S2O8_ini y_Fe_ini 0];% 0 0];

function dydt=odefun(t, y)

    dydt = zeros(3,1);

    dydt(1) = kLa*P/H*y(2) - kLa*y(1) - 2*y(4)*k_1-k_2*y(1)*y(4)-
k_3*y(4)*y(5)+k_4*y(5)+k_5+k_6;  %C_NO_liq

    dydt(2) = q/V_gas*y_NO_in - y(2)*(q/V_gas)  -
(y(2)+y_NO_in)*0.5*(kLa*V_liq*R*T/(H*V_gas)) ...
        + kLa*V_liq*R*T/(P*V_gas)*y(1)*1; %y_NO_gas

    dydt(3) = q/V_1*(y(2) - y(3));

    dydt(4) = -k_1*y(4)-k_2*y(1)*y(4)-k_3*y(4)*y(5)+k_6;

    dydt(5) = -k_3*y(4)*y(5)-(k_4+k_7)*y(5); %ferrous ion

    dydt(6) = 2*k_1*y(4);   %product of reaction 3

    %dydt(7) = 8*(y_S2O8_ini - y(4)) + q/V_liq*(y_NO_in - y(2))/(R*T);   %oxygen balance

%      dydt(8) = 2*(y_S2O8_ini - y(4)) - 2*y(5) - y(6);   %sulfate balance

    %dydt(5) = q/V_1*(y(2)-y(5));    %volume effect

end

tspan = [0 3900];

M = [1 0 0 0 0 0% 0 0

    0 1 0 0 0 0% 0 0

    0 0 1 0 0 0% 0 0

    0 0 0 1 0 0% 0 0

    0 0 0 0 1 0% 0 0

    0 0 0 0 0 1];% 0 0
```

```matlab
%0 0 0 0 0 0 0 0
%0 0 0 0 0 0 0 1];
options = odeset('Refine', 1, 'NonNegative', [1]);
T = 296;      %temperature, K
%parameters to be determined
kLa = 1.96e-2;  %mass transfer coefficient, s^-1 1.6, .48
k_1 = 1.18e-8;
k_2 = 2.59e-4;
k_3 = 1.46e-2;
k_4 = 2.53e-3;
k_5 = 1.22e-8;
k_6 = 1.36e-7;
k_7 = 5.23e-2;
k_sr= 6.24e-5;
[t, y]=ode45(@odefun, tspan, y0, options);
figure(1);
t = t + 60;
plot(t,y(:,5)*1e-3);
%   plot(t,y(:,4)/y_S2O8_ini);
hold on
 T = 303;      %temperature, K
%parameters to be determined
kLa = 2.12e-2;  %mass transfer coefficient, s^-1 1.6, .48
```

```matlab
k_1 = 1.32e-8;

k_2 = 3.89e-4;

k_3 = 3.05e-2;

k_4 = 3.96e-3;

k_5 = 1.92e-8;

k_6 = 2.12e-7;

k_7 = 7.65e-2;

k_sr= 8.40e-5;

[t, y]=ode45(@odefun, tspan, y0, options);

figure(1);

t = t + 60;

plot(t,y(:,5)*1e-3);
%    plot(t,y(:,4)/y_S2O8_ini);

hold on

T = 313;        %temperature, K

%parameters to be determined

kLa = 2.67e-2;  %mass transfer coefficient, s^-1 1.6, .48

k_1 = 2.79e-8;

k_2 = 4.58e-4;

k_3 = 6.15e-2;

k_4 = 8.89e-3;

k_5 = 2.75e-8;

k_6 = 3.81e-7;
```

```matlab
k_7 = 1.75e-1;

k_sr= 2.23e-4;

[t, y]=ode45(@odefun, tspan, y0, options);

figure(1);

t = t + 60;

plot(t,y(:,5)*1e-3);
%   plot(t,y(:,4)/y_S2O8_ini);

hold on

T = 323;        %temperature, K

%parameters to be determined

kLa = 3.36e-2;  %mass transfer coefficient, s^-1 1.6, .48

k_1 = 4.44e-8;

k_2 = 6.11e-4;

k_3 = 1.26e-1;

k_4 = 1.60e-2;

k_5 = 3.99e-8;

k_6 = 6.48e-7;

k_7 = 3.46e-1;

k_sr= 3.92e-4;

[t, y]=ode45(@odefun, tspan, y0, options);

figure(1);

t = t + 60;

plot(t,y(:,5)*1e-3);
```

```matlab
%    plot(t,y(:,4)/y_S2O8_ini);

    hold on

    T = 333;        %temperature, K

    %parameters to be determined

    kLa = 4.06e-2;  %mass transfer coefficient, s^-1 1.6, .48

    k_1 = 5.57e-8;

    k_2 = 6.85e-4;

    k_3 = 2.52e-1;

    k_4 = 3.02e-2;

    k_5 = 5.82e-8;

    k_6 = 9.53e-7;

    k_7 = 5.69e-1;

    k_sr= 5.72e-4;

    [t, y]=ode45(@odefun, tspan, y0, options);

    figure(1);

    t = t + 60;

    plot(t,y(:,5)*1e-3);

%    plot(t,y(:,4)/y_S2O8_ini);

    hold on

    T = 343;        %temperature, K

    %parameters to be determined

    kLa = 4.35e-2;  %mass transfer coefficient, s^-1 1.6, .48

    k_1 = 6.99e-8;
```

```matlab
k_2 = 8.57e-4;

k_3 = 6.00e-1;

k_4 = 6.71e-2;

k_5 = 8.49e-8;

k_6 = 1.40e-6;

k_7 = 1.09e-0;

k_sr= 1.15e-3;

[t, y]=ode45(@odefun, tspan, y0, options);

figure(1);

t = t + 60;

plot(t,y(:,5)*1e-3);
%    plot(t,y(:,4)/y_S2O8_ini);
hold on
T = 353;        %temperature, K
%parameters to be determined
kLa = 4.64e-2;  %mass transfer coefficient, s^-1 1.6, .48
k_1 = 8.77e-8;

k_2 = 1.22e-3;

k_3 = 1.42e-0;

k_4 = 1.18e-1;

k_5 = 1.44e-7;

k_6 = 2.25e-6;

k_7 = 1.73e-0;
```

```matlab
    k_sr= 1.71e-3;

    [t, y]=ode45(@odefun, tspan, y0, options);

    figure(1);

    t = t + 60;

    plot(t,y(:,5)*1e-3);
%   plot(t,y(:,4)/y_S2O8_ini);

    hold on

    T = 363;        %temperature, K

    %parameters to be determined

    kLa = 4.69e-2;  %mass transfer coefficient, s^-1 1.6, .48

    k_1 = 1.29e-7;

    k_2 = 1.59e-3;

    k_3 = 2.45e-0;

    k_4 = 2.12e-1;

    k_5 = 2.11e-7;

    k_6 = 3.30e-6;

    k_7 = 3.25e-0;

    k_sr= 2.54e-3;

    [t, y]=ode45(@odefun, tspan, y0, options);

    figure(1);

    t = t + 60;

    plot(t,y(:,5)*1e-3);
%   plot(t,y(:,4)/y_S2O8_ini);
```

```matlab
hold on

xlabel('Time(s)')

ylabel('Fe<2+> Concentration (M)')

legend('at 23degC','at 30degC', 'at 40degC', 'at 50degC', 'at 60degC','at 70degC','at 80degC','at 90degC')

end
```

### E.1.9 Code for S$_2$O$_8$ with different temperature

```matlab
function S2O8_difftemp_13rxn

clc

clear all

%Constants

R = 8.314;      %universal gas constant, J/mol.K

H = 5.223e4*1;    %henry's law constant, Pa/(mol/m^3)

%Parameters

q = 1.667e-6*1;   %gas flow rate, m^3/s

V_gas = 1.96e-5*1; %gas holdup, m^3, based on 1 cm height increase

V_liq = 1e-3;   %liquid volume, m^3

P = 101325;     %pressure, Pa

y_NO_in = 1010e-6; %mol fraction of NO, converted from mol fraction of 0.105%

V_1 = 1e-4*1;   %head space

V_2 = 1e-4*0;

y_Fe_ini = 0.01*1e3;  %concentration of persulfate, mol/m^3

y_S2O8_ini = 0.1*1e3;  %concentration of persulfate, mol/m^3
```

```matlab
y0 = [0 y_NO_in y_NO_in y_S2O8_ini y_Fe_ini 0];% 0 0];
function dydt=odefun(t, y)

    dydt = zeros(3,1);

    dydt(1) = kLa*P/H*y(2) - kLa*y(1) - 2*y(4)*k_1-k_2*y(1)*y(4)-
k_3*y(4)*y(5)+k_4*y(5)+k_5+k_6;  %C_NO_liq

    dydt(2) = q/V_gas*y_NO_in - y(2)*(q/V_gas)  -
(y(2)+y_NO_in)*0.5*(kLa*V_liq*R*T/(H*V_gas)) ...
        + kLa*V_liq*R*T/(P*V_gas)*y(1)*1; %y_NO_gas

    dydt(3) = q/V_1*(y(2) - y(3));

    dydt(4) = -k_1*y(4)-k_2*y(1)*y(4)-k_3*y(4)*y(5)+k_6;

    dydt(5) = -k_3*y(4)*y(5)-(k_4+k_7)*y(5); %ferrous ion

    dydt(6) = 2*k_1*y(4);   %product of reaction 3

    %dydt(7) = 8*(y_S2O8_ini - y(4)) + q/V_liq*(y_NO_in - y(2))/(R*T);   %oxygen balance
%       dydt(8) = 2*(y_S2O8_ini - y(4)) - 2*y(5) - y(6);   %sulfate balance

    %dydt(5) = q/V_1*(y(2)-y(5));    %volume effect

  end

  tspan = [0 3900];

  M = [1 0 0 0 0 0% 0 0
     0 1 0 0 0 0% 0 0
     0 0 1 0 0 0% 0 0
     0 0 0 1 0 0% 0 0
     0 0 0 0 1 0% 0 0
     0 0 0 0 0 1];% 0 0
```

```matlab
    %0 0 0 0 0 0 0 0

    %0 0 0 0 0 0 0 1];


    options = odeset('Refine', 1, 'NonNegative', [1]);

    T = 296;        %temperature, K

    %parameters to be determined

    kLa = 1.96e-2;  %mass transfer coefficient, s^-1 1.6, .48

    k_1 = 1.18e-8;

    k_2 = 2.59e-4;

    k_3 = 1.46e-2;

    k_4 = 2.53e-3;

    k_5 = 1.22e-8;

    k_6 = 1.36e-7;

    k_7 = 5.23e-2;

    k_sr= 6.24e-5;

    [t, y]=ode45(@odefun, tspan, y0, options);

    figure(1);

    t = t + 60;

    plot(t,y(:,4)*1e-3);
%    plot(t,y(:,4)/y_S2O8_ini);

    hold on

    T = 303;        %temperature, K

    %parameters to be determined
```

```
kLa = 2.12e-2;  %mass transfer coefficient, s^-1 1.6, .48

k_1 = 1.32e-8;

k_2 = 3.89e-4;

k_3 = 3.05e-2;

k_4 = 3.96e-3;

k_5 = 1.92e-8;

k_6 = 2.12e-7;

k_7 = 7.65e-2;

k_sr= 8.40e-5;

[t, y]=ode45(@odefun, tspan, y0, options);

figure(1);

t = t + 60;

plot(t,y(:,4)*1e-3);
%   plot(t,y(:,4)/y_S2O8_ini);
hold on

T = 313;       %temperature, K

%parameters to be determined

kLa = 2.67e-2;  %mass transfer coefficient, s^-1 1.6, .48

k_1 = 2.79e-8;

k_2 = 4.58e-4;

k_3 = 6.15e-2;

k_4 = 8.89e-3;

k_5 = 2.75e-8;
```

```matlab
    k_6 = 3.81e-7;

    k_7 = 1.75e-1;

    k_sr= 2.23e-4;

    [t, y]=ode45(@odefun, tspan, y0, options);

    figure(1);

    t = t + 60;

    plot(t,y(:,4)*1e-3);
%    plot(t,y(:,4)/y_S2O8_ini);

    hold on

    T = 323;      %temperature, K

    %parameters to be determined

    kLa = 3.36e-2;  %mass transfer coefficient, s^-1 1.6, .48

    k_1 = 4.44e-8;

    k_2 = 6.11e-4;

    k_3 = 1.26e-1;

    k_4 = 1.60e-2;

    k_5 = 3.99e-8;

    k_6 = 6.48e-7;

    k_7 = 3.46e-1;

    k_sr= 3.92e-4;

    [t, y]=ode45(@odefun, tspan, y0, options);

    figure(1);

    t = t + 60;
```

```matlab
    plot(t,y(:,4)*1e-3);
%   plot(t,y(:,4)/y_S2O8_ini);
    hold on
    T = 333;        %temperature, K
    %parameters to be determined
    kLa = 4.06e-2;  %mass transfer coefficient, s^-1 1.6, .48
    k_1 = 5.57e-8;
    k_2 = 6.85e-4;
    k_3 = 2.52e-1;
    k_4 = 3.02e-2;
    k_5 = 5.82e-8;
    k_6 = 9.53e-7;
    k_7 = 5.69e-1;
    k_sr= 5.72e-4;
    [t, y]=ode45(@odefun, tspan, y0, options);
    figure(1);
    t = t + 60;
    plot(t,y(:,4)*1e-3);
%   plot(t,y(:,4)/y_S2O8_ini);
    hold on
    T = 343;        %temperature, K
    %parameters to be determined
    kLa = 4.35e-2;  %mass transfer coefficient, s^-1 1.6, .48
```

```matlab
k_1 = 6.99e-8;

k_2 = 8.57e-4;

k_3 = 6.00e-1;

k_4 = 6.71e-2;

k_5 = 8.49e-8;

k_6 = 1.40e-6;

k_7 = 1.09e-0;

k_sr= 1.15e-3;

[t, y]=ode45(@odefun, tspan, y0, options);

figure(1);

t = t + 60;

plot(t,y(:,4)*1e-3);
%   plot(t,y(:,4)/y_S2O8_ini);

hold on

T = 353;       %temperature, K

%parameters to be determined

kLa = 4.64e-2;  %mass transfer coefficient, s^-1 1.6, .48

k_1 = 8.77e-8;

k_2 = 1.22e-3;

k_3 = 1.42e-0;

k_4 = 1.18e-1;

k_5 = 1.44e-7;

k_6 = 2.25e-6;
```

```matlab
k_7 = 1.73e-0;

k_sr= 1.71e-3;

[t, y]=ode45(@odefun, tspan, y0, options);

figure(1);

t = t + 60;

plot(t,y(:,4)*1e-3);
%   plot(t,y(:,4)/y_S2O8_ini);

hold on

T = 363;        %temperature, K

%parameters to be determined

kLa = 5.37e-2;  %mass transfer coefficient, s^-1 1.6, .48

k_1 = 1.29e-7;

k_2 = 1.59e-3;

k_3 = 2.45e-0;

k_4 = 2.12e-1;

k_5 = 2.11e-7;

k_6 = 3.30e-6;

k_7 = 3.25e-0;

k_sr= 2.54e-3;

[t, y]=ode45(@odefun, tspan, y0, options);

figure(1);

t = t + 60;

plot(t,y(:,4)*1e-3);
```

```matlab
%   plot(t,y(:,4)/y_S2O8_ini);

    hold on

    xlabel('Time(s)')

    ylabel('Fe<2+> Concentration (M)')

   legend('at 23degC','at 30degC', 'at 40degC', 'at 50degC', 'at 60degC','at 70degC','at 80degC','at

90degC')

end
```

## E.2 Modeling without PSS Approach

```matlab
function persulfate_mak_50_22rxn()

    clc

    clear all

%   conc1=xlsread('\50deg.xls','e1','C:C');

%    time30deg=xlsread('\50deg.xls','e1','D:D');

%    conc2=xlsread('\50deg.xls','e1','F:F');

% %   time50deg=xlsread('\50deg.xls','e1','D:D');

%    conc3=xlsread('\50deg.xls','e1','G:G');

% %   time60deg=xlsread('\50deg.xls','e1','D:D');

%    conc4=xlsread('\50deg.xls','e1','I:I');

% %  time40deg=xlsread('\40deg.xls','e1','D:D');

%    figure(1)

%    plot(time30deg, conc3,'r');

%    hold on

% figure(1)
```

```matlab
%   hold on

%   plot(time30deg, conc4,'r');

%   figure(1)

%   hold on

%   plot(time30deg, conc2,'r');

%   figure(1)

%   hold on

%   E1=plot(time30deg, conc1,'r');

 %Constants

   R = 8.314;     %universal gas constant, J/mol.K

   H_NO = 5.223e4*1;   %henry's law constant, Pa/(mol/m^3)

   H_NO2 = 2.48e3*1;   %henry's law constant, Pa/(mol/m^3)

   H_SO2 = 21*1;   %henry's law constant, Pa/(mol/m^3)

   %Parameters

   q = 1.667e-6*1;   %gas flow rate, m^3/s

   V_gas = 1.96e-5*1; %gas holdup, m^3, based on 1 cm height increase

   V_liq = 1e-3;   %liquid volume, m^3

   T = 323;       %temperature, K

   P = 101325;     %pressure, Pa

   y_NO_in = 1010e-6; %mol fraction of NO, converted from mol fraction of 0.105%

   y_NO2_in = 0e-6; %mol fraction of NO2, converted from mol fraction of 0.105%

   y_SO2_in = 1633e-6; %mol fraction of SO2, converted from mol fraction of 0.105%

   V_1 = 1e-4*1;   %head space
```

```
V_2 = 1e-4*0;
```

%parameters to be determined

```
kLa_NO = 3.36e-2;  %mass transfer coefficient, s^-1 1.6, .48

kLa_NO2 = 3.36e-2;  %mass transfer coefficient, s^-1 1.6, .48

kLa_SO2 = 3.36e-2;  %mass transfer coefficient, s^-1 1.6, .48

k_1 = 2.5e-7;

k_2 = 6.6e-2;

k_3 = 2.0e10;

k_4 = 1.0e8;%

k_5 = 9.8e8;

k_6 = 1.0e10;

k_7 = 4.5e9;

k_8_f = 1.7e-2;

k_8_b = 1e0;

k_9_f = 6.3e-8;

k_9_b = 1e0;

k_10 = 9.5e9;

k_11 = 5.5e9;

k_12 = 1.0e10;%

k_13 = 5.23e-8;%

k_14 = 6.5e-4;%

k_15 = 9.57e-2;%

k_16 = 8.62e-3;%
```

```matlab
k_17 = 4.33e-8;%

k_18 = 1.5e8;

k_19_f = 5.23e-4;

k_19_b = 6.48e0;

k_20 = 9.57e-2;

k_21 = 8.62e-3;

k_22 = 1.5e8;

function dydt=odefun(t, y)

    dydt = zeros(3,1);

    dydt(1) = q/V_gas*y_NO_in - y(1)*(q/V_gas)  -
(y(1)+y_NO_in)*0.5*(kLa_NO*V_liq*R*T/(H_NO*V_gas)) ...

        + kLa_NO*V_liq*R*T/(P*V_gas)*y(2)*1; %y_NO_gas

     dydt(2) = kLa_NO*P/H_NO*y(1) - kLa_NO*y(2) -k_3*y(2)*y(9)-k_14*y(2)*y(7);
%C_NO_liq

    dydt(3) = q/V_gas*y_NO2_in - y(3)*(q/V_gas)  -
(y(3)+y_NO2_in)*0.5*(kLa_NO2*V_liq*R*T/(H_NO2*V_gas)) ...

        + kLa_NO2*V_liq*R*T/(P*V_gas)*y(4)*1; %y_NO2_gas

    dydt(4) = kLa_NO2*P/H_NO2*y(3) - kLa_NO2*y(4)
+k_4*y(7)*y(10)+k_5*y(8)*y(10)+k_6*y(9)*y(10)...

        +k_14*y(2)*y(7)-k_18*y(4)^2*y(14)-k_22*y(4)^2*y(12);  %C_NO2_liq

    dydt(5) = q/V_gas*y_SO2_in - y(5)*(q/V_gas)  -
(y(5)+y_NO_in)*0.5*(kLa_SO2*V_liq*R*T/(H_SO2*V_gas)) ...

        + kLa_SO2*V_liq*R*T/(P*V_gas)*y(6)*1; %y_SO2_gas
```

dydt(6) = kLa_SO2*P/H_SO2*y(5) - kLa_SO2*y(6) -k_8_f*y(6)+k_8_b*y(11)*y(14)-k_16*y(6)*y(7);  %C_SO2_liq

dydt(7) = -k_1*y(7)-k_4*y(7)*y(10)-k_13*y(7)-k_14*y(2)*y(7)-k_15*y(7)*y(14)-k_16*y(6)*y(7)-k_17*y(7)*y(12);%S2O8<-2> ION

dydt(8) = 2*k_1*y(7)-k_2*y(8)-k_4*y(7)*y(10)-k_5*y(8)*y(10);% SO4<.-> ION

dydt(9) = k_2*y(8)-k_3*y(2)*y(9)-k_6*y(9)*y(10)-k_7*y(4)*y(9)-k_10*y(9)*y(14)-k_11*y(9)*y(12)-k_12*y(9)*y(13); %OH<.> ion

dydt(10) = k_3*y(2)*y(9)-k_4*y(7)*y(10)-k_5*y(8)*y(10)-k_6*y(9)*y(10)+2*k_18*y(4)^2*y(14)-k_19_f*y(10)*y(11)*y(14)^2 ...

        +k_19_b*y(15)-k_20*y(10)*y(11)*y(14)+2*k_22*y(4)^2*y(12);  %NO2<-> ION

dydt(11) = k_3*y(2)*y(9)+k_7*y(4)*y(9)+k_8_f*y(6)*y(10)-k_8_b*y(11)*y(14)+k_9_f*y(14)-k_9_b*y(11)*y(12) ...

        +3*k_18*y(4)^2*y(14)-k_19_f*y(10)*y(11)*y(14)^2+k_19_b*y(15)-k_20*y(10)*y(11)*y(14)+2*k_22*y(10)^2*y(12);  %H<+> ION

dydt(12) = k_9_f*y(14)-k_9_b*y(11)*y(12)-k_11*y(9)*y(12)-k_17*y(7)*y(12)-k_22*y(4)^2*y(12); %SO3<2-> ION

dydt(13) = k_10*y(9)*y(14)+k_11*y(9)*y(12)-k_12*y(9)*y(13);   %SO3<.-> ION

dydt(14) = k_8_f*y(6)*y(10)-k_8_b*y(11)*y(14)+k_9_f*y(14)-k_9_b*y(11)*y(12)-k_10*y(9)*y(14)-k_15*y(7)*y(14)-k_18*y(4)^2*y(14) ...

        -k_19_f*y(10)*y(11)*y(14)^2+2*k_19_b*y(15)-k_20*y(10)*y(11)*y(14)-k_21*y(14)*y(15);  %HSO3<-> ION

dydt(15) = k_19_f*y(10)*y(11)*y(14)^2-k_19_b*y(15)+k_21*y(14)*y(15); %HON(SO3)2<2-> ION

```matlab
    dydt(16) = k_20*y(10)*y(11)*y(14)-k_21*y(14)*y(15);    %ONSO3<-> ION

end

tspan = [0 3200];

M = [1 0 0 0 0 0 0 0 0 0 0 0 0 0 0 0

    0 1 0 0 0 0 0 0 0 0 0 0 0 0 0 0

    0 0 1 0 0 0 0 0 0 0 0 0 0 0 0 0

    0 0 0 1 0 0 0 0 0 0 0 0 0 0 0 0

    0 0 0 0 1 0 0 0 0 0 0 0 0 0 0 0

    0 0 0 0 0 1 0 0 0 0 0 0 0 0 0 0

    0 0 0 0 0 0 1 0 0 0 0 0 0 0 0 0

    0 0 0 0 0 0 0 1 0 0 0 0 0 0 0 0

    0 0 0 0 0 0 0 0 1 0 0 0 0 0 0 0

    0 0 0 0 0 0 0 0 0 1 0 0 0 0 0 0

    0 0 0 0 0 0 0 0 0 0 1 0 0 0 0 0

    0 0 0 0 0 0 0 0 0 0 0 1 0 0 0 0

    0 0 0 0 0 0 0 0 0 0 0 0 1 0 0 0

    0 0 0 0 0 0 0 0 0 0 0 0 0 1 0 0

    0 0 0 0 0 0 0 0 0 0 0 0 0 0 1 0

    0 0 0 0 0 0 0 0 0 0 0 0 0 0 0 1];

options = odeset('Refine', 1, 'NonNegative', [1]);

%    y_S2O8_ini = 0.01*1e3;  %concentration of persulfate, mol/m^3

%    y0 = [0 y_NO_in y_NO_in y_S2O8_ini 0 0];% 0 0];

%    [t, y]=ode45(@odefun, tspan, y0, options);
```

```matlab
%    figure(1);

%    t = t + 600;

%    plot(t,y(:,2)*1e6);

% %    plot(t,y(:,4)/y_S2O8_ini);

%    hold on

    y_S2O8_ini = 0.1*1e3;  %concentration of persulfate, mol/m^3

    y0 = [y_NO_in 0 y_NO2_in 0 y_SO2_in 0 y_S2O8_ini 0 0 0 0 0 0 0 0 0];% 0 0];

    [t, y]=ode45(@odefun, tspan, y0, options);

    figure(1);

    t = t + 600;

    E2=plot(t,y(:,1)*1e6);

%    plot(t,y(:,4)/y_S2O8_ini);

    y(end,2)*1e6

%    y_S2O8_ini = 0.05*1e3;  %concentration of persulfate, mol/m^3

%    y0 = [0 y_NO_in y_NO_in y_S2O8_ini y_Fe_ini 0];% 0 0];

%    [t, y]=ode45(@odefun, tspan, y0, options);

%    figure(1);

%    t = t + 600;

%    plot(t,y(:,2)*1e6);

% %    plot(t,y(:,4)/y_S2O8_ini);

%    y(end,2)*1e6

%    y_S2O8_ini = 0.1*1e3;  %concentration of persulfate, mol/m^3

%    y0 = [0 y_NO_in y_NO_in y_S2O8_ini y_Fe_ini 0];% 0 0];
```

```
%    [t, y]=ode45(@odefun, tspan, y0, options);

%    figure(1);

%    t = t + 600;

%    plot(t,y(:,2)*1e6);

% %   plot(t,y(:,4)/y_S2O8_ini);

%    y(end,2)*1e6

%    y_S2O8_ini = 0.2*1e3;  %concentration of persulfate, mol/m^3

%    y0 = [0 y_NO_in y_NO_in y_S2O8_ini y_Fe_ini 0];% 0 0];

%    [t, y]=ode45(@odefun, tspan, y0, options);

%    figure(1);

%    t = t + 600;

%    plot(t,y(:,2)*1e6);

% %   plot(t,y(:,4)/y_S2O8_ini);

%    y(end,2)*1e6

  xlabel('Time(s)')

  ylabel('NO Concentration (ppm)')

  legend([E1 E2],'Experimental', 'Model')

end
```

## Appendix F

### Summary of Experimental Data

Table F.1

*Experimental Data for Removal of Nitric Oxide (NO)*

| Condition / Run No | Temp. ($^0$C) | Inlet NO Conc. (ppm) | Inlet SO$_2$ Conc. (ppm) | Conc. of Persulfate (M) | Conc. of Fe$^{2+}$ (M) | Conc. of EDTA (M) | Initial pH | Final pH | NO Conv.** (%) | SO$_2$ Conv.** (%) |
|---|---|---|---|---|---|---|---|---|---|---|
| 1 | 50 | 753 | None | 0.1 | 0.01 | None | 3.311 | 3.130 | 69.87 | N/A |
| 2 | 50 | 753 | None | 0.1 | 0.01* | None | 3.342 | 3.202 | 72.19 | N/A |
| 3 | 60 | 753 | None | 0.1 | 0.01* | None | 3.165 | 2.829 | 83.52 | N/A |
| 4 | 60 | 753 | None | 0.1 | 0.01 | None | 3.468 | 2.714 | 82.07 | N/A |
| 5 | 40 | 753 | None | 0.1 | 0.01 | None | 3.334 | 3.331 | 54.56 | N/A |
| 6 | 40 | 753 | None | 0.1 | 0.01* | None | 3.289 | 3.220 | 51.23 | N/A |
| 7 | 30 | 753 | None | 0.1 | 0.01* | None | 3.385 | 3.133 | 35.73 | N/A |
| 8 | 30 | 753 | None | 0.1 | 0.01 | None | 3.348 | 3.281 | 31.25 | N/A |
| 9 | 30 | 753 | None | 0.1 | 0.02* | None | 3.326 | 3.189 | 36.92 | N/A |

| 10 | 40 | 753 | None | 0.1 | 0.02* | None | 3.295 | 3.103 | 55.19 | N/A |
|----|----|-----|------|-----|-------|------|-------|-------|-------|-----|
| 11 | 50 | 753 | None | 0.1 | 0.02* | None | 3.010 | 2.749 | 73.84 | N/A |
| 12 | 60 | 753 | None | 0.1 | 0.02* | None | 2.936 | 2.727 | 84.77 | N/A |
| 13 | 70 | 753 | None | 0.1 | 0.02* | None | 3.869 | 3.420 | 94.23 | N/A |
| 14 | 70 | 753 | None | 0.1 | 0.01* | None | 4.021 | 3.834 | 96.28 | N/A |
| 15 | 30 | 753 | None | 0.1 | 0.01 | 0.01 | 5.914 | 5.281 | 55.64 | N/A |
| 16 | 40 | 753 | None | 0.1 | 0.01 | 0.01 | 5.802 | 5.573 | 65.07 | N/A |
| 17 | 50 | 753 | None | 0.1 | 0.01 | 0.01 | 5.849 | 5.018 | 77.20 | N/A |
| 18 | 40 | 753 | None | 0.1 | 0.01 | 0.005 | 5.282 | 5.121 | 58.17 | N/A |
| 19 | 40 | 753 | None | 0.1 | 0.01 | 0.015 | 5.985 | 5.196 | 64.10 | N/A |
| 20 | 40 | 753 | None | 0.1 | 0.01 | 0.02 | 5.251 | 5.004 | 63.21 | N/A |
| 21 | 40 | 753 | None | 0.1 | 0.01 | 0.025 | 5.381 | 5.222 | 61.52 | N/A |
| 22 | 40 | 753 | None | 0.1 | 0.01 | 0.03 | 5.619 | 5.412 | 60.62 | N/A |
| 23 | 50 | 753 | None | 0.1 | 0.01 | 0.005 | 5.341 | 5.322 | 74.05 | N/A |
| 24 | 50 | 753 | None | 0.1 | 0.01 | 0.015 | 5.652 | 5.109 | 76.63 | N/A |
| 25 | 50 | 753 | None | 0.1 | 0.01 | 0.02 | 5.231 | 5.089 | 74.18 | N/A |
| 26 | 50 | 753 | None | 0.1 | 0.01 | 0.025 | 5.788 | 5.348 | 71.46 | N/A |

| 27 | 50 | 753 | None | 0.1 | 0.01 | 0.03 | 5.652 | 5.211 | 67.45 | N/A |
|----|----|-----|------|-----|------|-------|-------|-------|-------|-----|
| 28 | 60 | 753 | None | 0.1 | 0.01 | 0.005 | 5.952 | 5.096 | 83.45 | N/A |
| 29 | 60 | 753 | None | 0.1 | 0.01 | 0.015 | 5.943 | 5.085 | 85.56 | N/A |
| 30 | 60 | 753 | None | 0.1 | 0.01 | 0.02 | 5.929 | 5.079 | 82.12 | N/A |
| 31 | 60 | 753 | None | 0.1 | 0.01 | 0.025 | 5.623 | 5.129 | 81.16 | N/A |
| 32 | 60 | 753 | None | 0.1 | 0.01 | 0.03 | 5.792 | 5.146 | 78.13 | N/A |
| 33 | 30 | 753 | None | 0.1 | 0.01* | None | 3.290 | 3.227 | 34.79 | N/A |
| 34 | 50 | 753 | None | 0.1 | 0.01* | None | 3.977 | 3.017 | 73.17 | N/A |
| 35 | 40 | 753 | None | 0.1 | 0.01* | None | 2.998 | 2.967 | 54.47 | N/A |
| 36 | 50 | 753 | None | 0.1 | 0.01 | None | 3.006 | 2.924 | 70.92 | N/A |
| 37 | 50 | 753 | None | 0.1* | 0.01 | None | 3.185 | 3.119 | 65.87 | N/A |
| 38 | 50 | 753 | None | 0.1 | 0.01* | None | 3.239 | 3.207 | 69.19 | N/A |
| 39 | 50 | 753 | None | 0.1* | 0.01* | None | 3.169 | 3.150 | 66.53 | N/A |
| 40 | 50 | 753 | None | 0.1* | 0.01 | None | 3.278 | 3.225 | 63.28 | N/A |
| 41 | 50 | 753 | None | 0.1 | 0.01 | None | 3.079 | 2.919 | 69.53 | N/A |
| 42 | 60 | 753 | None | 0.1 | 0.01 | 0.01 | 6.257 | 5.949 | 87.32 | N/A |

| | | | | | | | | | | |
|---|---|---|---|---|---|---|---|---|---|---|
| 43 | 70 | 753 | None | 0.1 | 0.01 | 0.01 | 6.109 | 5.840 | 95.43 | N/A |
| 44 | 50 | 753 | None | 0.1 | 0.01 | None | 3.695 | 3.520 | - | N/A |
| 45 | 50 | 753 | None | 0.1 | 0.005 | None | 3.775 | 3.592 | - | N/A |
| 46 | 50 | 753 | None | 0.1 | 0.01 | None | 3.714 | 3.571 | - | N/A |
| 47 | 50 | 753 | None | 0.1 | 0.02 | None | 3.629 | 3.471 | - | N/A |
| 48 | 50 | 753 | None | 0.1 | 0.005 | None | 3.539 | 3.229 | - | N/A |
| 49 | 50 | 753 | None | 0.1 | 0.01 | 0.01 | 6.531 | 6.475 | - | N/A |
| 50 | 50 | 753 | None | 0.1 | 0.02 | 0.01 | 5.876 | 5.578 | - | N/A |
| 51 | 50 | 753 | None | 0.1 | 0.005 | 0.005 | 5.403 | 5.211 | - | N/A |
| 52 | 50 | 753 | None | 0.1 | 0.01 | 0.01 | 4.279 | 3.971 | - | N/A |
| 53 | 50 | 753 | None | 0.1 | 0.02 | 0.02 | 7.352 | 6.967 | - | N/A |
| 54 | 50 | 753 | None | 0.1 | 0.01 | 0.01 | 7.438 | 6.292 | - | N/A |
| 55 | 50 | 753 | None | 0.1 | 0.01 | 0.01 | 10.328 | 9.408 | 60.29 | N/A |
| 56 | 30 | 753 | None | 0.1 | 0.01 | 0.01 | 9.749 | 8.678 | 33.92 | N/A |
| 57 | 40 | 753 | None | 0.1 | 0.01 | 0.01 | 9.104 | 8.461 | 60.02 | N/A |
| 58 | 50 | 753 | None | 0.1 | 0.01 | 0.01 | 9.454 | 9.208 | 65.15 | N/A |

| 59 | 50 | 753 | None | 0.1 | 0.01 | 0.01 | 4.443 | 4.321 | 40.02 | N/A |
|----|----|-----|------|------|------|------|-------|-------|-------|-----|
| 60 | 50 | 753 | None | 0.1 | 0.02 | 0.02 | 6.336 | 6.223 | 71.23 | N/A |
| 61 | 23 | 753 | None | 0.1 | 0.01 | 0.01 | 6.628 | 6.329 | 48.47 | N/A |
| 62 | 30 | 753 | None | 0.1 | 0.01 | 0.01 | 5.985 | 5.873 | 55.64 | N/A |
| 63 | 40 | 753 | None | 0.1 | 0.01 | 0.01 | 6.232 | 6.192 | 65.07 | N/A |
| 64 | 50 | 753 | None | 0.1 | 0.01 | 0.01 | 6.251 | 6.102 | 77.82 | N/A |
| 65 | 60 | 753 | None | 0.1 | 0.01 | 0.01 | 5.987 | 5.780 | 86.99 | N/A |
| 67 | 70 | 753 | None | 0.1 | 0.01 | 0.01 | 6.692 | 6.231 | 96.28 | N/A |
| 68 | 23 | 753 | None | 0.2 | 0.01 | 0.01 | 4.612 | 4.470 | 51.53 | N/A |
| 69 | 30 | 753 | None | 0.2 | 0.01 | 0.01 | 4.881 | 4.588 | 58.57 | N/A |
| 70 | 40 | 753 | None | 0.2 | 0.01 | 0.01 | 4.446 | 4.193 | 67.20 | N/A |
| 71 | 50 | 753 | None | 0.2 | 0.01 | 0.01 | 4.087 | 3.805 | 78.22 | N/A |
| 72 | 60 | 753 | None | 0.2 | 0.01 | 0.01 | 3.703 | 3.462 | 87.78 | N/A |
| 73 | 70 | 753 | None | 0.2 | 0.01 | 0.01 | 3.861 | 3.637 | 97.34 | N/A |
| 74 | 23 | 753 | None | 0.05 | 0.01 | 0.01 | 7.662 | 7.359 | 42.76 | N/A |
| 75 | 30 | 753 | None | 0.05 | 0.01 | 0.01 | 7.398 | 7.102 | 49.54 | N/A |

| 76 | 40 | 753 | None | 0.05 | 0.01 | 0.01 | 7.432 | 7.156 | 59.50 | N/A |
|----|----|-----|------|------|------|------|-------|-------|-------|-----|
| 77 | 50 | 753 | None | 0.05 | 0.01 | 0.01 | 7.342 | 7.053 | 67.73 | N/A |
| 78 | 60 | 753 | None | 0.05 | 0.01 | 0.01 | 7.229 | 6.899 | 79.55 | N/A |
| 79 | 70 | 753 | None | 0.05 | 0.01 | 0.01 | 7.010 | 6.832 | 92.43 | N/A |
| 80 | 23 | 753 | None | 0.1  | 0.02 | 0.02 | 7.323 | 7.143 | 52.59 | N/A |
| 81 | 30 | 753 | None | 0.1  | 0.02 | 0.02 | 7.096 | 6.952 | 61.75 | N/A |
| 82 | 40 | 753 | None | 0.1  | 0.02 | 0.02 | 7.279 | 7.009 | 66.14 | N/A |
| 83 | 50 | 753 | None | 0.1  | 0.02 | 0.02 | 7.102 | 6.895 | 73.57 | N/A |
| 84 | 60 | 753 | None | 0.1  | 0.02 | 0.02 | 7.082 | 6.765 | 76.00 | N/A |
| 85 | 70 | 753 | None | 0.1  | 0.02 | 0.02 | 7.116 | 6.903 | 29.22 | N/A |
| 86 | 23 | 753 | None | 0.1  | 0.005| 0.005| 4.723 | 4.466 | 37.98 | N/A |
| 87 | 30 | 753 | None | 0.1  | 0.005| 0.005| 4.597 | 4.240 | 48.74 | N/A |
| 88 | 40 | 753 | None | 0.1  | 0.005| 0.005| 3.821 | 3.652 | 60.69 | N/A |
| 89 | 50 | 753 | None | 0.1  | 0.005| 0.005| 4.134 | 3.785 | 70.65 | N/A |
| 90 | 60 | 753 | None | 0.1  | 0.005| 0.005| 4.232 | 3.993 | 77.29 | N/A |
| 91 | 70 | 753 | None | 0.1  | 0.005| 0.005| 3.939 | 3.726 | 83.40 | N/A |

| 92 | 23 | 753 | None | 0.1 | 0.005 | 0.05 | 6.982 | 6.673 | 51.26 | N/A |
|-----|-----|-----|------|-----|-------|------|--------|--------|-------|-----|
| 93 | 30 | 753 | None | 0.1 | 0.005 | 0.05 | 7.503 | 7.212 | 61.15 | N/A |
| 94 | 40 | 753 | None | 0.1 | 0.005 | 0.05 | 6.827 | 6.661 | 19.12 | N/A |
| 95 | 50 | 753 | None | 0.1 | 0.005 | 0.05 | 8.102 | 7.853 | 13.28 | N/A |
| 96 | 60 | 753 | None | 0.1 | 0.005 | 0.05 | 7.693 | 7.123 | 3.85 | N/A |
| 97 | 70 | 753 | None | 0.1 | 0.005 | 0.05 | 7.520 | 6.905 | 0.40 | N/A |
| 98 | 40 | 753 | None | 0.1 | 0.01 | 0.01 | 2.139 | 2.057 | 41.43 | N/A |
| 99 | 40 | 753 | None | 0.1 | 0.01 | 0.01 | 4.346 | 4.187 | 58.03 | N/A |
| 100 | 40 | 753 | None | 0.1 | 0.01 | 0.01 | 6.234 | 5.994 | 65.07 | N/A |
| 101 | 40 | 753 | None | 0.1 | 0.01 | 0.01 | 7.943 | 7.872 | 62.42 | N/A |
| 102 | 40 | 753 | None | 0.1 | 0.01 | 0.01 | 9.871 | 9.615 | 51.79 | N/A |
| 103 | 40 | 753 | None | 0.1 | 0.01 | 0.01 | 12.331 | 11.564 | 33.33 | N/A |
| 104 | 50 | 753 | None | 0.1 | 0.01 | 0.01 | 2.023 | 1.975 | 46.48 | N/A |
| 105 | 50 | 753 | None | 0.1 | 0.01 | 0.01 | 3.899 | 3.801 | 66.14 | N/A |
| 106 | 50 | 753 | None | 0.1 | 0.01 | 0.01 | 6.103 | 5.987 | 77.82 | N/A |
| 107 | 50 | 753 | None | 0.1 | 0.01 | 0.01 | 8.521 | 8.220 | 73.97 | N/A |

| 108 | 50 | 753 | None | 0.1 | 0.01 | 0.01 | 10.210 | 9.901 | 61.49 | N/A |
| --- | --- | --- | --- | --- | --- | --- | --- | --- | --- | --- |
| 109 | 50 | 753 | None | 0.1 | 0.01 | 0.01 | 11.895 | 11.213 | 24.89 | N/A |
| 110 | 30 | ~500 | ~1800 | 0.1 | 0.01 | None | 7.348 | 7.125 | 40.69 | 98.30 |
| 111 | 30 | ~500 | ~1800 | 0.1 | 0.01 | 0.01 | 7.873 | 7.002 | 51.90 | ~100.00 |

*Injection from side, **NO and $SO_2$ conversion determined by eq 4.1 with average output concentration $\geq$ 3000 s.

Table F.2

*Spectrophotometric Determination of Iron Species' at 50 $^0C$ (Initial Persulfate 0.1 M, Initial Fe$^{2+}$ 0.005 M, Initial EDTA 0 M)*

| Sample withdrawal Time (s) | Fe$^{2+}$ Conc. | | Fe$^{3+}$ Conc. | | Fe$^{II}$-EDTA Conc. | | Total Fe Conc. | |
|---|---|---|---|---|---|---|---|---|
| | ppm | M | ppm | M | ppm | M | ppm | M |
| 30 | 261.42 | 0.004681 | 12.48 | 0.000223 | - | - | 273.9 | 0.004905 |
| 60 | 263.15 | 0.004712 | 9.45 | 0.000169 | - | - | 272.6 | 0.004881 |
| 80 | 1.23 | 2.2E-05 | 270.2 | 0.004838 | - | - | 271.43 | 0.00486 |
| 380 | 1.02 | 1.83E-05 | 275.49 | 0.004933 | - | - | 276.51 | 0.004951 |
| 440 | 0.79 | 1.41E-05 | 269.46 | 0.004825 | - | - | 270.25 | 0.004839 |
| 500 | 0.75 | 1.34E-05 | 275.64 | 0.004936 | - | - | 276.39 | 0.004949 |
| 680 | 0.3 | 5.37E-06 | 259.96 | 0.004655 | - | - | 260.26 | 0.00466 |
| 980 | 0.52 | 9.31E-06 | 255.41 | 0.004574 | - | - | 255.93 | 0.004583 |
| 1580 | 0.41 | 7.34E-06 | 258.91 | 0.004636 | - | - | 259.32 | 0.004644 |
| 2180 | 0.24 | 4.3E-06 | 261 | 0.004674 | - | - | 261.24 | 0.004678 |
| 3980 | 0 | 0 | 256.19 | 0.004588 | - | - | 256.19 | 0.004588 |

Table F.3

*Spectrophotometric Determination of Iron Species' at 50 $^0C$ (Initial Persulfate 0.1 M, Initial Fe$^{2+}$ 0.01 M, Initial EDTA 0 M)*

| Sample withdrawal Time (s) | Fe$^{2+}$ Conc. | | Fe$^{3+}$ Conc. | | Fe$^{II}$-EDTA Conc. | | Total Fe Conc. | |
|---|---|---|---|---|---|---|---|---|
| | ppm | M | ppm | M | ppm | M | ppm | M |
| 30 | 545.29 | 0.009764 | 14.38 | 0.010022 | - | - | 559.67 | 0.000257 |
| 60 | 540.23 | 0.009674 | 12.11 | 0.009891 | - | - | 552.34 | 0.000217 |
| 80 | 12.52 | 0.000224 | 550.45 | 0.010081 | - | - | 562.97 | 0.009857 |
| 380 | 8.28 | 0.000148 | 538.96 | 0.009799 | - | - | 547.24 | 0.009651 |
| 440 | 6.62 | 0.000119 | 535.61 | 0.00971 | - | - | 542.23 | 0.009591 |
| 500 | 7.29 | 0.000131 | 544.82 | 0.009886 | - | - | 552.11 | 0.009756 |
| 680 | 7.77 | 0.000139 | 529.76 | 0.009625 | - | - | 537.53 | 0.009486 |
| 980 | 6.23 | 0.000112 | 525 | 0.009513 | - | - | 531.23 | 0.009401 |
| 1580 | 5.78 | 0.000104 | 538.91 | 0.009754 | - | - | 544.69 | 0.00965 |
| 2180 | 5.33 | 9.54E-05 | 526.9 | 0.00953 | - | - | 532.23 | 0.009435 |
| 3980 | 4.62 | 8.27E-05 | 518.8 | 0.009373 | - | - | 523.42 | 0.00929 |

Table F.4

*Spectrophotometric Determination of Iron Species' at 50 $^0C$ (Initial Persulfate 0.1 M, Initial $Fe^{2+}$ 0.02 M, Initial EDTA 0 M)*

| Sample withdrawal Time (s) | $Fe^{2+}$ Conc. | | $Fe^{3+}$ Conc. | | $Fe^{II}$-EDTA Conc. | | Total Fe Conc. | |
|---|---|---|---|---|---|---|---|---|
| | ppm | M | ppm | M | ppm | M | ppm | M |
| 30 | 1035.75 | 0.018547 | 56.81 | 0.001017 | - | - | 1092.56 | 0.019564 |
| 60 | 1033.41 | 0.018505 | 53.08 | 0.00095 | - | - | 1086.49 | 0.019455 |
| 80 | 27.94 | 0.0005 | 1057.14 | 0.01893 | - | - | 1085.08 | 0.01943 |
| 380 | 25.73 | 0.000461 | 1043.51 | 0.018686 | - | - | 1069.24 | 0.019147 |
| 440 | 21.33 | 0.000382 | 1070.88 | 0.019176 | - | - | 1092.21 | 0.019558 |
| 500 | 15.15 | 0.000271 | 1067.44 | 0.019114 | - | - | 1082.59 | 0.019386 |
| 680 | 11.29 | 0.000202 | 1064.23 | 0.019057 | - | - | 1075.52 | 0.019259 |
| 980 | 12.57 | 0.000225 | 1042.72 | 0.018672 | - | - | 1055.29 | 0.018897 |
| 1580 | 8.39 | 0.00015 | 1059.18 | 0.018966 | - | - | 1067.57 | 0.019117 |
| 2180 | 9.54 | 0.000171 | 1036.23 | 0.018555 | - | - | 1045.77 | 0.018726 |
| 3980 | 6.54 | 0.000117 | 1026.44 | 0.01838 | - | - | 1032.98 | 0.018497 |

Table F.5

*Spectrophotometric Determination of Iron Species' at 50 $^0C$ (Initial Persulfate 0.1 M, Initial $Fe^{2+}$ 0.005 M, Initial EDTA 0.005 M)*

| Sample withdrawal Time (s) | $Fe^{2+}$ Conc. | | $Fe^{3+}$ Conc. | | $Fe^{II}$-EDTA Conc. | | Total Fe Conc. | |
|---|---|---|---|---|---|---|---|---|
| | ppm | M | ppm | M | ppm | M | ppm | M |
| 30 | 259.79 | 0.00465 | 15.3 | 0.00027 | - | 0 | 275.09 | 0.00493 |
| 60 | 90.63 | 0.00162 | 6.2 | 0.00011 | - | 0.00315 | 96.83 | 0.00173 |
| 80 | 3.67 | 6.6E-05 | 175.81 | 0.00315 | - | 0.00128 | 179.48 | 0.00321 |
| 380 | 5.54 | 9.9E-05 | 163.67 | 0.00293 | - | 0.00125 | 169.21 | 0.00303 |
| 440 | 4.6 | 8.2E-05 | 169.3 | 0.00303 | - | 0.00115 | 173.9 | 0.00311 |
| 500 | 4.73 | 8.5E-05 | 164.09 | 0.00294 | - | 0.00134 | 168.82 | 0.00302 |
| 680 | 4.03 | 7.2E-05 | 162.11 | 0.0029 | - | 0.00132 | 166.14 | 0.00298 |
| 980 | 2.92 | 5.2E-05 | 154.73 | 0.00277 | - | 0.00123 | 157.65 | 0.00282 |
| 1580 | 4.81 | 8.6E-05 | 147.59 | 0.00264 | - | 0.00114 | 152.4 | 0.00273 |
| 2180 | 5 | 9E-05 | 153.04 | 0.00274 | - | 0.0012 | 158.04 | 0.00283 |
| 3980 | 3.64 | 6.5E-05 | 147.2 | 0.00264 | - | 0.00111 | 150.84 | 0.0027 |

Table F.6

*Spectrophotometric Determination of Iron Species' at 50 $^0C$ (Initial Persulfate 0.1 M, Initial Fe$^{2+}$ 0.005 M, Initial EDTA 0.01 M)*

| Sample withdrawal Time (s) | Fe$^{2+}$ Conc. | | Fe$^{3+}$ Conc. | | Fe$^{II}$-EDTA Conc. | | Total Fe Conc. | |
|---|---|---|---|---|---|---|---|---|
| | ppm | M | ppm | M | ppm | M | ppm | M |
| 30 | 263.14 | 0.00471 | 12.53 | 0.00022 | - | 0 | 275.67 | 0.00494 |
| 60 | 81.43 | 0.00146 | 9.83 | 0.00018 | - | 0.003347 | 91.26 | 0.00498 |
| 80 | 4.29 | 7.7E-05 | 166.68 | 0.00298 | - | 0.001323 | 170.97 | 0.00438 |
| 380 | 3.1 | 5.6E-05 | 154.96 | 0.00277 | - | 0.001429 | 158.06 | 0.00426 |
| 440 | 3.92 | 7E-05 | 157.03 | 0.00281 | - | 0.00152 | 160.95 | 0.0044 |
| 500 | 4.52 | 8.1E-05 | 145.58 | 0.00261 | - | 0.001313 | 150.1 | 0.004 |
| 680 | 3.23 | 5.8E-05 | 139.88 | 0.0025 | - | 0.001312 | 143.11 | 0.00387 |
| 980 | 3.53 | 6.3E-05 | 142.63 | 0.00255 | - | 0.001479 | 146.16 | 0.0041 |
| 1580 | 3.28 | 5.9E-05 | 139.62 | 0.0025 | - | 0.001423 | 142.9 | 0.00398 |
| 2180 | 2.67 | 4.8E-05 | 134.56 | 0.00241 | - | 0.001382 | 137.23 | 0.00384 |
| 3980 | 3.82 | 6.8E-05 | 129.9 | 0.00233 | - | 0.001212 | 133.72 | 0.00361 |

Table F.7

*Spectrophotometric Determination of Iron Species' at 50 $^0C$ (Initial Persulfate 0.1 M, Initial $Fe^{2+}$ 0.005 M, Initial EDTA 0.02 M)*

| Sample withdrawal Time (s) | $Fe^{2+}$ Conc. | | $Fe^{3+}$ Conc. | | $Fe^{II}$-EDTA Conc. | | Total Fe Conc. | |
|---|---|---|---|---|---|---|---|---|
| | ppm | M | ppm | M | ppm | M | ppm | M |
| 30 | 252.59 | 0.004523 | 20.94 | 0.000375 | - | 0 | 273.53 | 0.004898 |
| 60 | 57 | 0.001021 | 5.99 | 0.000107 | - | 0.003672 | 62.99 | 0.001128 |
| 80 | 3.77 | 6.75E-05 | 153.27 | 0.002745 | - | 0.001723 | 157.04 | 0.002812 |
| 380 | 2.19 | 3.92E-05 | 144.29 | 0.002584 | - | 0.001625 | 146.48 | 0.002623 |
| 440 | 4.05 | 7.25E-05 | 136.23 | 0.002439 | - | 0.001523 | 140.28 | 0.002512 |
| 500 | 3.47 | 6.21E-05 | 138.54 | 0.002481 | - | 0.001832 | 142.01 | 0.002543 |
| 680 | 3.21 | 5.75E-05 | 149.35 | 0.002674 | - | 0.001912 | 152.56 | 0.002732 |
| 980 | 2.98 | 5.34E-05 | 154.33 | 0.002764 | - | 0.00175 | 157.31 | 0.002817 |
| 1580 | 3.48 | 6.23E-05 | 133.84 | 0.002397 | - | 0.001785 | 137.32 | 0.002459 |
| 2180 | 2.9 | 5.19E-05 | 126.83 | 0.002271 | - | 0.001621 | 129.73 | 0.002323 |
| 3980 | 3.98 | 7.13E-05 | 133.51 | 0.002391 | - | 0.001689 | 137.49 | 0.002462 |

Table F.8

*Spectrophotometric Determination of Iron Species' at 50 $^0C$ (Initial Persulfate 0.1 M, Initial Fe$^{2+}$ 0.01 M, Initial EDTA 0.005 M)*

| Sample withdrawal Time (s) | Fe$^{2+}$ Conc. | | Fe$^{3+}$ Conc. | | Fe$^{II}$-EDTA Conc. | | Total Fe Conc. | |
|---|---|---|---|---|---|---|---|---|
| | ppm | M | ppm | M | ppm | M | ppm | M |
| 30 | 526.45 | 0.00943 | 16.2 | 0.00029 | - | 0 | 542.65 | 0.00972 |
| 60 | 280.73 | 0.00503 | 72.26 | 0.00129 | - | 0.00325 | 352.99 | 0.00632 |
| 80 | 5.75 | 0.0001 | 369.69 | 0.00662 | - | 0.00221 | 375.44 | 0.00672 |
| 380 | 5.47 | 9.8E-05 | 358.08 | 0.00641 | - | 0.00218 | 363.55 | 0.00651 |
| 440 | 4.85 | 8.7E-05 | 348.25 | 0.00624 | - | 0.00227 | 353.1 | 0.00632 |
| 500 | 4.24 | 7.6E-05 | 354.11 | 0.00634 | - | 0.00205 | 358.35 | 0.00642 |
| 680 | 6.87 | 0.00012 | 355.39 | 0.00636 | - | 0.00212 | 362.26 | 0.00649 |
| 980 | 6.09 | 0.00011 | 346.91 | 0.00621 | - | 0.00203 | 353 | 0.00632 |
| 1580 | 5.13 | 9.2E-05 | 341.5 | 0.00612 | - | 0.00221 | 346.63 | 0.00621 |
| 2180 | 4.86 | 8.7E-05 | 347.91 | 0.00623 | - | 0.00202 | 352.77 | 0.00632 |
| 3980 | 5.3 | 9.5E-05 | 348.92 | 0.00625 | - | 0.00208 | 354.22 | 0.00634 |

Table F.9

*Spectrophotometric Determination of Iron Species' at 50 $^0C$ (Initial Persulfate 0.1 M, Initial Fe$^{2+}$ 0.01 M, Initial EDTA 0.01 M)*

| Sample withdrawal Time (s) | Fe$^{2+}$ Conc. | | Fe$^{3+}$ Conc. | | Fe$^{II}$-EDTA Conc. | | Total Fe Conc. | |
|---|---|---|---|---|---|---|---|---|
| | ppm | M | ppm | M | ppm | M | ppm | M |
| 30 | 522.19 | 0.00935 | 35.17 | 0.00063 | - | 0 | 557.36 | 0.00998 |
| 60 | 150.07 | 0.00269 | 36.99 | 0.00066 | - | 0.00652 | 187.06 | 0.00987 |
| 80 | 12.78 | 0.00023 | 350.8 | 0.00628 | - | 0.00268 | 363.58 | 0.00919 |
| 380 | 8.46 | 0.00015 | 346 | 0.0062 | - | 0.00268 | 354.46 | 0.00903 |
| 440 | 6.62 | 0.00012 | 317.83 | 0.00569 | - | 0.00277 | 324.45 | 0.00857 |
| 500 | 7.09 | 0.00013 | 329.75 | 0.0059 | - | 0.00263 | 336.84 | 0.00866 |
| 680 | 6.23 | 0.00011 | 339.93 | 0.00609 | - | 0.00255 | 346.16 | 0.00875 |
| 980 | 5.53 | 9.9E-05 | 325.7 | 0.00583 | - | 0.00247 | 331.23 | 0.0084 |
| 1580 | 7.23 | 0.00013 | 335.67 | 0.00601 | - | 0.00261 | 342.9 | 0.00875 |
| 2180 | 4.27 | 7.6E-05 | 334.46 | 0.00599 | - | 0.00261 | 338.73 | 0.00868 |
| 3980 | 4.5 | 8.1E-05 | 329.23 | 0.0059 | - | 0.00251 | 333.73 | 0.00849 |

Table F.10

*Spectrophotometric Determination of Iron Species' at 50 $^0C$ (Initial Persulfate 0.1 M, Initial Fe$^{2+}$ 0.01 M, Initial EDTA 0.02 M)*

| Sample withdrawal Time (s) | Fe$^{2+}$ Conc. | | Fe$^{3+}$ Conc. | | Fe$^{II}$-EDTA Conc. | | Total Fe Conc. | |
|---|---|---|---|---|---|---|---|---|
| | ppm | M | ppm | M | ppm | M | ppm | M |
| 30 | 526.45 | 0.009427 | 11.84 | 0.000212 | - | 0 | 538.29 | 0.009639 |
| 60 | 135.59 | 0.002428 | 29.87 | 0.000535 | - | 0.006939 | 165.46 | 0.002963 |
| 80 | 8.71 | 0.000156 | 327.58 | 0.005866 | - | 0.003052 | 336.29 | 0.006022 |
| 380 | 10 | 0.000179 | 332.44 | 0.005953 | - | 0.002917 | 342.44 | 0.006132 |
| 440 | 10.88 | 0.000195 | 319.33 | 0.005718 | - | 0.002846 | 330.21 | 0.005913 |
| 500 | 11.33 | 0.000203 | 308.77 | 0.005529 | - | 0.003012 | 320.1 | 0.005732 |
| 680 | 6.31 | 0.000113 | 326.29 | 0.005843 | - | 0.002956 | 332.6 | 0.005956 |
| 980 | 6.98 | 0.000125 | 326.75 | 0.005851 | - | 0.002723 | 333.73 | 0.005976 |
| 1580 | 7.65 | 0.000137 | 306.2 | 0.005483 | - | 0.002815 | 313.85 | 0.00562 |
| 2180 | 9.05 | 0.000162 | 331.8 | 0.005941 | - | 0.00289 | 340.85 | 0.006104 |
| 3980 | 9.55 | 0.000171 | 313.23 | 0.005609 | - | 0.002733 | 322.78 | 0.00578 |

Table F.11

*Spectrophotometric Determination of Iron Species' at 50 $^0C$ (Initial Persulfate 0.1 M, Initial Fe$^{2+}$ 0.02 M, Initial EDTA 0.005 M)*

| Sample withdrawal Time (s) | Fe$^{2+}$ Conc. | | Fe$^{3+}$ Conc. | | Fe$^{II}$-EDTA Conc. | | Total Fe Conc. | |
|---|---|---|---|---|---|---|---|---|
| | ppm | M | ppm | M | ppm | M | ppm | M |
| 30 | 1051.17 | 0.01882 | 63.03 | 0.00113 | - | 0 | 1114.2 | 0.01995 |
| 60 | 827.06 | 0.01481 | 20.14 | 0.00036 | - | 0.00433 | 847.2 | 0.01517 |
| 80 | 12.45 | 0.00022 | 838.05 | 0.01501 | - | 0.00412 | 850.5 | 0.01523 |
| 380 | 11 | 0.0002 | 787 | 0.01409 | - | 0.00393 | 798 | 0.01429 |
| 440 | 10.33 | 0.00018 | 808.91 | 0.01448 | - | 0.004 | 819.24 | 0.01467 |
| 500 | 9.6 | 0.00017 | 829.19 | 0.01485 | - | 0.00397 | 838.79 | 0.01502 |
| 680 | 11.33 | 0.0002 | 814.06 | 0.01458 | - | 0.00413 | 825.39 | 0.01478 |
| 980 | 11.95 | 0.00021 | 802.27 | 0.01437 | - | 0.00401 | 814.22 | 0.01458 |
| 1580 | 11.61 | 0.00021 | 779.15 | 0.01395 | - | 0.00418 | 790.76 | 0.01416 |
| 2180 | 9.3 | 0.00017 | 812.73 | 0.01455 | - | 0.0039 | 822.03 | 0.01472 |
| 3980 | 10.78 | 0.00019 | 809.58 | 0.0145 | - | 0.0038 | 820.36 | 0.01469 |

Table F.12

*Spectrophotometric Determination of Iron Species' at 50 $^0C$ (Initial Persulfate 0.1 M, Initial $Fe^{2+}$ 0.02 M, Initial EDTA 0.01 M)*

| Sample withdrawal Time (s) | $Fe^{2+}$ Conc. | | $Fe^{3+}$ Conc. | | $Fe^{II}$-EDTA Conc. | | Total Fe Conc. | |
|---|---|---|---|---|---|---|---|---|
| | ppm | M | ppm | M | ppm | M | ppm | M |
| 30 | 1055.12 | 0.01889 | 59.95 | 0.00107 | - | 0 | 1115.07 | 0.019967 |
| 60 | 724.57 | 0.01297 | 66.41 | 0.00119 | - | 0.005183 | 790.98 | 0.019347 |
| 80 | 5.72 | 0.0001 | 781.67 | 0.014 | - | 0.004029 | 787.39 | 0.018129 |
| 380 | 5.17 | 9.3E-05 | 738.83 | 0.01323 | - | 0.00435 | 744 | 0.017673 |
| 440 | 7.21 | 0.00013 | 730.82 | 0.01309 | - | 0.004242 | 738.03 | 0.017458 |
| 500 | 6.2 | 0.00011 | 775.86 | 0.01389 | - | 0.004129 | 782.06 | 0.018133 |
| 680 | 7.57 | 0.00014 | 754.8 | 0.01352 | - | 0.004316 | 762.37 | 0.017968 |
| 980 | 3.83 | 6.9E-05 | 742.33 | 0.01329 | - | 0.004621 | 746.16 | 0.017982 |
| 1580 | 4.92 | 8.8E-05 | 737.98 | 0.01321 | - | 0.00492 | 742.9 | 0.018223 |
| 2180 | 9.54 | 0.00017 | 729.19 | 0.01306 | - | 0.004411 | 738.73 | 0.017639 |
| 3980 | 6.17 | 0.00011 | 726.55 | 0.01301 | - | 0.0044 | 732.72 | 0.017521 |

Table F.13

*Spectrophotometric Determination of Iron Species' at 50 $^0C$ (Initial Persulfate 0.1 M, Initial $Fe^{2+}$ 0.02 M, Initial EDTA 0.02 M)*

| Sample withdrawal Time (s) | $Fe^{2+}$ Conc. | | $Fe^{3+}$ Conc. | | $Fe^{II}$-EDTA Conc. | | Total Fe Conc. | |
|---|---|---|---|---|---|---|---|---|
| | ppm | M | ppm | M | ppm | M | ppm | M |
| 30 | 1044.86 | 0.01871 | 29.15 | 0.000522 | - | 0 | 1074.01 | 0.019232 |
| 60 | 477.47 | 0.00855 | 43.28 | 0.000775 | - | 0.009874 | 520.75 | 0.009325 |
| 80 | 5.64 | 0.000101 | 768.36 | 0.013759 | - | 0.004675 | 774 | 0.01386 |
| 380 | 4.78 | 8.56E-05 | 794.92 | 0.014234 | - | 0.005083 | 799.7 | 0.01432 |
| 440 | 4.54 | 8.13E-05 | 775.56 | 0.013888 | - | 0.004842 | 780.1 | 0.013969 |
| 500 | 5.27 | 9.44E-05 | 733.56 | 0.013136 | - | 0.005163 | 738.83 | 0.01323 |
| 680 | 6.75 | 0.000121 | 734.31 | 0.013149 | - | 0.00518 | 741.06 | 0.01327 |
| 980 | 8.71 | 0.000156 | 740.89 | 0.013267 | - | 0.005904 | 749.6 | 0.013423 |
| 1580 | 7.37 | 0.000132 | 714.13 | 0.012788 | - | 0.005569 | 721.5 | 0.01292 |
| 2180 | 5.05 | 9.04E-05 | 725.15 | 0.012985 | - | 0.005176 | 730.2 | 0.013075 |
| 3980 | 5.45 | 9.76E-05 | 734.44 | 0.013151 | - | 0.004997 | 739.89 | 0.013249 |